General Disclaimer

One or more of the Following Statements may affect this Document

- This document has been reproduced from the best copy furnished by the organizational source. It is being released in the interest of making available as much information as possible.

- This document may contain data, which exceeds the sheet parameters. It was furnished in this condition by the organizational source and is the best copy available.

- This document may contain tone-on-tone or color graphs, charts and/or pictures, which have been reproduced in black and white.

- This document is paginated as submitted by the original source.

- Portions of this document are not fully legible due to the historical nature of some of the material. However, it is the best reproduction available from the original submission.

X-951-75-211
PREPRINT

NASA TM X- 70994

20 AND 30 GHz MILLIMETER WAVE EXPERIMENTS WITH THE ATS-6 SATELLITE

LOUIS J. IPPOLITO

AUGUST 1975

GSFC

GODDARD SPACE FLIGHT CENTER
GREENBELT, MARYLAND

20 AND 30 GHZ MILLIMETER WAVE EXPERIMENTS WITH THE ATS-6 SATELLITE

ABSTRACT

The ATS-6 (Applications Technology Satellite) Millimeter Wave Experiment, developed and implemented by the NASA Goddard Space Flight Center (GSFC), has provided the first direct measurements of 20 and 30 GHz earth-space links from an orbiting satellite. Studies at eleven locations in the continental United States were directed at an evaluation of rain attenuation effects, scintillations, depolarization, site diversity, coherence bandwidth, and analog and digital communications techniques. In addition to direct measurements on the 20 and 30 GHz links, methods of attenuation prediction with radars, rain gauges and radiometers were developed and compared with the directly measured attenuation.

This report contains the first comprehensive publication of initial data results of the ATS-6 Millimeter Wave Experiment from the major participating organizations.

The first section describes the experiment objectives, flight hardware, and modes of operation. The remaining six sections present papers prepared by the major participating organizations in the experiment. The papers present a comprehensive summary of the significant results of the initial eleven months of ATS-6 experiment measurements and related radiometric, radar and radio-meteorology studies.

CONTENTS

THE ATS-6 MILLIMETER WAVE EXPERIMENT

INTRODUCTION

The ATS-6 (Applications Technology Satellite) Millimeter Wave Experiment, developed and implemented by the NASA Goddard Space Flight Center (GSFC), has provided the first direct measurements of 20 and 30 GHz earth-space links from an orbiting satellite. Studies at eleven locations in the continental United States were directed at an evaluation of rain attenuation effects, scintillations, depolarization, site diversity, coherence bandwidth, and analog and digital communications techniques. In addition to direct measurements on the 20 and 30 GHz links, methods of attenuation prediction with radars, rain gauges and radiometers were developed and compared with the directly measured attenuation.

This section presents a summary of the satellite hardware, experiment configuration and operations. The following sections present data measurements and analysis results from a number of the participating organizations in the experiment.

The ATS-6 Millimeter Wave Experiment, (MWE), is designed to measure and evaluate the propagation characteristics of space-to-earth links centered at 20 GHz and 30 GHz.[1] The ATS-6 MWE is the second NASA flight experiment to evaluate propagation effects above 10 GHz. The first experiment, launched on-board the ATS-5 in July 1969, provided measurements at 15.3 GHz and 31.65 GHz.[2]

The ATS-6 was successfully launched into synchronous orbit at 13:00 GMT on Thursday, 30 May 1974, aboard the Titan IIIC launch vehicle, number C-27 (Figure 1-1). Spacecraft weight at the time of lift-off was 1396 Kg (3078.3 pounds), including the 48 Kg adapter which remained attached at spacecraft separation. Injection occurred at 19:30:49 GMT into a near perfect orbit. The automatic separation and deployment sequence was successfully completed and the spacecraft was commanded through the sun and earth acquisition, and yaw reference sequences, and with all operations being completed by 02:19 GMT the day after launch. During the next two weeks of flight, the spacecraft was commanded into its normal in-orbit configuration and all systems were evaluated. Following this spacecraft checkout phase, a series of tests were conducted to evaluate the performance of the on-board experiment systems and their respective ground system interfaces. At the end of the first month of flight, all

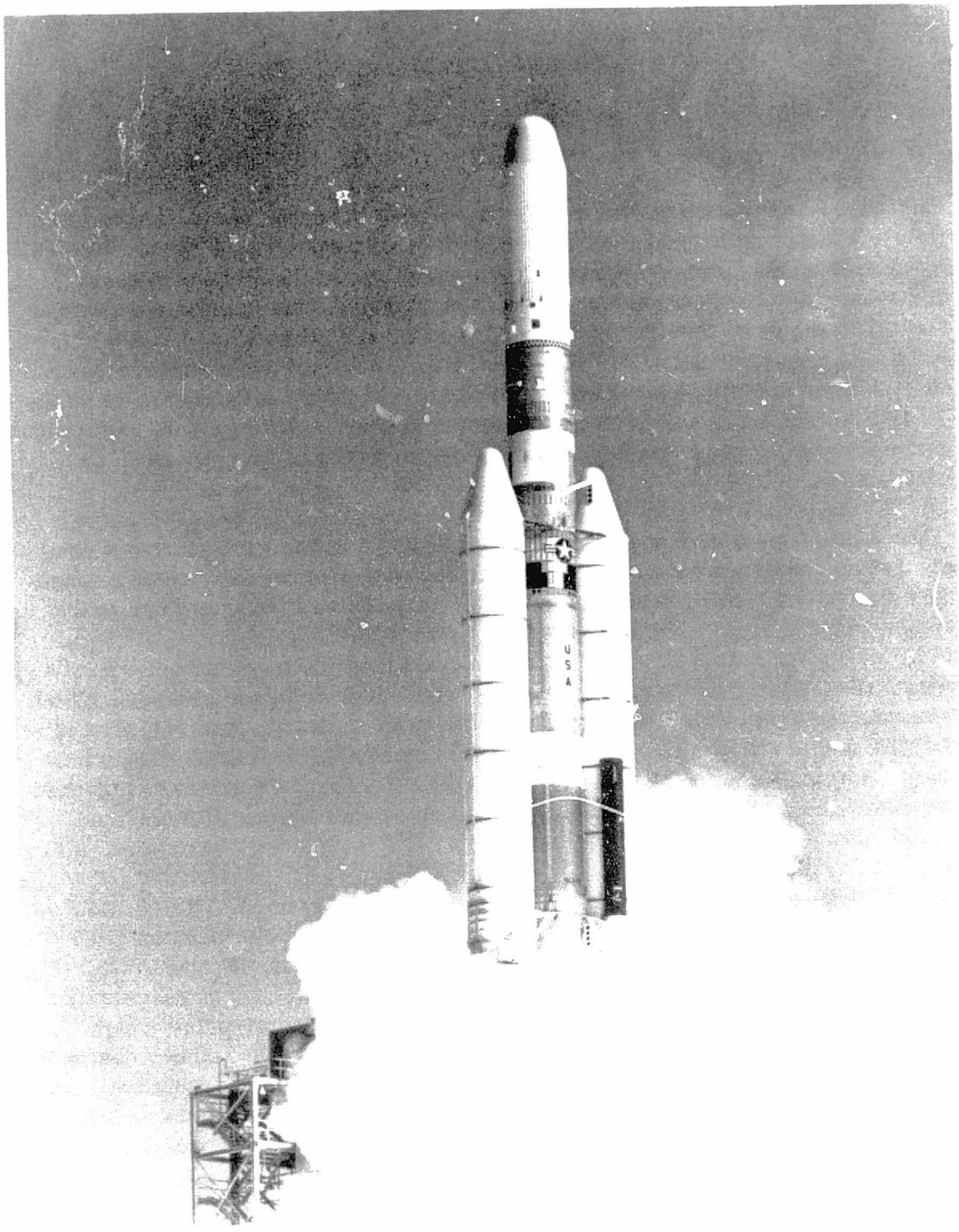

Figure 1-1. ATS-6 Launch, May 30, 1974.

systems had been successfully evaluated with very few anomalies encountered, and the spacecraft was declared operational.

SATELLITE HARDWARE

The major elements of the MWE satellite system are shown in Figure 1-2. The experiment has three modes of operation; CW, multitone, and communications, selectable at 20 and/or 30 GHz. In the CW mode, a 10 GHz signal is developed by multiplication from the 5 MHz master oscillator, then doubled for the 20 GHz carrier and tripled for the 30 GHz carrier. The carriers are then used to drive 2 watt traveling wave tube amplifiers, (TWTA), and then transmitted through either of two antenna systems to the earth. The parabolic antenna is used when a narrow spot beam is required, and the horn antennas are used for wide coverage of the continental United States area.

In the multitone mode, a 180 MHz signal is developed from the 5 MHz master oscillator and used to phase modulate the 10 GHz carriers in the 20 and 30 GHz chains. A comb of 9 tones is generated, four on either side of the carrier spaced 180 MHz apart, resulting in a total spectrum of 1440 MHz. This signal is used to evaluate the coherence bandwidth characteristics of the space-to-earth path. In the communications mode, the 150 MHz I.F. from the spacecraft is used to drive an upconverter which produces a 30.150 GHz or 20.150 GHz transmitted signal for communications tests. Bandwidths of 25 MHz or 12 MHz are available, on command, for the 150 MHz IF signal. The uplink frequency of the spacecraft transponder is one of three in the 6 GHz band, and the downlink is one of three in the 4 GHz band.

The experiment hardware, located in the ATS-6 Earth Viewing Module (EVM), is physically divided into four units shown in Figure 1-3; a) the RF multiplier; b), the 20/30 GHz modulator/power amplifier; c), the 20/30 GHz horn antenna assembly, and, d), the .45 meter 20/30 GHz parabolic antenna. The package weighs a total of 91.4 lbs., and consumes about 39 watts with one TWTA on, and 70 watts with both frequencies operating. The frequency deviation of the oscillator was measured at about 1 part in 10^{10} over a temperature range of -10° to 50° C.

MODES OF OPERATION

The experiment is commandable into three modes of operation: a continuous wave mode in which the 20 and 30 GHz carriers only are transmitted; a multitone mode in which nine spectral lines spaced 180 MHz apart and centered at

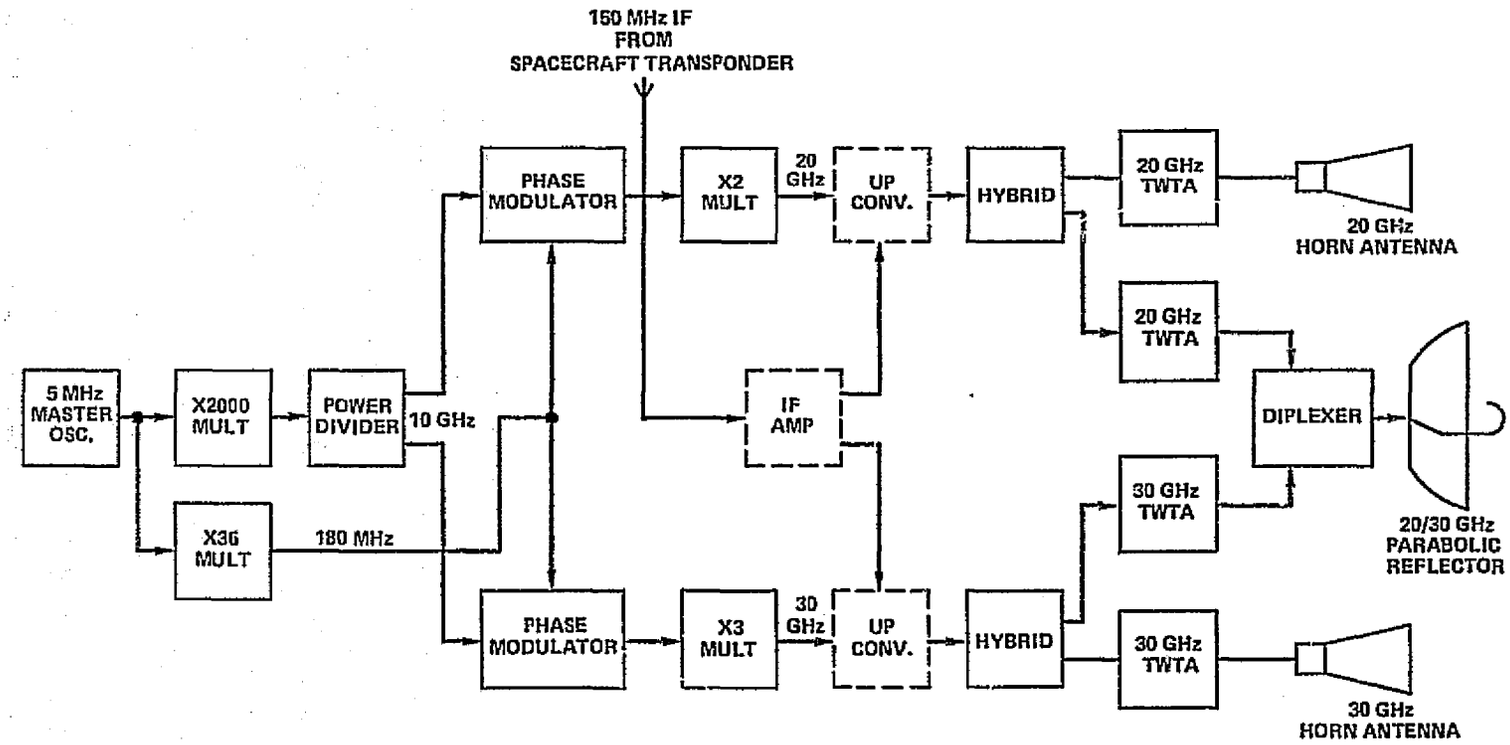

Figure 1-2. ATS-6 Millimeter Wave Experiment Flight Hardware Elements

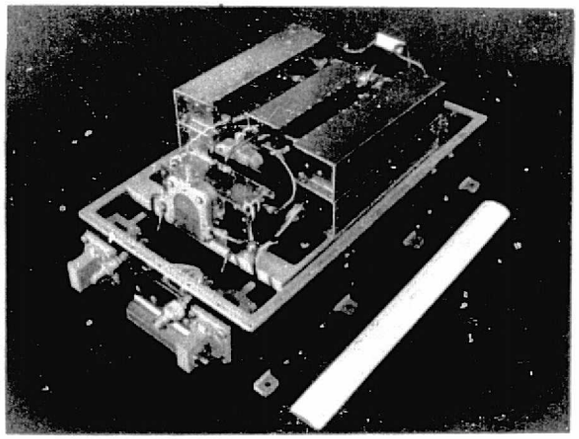

(a) RF Multiplier

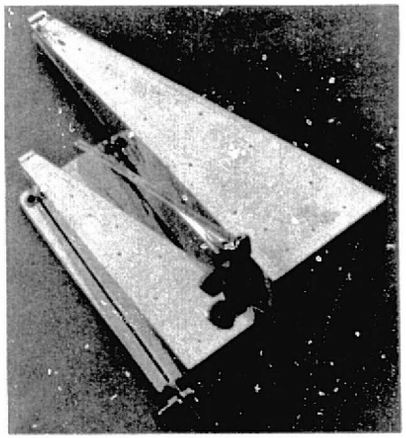

(b) 20/30 GHz Modulator/Power Amplifier

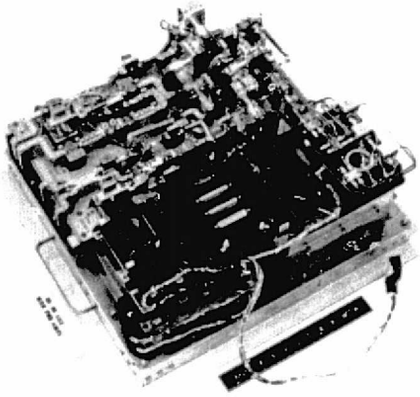

(c) 20/30 GHz Horn Antenna Assembly

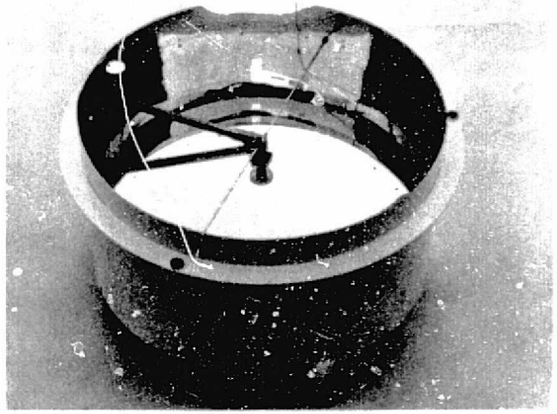

(d) 20/30 GHz Parabolic Antenna

Figure 1-3. Millimeter Wave Experiment Flight Hardware.

20 GHz and at 30 GHz are transmitted; and a communications mode in which the FM communications signals received on the spacecraft transponder are retransmitted at 20.15 and 30.15 GHz.

Simplified block diagrams of the experiment configuration for the CW mode are shown in Figure 1-4 for the cases of radiation from the horn antennas and the parabolic antenna, respectively. In each case a 10 GHz signal is generated in the RF multiplier which uses a very stable 5 MHz crystal oscillator as a reference. The 10 GHz signal is applied to X2 and X3 frequency multipliers and the resulting 20 and 30 GHz signals are amplified by TWTAs for radiation by the antennas.

Simplified block diagrams of the experiment configuration for the multitone mode are shown in Figure 1-5 for the cases of horn antennas and parabolic antenna, respectively. In this mode a 180 MHz modulating signal is derived from the same 5 MHz master oscillator as the 10 GHz. The 180 MHz signal drives the phase modulators at 10 GHz and the modulated signal is frequency multiplied X2 and X3 to achieve multitone spectrums at 20 and 30 GHz. The 20 and 30 GHz multitone signals are amplified by traveling-wave tube amplifiers (TWTAs) for radiation by the antennas.

The configuration of the experiment for the communications mode is shown in simplified form in Figure 1-6. In this mode the 10 GHz signal is again frequency multiplied to 20 and 30 GHz as in the CW mode, and these two frequencies are used to pump two upconverters. Signal drive for the upconverters consists of the frequency modulated 150 MHz IF signal from the spacecraft transponder suitably amplified by an IF amplifier. The resulting 20.15 and 30.15 GHz FM signals are then amplified by TWTAs for radiation by the parabolic antenna.

Three antennas are provided in the experiment: a 20 GHz horn antenna, a 30 GHz horn antenna, and a 20/30 GHz parabolic antenna. In each case the radiated RF is linearly polarized with the plane of the E-vector aligned to the north-south axis of the spacecraft. For both horn antennas the 3 dB bandwidths are approximately 6 degrees in the north-south direction and approximately 8 degrees in the east-west direction. The parabolic antenna provides a 3 dB beamwidth of approximately 2.3 degrees at 20 GHz and approximately 1.6 degrees at 30 GHz. The effective isotropic radiated power (EIRP) of the antennas at the peak of the beam based on measured performance, is listed in Table 1-1.

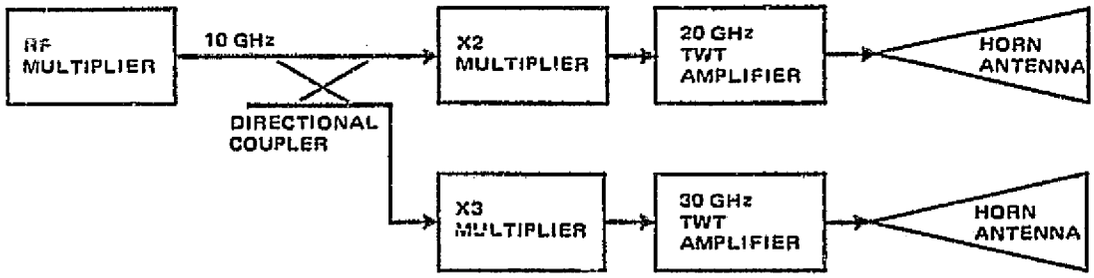

a) USING HORN ANTENNAS

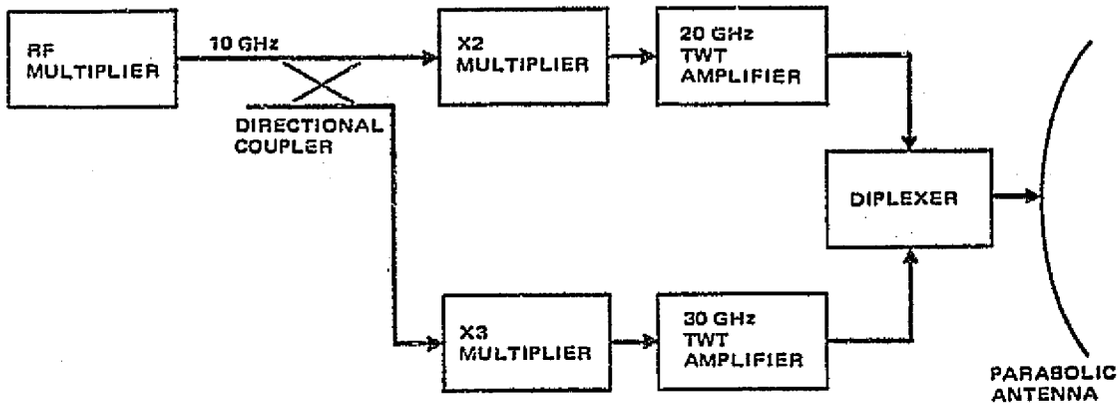

b) USING PARABOLIC ANTENNA

Figure 1-4. CW Mode Simplified Block Diagram

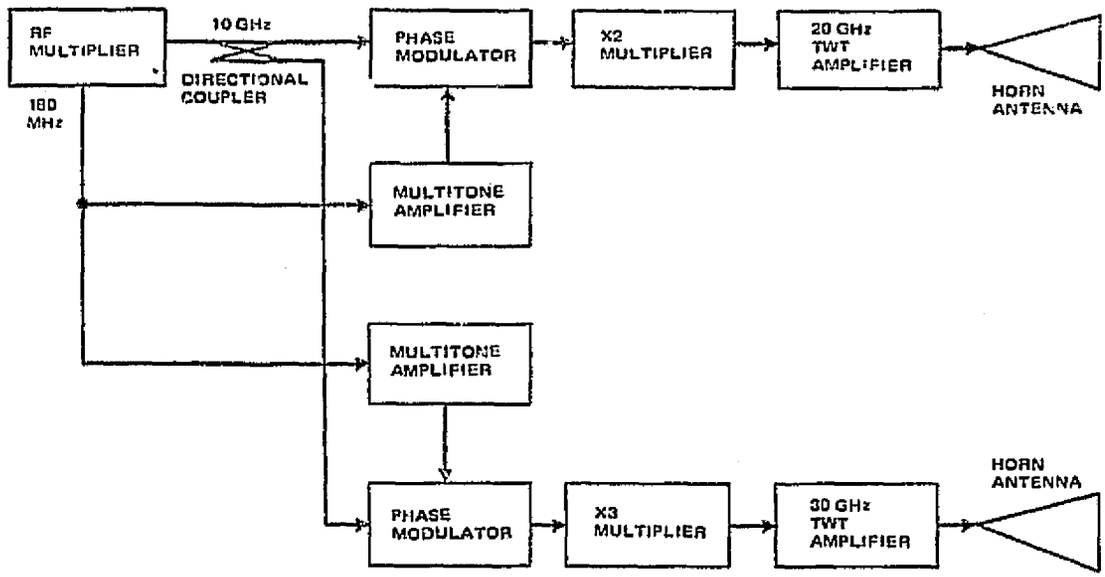

a) USING HORN ANTENNAS

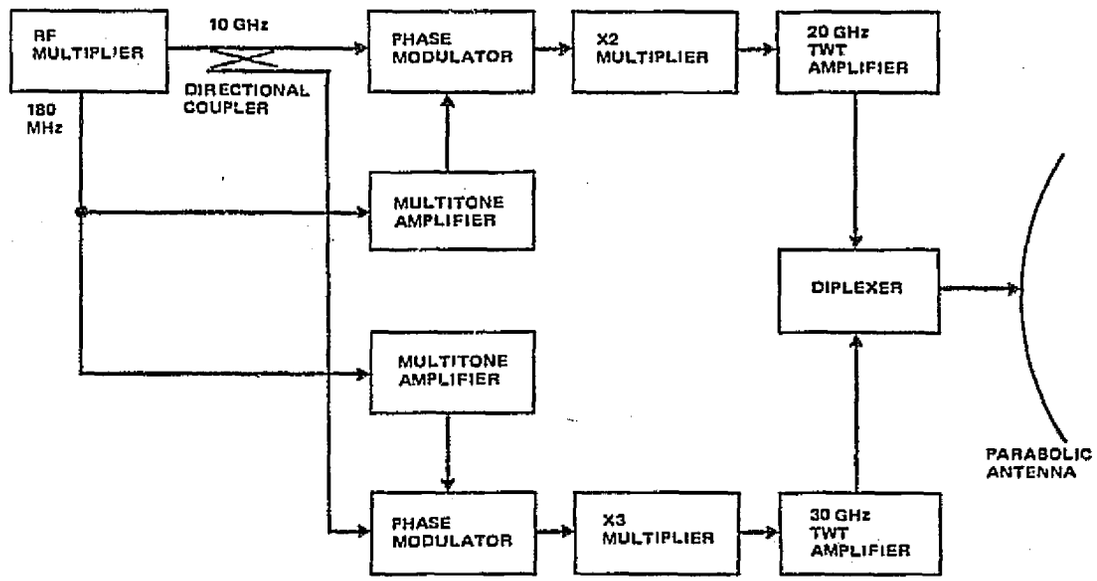

b) USING PARABOLIC ANTENNA

Figure 1-5. Multitone Mode Simplified Block Diagram

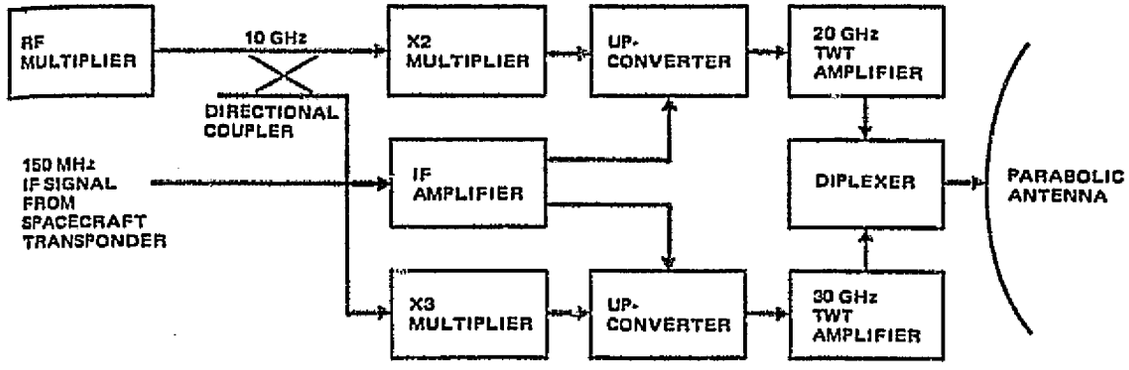

Figure 1-6. Communications Mode Simplified Block Diagram

Table 1-1. EIRP at Antenna Beam Maximum

Antenna	EIRP, dBm	
	20 GHz	30 GHz
Horn		
CW mode	61.0	59.8
Multitone mode	60.1	59.9
Communications mode	60.3	60.1
Parabolic		
CW mode	70.3	73.6
Multitone mode	70.2	73.8
Communications mode	71.3	73.3

GROUND TERMINAL LOCATIONS

The ATS-6 MWE consists of ground terminals at eleven locations throughout the United States. The prime facility is the NASA Station at Rosman, North Carolina, which is equipped to measure 20 and 30 GHz attenuation, coherence bandwidth, communications link characterization and prediction techniques with radars and rain gauges. A second NASA terminal, located at the Goddard Space Flight Center, GSFC, Greenbelt, Maryland, performs 20 and 30 GHz attenuation measurements, and scintillation studies.

A major element of the ATS-6 MWE involved the participation of a number of organizations with unique specialties in the millimeter wave propagation area.

Nine organizations with thirteen ground terminals participated in the ATS-6; their locations and major areas of measurement are summarized in Table 1-2.

All terminals were equipped to measure attenuation at 20, 30 GHz, or both, and all except for Bell Laboratories had rain gauge measurements as well. The Washington DC Area Diversity Experiment consisted of four terminals in the Washington metropolitan area which jointly observed 20 GHz attenuation events from which site diversity statistics were developed.

Most of the participating stations used receiver systems that were designed for the ATS-5 program and converted to 20 and 30 GHz for use on the ATS-6 MWE.[3] Antenna sizes varied from 1.2 to 18.3 m (see Table 1-2) and the front-end characteristics varied with the particular sites. Descriptions of the ground systems will be included in the papers from the participating organizations.

EXPERIMENT OPERATIONS

The Millimeter Wave Experiment flight hardware was first energized on June 13, 1974, and all modes were operational except for the 20 GHz horn antenna TWTA. Repeated attempts to energize the 20 GHz horn antenna were unsuccessful. All other modes have performed within the expected parameters.

The MWE operated with both scheduled tests, and unscheduled periods when a call up was requested by a participant. Other ATS-6 experiments, primarily HET and PLACE, had priority for operations of the MWE, hence all request periods could not be honored. Figure 1-7 summarizes the hours of on-time, both scheduled and unscheduled for the 13 months of MWE operations. The number of requests granted for each month is also shown. For many of the request periods more than one ground terminal was monitoring the satellite signal; the numbers on the figure only indicate the initial request.

The ATS-6 MWE has logged over 1143 hours of operations, in all modes, since launch; over 900 of these hours were for unscheduled 'call-up' measurements during rain periods or special tests.

MWE operations at the new spacecraft location at 35° East longitude are continuing at both 20 and 30 GHz, and further tests are planned when the ATS-6 returns to 105° West longitude in 1976.

Table 1-2
ATS-6 MWE Participating

LOCATION, ORGANIZATION	ELEVATION ANGLE (ANTENNA DIA.)	MAJOR AREAS OF INVESTIGATION
ROSMAN, N. CAROLINA NASA GSFC	47 (15 ft)	PRIME FACILITY 20 & 30 GHz–ATTENUATION, COHERENCE BANDWIDTH, DIFFERENTIAL PHASE EFFECTS, SCINTILLATION, COMMUNICATIONS LINKS, RADARS, RADIOMETERS, RAIN GAGE NETWORK
GREENBELT, MARYLAND NASA GSFC	41 (10 ft)	20 & 30 GHz–ATTENUATION, SITE DIVERSITY**, RADIOMETERS
AUSTIN, TEXAS UNIV. OF TEXAS (2)*	54 (5, 10 ft)	30 GHz–ATTENUATION, 2 TERMINAL SITE DIVERSITY, RADIOMETER
BLACKSBURG, VIRGINIA VPI & SU*	45 (4 ft)	20 GHz–ATTENUATION, DEPOLARIZATION
CLARKSBURG, MARYLAND COMSAT (2)*	41 (10, 15 ft)	20 & 30 GHz–ATTENUATION, SITE DIVERSITY**, RADIOMETERS
COLUMBUS, OHIO OHIO STATE UNIV. (3)*	42 (10, 15 ft)	20 & 30 GHz–ATTENUATION, 3 TERMINAL SITE DIVERSITY, SCINTILLATION, RADARS, RADIOMETERS
HOLMDEL, NEW JERSEY BELL LABORATORIES	39 (12 ft)	20 GHz–DEPOLARIZATION
BALTIMORE, MARYLAND WESTINGHOUSE*	41 (12 ft)	20 GHz–ATTENUATION; SITE DIVERSITY**
WALDORF, MARYLAND NRL*	42 (60 ft)	20 & 30 GHz–ATTENUATION; SITE DIVERSITY**, RADIOMETERS
RICHLAND, WASHINGTON BATTELLE N.W.*	31 (30 ft)	20 GHz–ATTENUATION, RADIOMETER
FT. MONMOUTH, N.J. USASCA	39 (15 ft)	30 GHz–ATTENUATION

*GSFC SUPPORTED PARTICIPATION
**WASHINGTON, D.C. AREA DIVERSITY EXPERIMENT

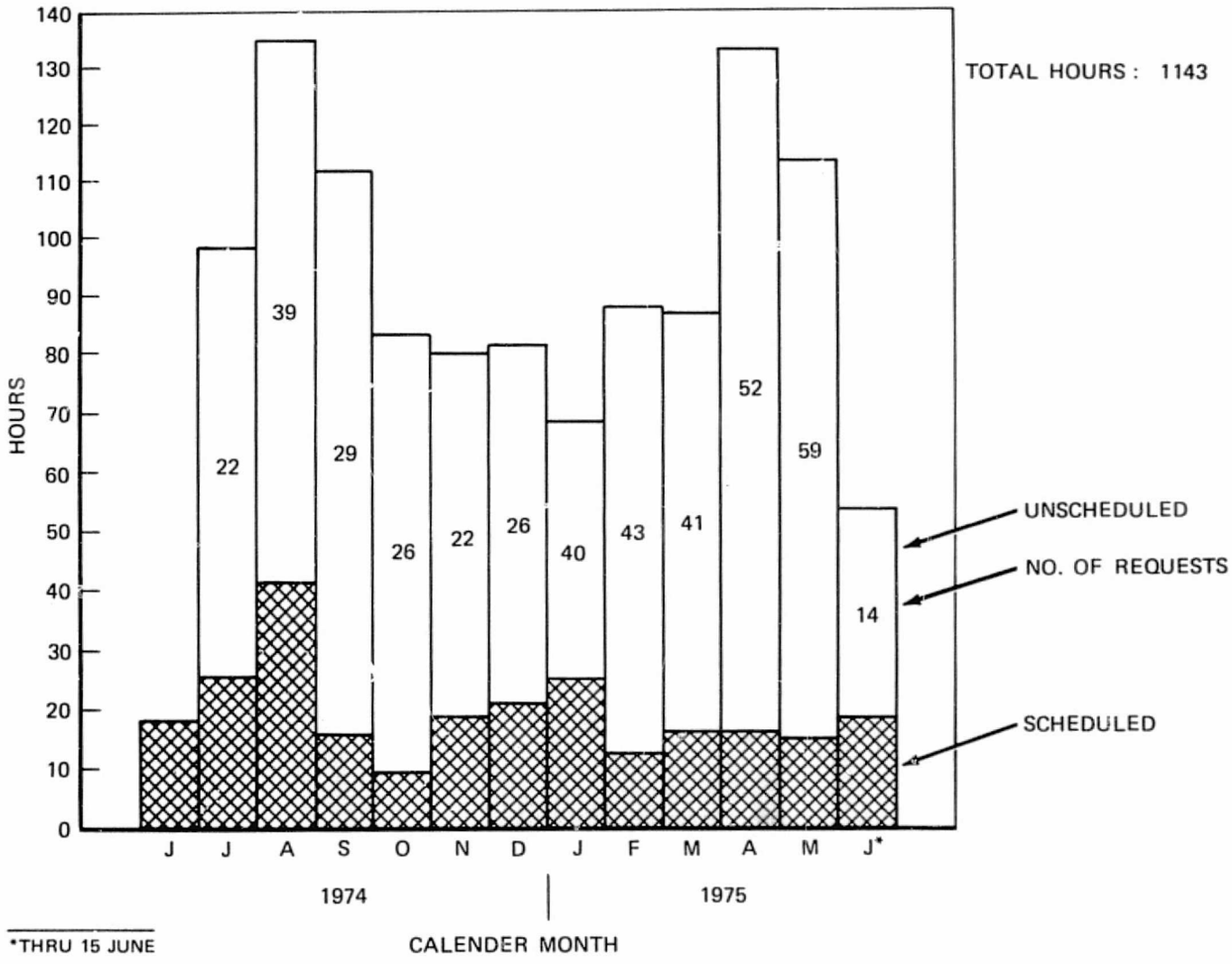

Figure 1-7. ATS-6 Millimeter Wave Experiment Hours of Spacecraft On-Time

REFERENCES

1-1. L. J. Ippolito, "The ATS-F Millimeter Wave Propagation Experiment," NASA Goddard Space Flight Center, Greenbelt, Maryland, Rep. X-751-71-460, October 1971.

1-2. L. J. Ippolito, "Effects of Precipitation on 15.3 and 31.65 GHz Earth Space Transmissions with the ATS-5 Satellite, Proc. IEEE, Vol. 59, No. 2, pp. 189-205, February 1971.

1-3. C. D. Calhoon, Jr., "ATS-F Millimeter Wave Experiment Ground Receiver Systems for NASA Sponsored Participating Stations", NASA Goddard Space Flight Center, Greenbelt, Maryland, Rep. X-751-73-3, January 1973.

ATS-6 ATTENUATION AND DIVERSITY MEASUREMENTS AT 20 AND 30 GHz

W. J. Vogel
A. W. Straiton
B. M. Fannin
N. K. Wagner
Electrical Engineering Research Laboratory
The University of Texas at Austin
Austin, Texas

1. INTRODUCTION

A. General

Satellite-terrestrial communication systems depend upon the propagation of electromagnetic waves through the atmosphere. A successful design of such a system is one that meets realistic specifications. These must be based on the knowledge of any limitations introduced by the atmosphere. At millimeter wave frequencies for elevation angles above about 15° mainly two mechanisms exist that introduce limitations: (1) the absorption and reradiation of radio waves by oxygen and water vapor and (2) the absorption and scattering of radio waves by precipitation. While the first can be essentially determined (Straiton, 1975) the second one requires that propagation measurements be made. This is so because while the interaction can be theoretically analyzed if the physical parameters of the precipitation are known (Vogel et al. 1973) the frequency of occurrence and the severity of precipitation events are not well enough defined to allow a purely theoretical prediction.

For this purpose and in anticipation of the future need of satellite systems operating at 20 and 30 GHz NASA's ATS-6 satellite included a millimeter wave experiment. The signals from the 20 and 30 GHz transmitters could be used by participating experimenters for pertinent measurements. This report describes the efforts by the Electrical Engineering Research Laboratory, The University of Texas at Austin.

B. Experiment Objectives

The information to be presented here has been obtained in three ways.

1. Statistical data has been collected on the attenuation due to the atmosphere for the transmission from the satellite at both 20 and 30 GHz. The 30 GHz data has been taken by using the satellite signal and the 20 GHz data has been obtained by radiometric means. From the 20 GHz data the 30 GHz attenuation could be estimated for the times during which the satellite signal was not received because of the unavailability of the transmitter or rare failures of the receiver.

2. Space diversity studies have been carried out by having a radiometer and a receiver located at Balcones Research Center and a second radiometer and a second receiver located on the Main Campus of The University of Texas at a distance of 11 km to the south. This distance was selected on the basis of the results of the ATS-5 satellite experiments which indicated that thunderstorms that produced attenuation of a severe nature were commonly less than 12 km in diameter. The thunderstorms whose width is less than the separation of the terminals would not be covering both stations at the same time.

3. Data obtained from the Weather Bureau both by radar and by other techniques have been compared to the measured attenuations. This has the objective of trying to extrapolate the measurements made in Austin to other sites which might later be used for ground terminals and for which similar meteorological data are available. For this extrapolation an understanding of the nature of the thunderstorm is important background information. The results of studies made on the ATS-5 satellite indicated that severe attenuations were experienced only during the periods of very severe thunderstorms. The area around Austin, Texas has a relatively high number of thunderstorms per year and, therefore, provides a location where this effect can be studied effectively.

C. Organization of Paper

In Chapter II the ground station instrumentation and the operational procedures and statistics will be described. Chapter III is devoted to the meteorological characterization of Austin. Besides a general climatology it includes various relevant statistics published by the U. S. Weather Bureau and explains where and how the weather data were obtained. The results of the measurements are given in Chapter IV both from a single site point of view and a diversity one. Conclusions are presented in Chapter V.

II. GROUND STATIONS

A. Instrumentation

1. Antennas

The two ground stations had different antenna systems. The northern site (at Balcones Research Center) utilized two 3 m parabolic dishes attached side by side to one azimuth-elevation steerable converted ballistic radar mount (see Fig. 2-1, a). The pointing of these antennas was controlled by the observer with setting accuracy within .03°. Both antennas had prime focus feeds. For this purpose each had a 30 cm long aluminum cylinder with 23.5 cm diameter mounted at the focus which served as universal receiver box. The side pointed towards the dish was covered by a half sphere plexiglass radome of 7.5 cm radius with the focal point at its center. The thickness was selected to achieve a quarter wave match at either 20 or 30 GHz. This way reflections off the radome were minimized. The outside was coated with water repellant (Silanox 101) causing immediate beading and runoff to any water on it. The antenna for the second site (on the Campus of The University of Texas) was a 1.5 m converted searchlight (see Figure 2-1, b). It was outfitted with a stepping motor and digital shaft encoders to allow automatic pointing in azimuth and elevation to within .02°. This antenna had a prime focus feed support structure. For the simultaneous operation at 20 and 30 GHz the feeds were placed into the focus side by side. This caused the two beams to be slightly divergent. The front of the antenna was covered with a plexiglass plate (matched to 20 GHz and coated with water repellant), enclosing both the antenna and the receiver box.

To prevent condensation refrigerated air was blown into this cavity. Minimum elevation angles at BRC were 15° to the east and west because of the structure of the mount and about 35° on Campus because of adjacent buildings.

2. Satellite Receivers

The 30 GHz satellite receivers had superheterodyne front ends in which 28.95 GHz crystal multiplier local oscillators were mixed with the signal from the feed into a 1.05 GHz IF. This allowed the utilization of back ends built for the ATS-5 experiment by Martin-Marietta. These receivers have been documented elsewhere (Martin-Marietta, 1969). They are phase-locked loop receivers in which the down converted carrier is locked to a 10 MHz crystal oscillator. The noise bandwidth of these receivers is 50-100 Hz. With the typical 12 dB SSB noise figure of the mixers the noise power of the receivers $P_N = kTB$ is -142 dBm. To improve the reliability of the local oscillators in continuous operation even during the hottest summer weather all active front

Figure 2-1a. Balcones Research Center Antenna System

Figure 2-1b. University Campus Site Antenna

end components were mounted on a water cooled plate. This could be inserted into the focal cylinder of the 3 m antenna or the support structure of the 1.5 m antenna. Figure 2-2, a gives a block diagram of the satellite receivers. The fade margins when the satellite was pointed at Rosman, N. C. and was transmitting through the 30 GHz horn antenna were better than about 33 dB for both receivers. The only small difference between the 3 m and 1.5 m antenna systems can be explained by the fact that the 3 m dish is degraded at 30 GHz and the mixer with the better noise figure was used for the smaller antenna.

3. Radiometers

The 20 GHz sky-noise radiometers were Dicke switched receivers. Their local oscillator frequency was chosen to coincide with the first lower sideband frequency of the 20 GHz satellite transmitter at 19.82 GHz. Thus it was ensured that the 30 MHz IF (total bandwidth = 20 MHz) would not allow any satellite signals to introduce errors into the measurements. For additional isolation the radiometers were approximately cross-polarized to the satellite signals. Even during clear air propagation conditions no satellite signals were ever noted in the radiometer outputs. A plot of the spectrum is given in Figure 2-2, b.

The sensitivity of the radiometers was about 1°K which a 1 sec integration time. Their block diagram is given in Figure 2-3. The components were mounted on a water-cooled plate. For the searchlight system they shared the plate with the satellite receiver.

4. Station Location

Site 1 at the Balcones Research Center (BRC) was located at the northern edge of Austin, Texas. Its coordinates are shown in Figure 2-4. Site 2 on the Campus of The University of Texas was 11 km to the south. Figure 2-5 gives the relevant data and shows that the two sites were almost aligned along the direction of the satellite.

B. Calibration

1. Satellite Receivers

Because of weight and space limitations for the front end all calibrations were performed by attenuating the satellite signal with a calibrated attenuator during periods when no rain was in the propagation path. Since the attenuation was introduced in the IF (1.05 GHz BRC site; 60 MHz Campus site) noise generated in the front end was attenuated too. Therefore the attenuation at 30 GHz has to be related to the attenuation at the IF level by

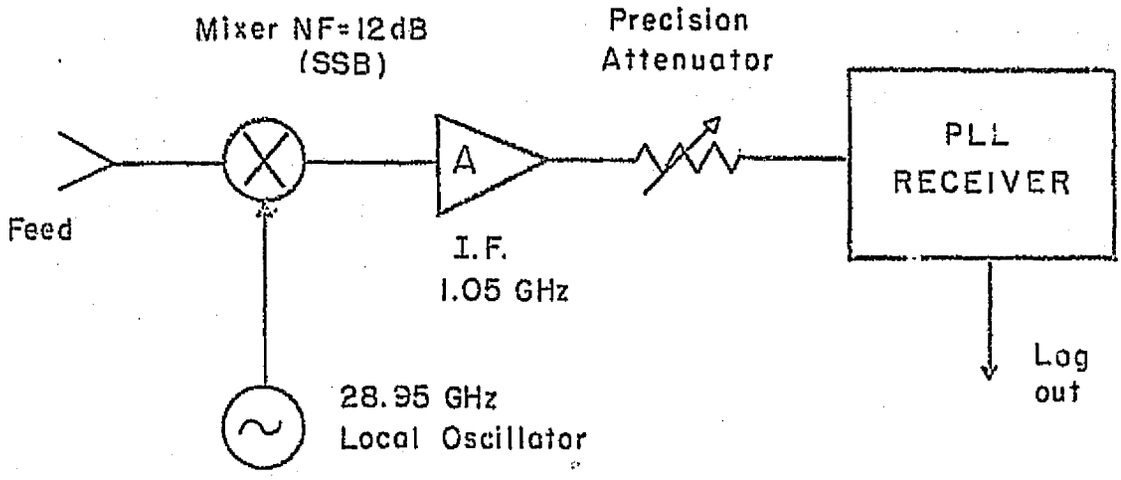

Figure 2-2a. Satellite Receiver Block Diagram

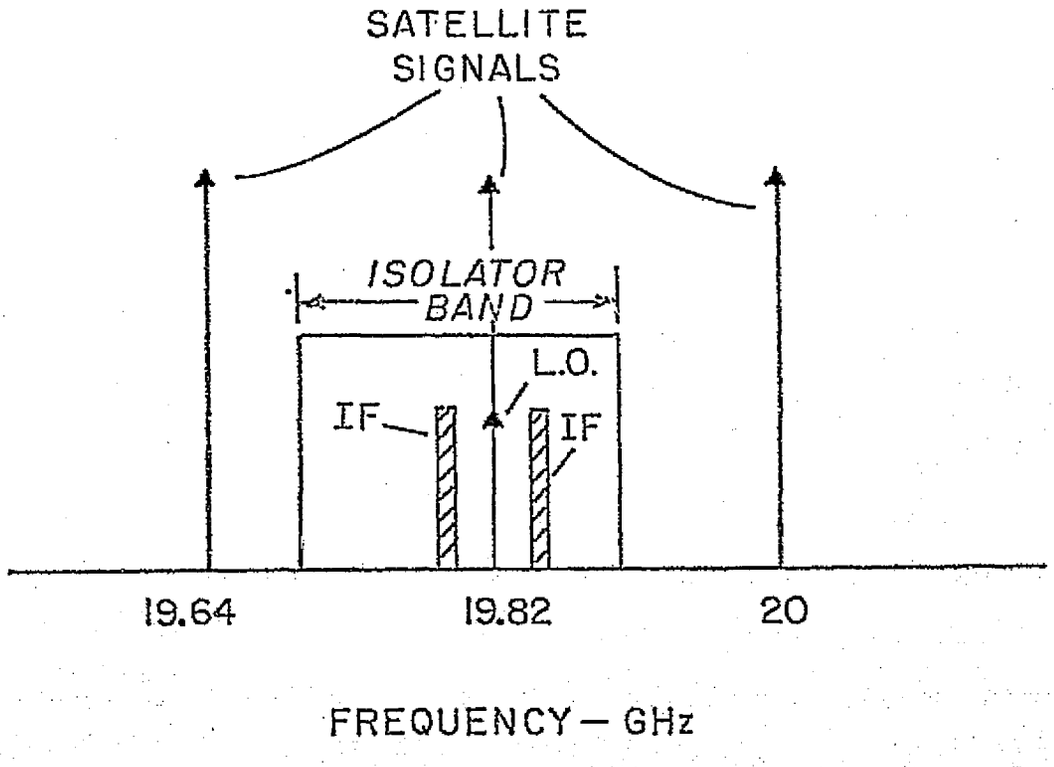

Figure 2-2b. Spectrum for 20 GHz Radiometer.

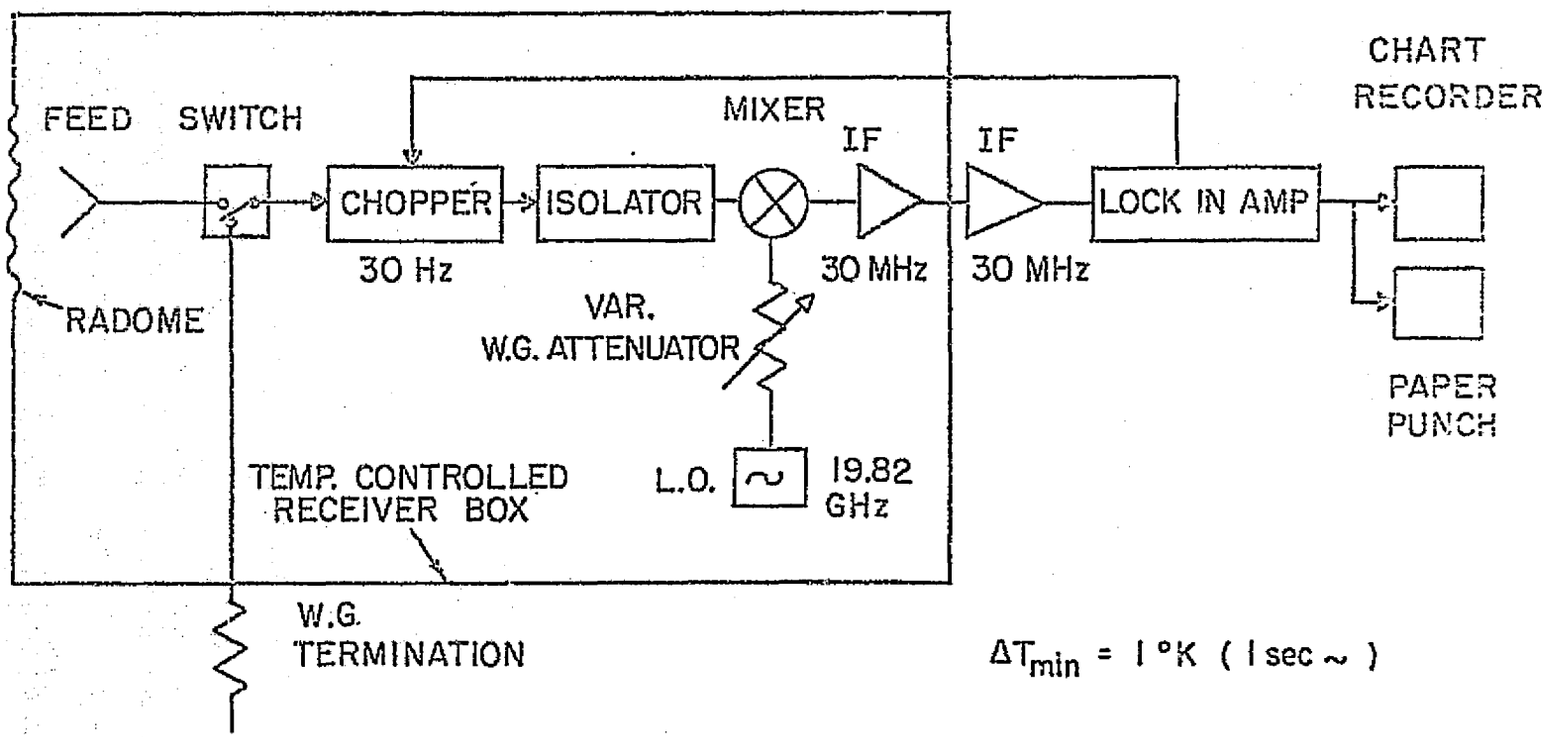

Figure 2-3. 20 GHz Radiometer System Simplified Block Diagram

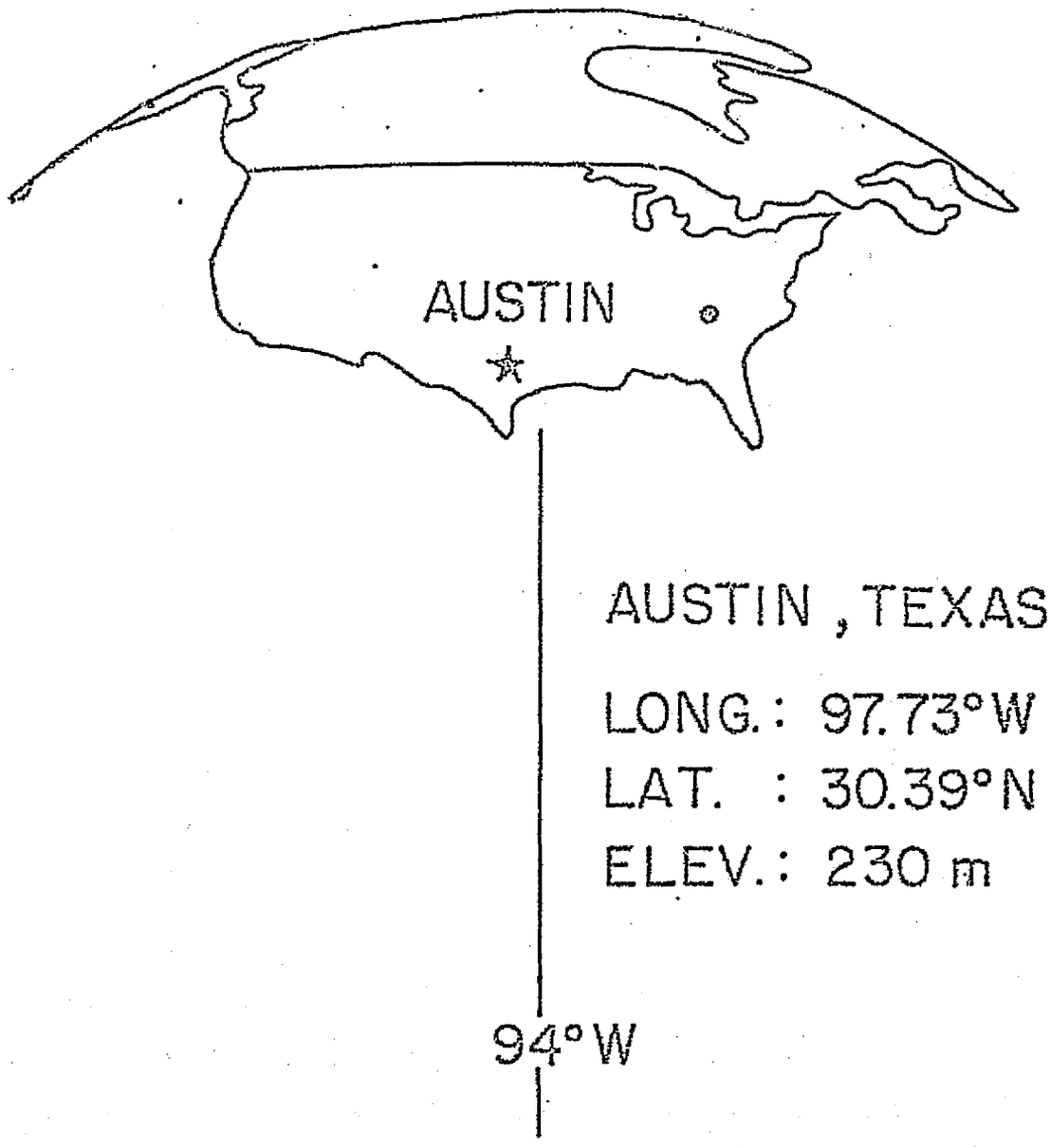

Figure 2-4. Geography seen from Satellite

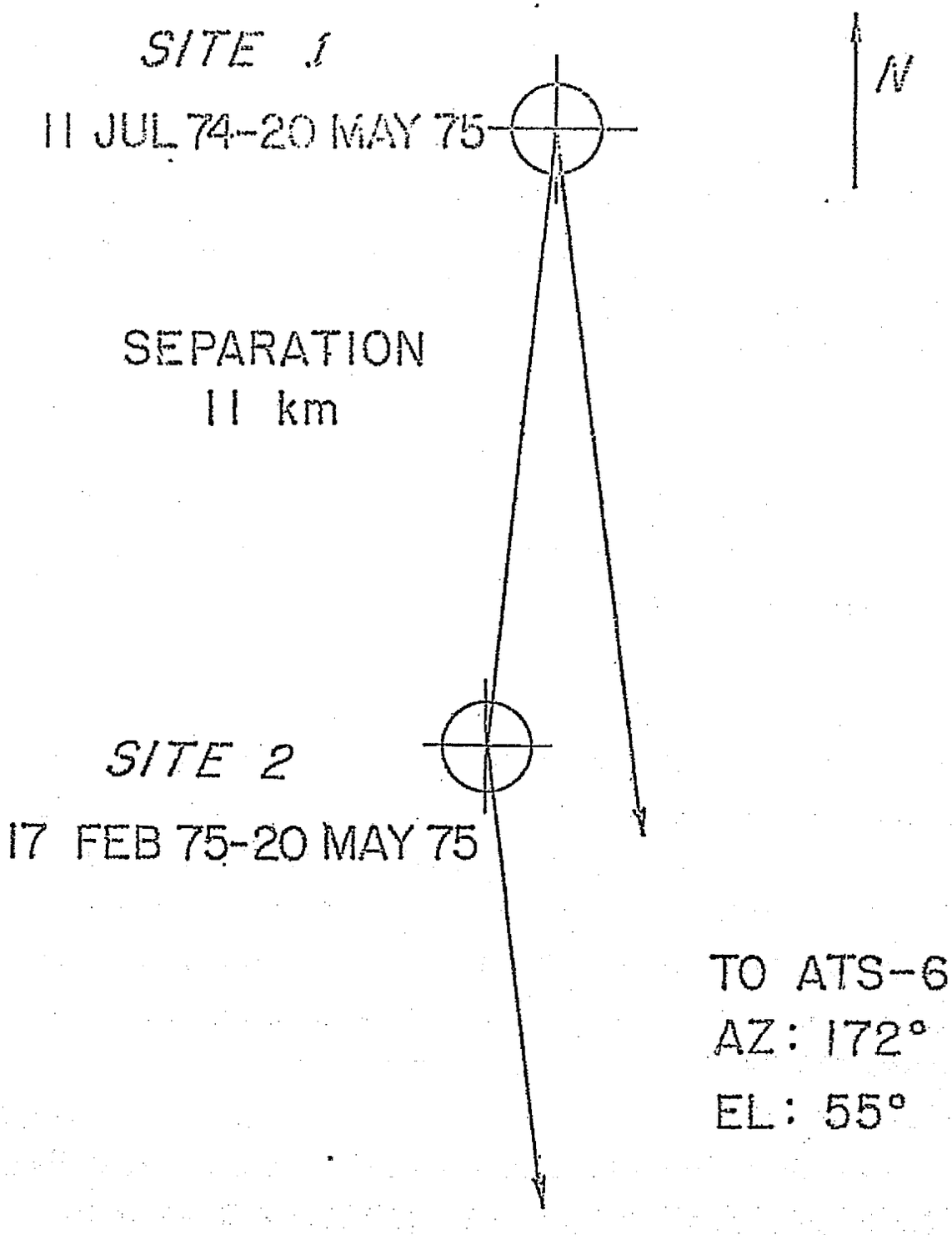

Figure 2-5. Station Lay-out in Austin, Texas

$$L_{RF} = L_{IF} + \{SNR - 10 \log(10^{SNR/10} - 10^{L_{IF}/10} + 1)\} \quad (1)$$

where SNR is the signal-to-noise ratio in dB under clear weather transmission conditions. L_{RF}, L_{IF} are the RF and IF attenuation in dB. Because of the difficulty in exactly measuring the SNR of the phase locked receiver for all the possible clear-air levels which existed for the many combinations of pointing and mode of the spacecraft, the data analysis was restricted to a maximum fade depth of 25 dB. For these levels the above relation simplifies to

$$L_{RF} \approx L_{IF}. \quad (2)$$

Calibrations were performed as frequently as the weather and the operation of the satellite allowed. At the BRC station this was typically at least once for each turn-on period and each spacecraft pointing. At the automated receiver site on Campus calibrations were made typically once during days with attenuation events. The accuracy of the calibrations is estimated to be ±.5 dB.

2. Radiometers

The radiometers were calibrated about once a week during cloudless periods. Since they operated in a temperature controlled environment of about 40°C the "hot" point was found by disconnecting the IF preamplifiers from the IF amplifier. The output then corresponds to a zero signal level at the chopper frequency and equals the temperature of the chopper, typically 303°K. The second point to define the linear relationship between sky temperature and radiometer output voltage was found by calculating the clear air sky-noise temperature from a measurement of the absolute ground humidity, resulting in typically between 15 and 25°K. This method of calibration has the advantage that the losses from the input of the antenna to the output of the feed need not be measured. It is estimated that the absolute accuracy of the calibrations is ±5°K at low sky temperatures and ±2°K at high sky temperatures.

3. Clocks

Since the data from each of the two stations has to be compared, another calibration was required, consisting of synchronizing a 60 Hz clock at each site. This was done with a WWV receiver and over the telephone. The clocks were checked regularly and discrepancies were kept to less than 1 sec.

C. Operation

Regular observations of the 30 GHz satellite signal started at the BRC site on 11 July 1974 and lasted until 20 May 1975 for a total of 314 days. The 20 GHz radiometer at this site was put into operation on 30 October 1974 and continued until 20 May 1975 for a total of 203 days. During the period from 11 July 1974 to 30 October 1974 the station could be made operational in about the time it took to have the satellite transmitter turned on. This fact combined with a relative high priority assured that few attenuation events were missed. The geographical location of Austin (see Figure 2-4) proved to be of significant advantage. Regardless of the pointing of the spacecraft including Alaska we almost always stayed within the 3 dB beamwidth of the 30 GHz horn. Therefore we could utilize the transmitter while other experiments were conducted (as long as no other restrictions on the satellite prevented this). All systems, except the antenna drive were in continuous operation or standby. This allowed monitoring of the system, eliminated warm-up problems and assured instantaneous response to the weather. The antenna was pointed manually for satellite observations with the pointing coordinates supplied to us by ATSOCC and peaked regularly.

The second station, on the Campus of The University of Texas, as in operation from 17 February 1975 to 20 May 1975 for a total of 93 days. This station operated fully automated. The antenna was kept pointed at all times by the antenna controller which also used the ATSOCC supplied pointing data as input. The PLL receiver continuously searched over a range of ±12 kHz around the 30 GHz carrier and locked on to the signal if present. The outputs from the radiometer and the receiver were sampled every 10 min. in clear weather and every 20 sec if the sky temperature exceeded 80°K. The data, with the time and rain gauge information were then punched out on paper tape.

III. METEOROLOGY OF AUSTIN

A. Thunderstorm Climatology for Central Texas

High attenuation events were always associated with thunderstorms in the Austin area. The storm climatology is given to help in the interpretation of the attenuation data.

Information on thunderstorms in Central Texas is given in Table 2-1. The frequency of occurrence refers to the mean over a thirty year observational period and was obtained from Local Climatological Data for Austin, Texas.

The other information was obtained from Mr. William Hare, Meteorologist in Charge at the National Weather Service Meteorological Observatory, Radar Center, Hondo, Texas. Data obtained from the radar at Hondo (which includes Austin in the scope area) for the two years this site has been in operation were used. These data should be fairly representative of the Austin area. Cloud (thunderstorm) tops are given in 1000's of feet above mean-sea-level, the translational speed of the individual rain cells is given in knots, and the direction of movement of the rain cells is given as the direction from true north from which the cell is moving. It should be pointed out that when the showers are arranged in a line (a small line) as they frequently are in the spring (March through May) the line usually moves from 300° to 310° (i.e. from the northwest). The individual shower cells within the line, however, move in the direction as indicated in the Table.

Thunderstorm frequency is bimodal, as shown in the Table.

Table 2-1
Thunderstorm Statistics for Central Texas

Month	Frequency of Occurrence	Height of Cloud Tops (1000's of feet)	Cell Speed (Knots)	Direction of Movement (degrees)
Jan	1	28	25	240
Feb	2	30	30	250
Mar	3	38	35	270
Apr	5	40	30	250
May	7	42	25	240
Jun	4	35	20	180
July	4	32	15	170
Aug	5	32	15	150
Sept	4	40	25	230
Oct	3	38	25	230
Nov	2	30	25	240
Dec	1	28	25	240

Thunderstorm frequency is bimodal, as shown in the Table. May and August have the highest observed mean frequencies (though the standard deviation is very large throughout the year). Maximum cloud tops occur almost concurrently with maximum frequency. Translational speed of individual cells is at a maximum in early spring (March) when mean wind speeds within the troposphere at this location are at a maximum. Minimum speeds are observed in late summer. The direction of movement of individual cells has a strong southwesterly to

westerly component most of the year, except in the summertime when cells move from the south (June) to southeast (August).

B. Meteorology for 11 July 1974 - 20 May 1975

The 40 year mean rainfall for 11 July - 20 May is 31.04 inches (78.8 cm) with a standard deviation of 8.76 inches (22.25 cm). The amount measured for 11 July 74 - 20 May 1975 was 34.5 inches (87.63 cm). During this 314 day period there were 54 days with more than 1 inch (2.54 cm) total precipitation. Significant attenuation events, defined by the 30 GHz attenuation exceeding 3 dB and/or the 20 GHz sky temperature exceeding 80°K were measured on 50 days.

A total of 37 thunderstorms occurred. The direction from which the rain cells were moving and their speed are given in Figure 2-6. The mean direction was 233° and the mean speed was 20.4 knots (37.7 km/hr). The tops of the clouds extended from 3 Km to 15.2 Km feet. Their relation to the measured attenuations will be given later.

Another quantity obtainable from the Weather Bureau is the grid value. It is a numerical indication, manually derived from a weather radar, of the rain intensity and percent coverage of the grid. The grid including Austin is a square with 80.47 km sides. The grid values are the integers 0 through 9. Their interpretation is given in Table 2-2. The last column in the table gives the percentage of time (based on the hourly reporting intervals by the Weather Bureau) each value was assigned to the Austin area.

IV. RESULTS

A. Single Site

The 20 GHz sky noise temperature and the 30 GHz attenuation of the satellite signals are shown in Figure 2-7 as they were recorded on paper charts during one typical rain storm. One notes that a general agreement between crests and valleys exists. The sky temperature curve seems to be relatively smoother, however. This can be explained with the following argument. The 20 GHz beam is wider for the same size antenna (compared to 30 GHz) and the noise power is received from the whole volume of the beam whereas the 30 GHz attenuation is caused by precipitation close to the line-of-sight. Other variations can be expected because of changes in the drop size distribution or by frozen particles in the path.

Table 2-2

Grid Value Code No.	Maximum Observed VIP Level	Coverage in Box	Rainfall Rate mm/hr	Intensity Category	Austin Grid % Time
0	No echoes				
1	1	Any VIP1	<2.5	Weak	
2	2	≤1/2 of VIP2		Moderate	3.7
3	2	>1/2 of VIP2	2.5 - 12.7		
4	3	≤1/2 of VIP3	12.7 - 25.4	Strong	1.1
5	3	>1/2 of VIP3			
6	4	≤1/2 of VIP3 and 4	25.4 - 50.8	Very Strong	.73
7	4	>1/2 of VIP3 and 4			
8	5 or 6	≤1/2 of VIP3 4, 5 and 6	>50.8	Intense or Extreme	.35
9	5 or 6	>1/2 of VIP3 4, 5 and 6	>50.8	Intense or Extreme	

(Ignore additional coverage by weak echoes for all DR code numbers above 1. Intensity categories and rainfall rates correspond to maximum observed VIP levels.)

Priority for additive data group giving row-colomn position of blocks with present or past severe weather or lines is: 1) +, 2), 3) /. No box shown more than once, group in left-to-right, top-to-bottom order.

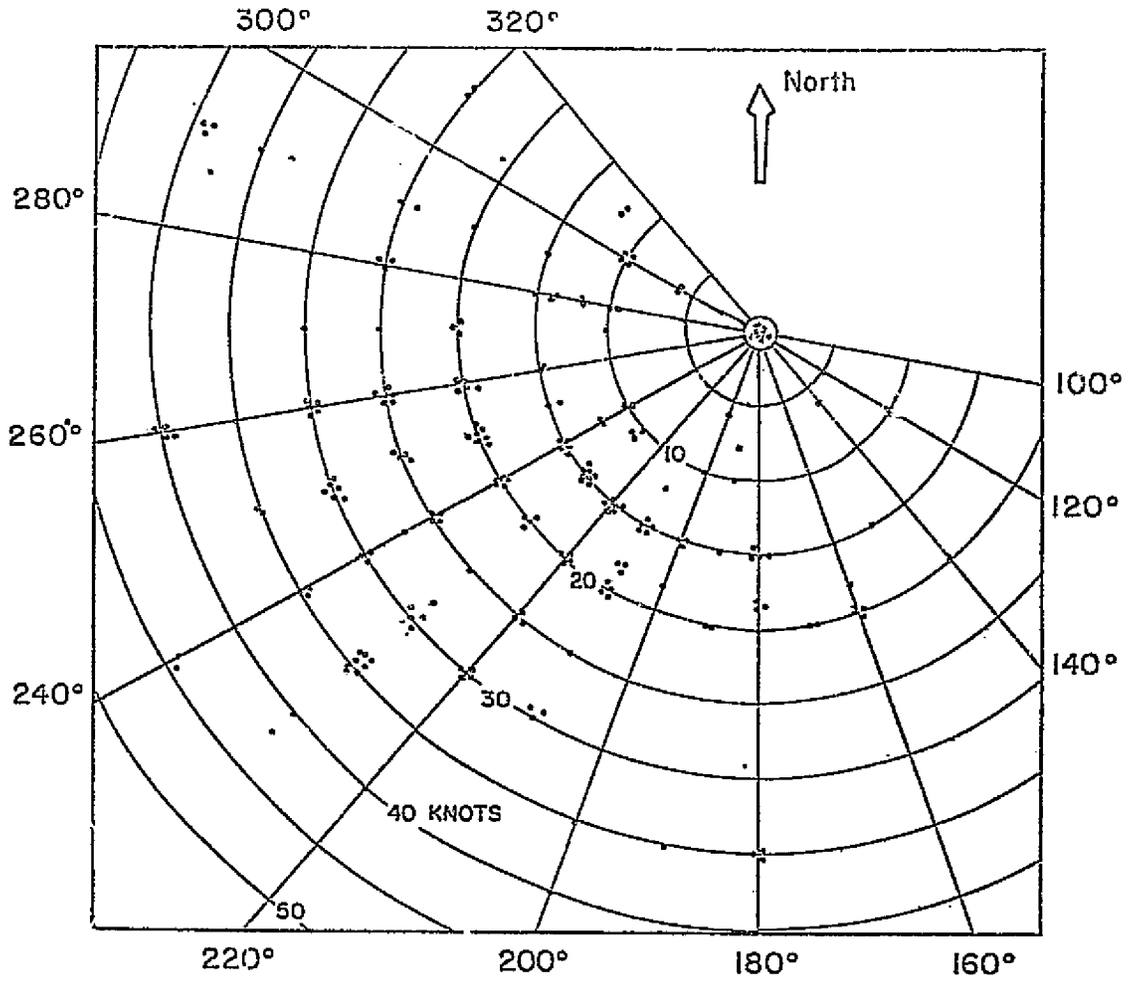

Figure 2-6. Direction from which storm cells moved and their speed (1 July 74 – 20 May 75)

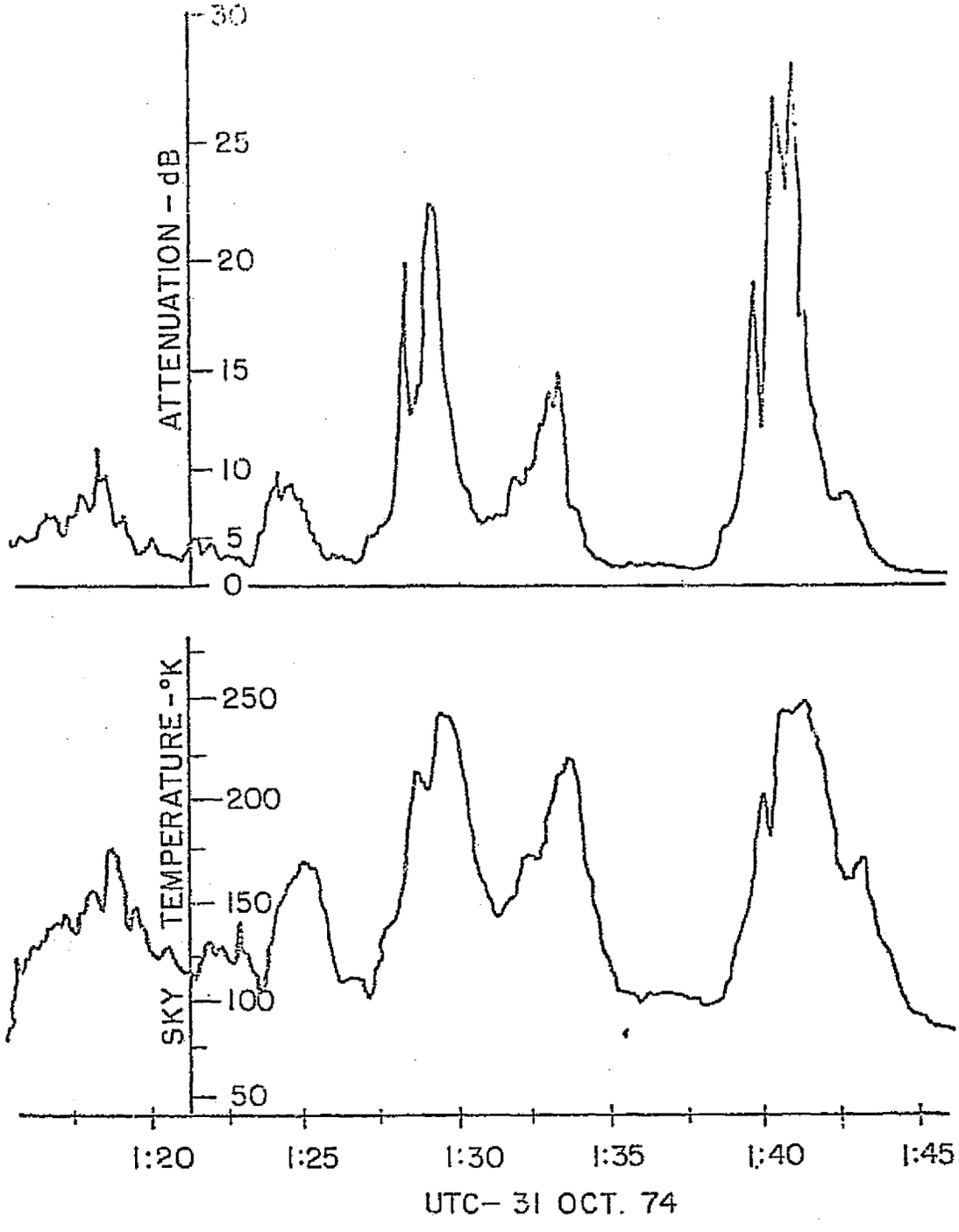

30 GHz ATTENUATION AND 20GHz SKY TEMPERATURE
UTBALC - ATS-6

Figure 2-7. 30 GHz attenuation and 20 GHz sky temperature UTBALC-ATS-6

Assuming the rain to be an absorbing, non-scattering medium with a physical temperature of 284°K, the measured noise temperature T_{sky} can be converted to attenuation A with

$$A = 10 \log \left[\frac{284}{284 - T_{sky}} \right] \text{ dB.} \qquad (3)$$

This formula can be derived from the theory of radiative transfer (e.g. Kraus, 1966). It can be used with reasonable accuracy for attenuations of up to about 10 dB. Figure 2-8 shows the measured 30 GHz attenuation plotted versus the calculated 20 GHz attenuation for the BRC site. Each point represents a sample taken at one minute intervals for most of the periods for which such simultaneous data were available. In the average the ratio between the two attenuations is 2.65. The straight line drawn through the points does not intercept at (0, 0) because the 30 GHz values do not include the attenuation caused by oxygen and water vapor. The 20 GHz attenuations include these losses because they contribute to the sky noise temperature. Therefore to find the attenuation ratio due to precipitation the abscissa zero should be shifted to the intercept. Figure 2-9 shows the same kind of plot for data collected on 28 April 75 at the Campus site with essentially the same slope. The spread of the points in Figure 2-8 is larger than in Figure 2-9 because the values were taken from strip chart recordings at the BRC site as compared to digital recordings at the Campus site. The relationship between the 20 GHz and the 30 GHz values is well enough defindd to allow an estimation of the 30 GHz attenuation from 20 GHz sky temperature data.

The fade histogram for the 30 GHz attenuation at the BRC site from 11 July 1974 to 20 May 1975 is given in Figure 2-10. The dark areas derive from direct measurements and the light ones are based on the 20 GHz sky temperature for times when the satellite was not available.

The 5 dB level, for instance, was exceeded for a total of 18.17 hours while the satellite was on and 11.45 hours while it was off. Table 2-3 summarizes these results.

The satellite was available for an average of 61.4% of the measured attenuation events. As stated earlier the availability was much higher before November 1974 than afterwards.

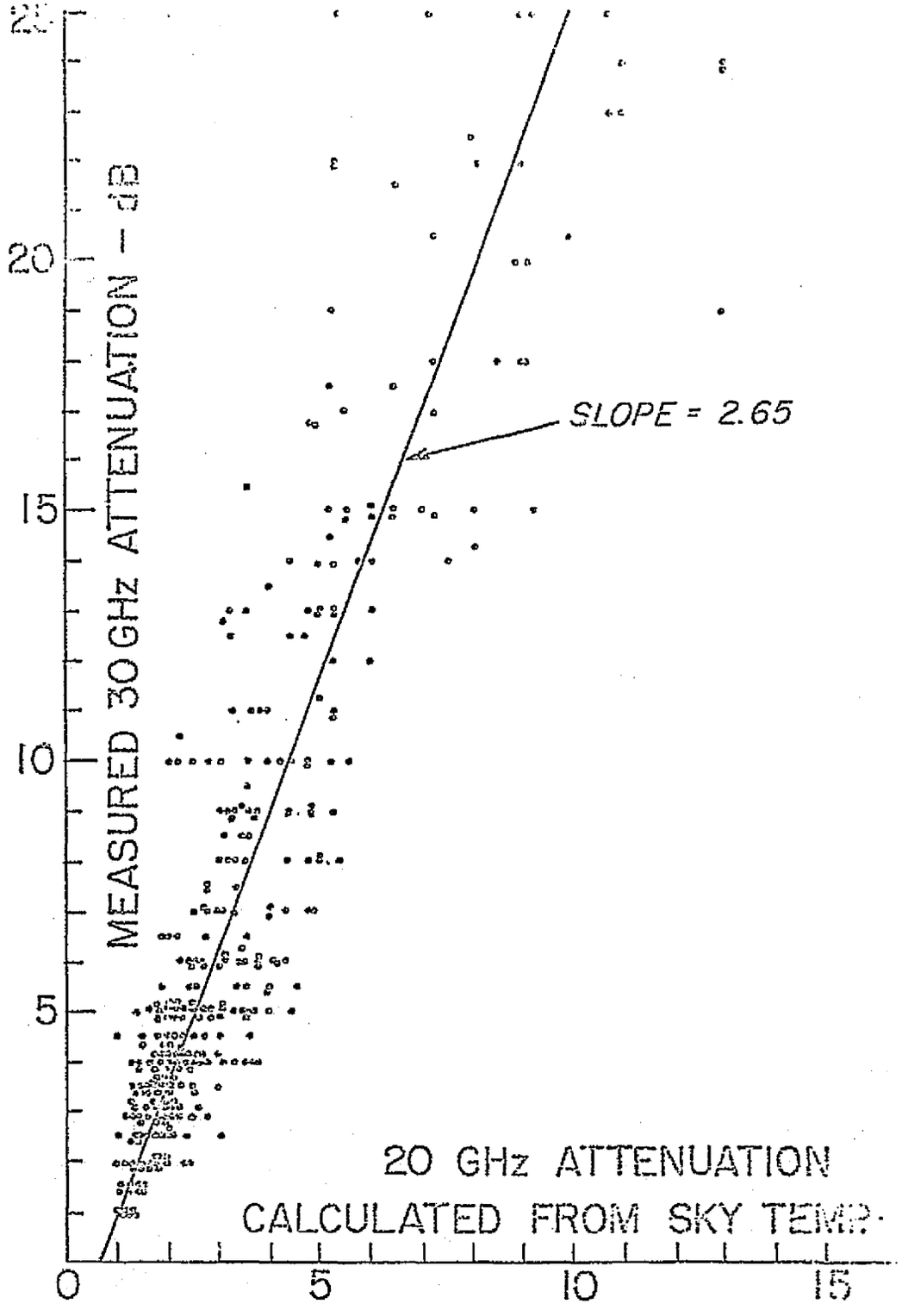

Figure 2-8. 20 GHz versus 30 GHz attenuation

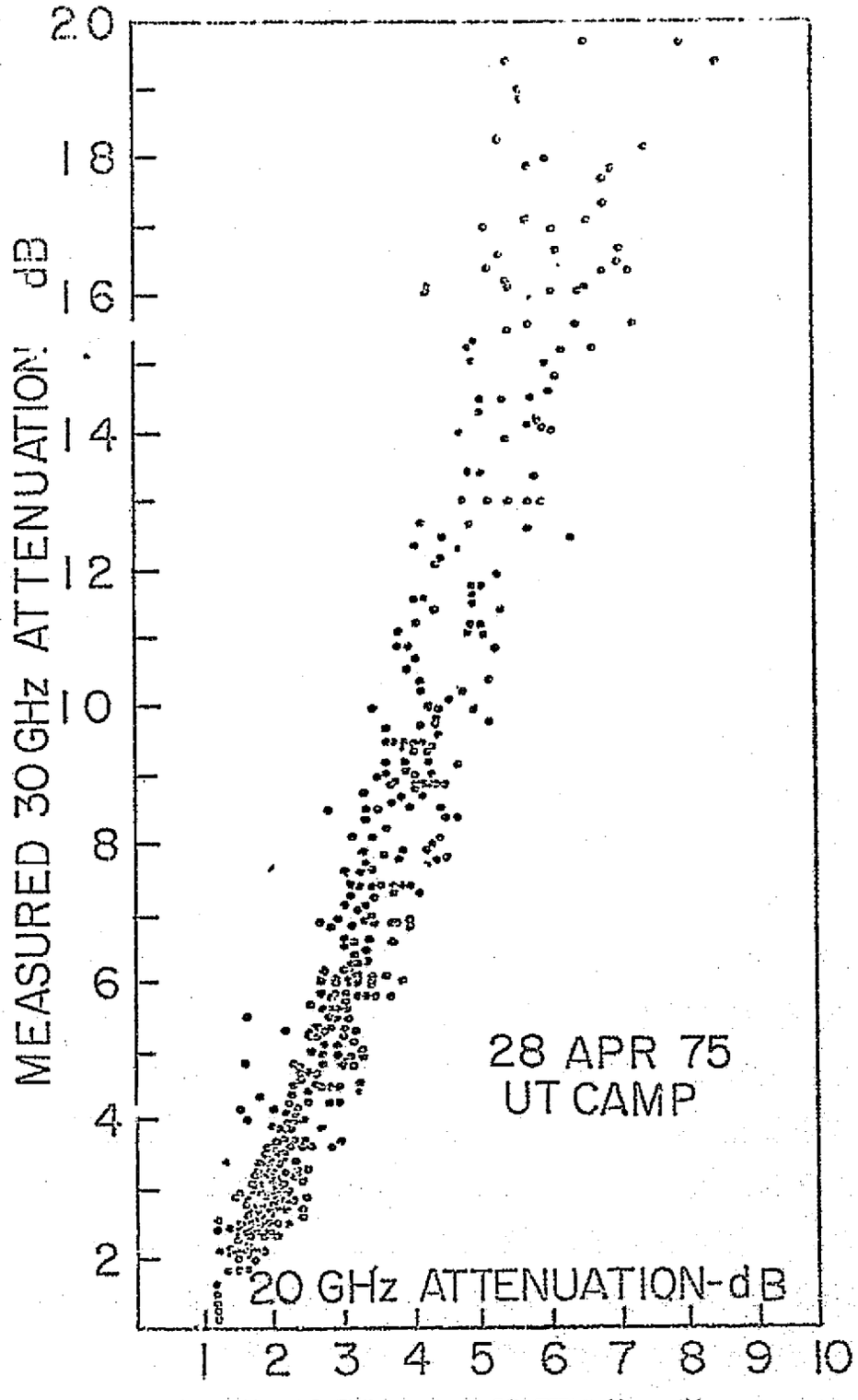

Figure 2-9. 20 GHz versus 30 GHz attenuation

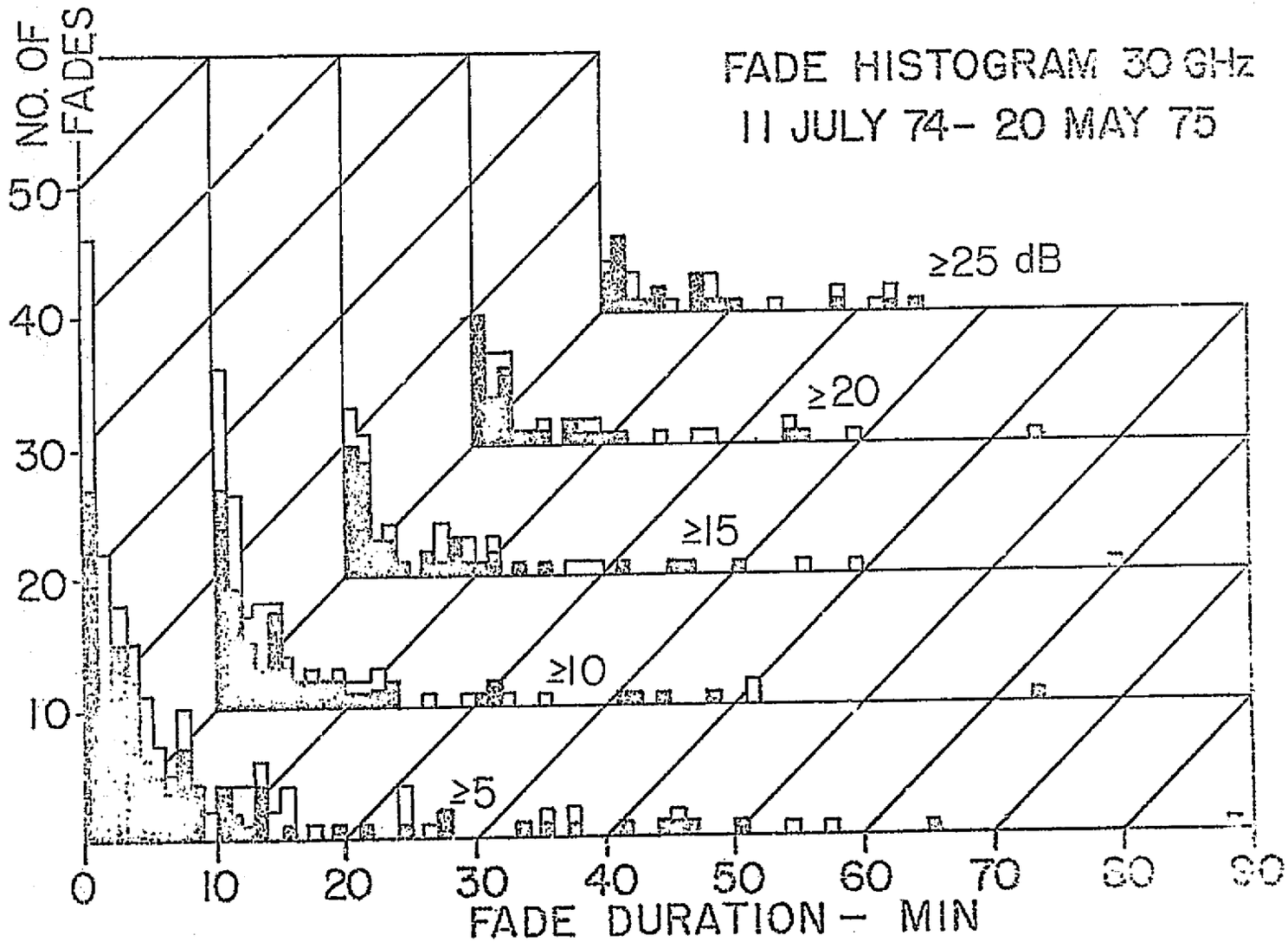

Figure 2-10. Fade histogram

Table 2-3

Attenuation exceeded at 30 GHz:	Time (hrs) Satellite		Total (hrs)
	On	Off	
5 dB	18.17	11.45	29.62
10	8.45	4.33	12.76
15	5.73	3.33	9.07
20	3.37	2.35	5.72
25	2.55	1.82	4.37

The cumulative probability in percent of time the 30 GHz attenuation exceeds a certain fade depth is given in Fig. 2-11 for fades between 5 and 25 dB. It can be seen that in Austin, Texas 10 dB attenuation is exceeded at 30 GHz for .17% and 25 dB for .058% of the time. This corresponds to about 15 and 5 hours respectively, on an annual basis.

A comparison of rain rates (measured with one tipping bucket at the antenna) with the attenuation at 30 GHz as given in Fig. 2-12 shows that it is not possible to predict the fade depth from point rain data. The effective path lengths L that have been added to the plot are based on the theoretical relationship between rain rate and attenuation for homogeneous rain. They vary over an order of magnitude for a given rate. A statistical comparison of these data has been made also. For this purpose the attenuations A and rain rates R for equal cumulative probabilities were compared. The effective cloud heights were then derived with

$$H_{eff} = \frac{A}{A_{theoretical}(R)} \times \sin(\text{angle of elevation}) \qquad (4)$$

The results are given in Table 2-4. From these data one would conclude that the highest attenuation occurs when the clouds are lowest. This is probably due to the higher probability of rain occurring at the gauge when clouds are low. The data, in Table 2-4, are in contradiction to the results from the ATS-5 experiment, where a direct correlation of attenuation with cloud heights was found (Straiton, 1971). It also does not agree with the cloud height data obtained from the Weather Bureau for this experiment. Figure 2-13 is derived from the hourly location reports. It gives the maximum cloud height within the radar range of the weather station (250 × 250 miles) including the Austin area versus the maximum attenuation at 30 GHz that was measured. This figure establishes a minimum cloud top

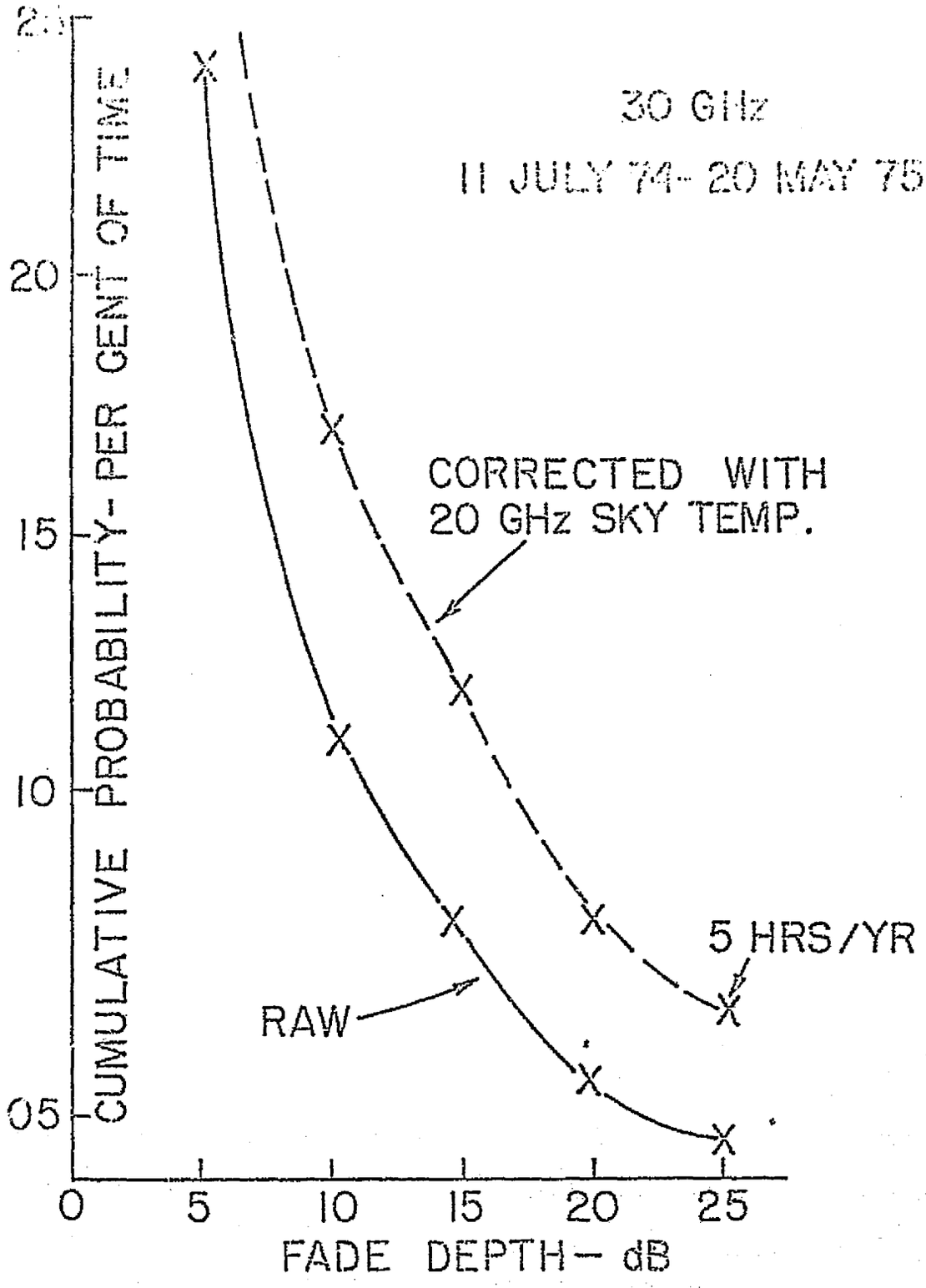

Figure 2-11. Cumulative fade probabilities at 30 GHz

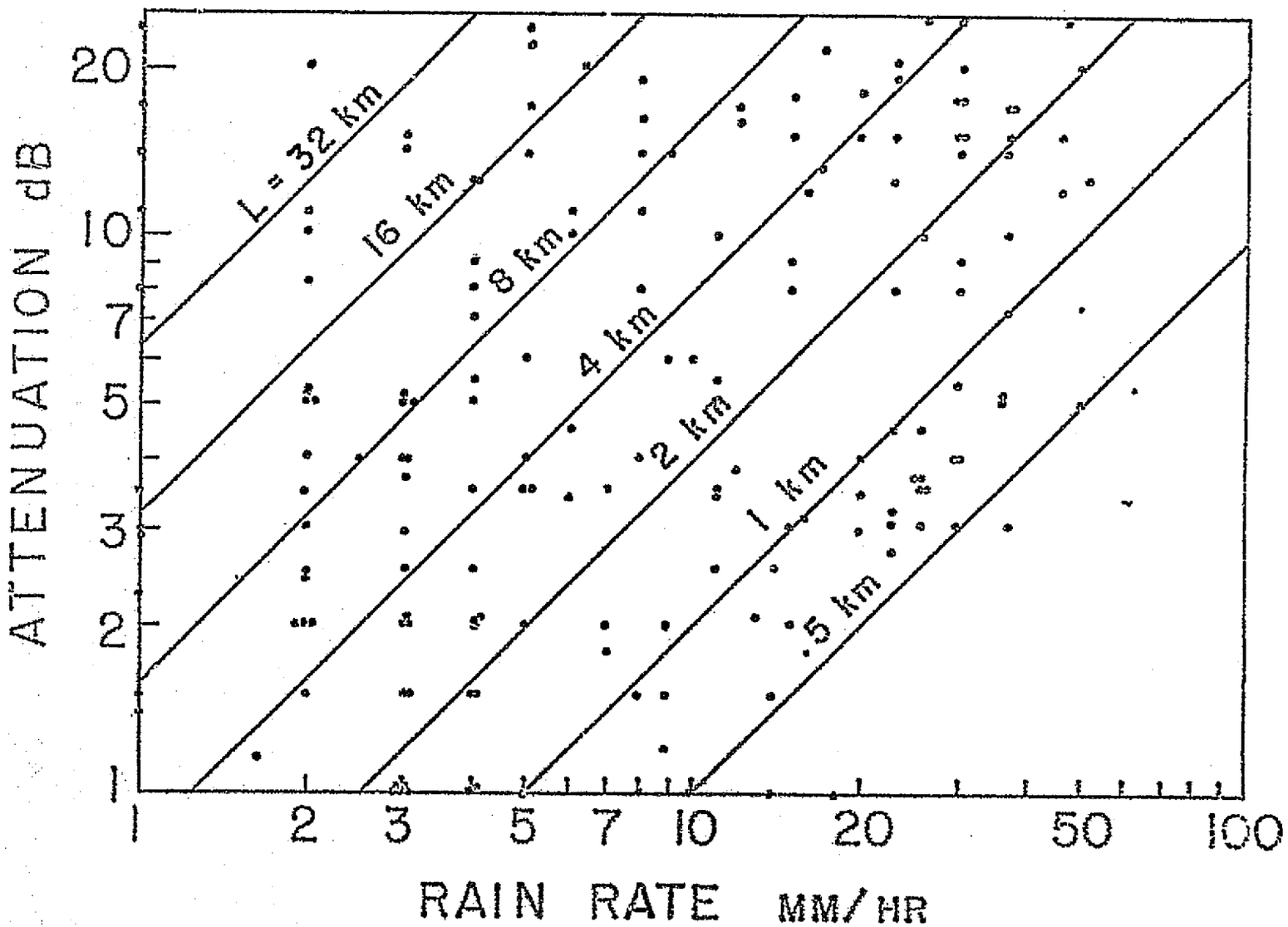

Figure 2-12. Attenuation versus point rain rate

Table 2-4
Probabilistic Effective Cloud Heights

Attenuation dB	Rain Rate mm/hr	A Theor. dB/km	Effective Cloud Top Height Feet
Exceeded for Equal Percentage			
5	3.4	.6	22,100
10	7	1.3	20,400
15	9.6	1.75	22,700
20	17.5	3.2	16,600
25	24	4.4	15,100

height increasing roughly linearly with increasing attenuation. The scatter of points above this line relates to the fact that higher clouds were present at other locations and did not cause attenuation at the receiver site. The relation between attenuation and cloud height suggested by Fig. 2-13 is roughly

$$A = 1.62 \cdot H \cdot \operatorname{cosec}(\epsilon)\ \text{dB} \qquad (5)$$

where H is the cloud height in km and ϵ is the angle of elevation.

Figure 2-14 shows a plot of the attenuation versus the associated values assigned by the Weather Bureau radar at Hondo for the Austin grid. Because of the areal extent of the grid, a correlation of attenuation versus grid value is not apparent.

B. Space Diversity Results

The measured cumulative probabilities of the fade depth for the single sites and the joint probability for the pair of satellite receivers operating at 30 GHz have been plotted in Fig. 2-15. In these plots use has been made of the 20 GHz sky temperatures to augment the fade data for times of satellite unavailability. For the single sites the 93 day Campus statistics and the 314 day BRC statistics agree very closely. The 93 day BRC probabilities deviate for the higher fades. This type of behavior can be expected, considering the relatively short period of sampling. In this plot 100% of the time represents the total 93 days of common operation. If one were to multiply the single site probabilities to get the joint probability of fades with zero correlation the measured joint probability is far above the calculated value indicating some correlation of attenuation at the two sites existed. Naturally during the extended periods of clear weather both

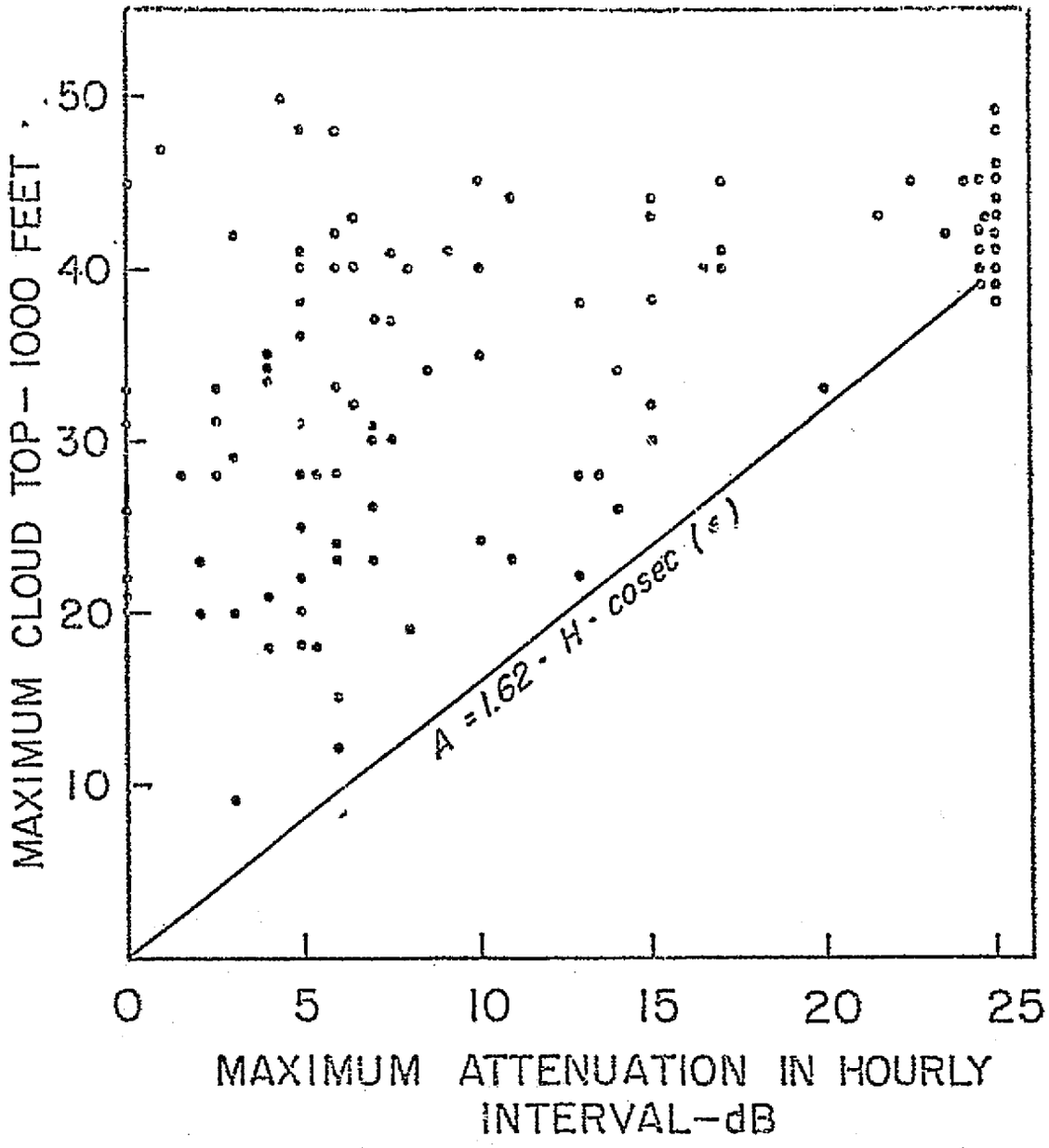

Figure 2-13. Cloud top height versus attenuation at 30 GHz

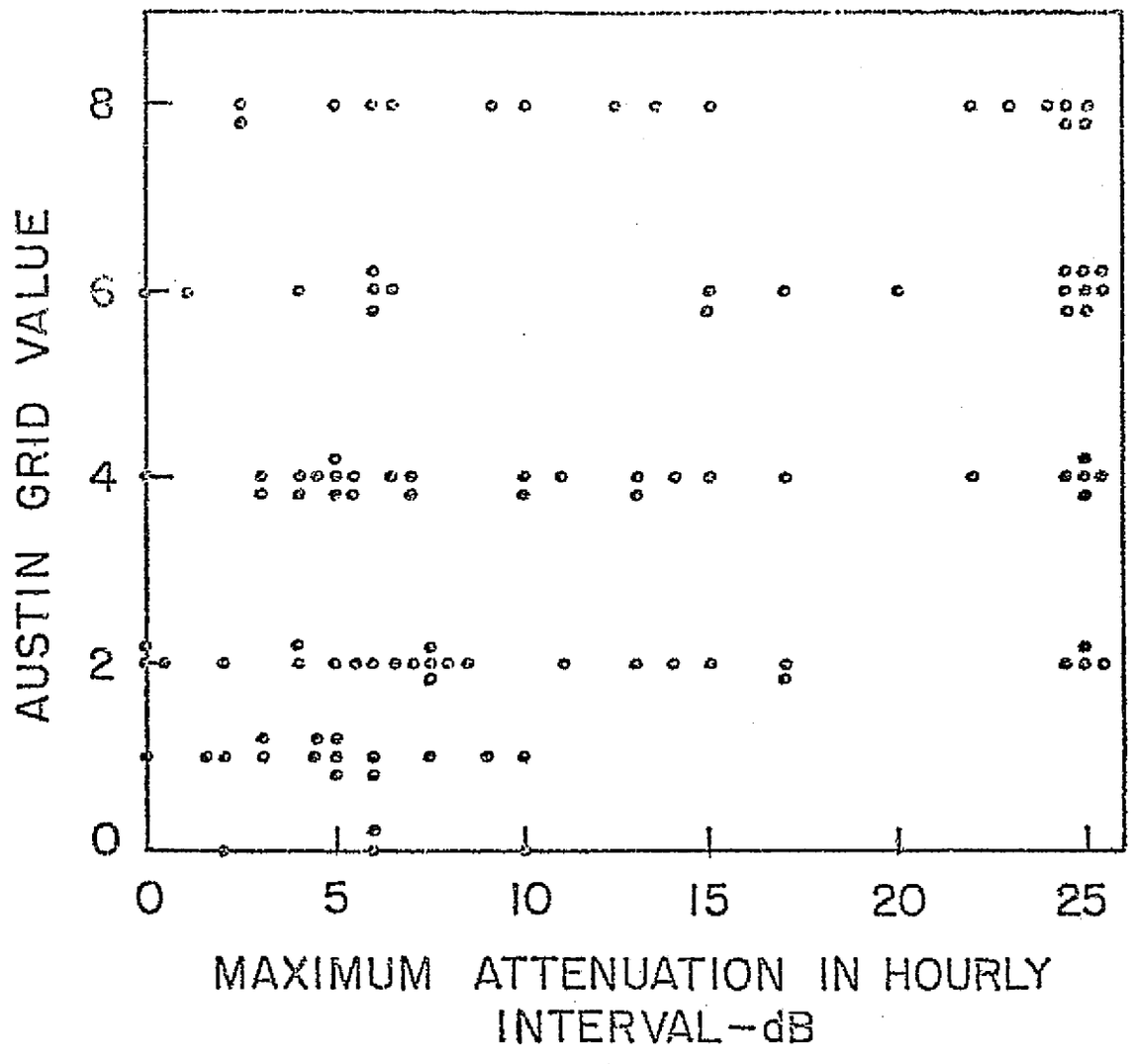

Figure 2-14. Grid value versus attenuation at 30 GHz

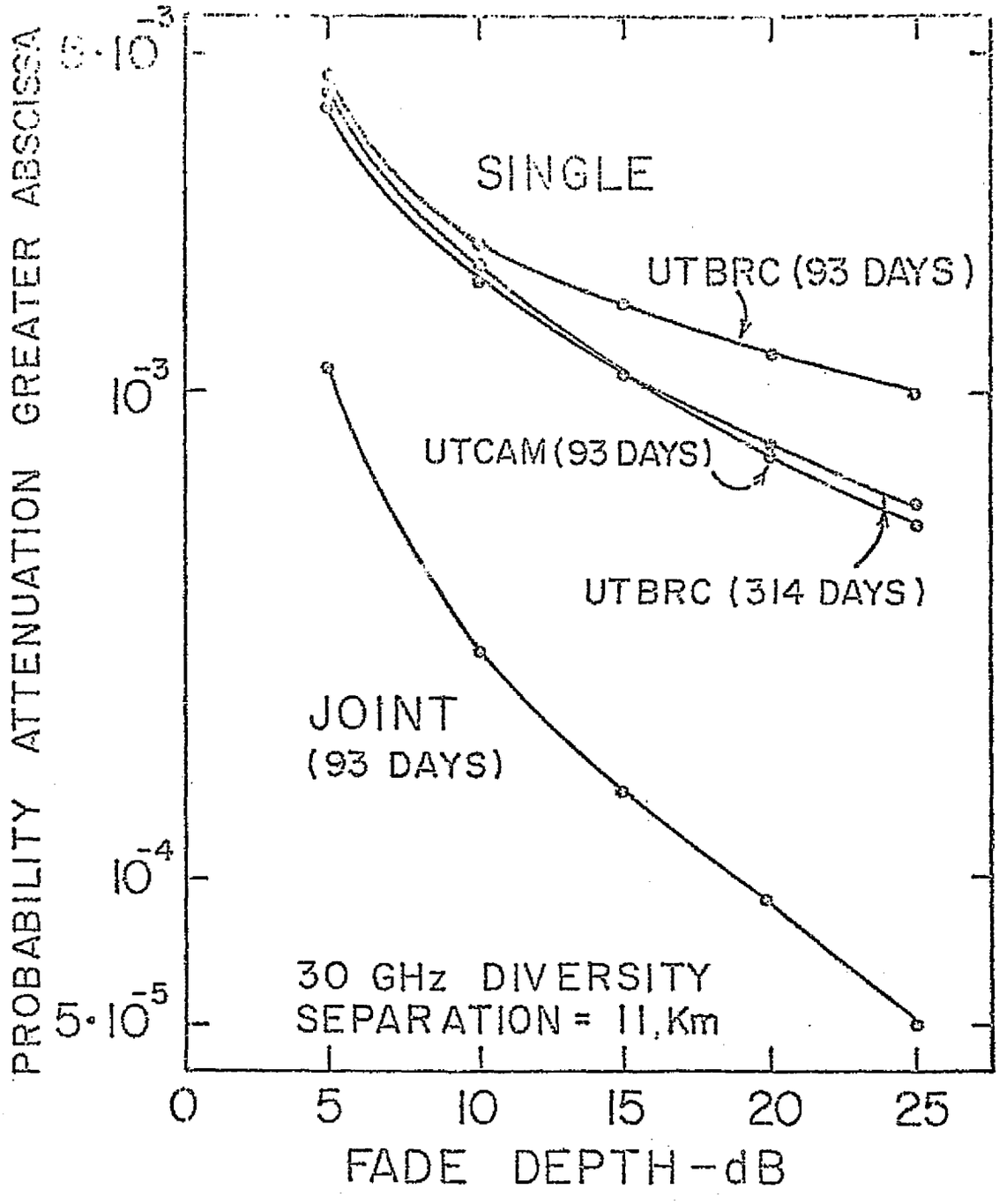

Figure 2-15. Diversity results

stations are correlated. Therefore the curves have been redrawn in Fig. 2-16 as conditional probabilities. The 100% time base is now the time during which the attenuation exceeded 2 dB at either station, thereby eliminating the correlated clear weather data. It can be seen that the joint probability now approaches the squared single site probability much closer. Naturally the result would differ if one conditioned the probabilities on another fade level. The diversity gain has been defined by Hodge (1974) as the reduction in fade depth for equal probabilities. This gain has been plotted in Fig. 2-17 versus the single station attenuation. The points lie on a straight line defined by

$$\text{diversity gain} = (.7)\,\text{attenuation}. \tag{6}$$

Another way of looking at the data is todetermine the diversity advantage which is the factor by which the probability that simultaneous fades exceed a certain levelis decreased. In our case this value varies between 3 and 11 for attenuations between 5 and 25 dB. The curve is given in Fig. 2-18.

V. CONCLUSIONS

Satellite propagation experiments that require unscheduled transmission in response to the weather while all other experiments sharing the spacecraft can be scheduled ahead are at an obvious disadvantage when it comes to full coverage of all fade events. Despite this nearly complete coverage was achieved here for the following reasons: (1) The geographical location of the stations and the type of measurements made allowed reception largely independent of the spacecraft pointing and (2) the simultaneous operation of 20 GHz radiometers served both as an effective way of judging if the conditions required a request of the satellite transmitter and, if the request was denied, the sky temperature data could be used to derive the 30 GHz attenuation.

If commercially operating satellite communication links are restricted to a 10 dB fade margin (for economic reasons for instance) then our measurements show that one station in Austin would achieve 99.83% reliability and a diversity pair with 11 km separation would achieve 99.99% reliability, as far as weather influences are concerned. To achieve the same reliability with only one station the fade margin would have to be increased by over 20 dB, which may be unfeasible.

Of all the weather data obtained from the U. S. Weather Bureau the maximum cloud tops show the best correlation to the attenuation data. It should be worthwhile to make such measurements directly at the site of a propagation experiment to exclude the points in Fig. 2-13 not relating directly to the experiment site. A linear relation between attenuation and cloud height is suggested by the

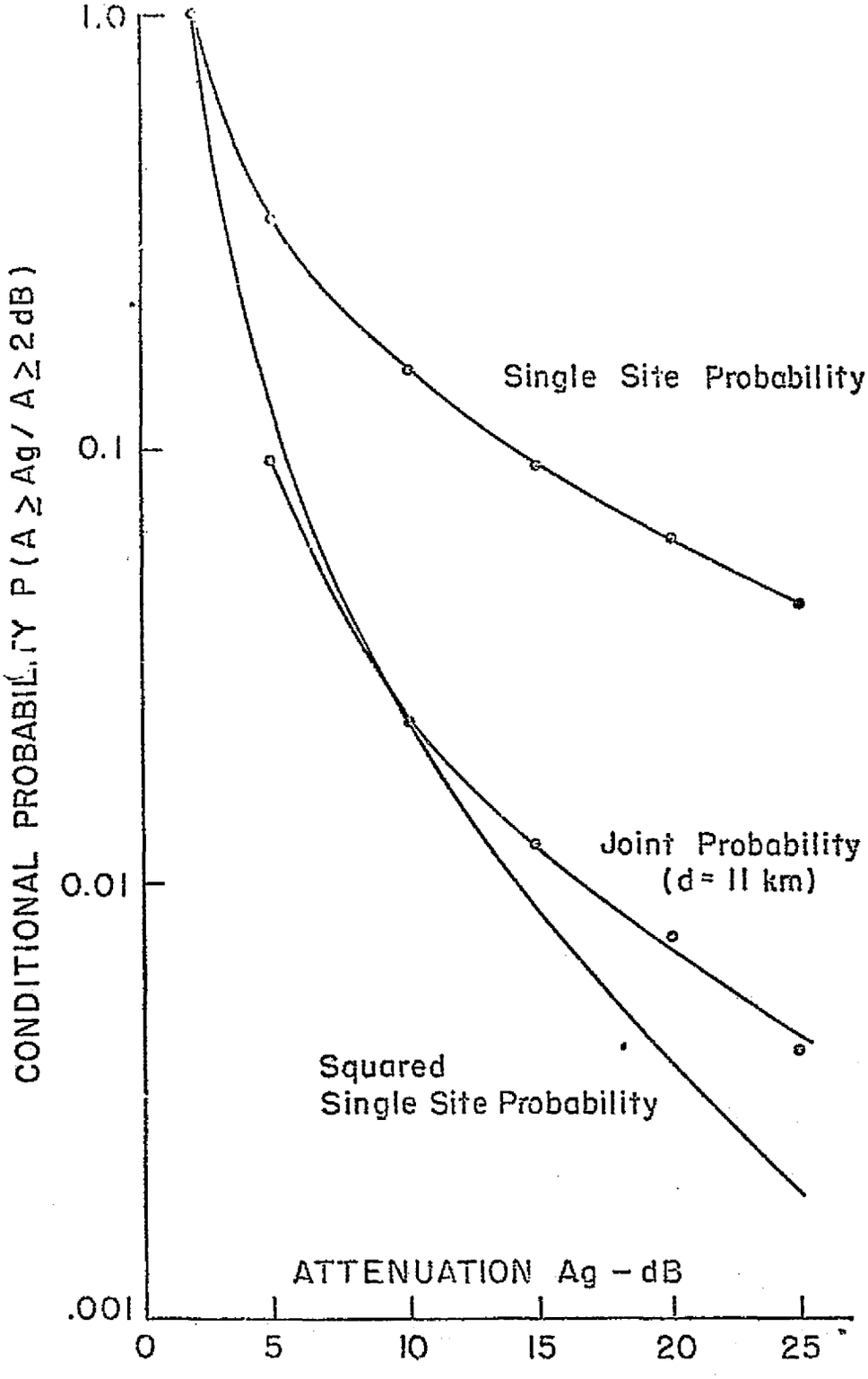

Figure 2-16. Conditional space diversity for A ≥ 2 dB

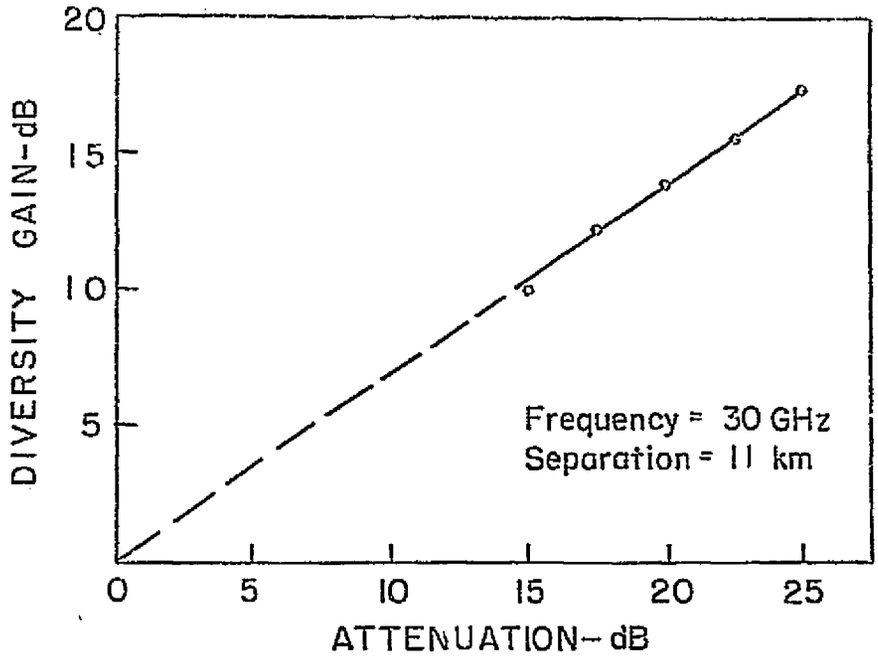

Figure 2-17. Diversity gain as a function of single site attenuation

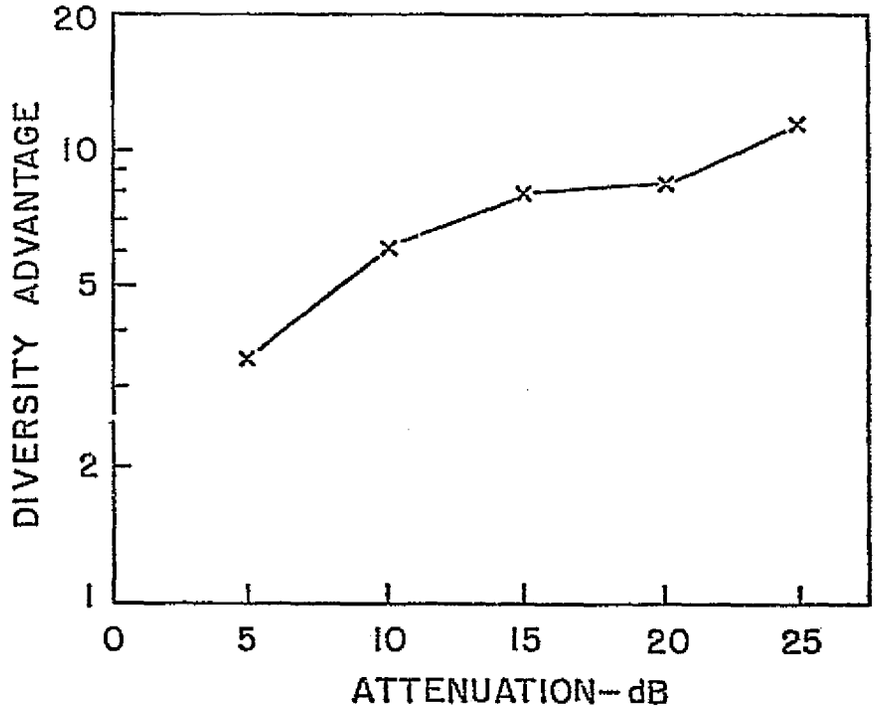

Figure 2-18. The diversity advantage of 2 receiver sites at 30 GHz

data. Other weather parameters, such as rain rate or grid value show very little promise of allowing an estimate of attenuations. Many of the Weather Bureau data are qualitative rather than quantitative and are not well suited for analysis.

REFERENCES

Kraus, J. D., Radio Astronomy, McGraw-Hill Book, Co., N.Y., 1966.

Martin Marietta Corporation, Prepared by "15.3 GHz Ground Receiver Systems for the ATS Millimeter Wave Propagation Experiment," Final Technical Report, Report No. OR 10265, Sept. 1969.

Straiton, A. W., "The Absorption and Reradiation of Radio Waves by Oxygen and Water in the Atmosphere," IEEE Trans. Antennas Propagat., Vol. AP-23, July 1975.

Vogel, W. J., B. M. Fannin, and A. W. Straiton, "Polarization Effects for Millimeter Wave Propagation in Rain," Tech. Rept. No. 73-1, Electrical Engineering Research Laboratory, The University of Texas, Austin, Texas, Dec. 1973.

Straiton, A. W., et al., "ATS-5 Signal Characteristics at 15.3 GHz and Related Experiments at 15 and 35 GHz," Part I, Final Technical Report ATS-% Millimeter Wave Experiments, Electrical Engineering Research Laboratory, The University of Texas, Austin, Texas, 1971.

Hodge, D. B., "Space Diversity for Reception of Satellite Signals," Dept. Elec. Eng., Ohio State University, Columbus, Ohio, Tech. Rept. 2374-16, Oct. 1974.

INITIAL RESULTS OF OSU 20 AND 30 GHZ ATS-6 PROPAGATION MEASUREMENTS

D. B. Hodge, D. M. Theobold, and R. C. Taylor
The Ohio State University
Columbus, Ohio

INTRODUCTION

This program is motivated by the increasing demand for utilization of the frequency spectrum above 10 GHz. The kinds of usage under current development range from remote sensing to communications. Nevertheless, the reliable usage of these frequencies, whatever the application, is extremely dependent upon a thorough knowledge of the interactions between propagating millimeter waves and precipitation. In particular, the severest atmospheric attenuation rates are encountered by increased radiometric noise emission and scattering. In the case of satellite applications, these effects can occur on slant paths from the earth's surface upward to heights on the order of 10 to 20 km and, thus, cannot be measured on terrestrial propagation paths.

The objective of this experiment is to determine the reliability improvement resulting from the use of path diversity on millimeter wavelength, earth-satellite communication links. This will be accomplished by measuring the path attenuation observed on 20 and 30 GHz ATS-6 downlinks at two spatially separated ground terminals. Radiometric noise emission at 20 and 30 GHz along these same propagation paths will also be recorded for correlation with the attenuation date. A third remote terminal will record 20 GHz radiometric noise emission along a propagation path directed toward the position of the ATS-6 satellite to provide an additional estimate of path attenuation and diversity performance. Measurements of radar backscatter and radiometric noise emission at 3, 9, and 15 GHz over the regions through which the propagation paths to the remote terminals pass will also be made using the OSU High-Resolution Radar/Radiometer System and the OSU Low-Resolution Radar System. Finally, a cooperative experiment with the Comsat Corp. will provide downlink attenuation on four spatially separated propagation paths at 17.8 GHz and on one path at 13.2 GHz.

LOCATION OF GROUND TERMINALS

The ground terminals are located approximately as shown in Figure 3-1. The three OSU terminals (fixed, transportable, and unmanned) located approximately

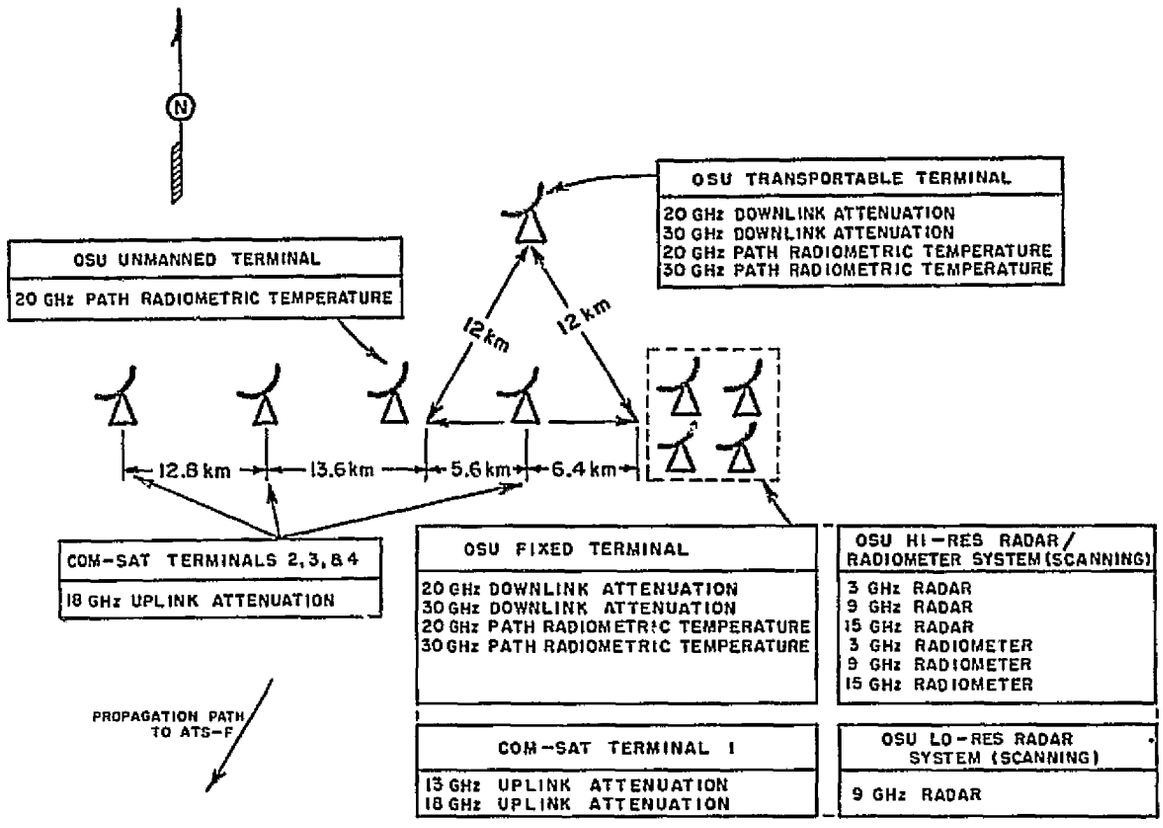

Figure 3-1. ATS-F diversity experiment, ElectroScience Laboratory, Ohio State University, Columbus, Ohio.

at the vertices of an equilateral triangle having 12 Km sides are shown in Figures 3-2, 3-3, and 3-4. This arrangement permits one baseline to be oriented along the east-west baseline chosen by the Comsat Corp., and, consequently, provides correlation with their data. The second baseline is oriented in nearly a northwest-southeast direction, the direction for which optimum diversity improvement is expected. [3-1] This orientation also permits correlation with data resulting from the ATS-5 15.3 GHz millimeter wave experiment. [3-2] The third baseline is almost perpendicular to the optimum orientation for the purpose of comparison. The spacing of 12 Km was chosen since nearly optimum performance is expected for terminal spacings greater than 8-10 Km. 3. Also, since all three baselines are nearly equal direct comparisons of the resulting data is possible.

A summary of the types of observations and frequencies at the various terminals is presented in Figure 3-5.

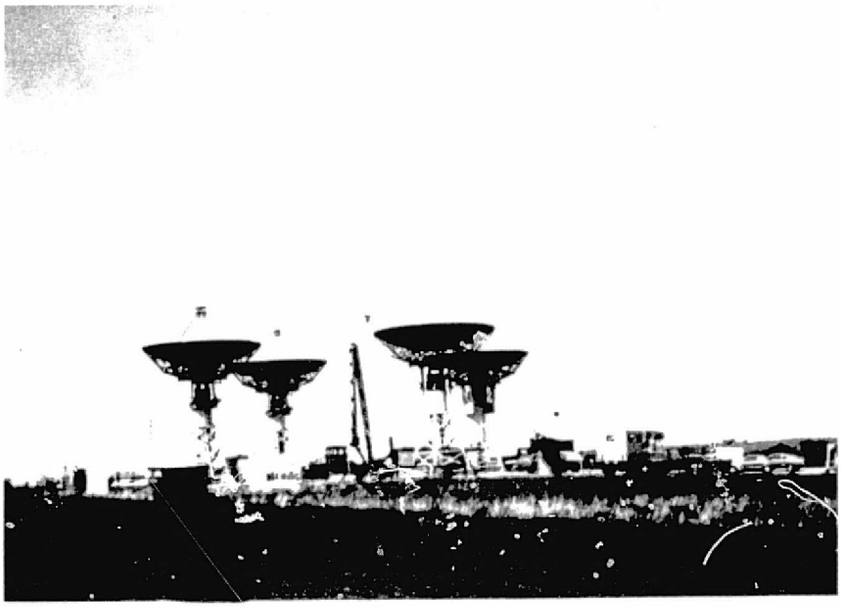

Figure 3-2. OSU Fixed Terminal.

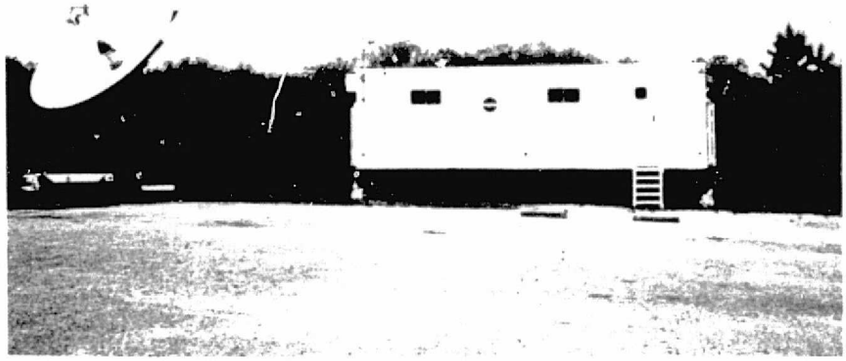

Figure 3-3. OSU Transportable Terminal.

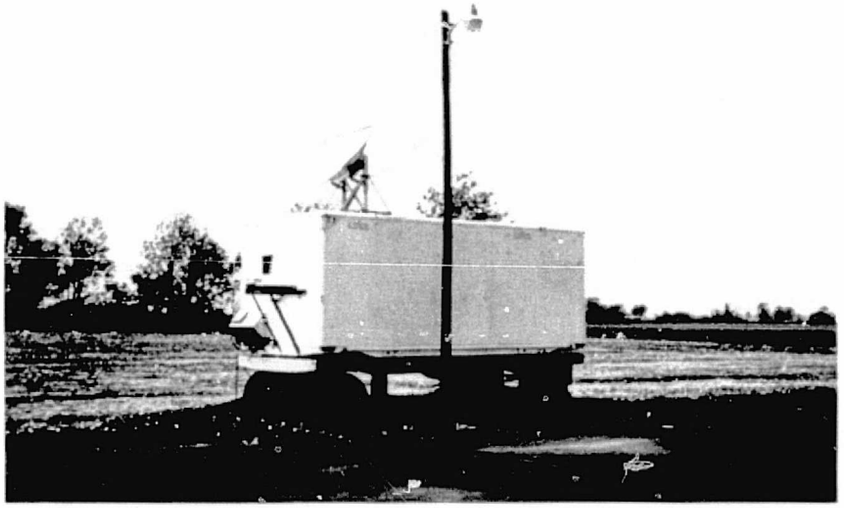

Figure 3-4. OSU Unmanned Terminal.

Freq.	Fixed Terminal	Transportal Terminal	Unmanned Terminal	Outlying COMSAT Terminals
3.1 GHz	ST			
9.3	ST			
13.2	A			
15.6	ST			
17.8	A			A
20	A T	A T	T	
30	A T	A T		

A = Attenuation T = Radiometric Temperature S = Radar Backscatter

Figure 3-5. Frequencies and types of measurements at the various terminals.

TRANSPORTABLE TERMINAL

The OSU Transportable 20/30 GHz Ground Terminal is housed in a 2.3 × 9 meter semi-trailer. The heating and cooling unit for the semi-trailer is contained in a small 2-wheel trailer and the 4.6 m parabolic antenna is mounted on a 2.4 × 5.5 m trailer.

The primary Transportable Terminal instrumentation consists of the 20 and 30 GHz receiver/radiometers. These NASA supplied receiver/radiometers were built by the Martin-Marietta Corp. and are described in detail in Reference 3-4. The outputs of these receivers and radiometers are sampled, digitized, and merged with terminal status bits. The resulting digital data blocks are transmitted via a duplex telephone line to the Fixed Terminal for recording. A simplified block diagram of the transportable Terminal is shown in Figure 3-6.

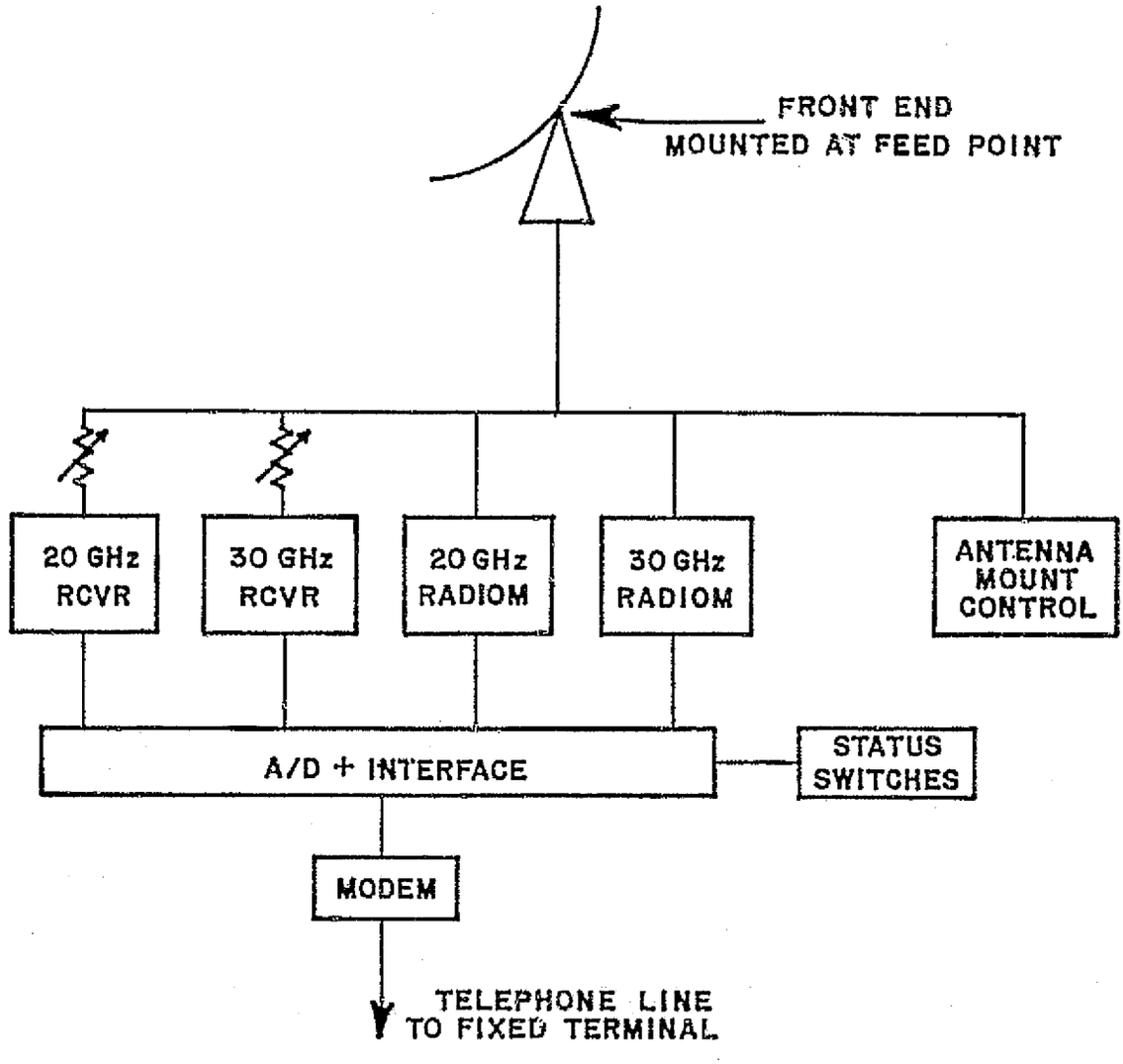

Figure 3-6. Simplified block diagram of OSU Transportable 20/30 GHz Ground Terminal.

The transportable antenna is a 4.6 m, Cassegrainian fed, parabolic antenna. The antenna pedestal consists of an azimuth-over-elevation-over-azimuth mount so that the polarization is fully controllable. All front end hardware is mounted in a cylindrical silo located immediately behind the feed horn. The RMS surface tolerance of the fiberglass parabolic surface is 1.14 mm or 0.076λ at 20 GHz and 0.114λ at 30 GHz.

The feed horn is a square corrugated horn tapered to reduce illumination of the hyperbolic sub-reflector edge and, thus, to reduce side lobe levels. The feed horn design was provided by Professor L. Peters and Dr. C. Mentzer of the OSU ElectroScience Laboratory. The horn aperture is covered by a 0.2 mm teflon window. The measured SWR of the radome, horn, transition, diplexer combination was 1.04 at 30 GHz and 1.38 at 20 GHz. The 20 and 30 GHz measured patterns of the feed horn are shown in Figure 3-7.

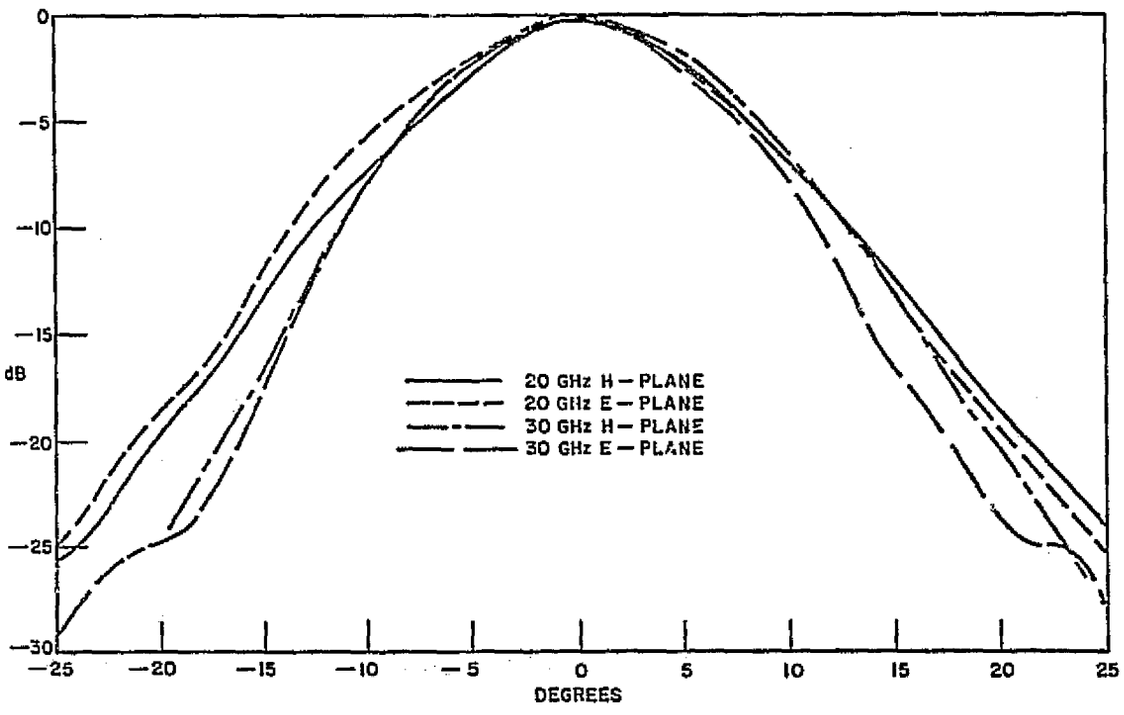

Figure 3-7. Transportable feed horn patterns.

The patterns of the Transportable antenna were measured using the 20 and 30 GHz ATS-6 downlink signals; these patterns are shown in Figures 3-8 and 3-9. These patterns are in the azimuth and elevation planes rather than the E- and H-planes. The broadening of the pattern in the azimuth plane is not fully understood at the present time. The feed horn has been realigned; however, this did not eliminate the problem. The polarization of the satellite signal at Columbus, Ohio, was calculated to be +12.8° clockwise from vertical when looking toward the satellite along the propagation path; this value agrees well with observation. The gain of the Transportable antenna is estimated to be 53.9 dB at 20 GHz and 57.5 dB at 30 GHz.

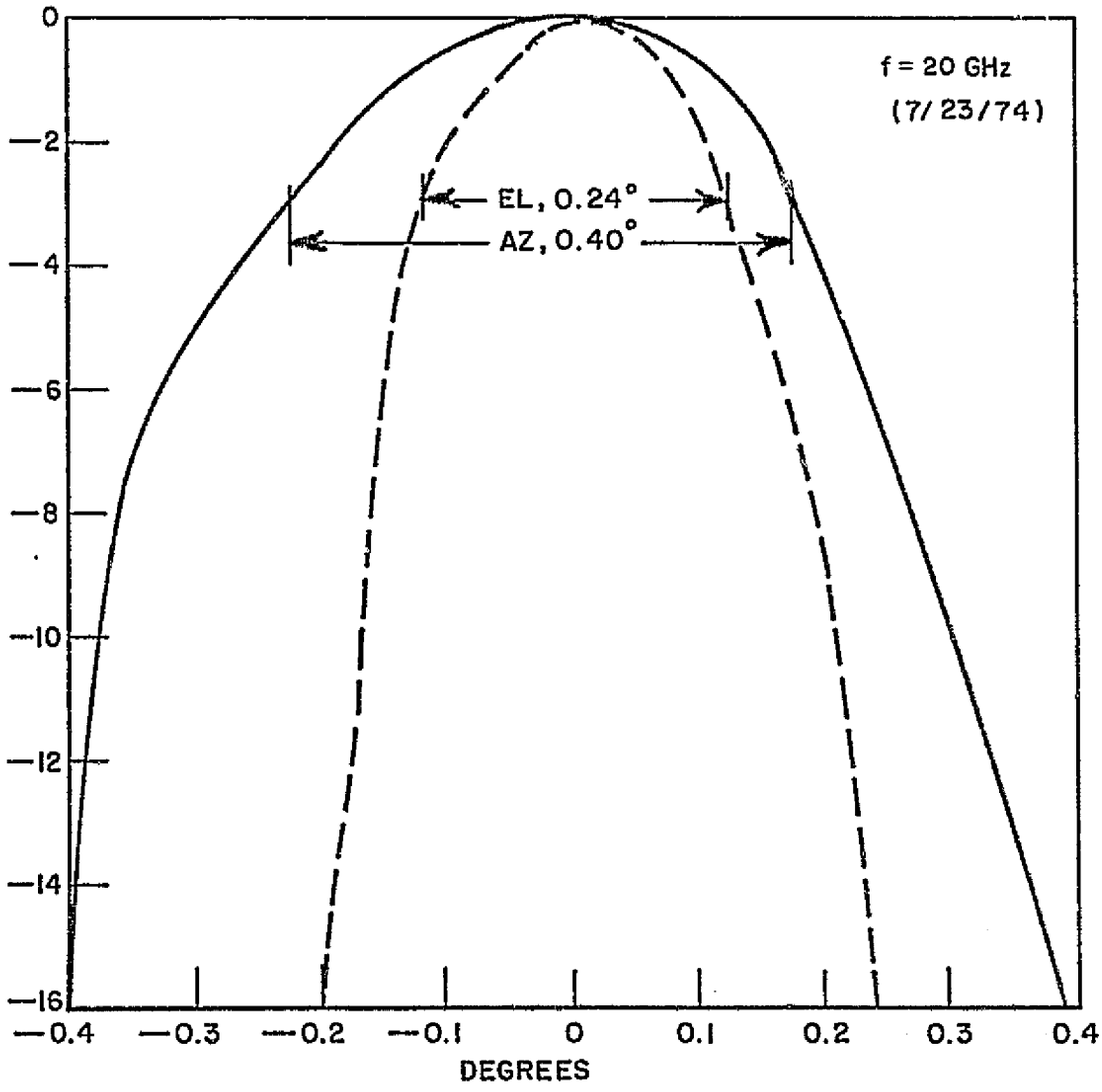

Figure 3-8. Transportable antenna pattern – 20 GHz.

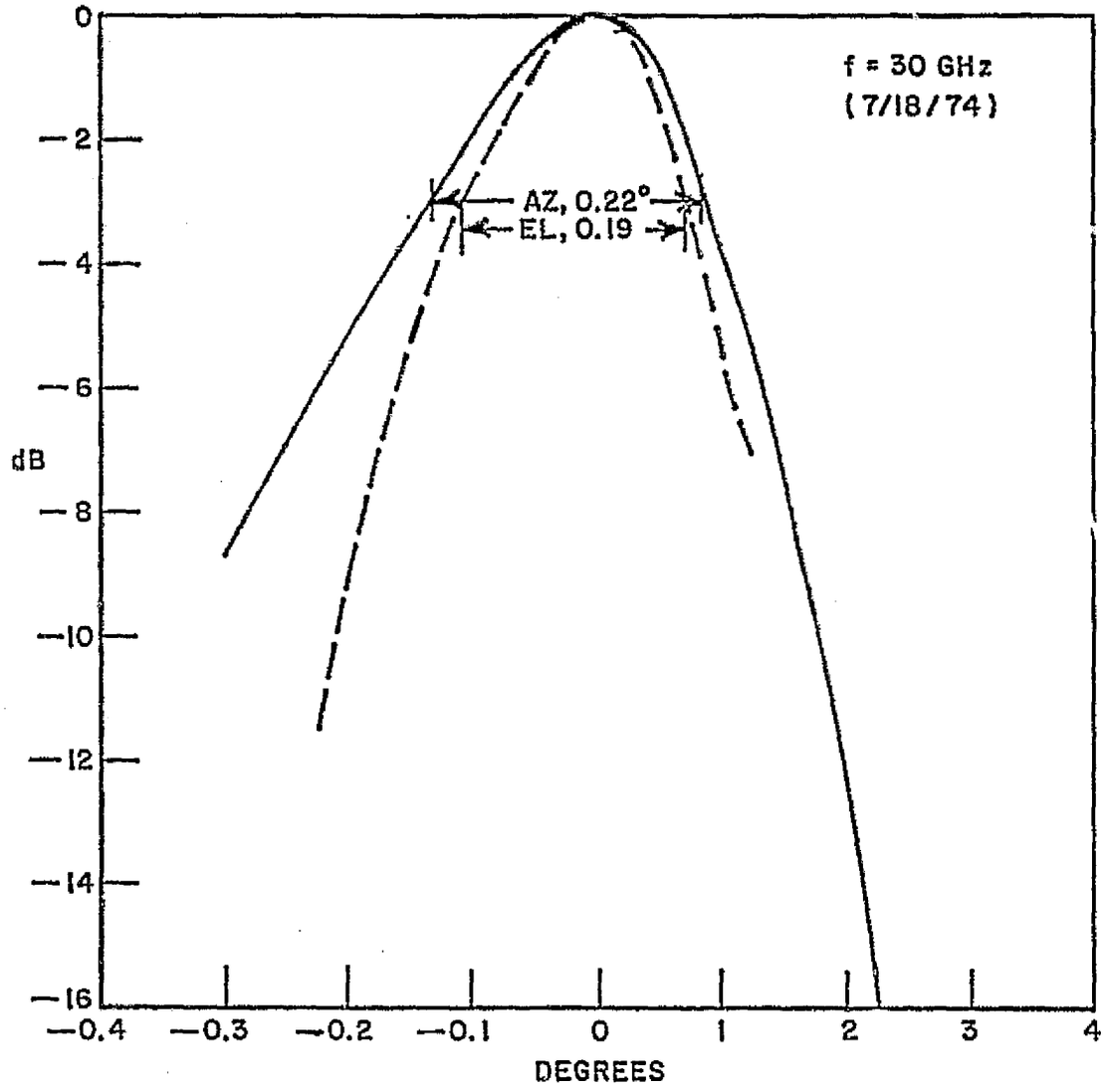

Figure 3-9. Transportable antenna pattern – 30 GHz.

The RF front ends for the 20/30 GHz receivers and radiometers are located in the silo of the Transportable antenna. The block diagram of the front ends is shown in Figure 3-10. These front ends are almost identical in electrical design to those described in Reference [3-4] hence, will not be discussed in detail here. The most significant difference is the addition of directional couplers following the waveguide calibrate switches which permit direct injection of RF signals into the receivers and radiometers.

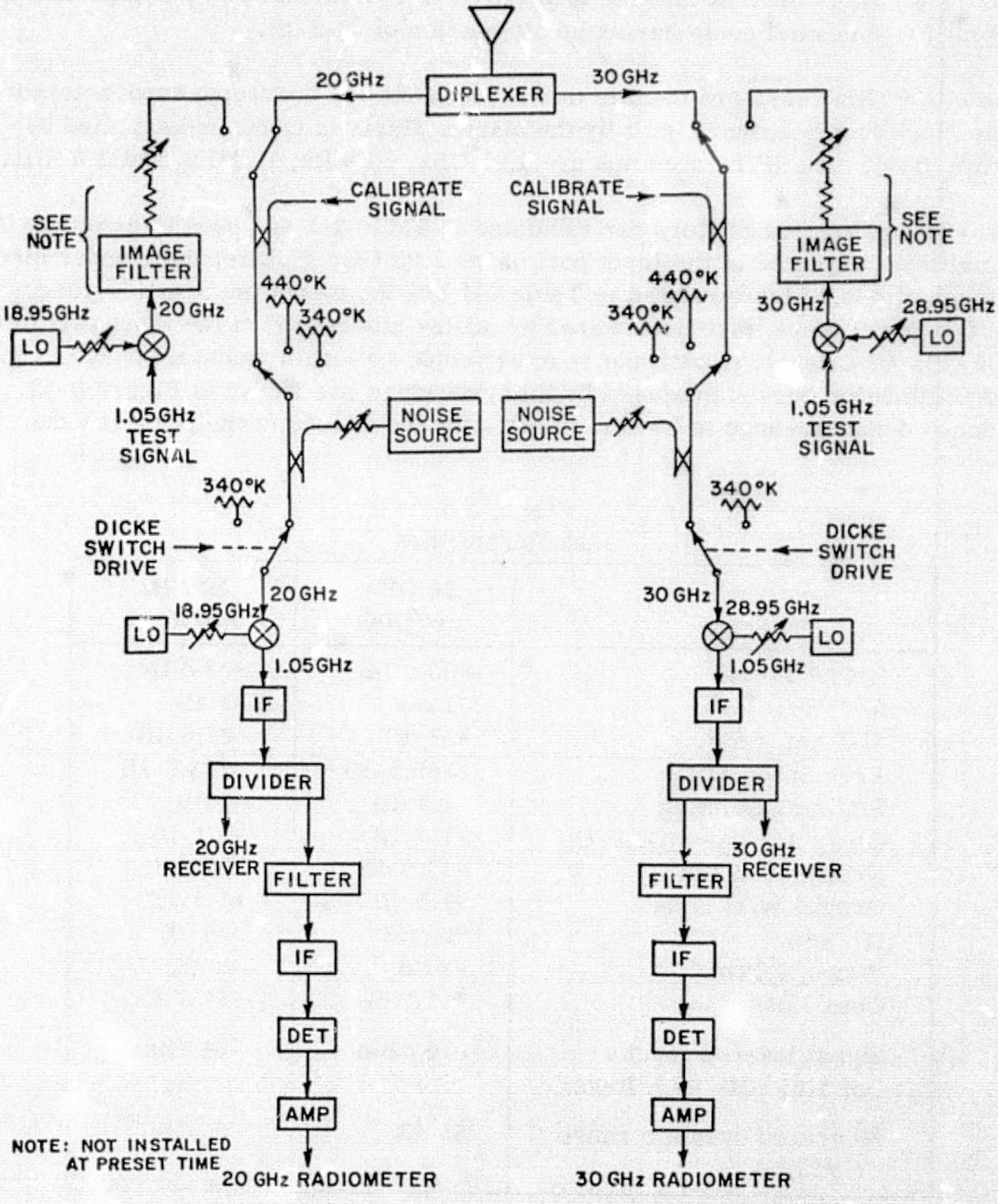

Figure 3-10. 20/30 GHz front end.

The front end components are mounted on a flat, rectangular plate with all 20 GHz components on one side and all 30 GHz components on the opposite side. The 1.05 GHz IF signal is brought into the transportable equipment now by means of a 128 ft (39 m) RG-9 coaxial cable having an attenuation of 11.8 dB.

The 20/30 GHz receivers used in this experiment are quadruple superheterodyne phase lock loop receivers built by the Martin-Marietta Corp. and supplied by NASA [3-4]. The IF frequencies are 1.05 GHz, 60 MHz, 10 MHz, and 2.5 KHz.

The various link parameters are tabulated in Table 3-1 and used to calculate the signal level expected at the input port of the 1.05 GHz PLL receiver under clear sky conditions. Also tabulated in Table 3-1 are the measured dynamic ranges of the two links; these were determined by adding attenuation at the input port of the 1.05 GHz PLL receiver until the receiver could no longer maintain phase lock. The calibration curves produced by this procedure are shown in Figure 3-11. The reduced dynamic range at 30 GHz is not fully understood at the present time.

Table 3-1
Link Parameters

	20 GHz cw/Dish	30 GHz cw/Horn
XMTR Power	+33 dBm	+33 dBm
S/C W/G loss	-1 dB	-1 dB
S/C Ant. Gain	+37 dB	+27.6 dB
Free Space Loss	-209.5 dB	-213.1 dB
S/C Ant. Pointing	-1.5 dB	-1 dB
Clear Air Loss (O ,H O)	-1.4 dB	-1.1 dB
Ground Ant. Gain	+53.9 dB	+57.5 dB
Ground W/G Loss	-1.5 dB	-1.5 dB
IF Gain	+30 dB	+30 dB
Power Splitter	-3 dB	-3 dB
Coax Loss	-11.8 dB	-11.8 dB
Signal level at input of 1.05 GHz PLL Revc.	-76 dBm	-84 dBm
Measured dynamic range (7/23/74	55 dB	35 dB

Independent calibrations of the 1.05 GHz PLL receivers were also performed by injecting 1.05 GHz signals of known level at the receiver inputs. These curves are shown in Figure 3-12.

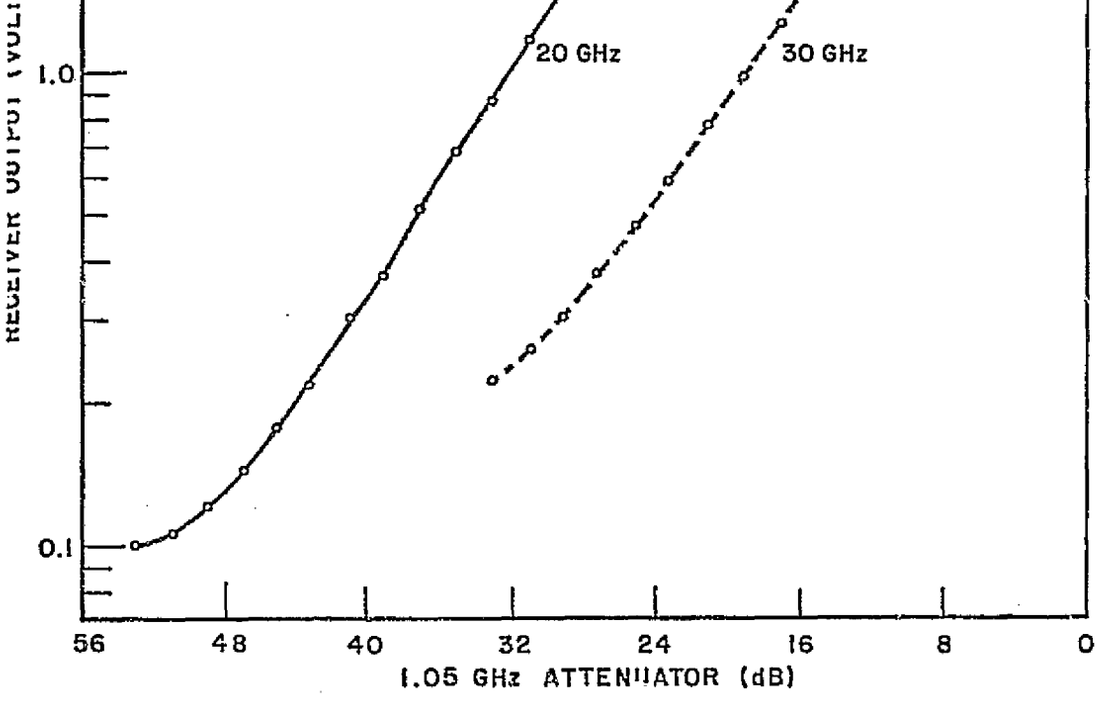

Figure 3-11. Link calibration using ATS-6 signal (7/22/74).

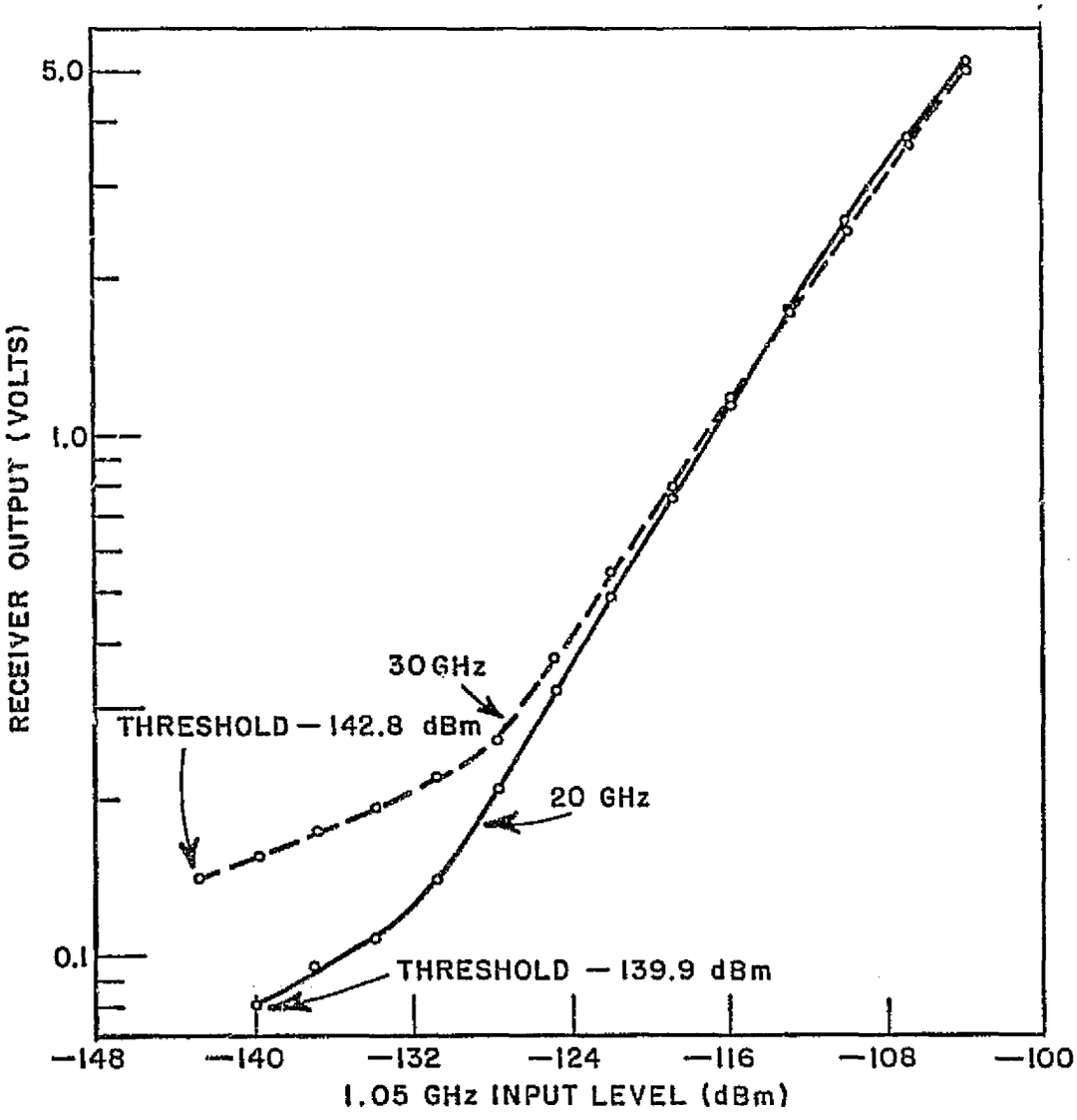

Figure 3-12. Receiver calibration (9/9/74).

The difference in received signal level between CW and multitone modes was checked on July 2, 1974, and the multitone level was found to be approximately 6.5 dB lower at both 20 and 30 GHz.

The difference in received signal level both with and without the Dicke switch operating has also been checked, and the level was found to be approximately 6 dB lower when this switch is operating.

FIXED TERMINAL

The Fixed 20/30 GHz Ground Terminal is located at the Ohio State University ElectroScience Laboratory Satellite Communication Facility, 1320 Kinnear Road, Columbus, Ohio. The geographical location of this site is latitude 40° 00' 10" and longitude 83° 02' 30" W; the site elevation is 252 m above sea level. Both the OSU High Resolution Radar/Radiometer and Low-Resolution Radar Systems are also located at this site [3-5]. In addition, a 13/18 GHz Comsat ATS-6 uplink terminal is located at this site.

The instrumentation at the Fixed Terminal consists of 20 and 30 GHZ Martin-Marietta phase lock loop receivers. 20 and 30 GHz radiometers were constructed by OSU following the design presented in Reference 4 and were added to these receivers.

The digital data handling for the entire experiment is performed at the fixed terminal. This function consists of digitizing and formating data obtained at the Fixed Terminal; these data are then merged with the data obtained from the two remote terminals as well as the High Resolution Radar/Radiometer System. All data are then recorded in real time on a single digital magnetic tape.

The 20/30 GHz Fixed Terminal antenna is a 4.6 m. Cassegrain fed, parabolic antenna. (See Figure 3-2). The RMS surface tolerance of this antenna is 0.64 mm or 0.043λ at 20 GHz and 0.064λ at 30 GHz. The antenna is mounted on an azimuth-over-elevation-over-azimuth pedestal so that the polarization can be remotely controlled. A square, corrugated horn is used to feed the antenna. The feed horn and the packaging of front end hardware are identical to those used for the OSU Transportable Terminal and were described in Reference [3-3].

The Fixed Terminal feed horn patterns are shown in Figure 3-13. The measured SWR of this feedhorn was 1.20 at 20 GHz and 1.19 at 30 GHz.

The patterns of the Fixed Terminal antenna were measured using the 20 and 30 GHz ATS-6 downlinks. These patterns are shown in Figures 3-14 and 3-15. The gain of the Fixed antenna is estimated to be 53.9 dB at 20 GHz and 57.5 dB at 30 GHz.

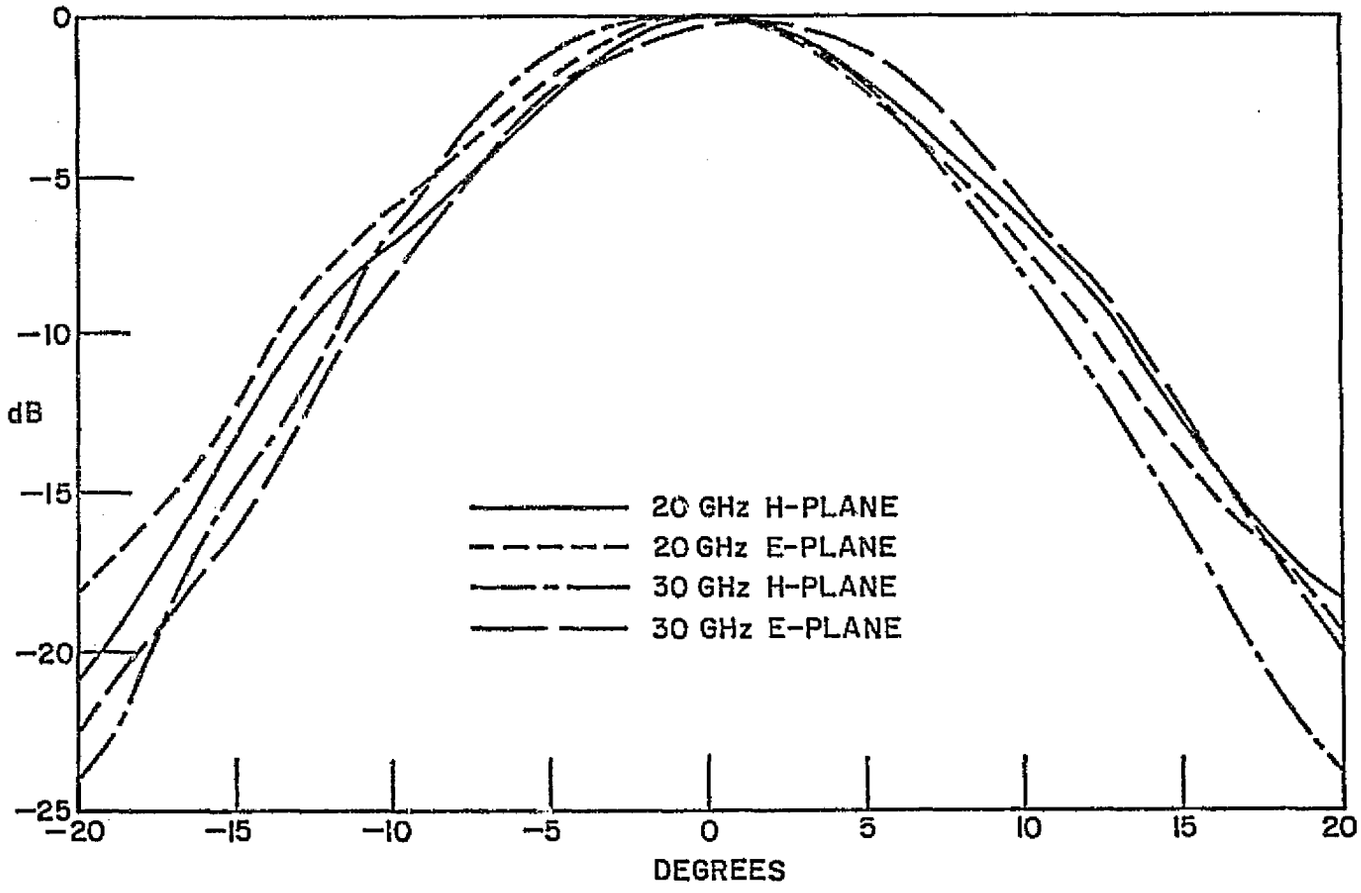

Figure 3-13. Fixed feed horn patterns.

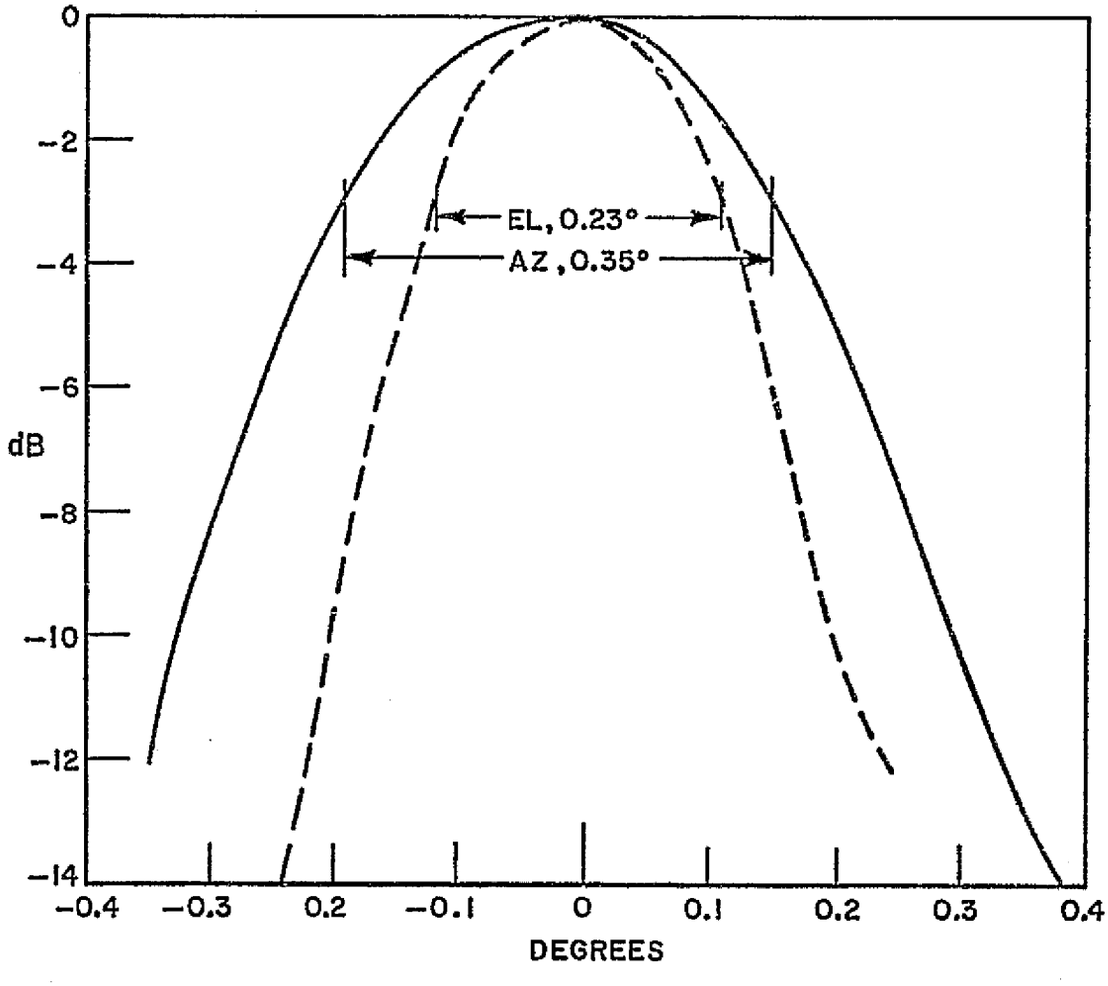

Figure 3-14. Fixed antenna pattern – 20 GHz.

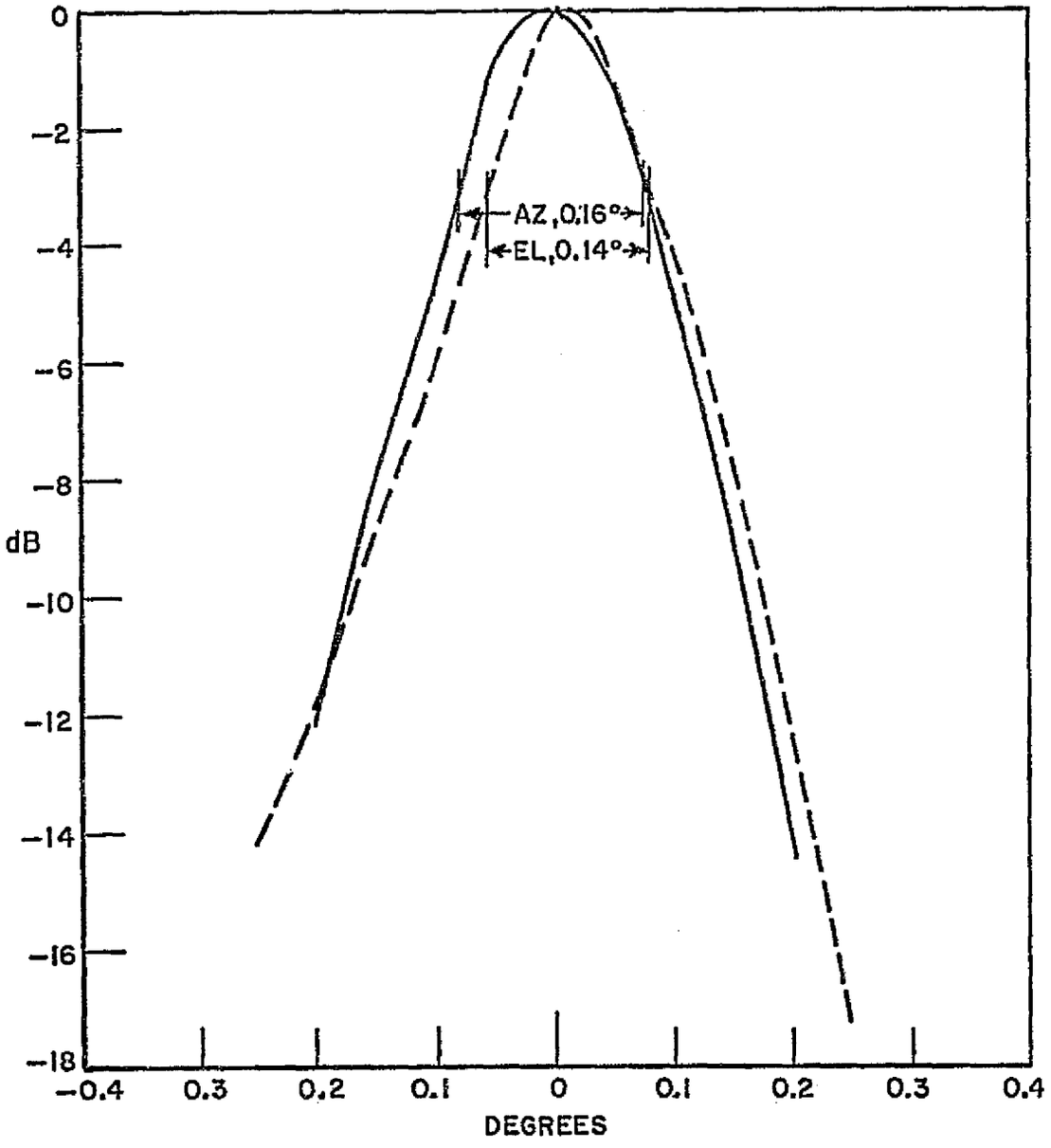

Figure 3-15. Fixed antenna pattern – 30 GHz.

The RF front ends for the 20/30 GHz receivers and radiometers are essentially identical to those used for the Transportable Terminal. The electrical design has been described in Ref. [3-4] and the physical arrangement of components was presented above. The RG-9 coaxial cable carrying the 1.05 GHz IF signal from the RF front end to the fixed receivers is 135 ft (41 m) long and has an attenuation of 12.4 dB.

The link parameters are the same of those listed in Table 1, Reference [3-2], with the exception of 0.6 dB additiona. coax loss in the case of the Fixed Terminal. The calculated signal levels at the input of the Fixed Terminal 1.05 GHz PLL receivers are -76 dBm at 20 GHz and -85 dBm at 30 GHz. These levels are for the 20 GHz cw/Dish and 30 GHz cw/Horn modes. Measured dynamic ranges at the Fixed Terminal are 55 dB at 20 GHz (8/27/74) and 51 dB at 30 GHz (1/24/75).

Calibration curves obtained using the ATS-6 signals and introducing attenuation at the inputs to the 1.05 GHz PLL receivers are shown in Figure 3-16 Calibration curves for the PLL receivers using locally injected 1.05 GHz signals are presented in Figure 3-17.

Margin measurements were performed on 6 June 1975 with the satellite antennas directed toward VPI. The margins were

	20 GHz	30 GHz
Transportable	46 dB	34 dB
Fixed	47 dB	37 dB

for the 20 GHz cw/Dish and 30 GHz cw/Horn modes.

DIGITAL DATA SYSTEM

All data acquired in this experiment are digitized and recorded on a common digital tape in real time. The data acquired at the remote terminals are digitized at the point of acquisition and transmitted to the Fixed Terminal via telephone lines. These data together with data from the High Resolution Radar/Radiometer System are merged and recorded on a single digital magnetic tape. In addition to these data, various status switches indicating operating modes and conditions are also monitored and recorded. The operator at the Fixed Terminal maintains control of the entire data system at all times.

The data acquisition system consists of an HP-2115-A minocomputer and control hardware, a digital magnetic tape deck, and two remote process controllers which

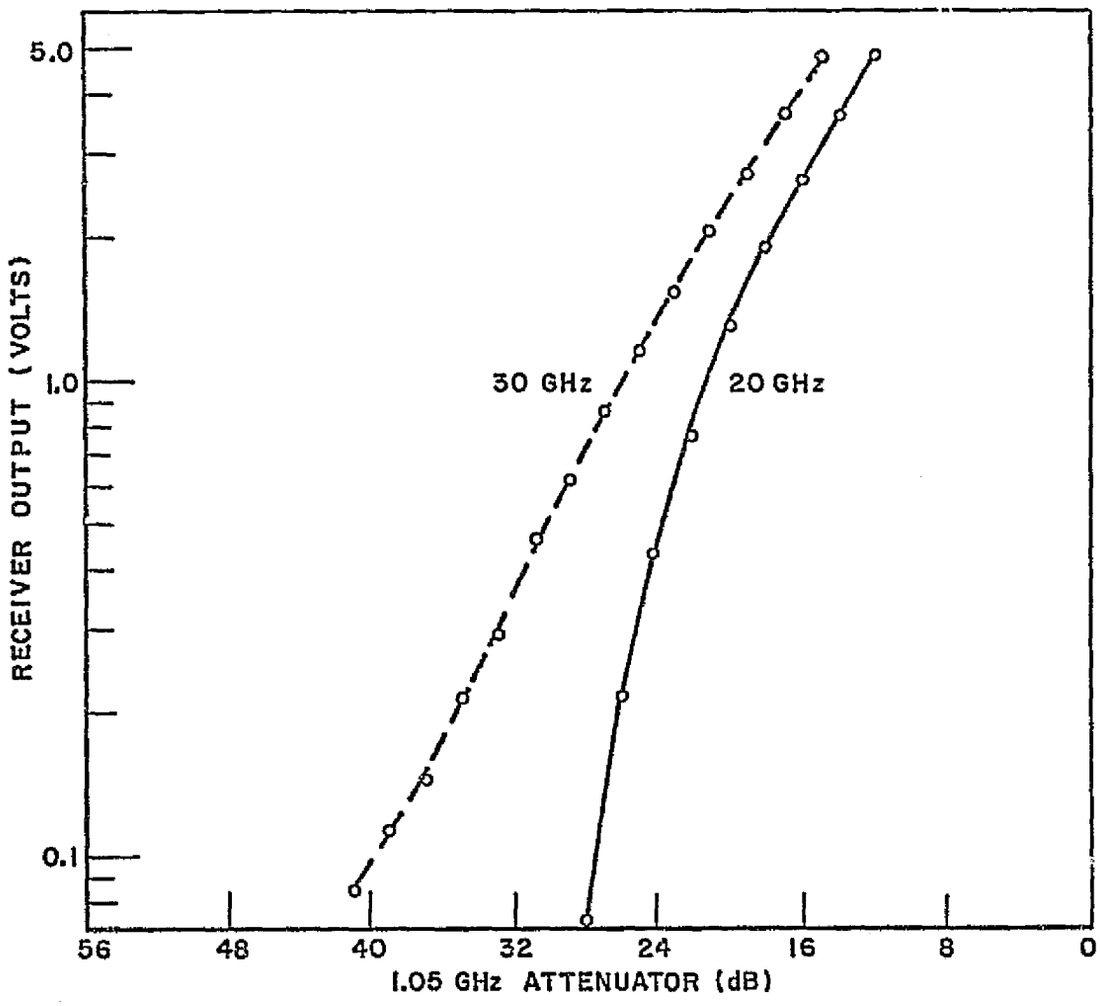

Figure 3-16. Link calibration using ATS-6 signal (1/24/75).

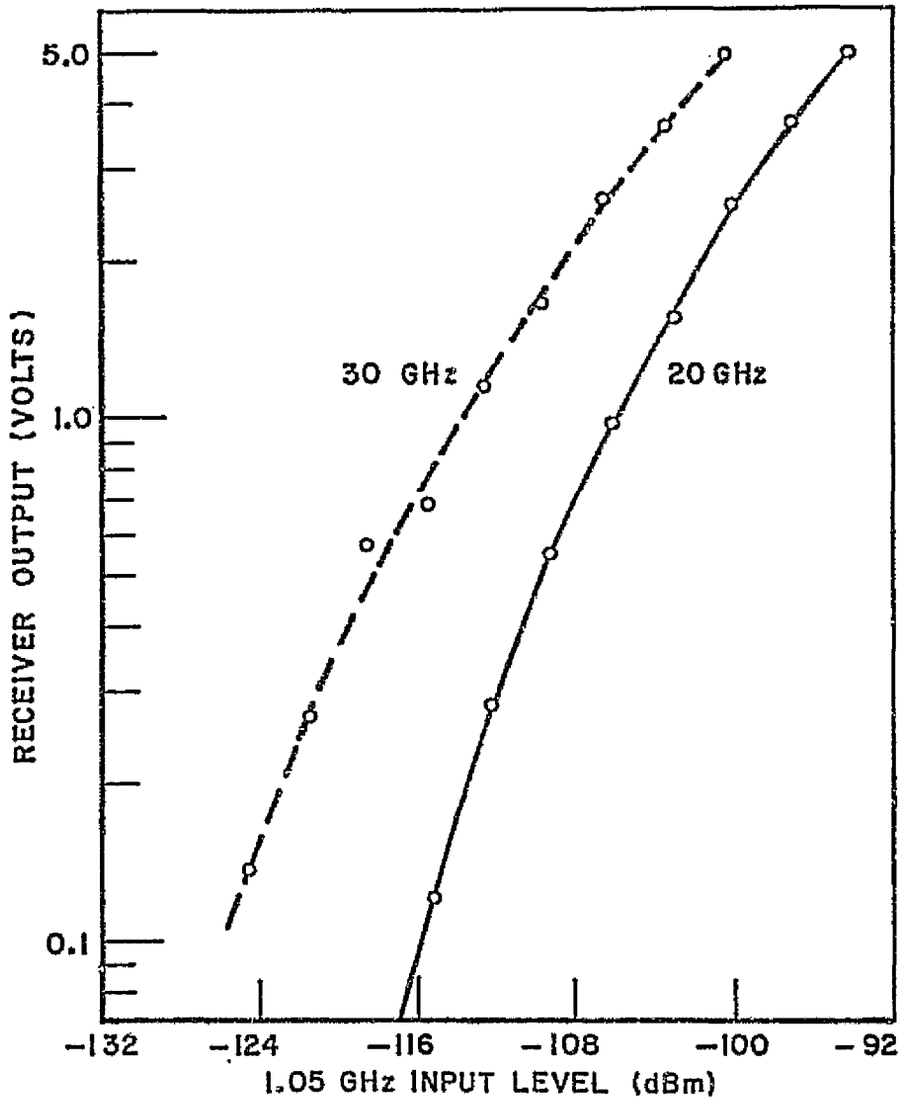

Figure 3-17. Receiver calibration (9/4/74).

are directed by the HP-2115-A via commercial telephone lines. One remote controller located at the Transportable Terminal acquires, buffers, and transfers data blocks at the request of the central computer. The data, sampled once a second, consist of status checks and the receiver and radiometer outputs from the Transportable Terminal. The remote controller, located at the Unmanned Terminal samples one radiometer, interrogates a status register, samples test voltages, or performs a control function at the request of the central computer and returns the desired word of information once a second. The central computer must request each word of data or status separately and the remote controller returns the desired word after a 400 msec. delay. The central computer, in addition to controlling the remote processors, examines the status and samples the receivers and radiometers of the Fixed Terminal at rates of 10 or 200 samples per second, and records all data on magnetic tape.

A/D conversion, status acquisition, and data transmission and reception are performed by three control units. The analog signals are multiplexed and then converted. All A/D conversions provide seven significant bits plus sign. Provisions were made for sixteen sampled analog channels at the Fixed Terminal and eight at the Transportable Terminal. An A/D controller operates the A/D converter and multiplexer and provides an interrupt signal to the I/O bus.

Data are transferred from the remote controllers to the Fixed Terminal data system via commercial voice-grade telephone lines. A pair of Vadic VA-1600 modems are used for data communication with the Transportable Terminal and two Bell System type 103 modems are used with the Unmanned Terminal. Modem controllers at each terminal provide the correct parallel-to-serial conversions, control, and interrupt logic.

EMPIRICAL DIVERSITY GAIN RELATION

Only a limited amount of diversity gain data exists for millimeter wavelength earth-space propagation paths. These data, consisting of measurements performed by the Ohio State University and Bell Telephone Laboratories, were collected and presented in an earlier publication [3-6]. The OSU data were obtained using the ATS-5 15.3 GHz downlink for attenuation measurements; and the BTL data were generated from 16 GHz radiometric temperature measurements along a nominal ATS-5 propagation path. In both cases the ground terminals were separated along a baseline oriented in approximately the NW-SE direction; the nominal look angles were 220° azimuth and 35° elevation. Even though these data were collected in different locations, the OSU data in Ohio and the BTL data in New Jersey, and over different time periods, the resulting diversity gain data were remarkably consistent.

Diversity gain is defined here as the difference between the path attenuations associated with the single terminal and diversity modes of operation for a given percentage time. Thus, diversity gain, G, is a function of the single terminal fade depth, A, as well as the terminal separation distance, D.

These data were used to generate an empirical relationship for diversity gain as a function of both separation distance and single terminal fade depth. First, it was recognized that the diversity gain data, Figure 3-18, behaved as

$$G = a(1 - e^{-bD}) \tag{1}$$

for each value of single terminal fade depth. Consequently, a minimum RMS error fit was performed for each fade depth; this procedure yielded a family of coefficients, a and b, which depended only upon the fade depth. These coefficients, Figures 3-19, 3-20, were also fit to closed form analytic expressions:

$$a = A - 3.6(1 - e^{-0.24A}) \tag{2}$$

$$b = 0.46(1 - e^{-0.26A}) \tag{3}$$

where G and A are expressed in dB and D is expressed in kilometers. Now, using Eqs. (1), (2), and (3), diversity gain was calculated as a function of terminal separation distance and single terminal fade depth. The results of these calculations are shown in Figure 3-18, it may be seen that the agreement between the empirical calculation and the data points is at worst approximately 0.75 dB. This agreement is well within the experimental accuracy of the experiment and emphasizes the consistency of these experimental data.

It is of interest to note that the linear portion of the curve relating the coefficient a to the single terminal fade depth intercepts the ordinate at about -3.6 dB. This coefficient may be interpreted as the difference between the diversity gain reached for large separation distances and the ideal diversity gain. Therefore, this result indicates that the diversity gain approaches a level approximately 3.6 dB below the ideal diversity gain as the terminal separation distance becomes large. This behavior is in accord with the concept of optimum diversity gain presented earlier [3-6].

It is also of interest to note that the coefficient b approaches a value of approximately 0.4 for large fade depths. This coefficient may be interpreted as the decay rate for diversity gain as a function of terminal separation distance. Thus, one may conclude that diversity performance is largely determined by storm cell cores having diameters on the order of 2.5 km.

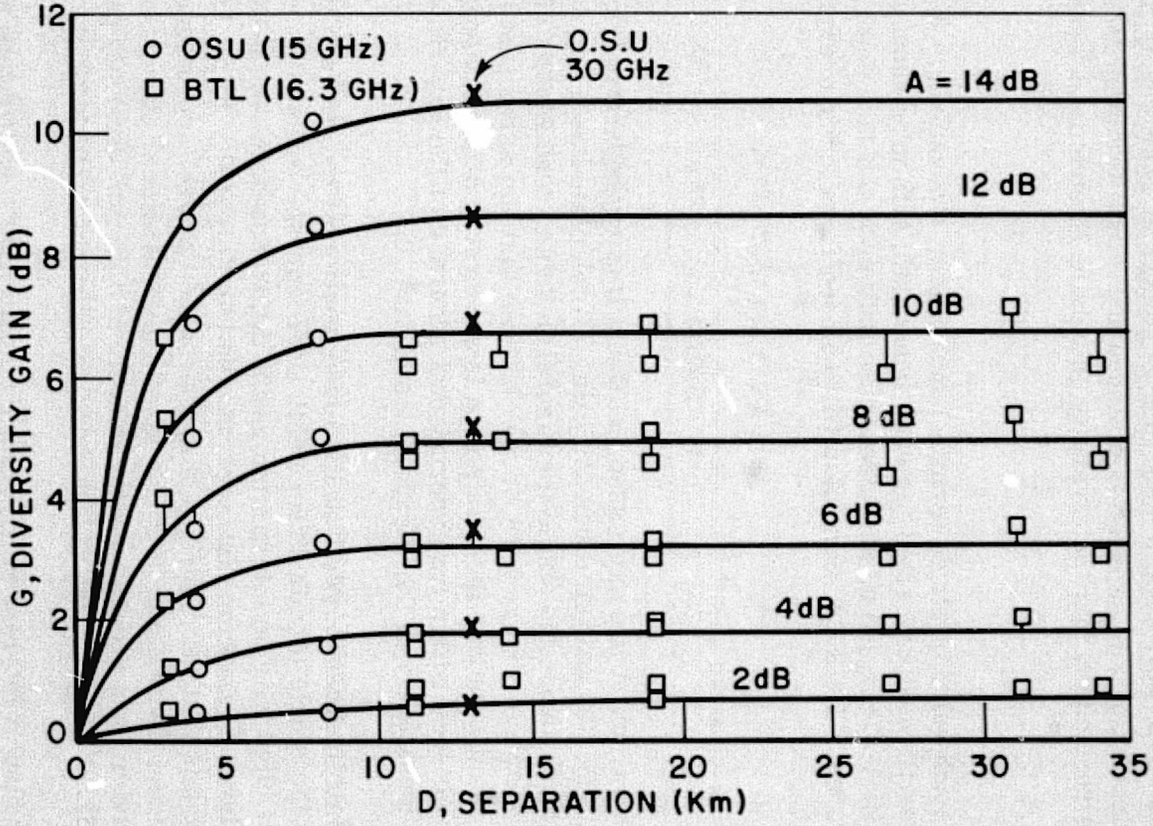

Figure 3-18. Diversity gain versus terminal separation distance.

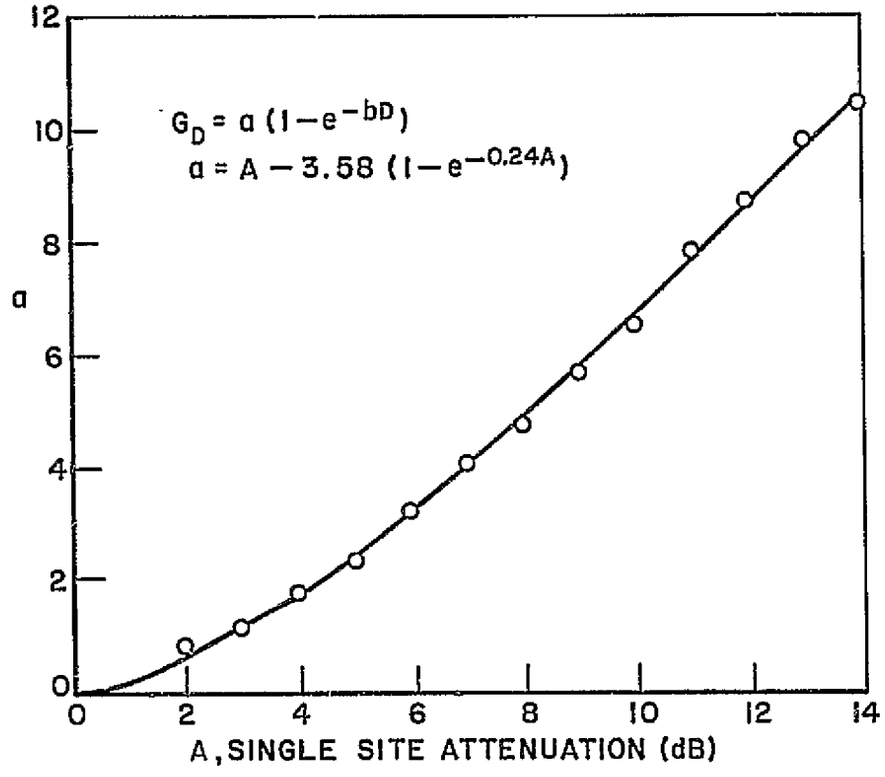

Figure 3-19. Coefficient a versus single site attenuation, A.

Finally, the empirically calculated diversity gain is presented as a function of single terminal fade depth in Figure 3-21. These curves show that the diversity gain has approached its optimum value, i.e., that value associated with an infinitely large separation distance, within 1 dB for terminal separation distances over 8 km.

PRELIMINARY ATS-6 30 GHz DIVERSITY DATA

The initial operation of the ATS-6 Millimeter Wave down link occurred on June 13, 1974. Both the 20 and 30 GHz signals were acquired at the OSU Transportable Terminal during this initial turn-on period. Data acquisition on the ATS-6 20 and 30 GHz downlinks terminated on 13 June 1975. All terminals remained operational until loss of signal as the satellite moved below the horizon. The total data acquisition periods were as follows:

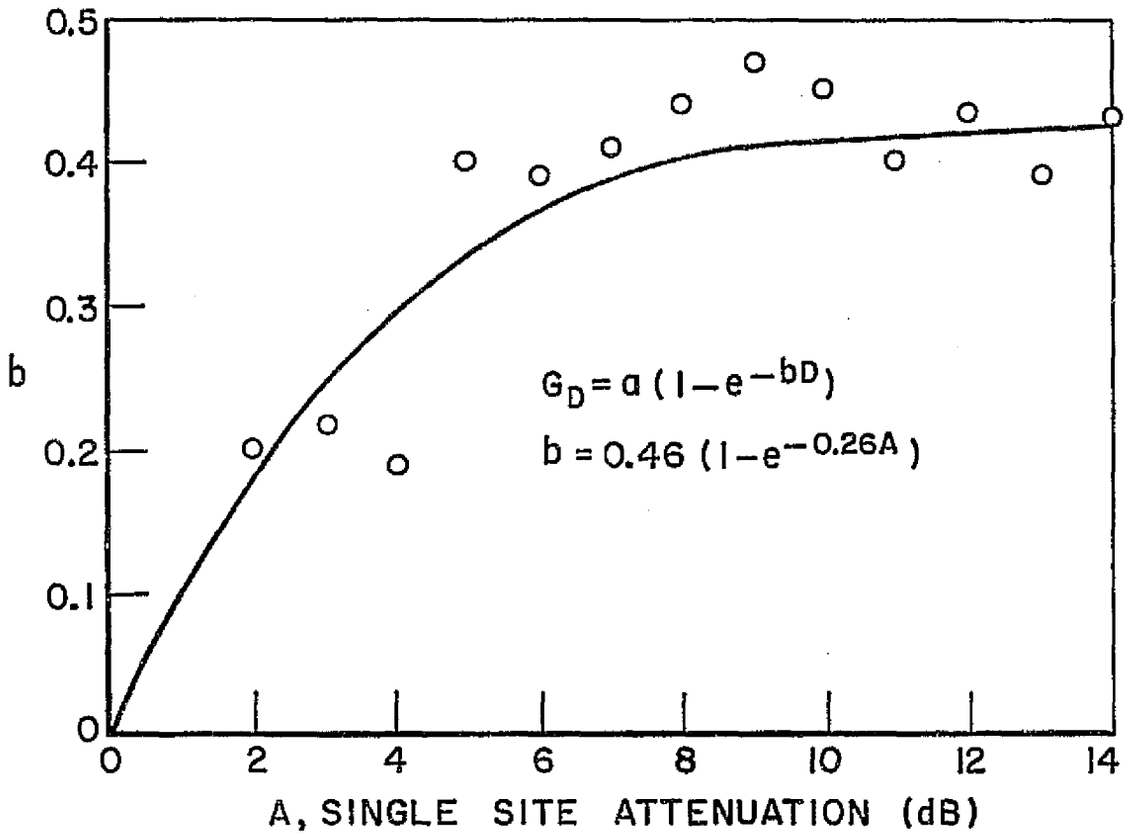

Figure 3-20. Coefficient b versus single sit attenuation, A.

Transportable	20 GHz	7,409 Min.
	30 GHz	9,281 Min.
Fixed	20 GHz	6,970 Min.
	30 GHz	8,317 Min.
Unmanned	20 GHz	5,438 Min.
TOTAL		37,415 Min.

Although a considerable amount of data has been colledted at the present time, only initial results for 30 GHz diversity behavior have been analyzed to date. Hence, the following discussion covers only 30 GHz downlink attenuation data from the Fixed and Transportable Terminals.

The relative locations of the ground terminals are shown in Figure 3-22. The nominal look angles to the ATS-6 synchronous satellite were 40° elevation and 200° azimuth.

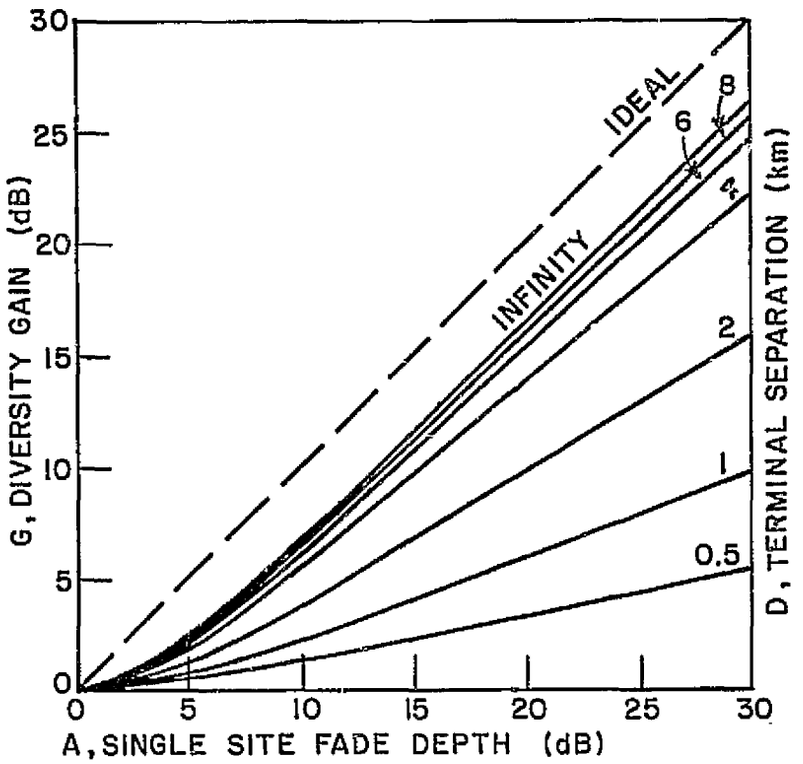

Figure 3-21. Diversity gain, G, versus single site fade depth, A.

Samples of the raw data from these terminals are presented in Figure 3-23. These curves represent the sampled outputs of the 30 GHz receivers before processing. The receiver outputs were sampled at a rate of 10 Hz although the plots were generated using 10 sample, i.e., 1 sec., averages. It should be noted that at approximately 22 minutes into this data period a 10 dB pad was switched out of the receiver input at the Transportable Terminal. The received signal at that terminal subsequently dropped below threshold for approximately 1 minute, and the 10 dB pad was reinserted at about 32 minutes into the data period. This same segment of data is shown in Figure 3-24 after conversion to a decibel scale and compensation for the pad changes. Finally, fade distributions were generated for this same data segment; these curves are shown in Figure 3-25.

A set of cumulative fade distribution for seven fade events which occurred during early Spring, 1975, are presented in Figure 3-26. It is interesting to note that the character of the diversity fade distribution has changed little from that shown in Figure 3-25 even though six additional fade events are included. Both terminals experienced fades to depths of 30 dB or more during one or more of these events.

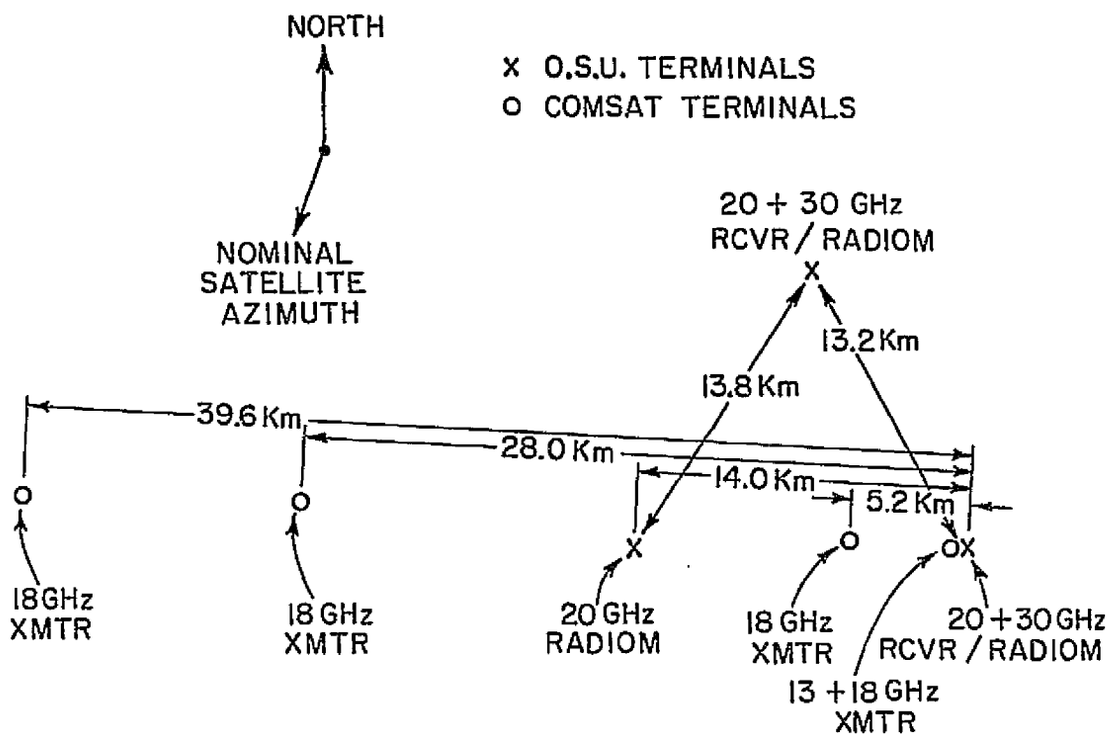

Figure 3-22. Ohio State University ATS-6 MMW Experiment site plan.

Diversity gain data were extracted from the curves shown in Figure 3-26, these 30 GHz diversity gain data points are shown in Figure 3-18 along with the empirically derived diversity gain curves. The agreement is exceptional; in fact, although not shown in this figure, the 30 GHz data points and the 15 GHz empirical results agree within 0.25 dB for all fade depths up to 30 dB. The calculations were not carried beyond this fade depth due to lack of data.

This preliminary result indicates that diversity gain is not a sensitive function of frequency. Alternatively, this result indicates that terminal separation distances of 8-10 km, which provide nearly optimum diversity gain at 15 GHz, will provide the same diversity improvement at 30 GHz. Clearly, this preliminary conclusion rests on a limited data base at the present time; nevertheless, the close agreement with earlier results tends to strengthen the credibility of this conclusion.

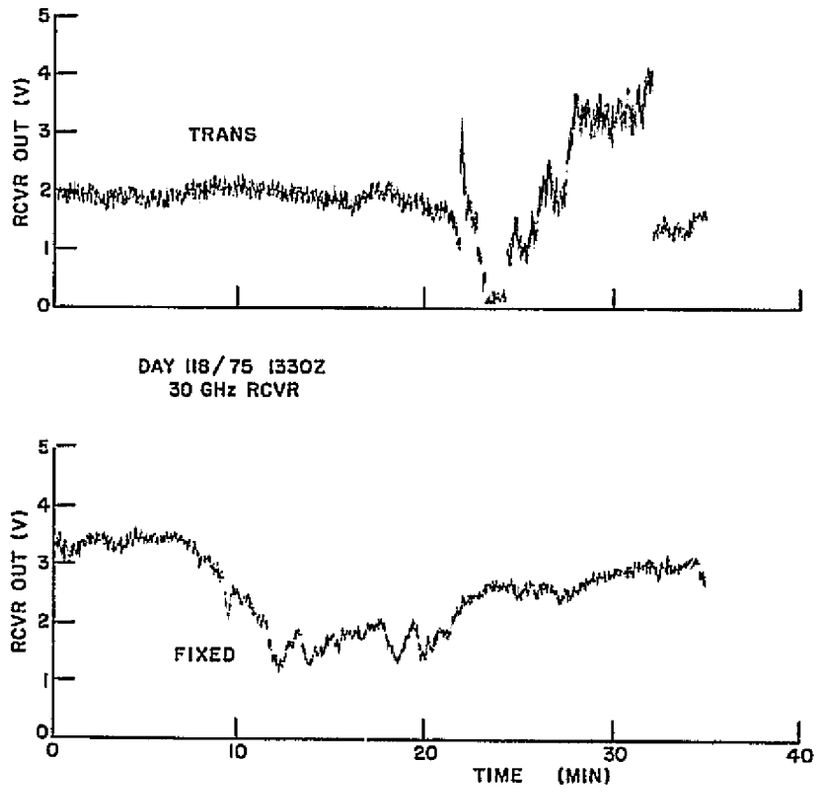

Figure 3-23. 30 GHz raw receiver data
(28 April 1975)

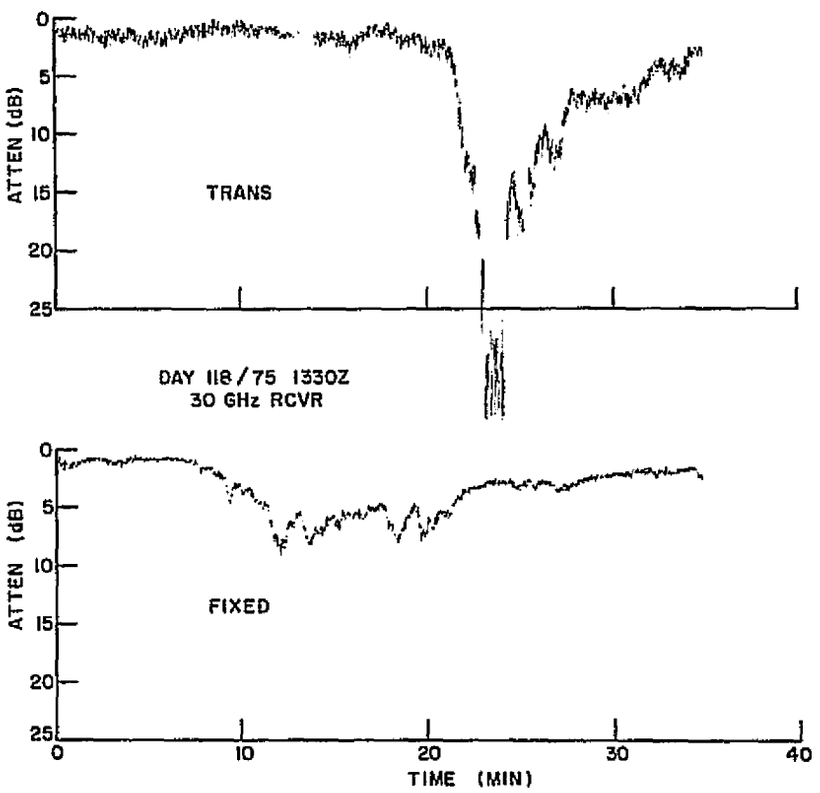

Figure 3-24. Preprocessed 30 GHz receiver data (28 April 1975)

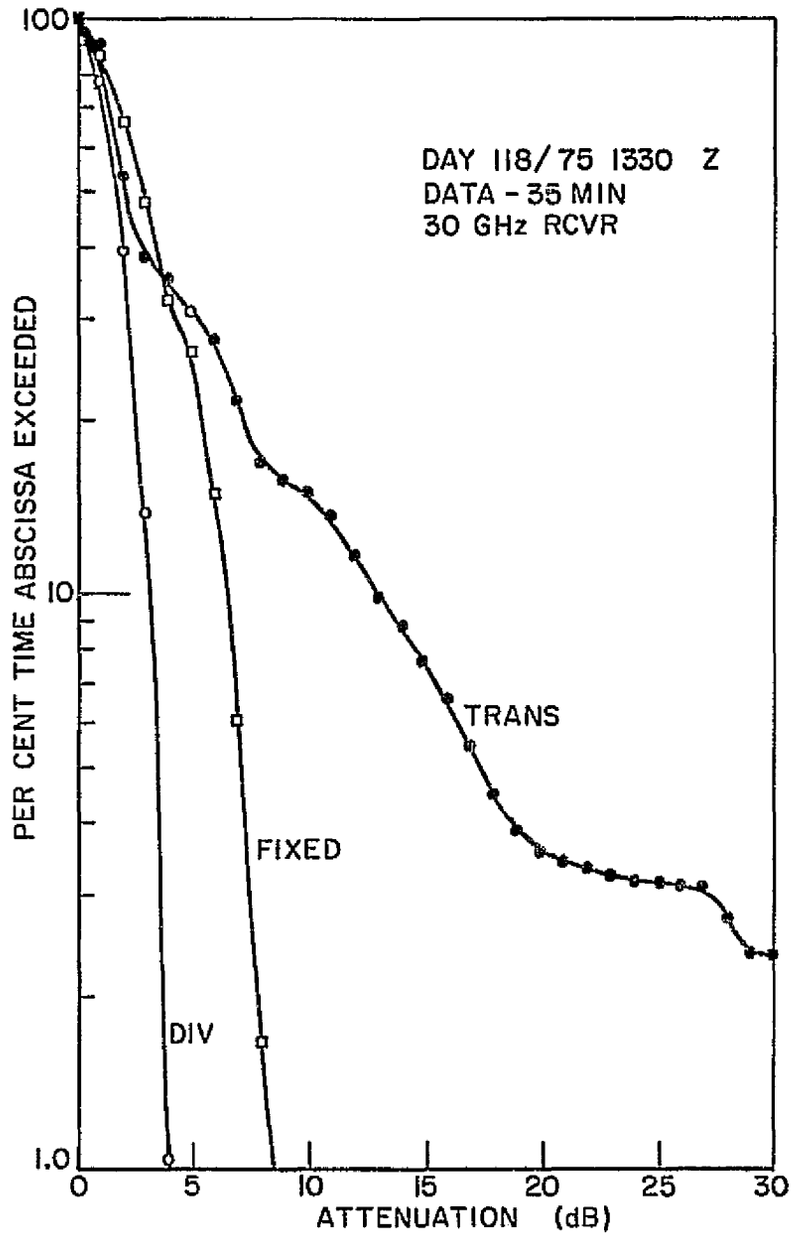

Figure 3-25. 30 GHz fade distribution
(28 April 1975)

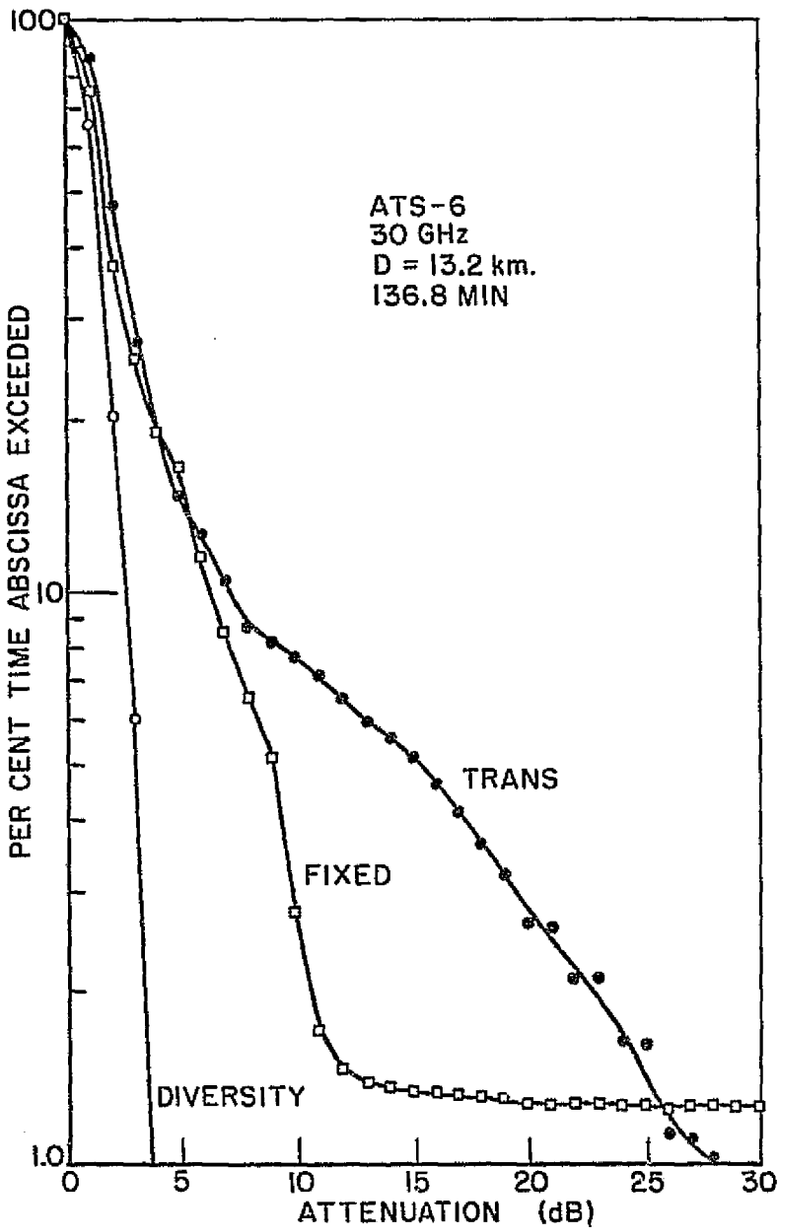

Figure 3-26. Cumulative 30 GHz fade distributions (7 events)

REFERENCES

[3-1] J. I. Strickland, "Radar Measurements of Site-Diversity Improvement During Precipitation," Proceedings of IUCRM Colloquim on the Fine Scale Structure of Precipitation and EM Propagation, Nice, France, p. IV-8, October, 1973.

[3-2] D. B. Hodge, "A 15.3 GHz Satellite-to-Ground Diversity Experiment Utilizing the ATS-5 Satellite, Report 2374-11, October 1972, The Ohio State University ElectroScience Laboratory, Department of Electrical Engineering; prepared under Grant NGR-008-080 for National Aeronautics and Space Administration.

[3-3] D. B. Hodge, "Space Diversity for Reception of Satellite Signals," Report 2374-16, October 1973, The Ohio State University ElectroScience Laboratory, Department of Electrical Engineering; prepared under Grant NGR-008-080 for National Aeronautics and Space Administration.

[3-4] C. D. Calhoon, Jr., "ATS-F Millimeter Wave Experiment Ground Receiver Systems for NASA Sponsored Participating Stations," NASA Goddard Space Flight Center, Greenbelt, Maryland, Rept. X-751-73-3, January 1973.

[3-5] D. B. Hodge and R. C. Taylor, "The Ohio State University ElectroScience Laboratory Radar/Radiometer Facilities for Precipitation Measurements," Report 2374-13, March 1973, The Ohio State University ElectroScience Laboratory, Department of Electrical Engineering; prepared under Grant No. NGR-008-080 for National Aeronautics and Space Administration.

[3-6] D. B. Hodge, "Path Diversity for Reception of Satellite Signals," Journal de Recherches Atmospheriques, V. 8, p. 443, June, 1974.

[3-7] D. B. Hodge, "Ats-F Millimeter Wavelength Propagation Experiment," Report 3863-1, July 1974, The Ohio State University ElectroScience Laboratory, Department of Electrical Engineering; prepared under Contract NAS5-21983 for National Aeronautics and Space Administration (NASA Goddard).

[3-8] D. B. Hodge and R. C. Taylor, "ATS-6 Millimeter Wavelength Propagation Experiment," Report 3863-2, September 1974, The Ohio State University ElectroScience Laboratory, Department of Electrical Engineering; prepared under Contract NAS5-21983 for National Aeronautics and Space Administration (NASA Goddard).

[3-9] D. B. Hodge and R. C. Taylor, "ATS-6 Millimeter Wavelength Propagation Experiment," Report 3863-3, March 1975, The Ohio State University ElectroScience Laboratory, Department of Electrical Engineering; prepared under Contract NAS5-21983 for National Aeronautics and Space Administration (NASA Goddard).

ATMOSPHERIC ATTENUATION MEASUREMENTS AND PREDICTION TECHNIQUES AT 20 & 30 GHz WITH THE ATS-6 SATELLITE

Louis J. Ippolito
NASA Goddard Space Flight Center
Greenbelt, Maryland

ABSTRACT

The ATS-6 (Applications Technology Satellite) Millimeter Wave Experiment provided direct rain attenuation measurements at 20 and 30 GHz at a number of locations in the continental United States. Studies at the NASA stations at Rosman, North Carolina and Greenbelt, Maryland were directed at an evaluation of rain attenuation statistics, attenuation ratio variations, scintillation effects, coherence bandwidth in a 1400 MHz band, and attenuation prediction techniques utilizing rain gauge, radar, and radiometer measurements coincident with the earth-space attenuation measurements.

Results of the first 10 months of measurements at Rosman and Greenbelt are presented with major emphasis on the impact of the results on earth-space system design.

INTRODUCTION

The radio frequency bands below 10 GHz presently support virtually all terrestrial and space communications links. Recent needs for additional capacity and expanding coverage have required the systems designer to look to higher frequency bands to provide the needed capabilities without sharing problems or inadequate bandwidth. The frequency bands above 10 GHz are presently allocated for all major space services, including fixed satellite, broadcast satellite, meteorological satellite, and terrestrial services such as fixed line-of-site, mobile, and radiolocation. Some of the bands are shared, many are exclusive or limited to two or three services.

In the design of space communications systems at millimeter wavelengths, consideration must be given to the effects of precipitation on the earth-space propagation path. At frequencies above about 10 GHz, absorption and scattering caused by rain, hail or wet snow can cause a reduction in signal level (attenuation) which

will reduce the reliability of the communications link. Other effects can be generated by precipitation events. They include: depolarization, amplitude and phase scintillations, and bandwidth decoherence. All of these factors can have a degrading effect on space communications at millimeter wavelengths.

The ATS-6 MWE is designed to measure and evaluate propagation characteristics of space-to-earth links at 20 and 30 GHz [1].

The measurements at Rosman and Greenbelt were accomplished in three areas:

The MWE provided the propagation characteristics of earth-to-space links at 20 and 30 GHz under defined meteorological conditions. Included were measurements of attenuation, phase, scintillations, and coherence bandwidth.

The experiment provided engineering data on communications links; 6 GHz up, and 4, 20 and 30 GHz down. Measurements on both analog video and digital biphase signals were made, and the effects of the millimeter space links evaluated.

The experiment also provided measurements and analyses for the development of methods of attenuation prediction from radar systems, rain gauge networks, and radiometers.

GROUND STATION EQUIPMENT

The prime NASA MWE ground terminal was at the NASA tracking station in Rosman, N. Carolina, located in the western part of the state (see Figure 4-1). The MWE used a 4.6 meter parabolic reflector antenna (Figure 4-2) with a dual frequency feed and RF front end mounted at the antenna. Telemetry and command for the ATS-6 is accomplished with a 26 meter antenna located about 60 meters from the MWE antenna, as seen in Figure 4-3.

The principal elements of the Rosman MWE ground equipment are shown in Figure 4-4.

The ground receiving system consists of the dual frequency feed and RF front end mounted at the feed point of the antenna; a phase-lock loop/signal processor; control and monitor unit; and radiometer chassis. Additionally, automatic calibration and test equipment is provided to facilitate performing the required amplitude and phase calibration.

Figure 4-5 shows the receiver system mounted in the three racks at the right side of the figure. Strip chart recorders, antenna pointing controls, and other support equipment are seen in the other racks.

Figure 4-1. NASA Rosman, N. Carolina Tracking Station

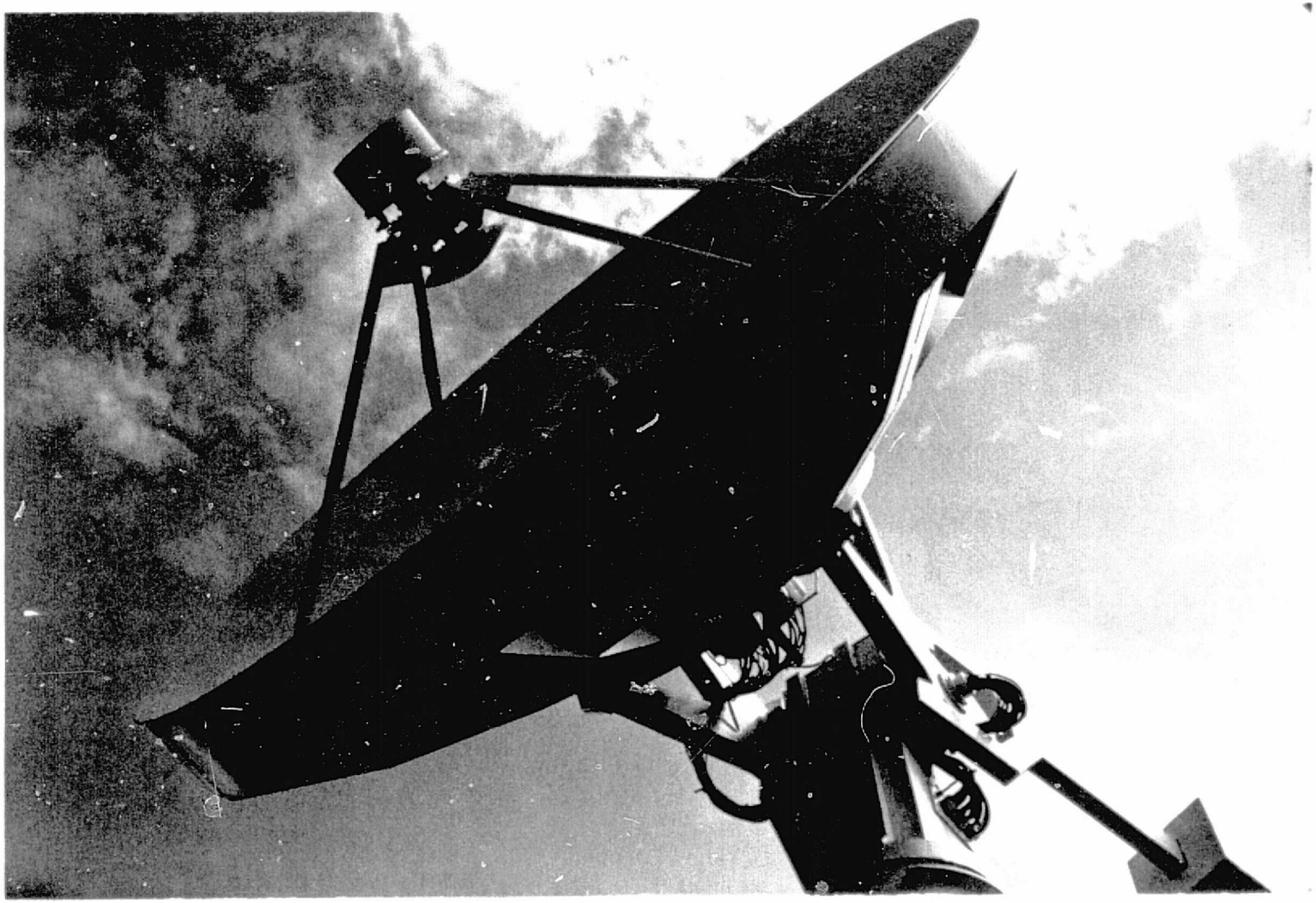

Figure 4-2. 4.6 Meter Antenna for Millimeter Wave Experiment, Rosman, N.C.

Figure 4-3. ATS-6 Tracking Antenna and MWE Antenna, Rosman, N.C.

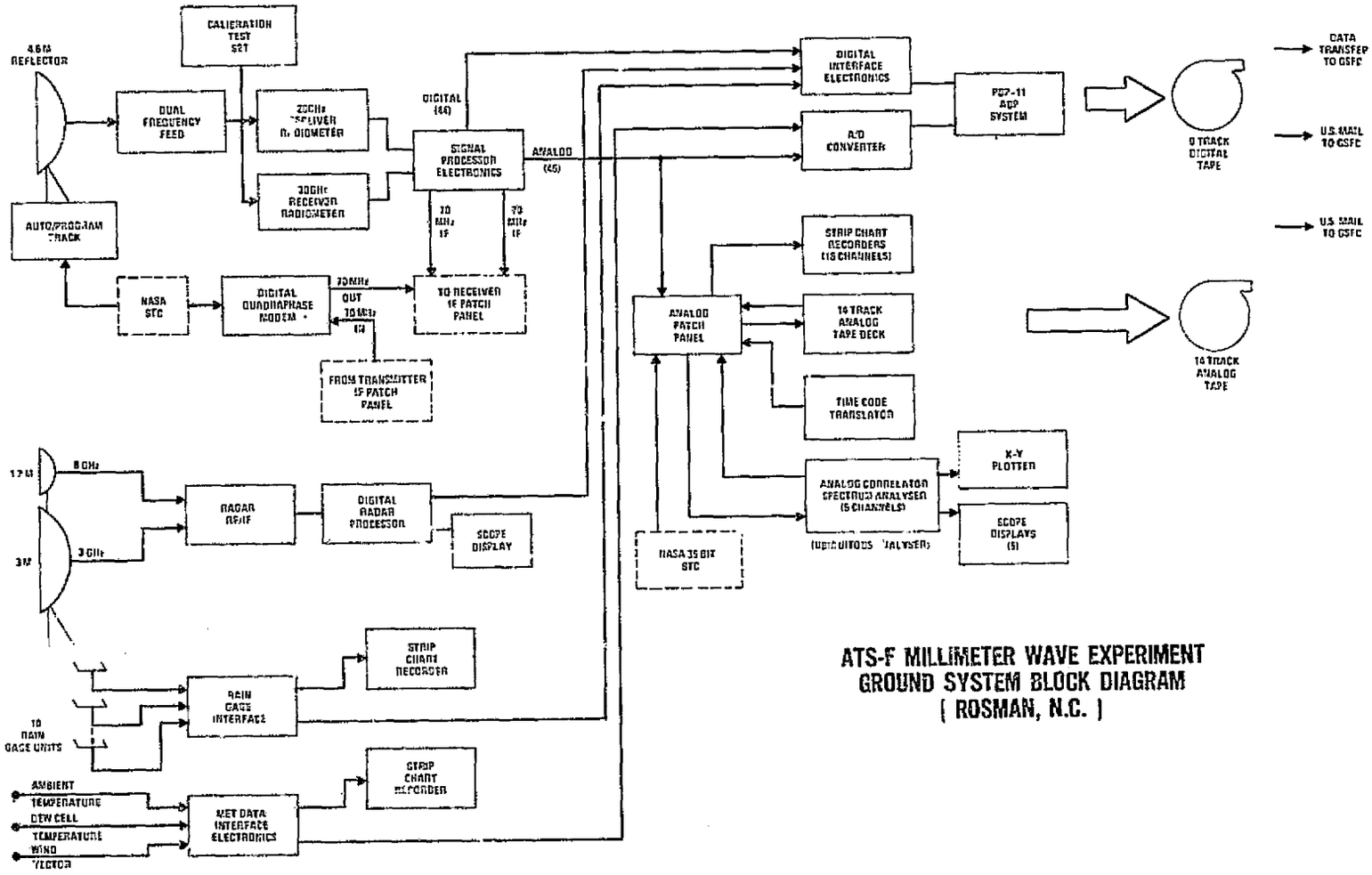

ATS-F MILLIMETER WAVE EXPERIMENT GROUND SYSTEM BLOCK DIAGRAM (ROSMAN, N.C.)

Figure 4-4. The NASA Rosman, N.C. MWE Ground Terminal

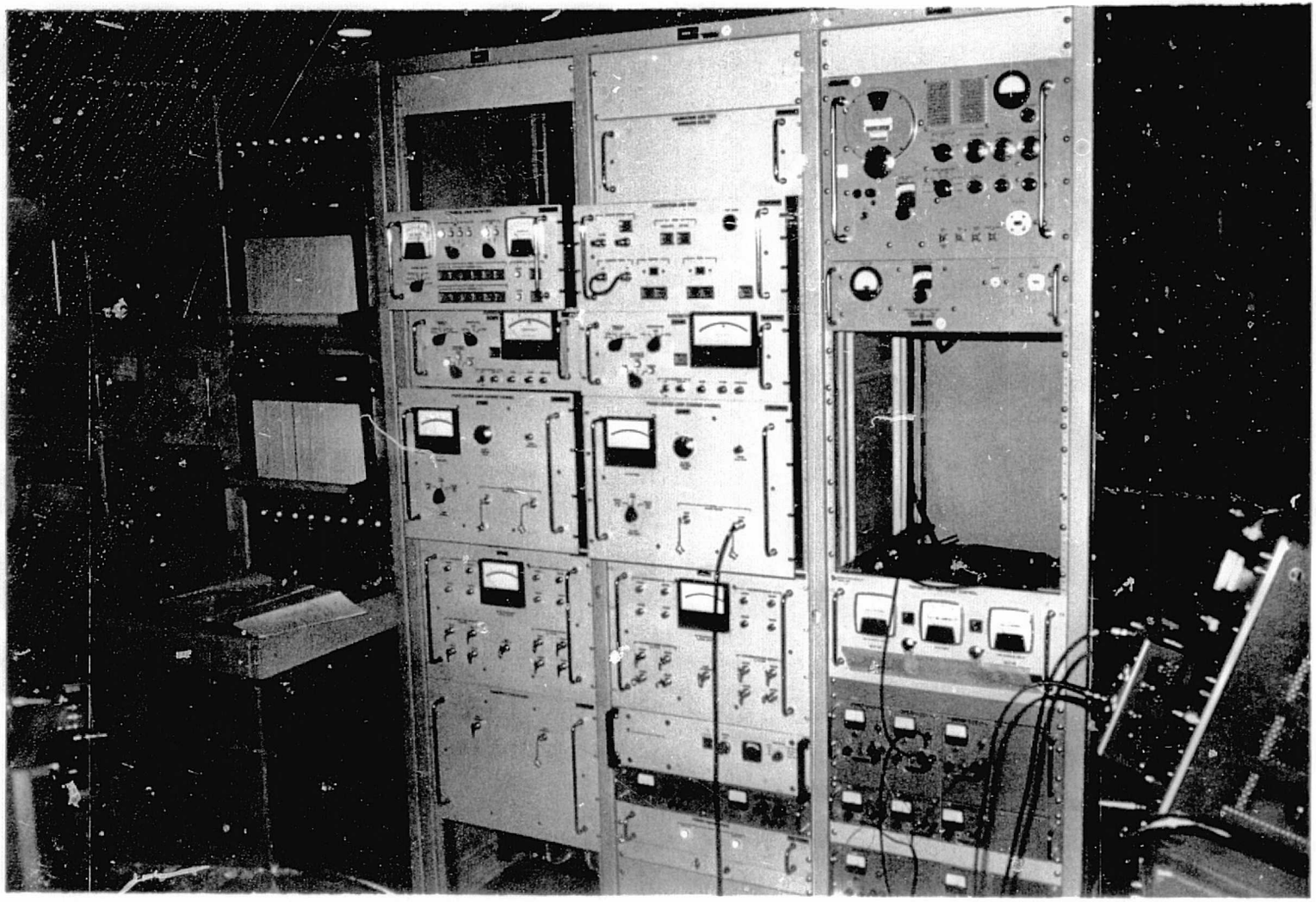

Figure 4-5. MWE 20 & 30 GHz Receiver, Rosman, N.C.

A corrugated feed horn provides the required broadband frequency performance (greater than 2 to 1), equal E and H phase beamwidths at 20 and 30 GHz, coincident phase centers, and high illumination efficiencies. A polarization rotation assembly provides the capability of remotely aligning the ground antenna polarization with that of the satellite antennas and operates at 20 GHz and 30 GHz with a ±1000 MHz bandwidth. A diplexer effectively separates the 20 and 30 GHz signals, directs them to their respective front ends, and provides the isolation necessary to prevent the LO signal of one mixer from getting through to the receiver of the opposite band.

The 4.6m parabolic antenna has 56 dB gain and a 0.23 degree halfpower beamwidth at 20 GHz, and 58 dB gain and 0.15 degree halfpower beamwidth at 30 GHz. Sidelobes for both frequencies are below 15 db. A remote feed polarization positioning technique is used and the autotrack is accomplished by scanning the subreflector in a conical scan mode (see subreflector on Figure 4-2). The program track capability utilizes a small digital processor to compare time and orbit data to track the satellite. The antenna system is capable of providing selectable conical scan autotracking and simultaneous reception at 20 GHz and 30 GHz.

The 20 and 30 GHz front ends are similar in design, and the block diagram of the 30 GHz system is shown in Figure 4-6.

The inputs are derived from the diplexer on two separate waveguide ports and the outputs are applied separately to the PLL/SP and radiometer IF's. The front ends are completely independent of each other. The receiver system front ends incorporate uncooled parametric amplifiers to provide moderately low system noise temperatures. Both front ends contain all of the circuits necessary to convert propagation/communications signals to an IF and process the radiometer signal through the video detector back to the original Dicke switching rate.

Two diplexers are used, one to separate the radiometric and propagation channels and the other to sum the propagation and radiometric inputs to the paramp. This prevents loss of 6 dB of propagation signal power when the radiometer is operating.

In order to minimize communications signal losses preceding the parametric amplifier for both frequencies, transfer switches are used to bypass the radiometer and propagation channels, including the two diplexers. The receiver noise figures are 4.6 dB at 20 GHz and 5.6 dB at 30 GHz, without the radiometer in the system.

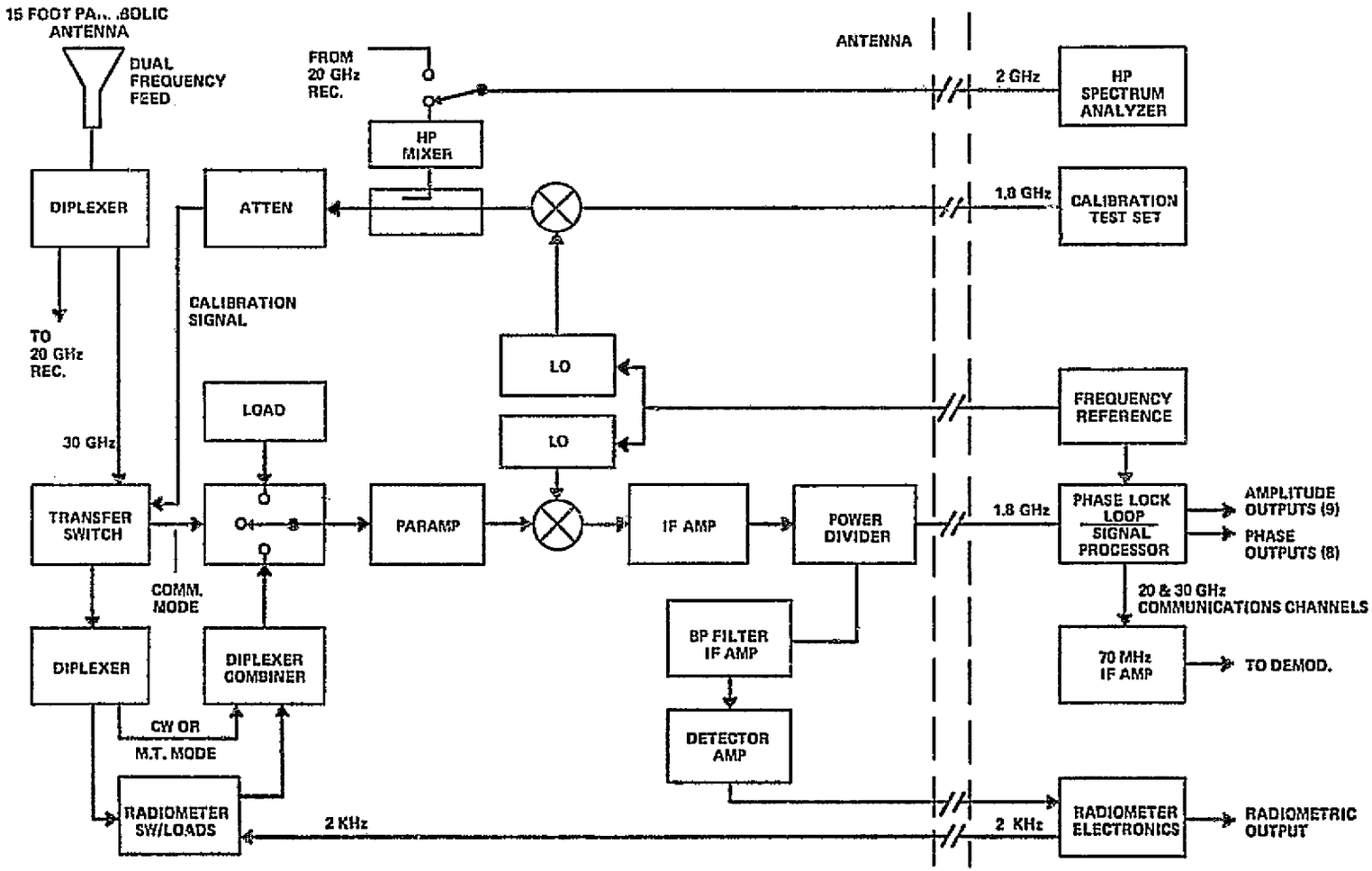

Figure 4-6. Front ends for Rosman, N.C. Terminal

The radiometer is designed to aid in the correlation of the received propagation signal characteristics with sky temperature. Simultaneous measurement of received signal characteristics and sky temperature using the same antenna permits a direct correlation to be done under various meteorological conditions. The radiometer is an absolute reading, self calibrating unit capable of measuring sky temperature over a range of 0 to 350 K. Additionally, a high isolation Dicke switch is included to allow sun temperature measurements.

The RF front end components used in the radiometer include one of the two transfer switches used to bypass the radiometer in the communications mode, two diplexers, a switching circulator for modulating the RF signal to operate the synchronous detector, calibration equipment consisting of a three position waveguide switch, two waveguide termination ovens with their control circuits and a solid state noise source with a waveguide attenuator and crossguide directional coupler. Other components include an IF amplifier, a power drive for splitting the IF signal between the CW receiver and the radiometer channel, and an envelope detector/video amplifier module. Additional radiometer circuits include a lock-in-amplifier and the control circuits to perform the calibration of the radiometer. The lock-in amplifier is basically a reference generator used to synchronize the RF switching with the reference signal to provide low level signal detection.

The radiometer utilizes a 100 MHz bandwidth centered at 20.270 or 30:270 GHz. The radiometer has a T_{min} sensitivity of 0.24°K and 0.87°K for a 10 second integration time at 20 GHz and 30 GHz, respectively. These sensitivities can be achieved at the Rosman site with the parametric amplifier on.

The Phase Lock Loop/Signal Processor (PLL/SP) processes the IF signals from the 20 GHz and 30 GHz front ends and provides the frequencies necessary to translate the IF signals to the required processing frequencies. The signal processor operates in two modes. In the multitone mode, there are 13 outputs provided which are proportional to the amplitude and phase of the nine MT signals. In the communications mode, the 20 and 30 GHz signals are translated to 70 MHz.

Each receiver system is calibrated using equipment whose signal level and frequency stability simulate those of the received propagation signal. The calibration and test equipment provides carriers at 20 and 30 GHz with 4 pairs of sidebands spaced 180 MHz apart and of equal amplitude. The signal levels are variable over a 45 db range in 3 db steps. An additional variation of 25 db is provided to simulate the spacecraft high gain antenna and CW capability. The phase of the carrier is varied over a 180 degree range, simulating a relative differential sideband phase of 360 degrees. The calibration system is completely automatic with preprogrammed circuits to control the amplitude and phase calibration.

The modulation signals from the PLL/SP are the four sidebands at 180, 360, 540, and 720 MHz. These signals are applied to a balanced modulator along with the 1.8 GHz carrier suppressed. Additional carrier suppression is realized in the carrier reject filter and sideband amplitude adjust circuit which reduces the carrier to at least 40 db below the sidebands. The sideband amplitude adjust circuit is a 9 channel band reject filter used to equalize the nine signals to within ±0.5 db or less. This sideband signal and the phase shifted carrier are combined and the resultant signal is a 9 line equal amplitude spectrum with a carrier at 1.8 GHz and four sidebands on either side of the carrier space 180 MHz apart. This signal is applied to an automatically controlled attenuator and sideband amplitude adjust circuit and is then transmitted to the RF front end with a low loss RG 218/U coaxial cable. Here the signal is plit, and applied to the 20 and 30 GHz upconverters. The output of the up-converters is attenuated by fixed attenuators to the levels required for receiver calibration.

In addition to the signal processor outputs a number of other functions are measured and recorded for later analysis, including 3 and 8 GHz radar, ten rain gauges, meteorological data, and "housekeeping" data. All parameters are recorded on a single 8-track digital tape with the aid of a PDP-11 minicomputer system, which sorts, formats, and samples the data as required (see Figure 4-4). Table 4-1 lists the parameters of the ATS-6 MPE recorded at Rosman, and indicates their major characteristics.

All experiment functions are controlled by the Experiment Status Panel (ESP), shown in Figure 4-7, which provides equipment status, fault status, antenna pointing inputs, spacecraft telemetry conditions, and other control functions.

Experiment data acquisition, formatting, calibration, and recording is accomplished with the PDP-11 computer system, shown with the ESP on Figure 4-8.

An analog recording system (see Figure 4-4) is also included for scintillation and bandwidth coherence measurements and analysis. A special purpose correlator/ spectrum analyser developed for the ATS-5 Millimeter Wave Experiment is used for detailed evaluation of the channel time-frequency characteristics.

The digital tape recorded at Rosman is transferred to GSFC via land lines, where final data reduction and analysis is accomplished. Data processing proceeds through three levels of reduction, with each succeeding step determined by the output of the step proceeding it. Figure 4-9 presents a three-dimensional description of the many output displays that are generated from the digital processing programs at GSFC. All reduction is accomplished on IBM System 360 facilities, and the output graphics are generated on 16 millimeter film strips for evaluation and storage.

Table 4-1
Data Parameters for the ATS-6 MWE

	Test Period Mode		Item	Signal Source	Digital Sample Rate (Per Second)	Digital Dynamic Range (Digital Counts)	Parameter Dynamic Range (Engineering Units)	Number of Separate Parameters Recorded
	CW	Multitone						
A			Propagation Parameters					
	X	X	20 GHz Carrier Amplitude	Receiver	20	8 bits	45 dB	1
		X	20 GHz Sideband Amplitude (8)	Receiver	20	8 bits	45 dB	8
		X	20 GHz Sideband Phase (4)	Receiver	20	8 bits	0-360 Degrees	4
	X	X	30 GHz Carrier Amplitude	Receiver	20	8 bits	45 dB	1
		X	30 GHz Sideband Amplitude (8)	Receiver	20	8 bits	45 dB	8
		X	30 GHz Sideband Phase (4)	Receiver	20	8 bits	0-360 Degrees	4
B			Meteorological Parameters					
	X	X	20 GHz Sky Temperature	Receiver	20	8 bits	0-350^{o}K	
	X	X	30 GHz Sky Temperature	Receiver	20	8 bits	0-350^{o}K	1
	X	X	Ground Ambient Temperature	Transducer	1	8 bits	0-110^{o}F	1
	X	X	Ground Wind Velocity	Transducer	1	8 bits	0-100 mph	1
	X	X	Ground Wind Direction	Transducer	1	8 bits	0-360^{o}	1
	X	X	X-Band Radar Backscatter	Radar	1 Range Interval	16 bits	80 dB	100
	X	X	S-Band Radar Backscatter	Radar	1/Range Interval	16 bits	80 dB	100
	X	X	Rainfall (Gauges 1-10)	Rain Gauge	1 Gauge	Tip No Tip Single Bit	.01 inches Up	10
C			Spacecraft Parameters					
	X	X	20 GHz Power Monitor	S/C Telemetry	1/3 Seconds	9 bits	0-3000 MW	2
	X	X	30 GHz Power Monitor	S/C Telemetry	1/3 Seconds	9 bits	0-3000 MW	2
	X	X	Multitone Mode	S/C Telemetry	1/3 Seconds	Discrete	ON OFF	1
	X	X	CW Mode	S/C Telemetry	1/3 Seconds	Discrete	ON OFF	1
D			Experiment Status					
	X	X	Grd. Antenna Azimuth Angle	Antenna	1	4 bit - BCD	0.00^{o}-360.00^{o}	1
	X	X	Grd. Antenna Elevation Angle	Antenna	1	4 bit - BCD	0.00^{o}-90.00^{o}	1
	X	X	Greenwich Mean Time	Time Code Translator	1	36 bits	Day:Hr:Min:Sec	1
	X		20 GHz, CW Mode	Control Panel	1	Discrete	Hi Low Off	1
		X	20 GHz, Multitone Mode	Control Panel	1	Discrete	Hi Low Off	1
	X		30 GHz, CW Mode	Control Panel	1	Discrete	Hi Low Off	1
		X	30 GHz, Multitone Mode	Control Panel	1	Discrete	Hi Low Off	1
	X	X	20 GHz, Calibrate Test Mode	Control Panel	1	Discrete	Cal Test	1
	X	X	30 GHz, Calibrate Test Mode	Control Panel	1	Discrete	Cal Test	1
	X	X	S/C Beam Pointing Earth Longitude	Voice	1	4 bit - BCD	0.00^{o}-180.00^{o}	1
	X	X	S/C Beam Pointing Earth Latitude	Voice	1	4 bit - BCD	0.00^{o}-90.00^{o}	1

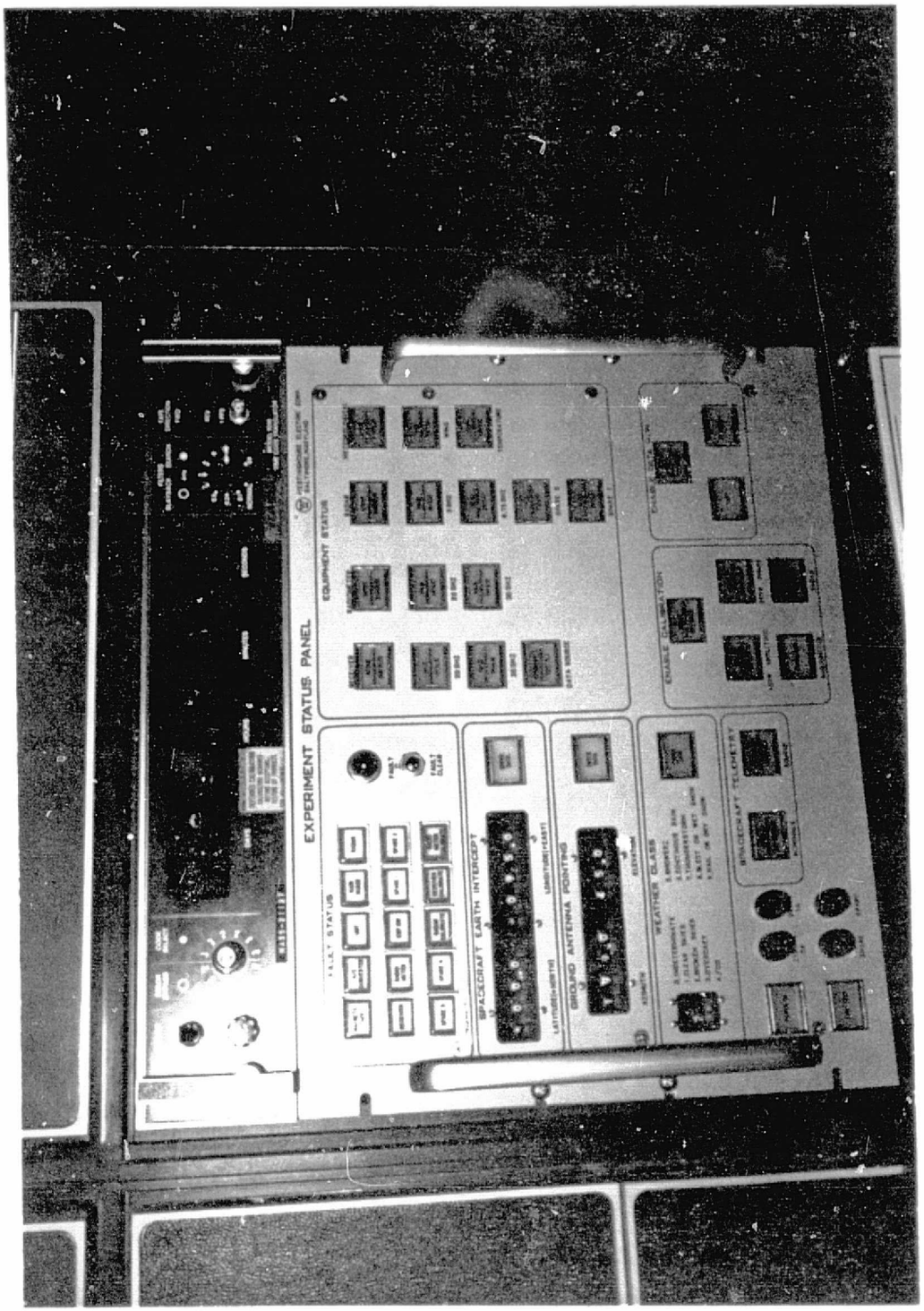

Figure 4-7. Experiment Status Panel, 'ESP'

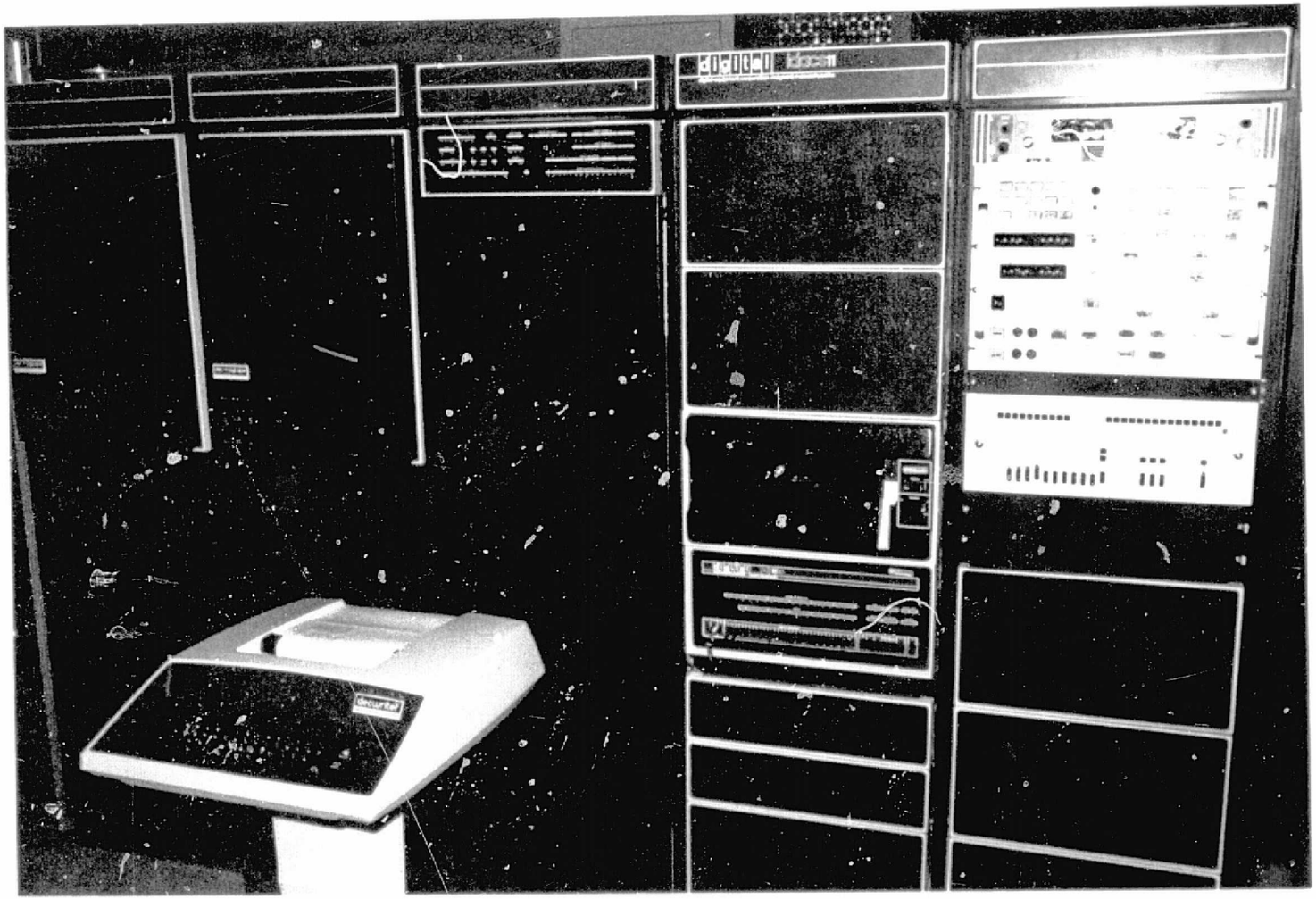

Figure 4-8. MWE Data Acquisition System, Rosman, N.C.

CENTRAL DATA PROCESSING OUTPUT DISPLAYS FOR ATS-F MILLIMETER WAVE EXPERIMENT

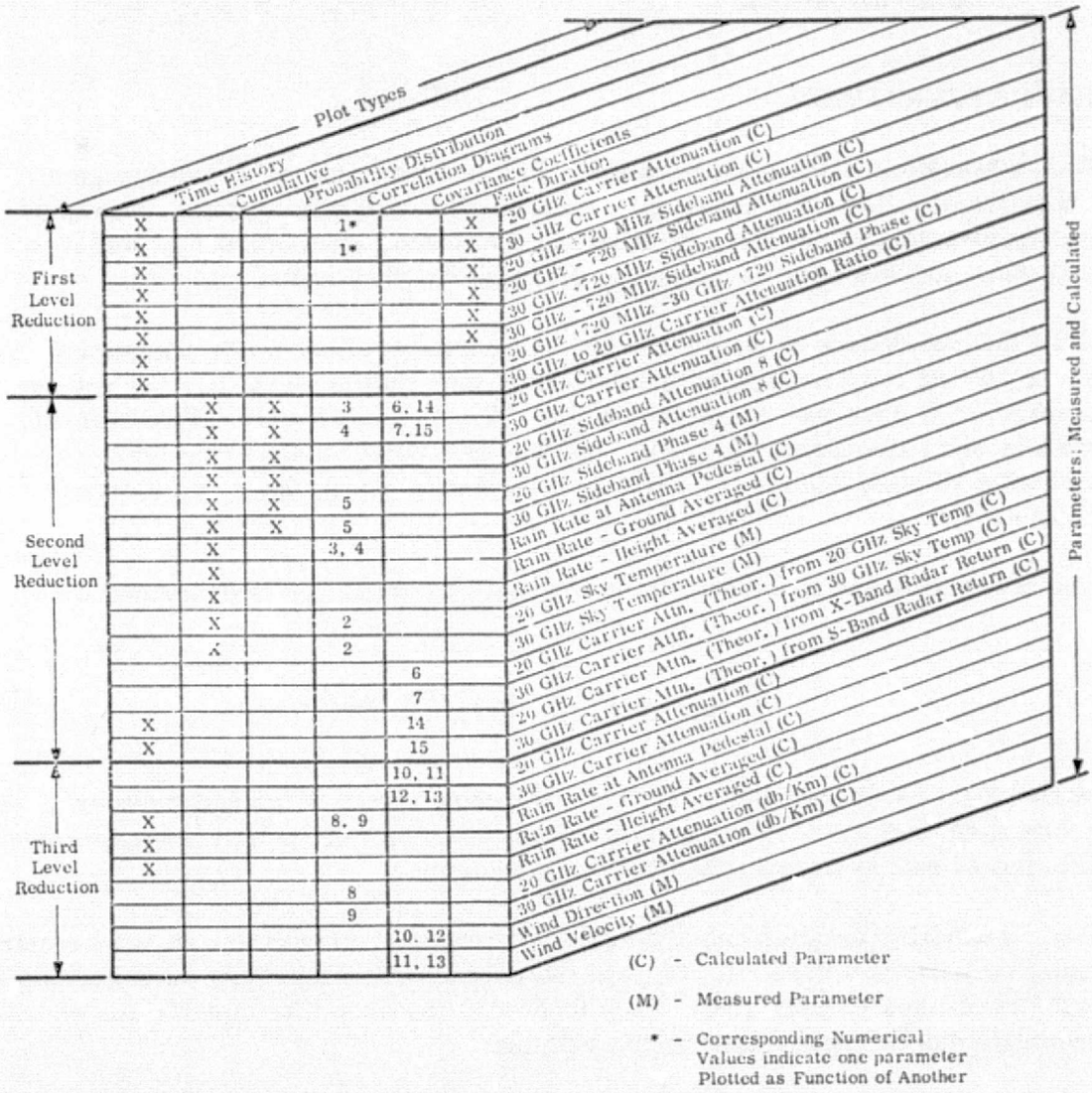

Figure 4-9. Central Data Processing Output Displays for the ATS-6 Millimeter Wave Experiment

The ground terminal at GSFC consists of a 3m parabolic antenna with manual tracking only. The GSFC receiver is similar to the Rosman unit, except that only the 20 and 30 GHz carriers can be received, and the front end does not utilize a paramp. Recording at GSFC is on analog tape and strip-chart only, with no digital processing.

RAIN ATTENUATION

Rain attenuation is the most perplexing problem encountered in the design and operation of millimeter wavelength space communications systems. Early investigators recognized the problems of rain induced attenuation, [3] and semi-empirical models were developed to describe the phenomena. [4], [5]

Over the last decade or so, direct measurements of earth-space attenuation above 10 GHz have been accomplished, first with radiometers [6], [7] and sun-trackers, [8] then with an earth satellite. [2], [9], [10], [16] More refined models were discussed, [11], [12] and the first steps in acquiring long term statistics of attenuation were begun at a number of frequencies and locations. [13-16]

The attenuation due to a distribution of spherical raindrops is described by:

$$A \frac{dB}{(km)} = 4.343 \int_0^\infty N(a)\, Q(a, \lambda)\, da \qquad (1)$$

where N (a) da is the number of drops per cubic meter with radii between a and a + da (cm), and Q (a, λ) is the attenuation cross section (m^2) of a single spherical drop of radius a (cm) at the wavelength λ (cm).

The relationship between raindrop size and rainfall rate was investigated empirically by Laws and Parsons, [17] and later distribution functions were developed by Marshall and Palmer [18]. They found that the drop size distribution measurements can be represented by the relation:

$$N(a) = N(o)\, e^{-\Lambda a} \qquad (2)$$

where N (o) is the value at zero radius, and

$$\Lambda = 82\, R^{-0.21} \qquad (3)$$

where R is the rainfall rate, in millimeters per hour.

The attenuation cross-section is calculated from the general solution of Maxwell's equations with a given refractive index of water for the wavelength of interest. Medhurst applied measured drop terminal velocities and the measured Laws and Parsons drop size distribution to calculate the attenuation coefficient for 2 to 100 GHz [5].

A simple exponential expression relating attenuation and rainfall rate, of the form

$$A \frac{(dB)}{(km)} = \alpha R^B \tag{4}$$

first proposed by Gunn and East [4], where α and B are frequency dependent constants, has shown reasonably good agreement with measured attenuation over short terrestrial paths. The attenuation coefficients for the ATS-6 MWE frequencies, assuming a Laws and Parsons drop size distribution, are:

$$A \frac{(dB)}{km} = 0.0687\ R^{1.1} \quad @20\ GHz \tag{5}$$

$$A \frac{(dB)}{km} = 0.1649\ R^{1.035} \quad @\ 30\ GHz \tag{6}$$

Figure 4-10 shows the attenuation as a function of rainfall rate, for path lengths of 1 and 5 Km. The path length is important in earth-space attenuation, and, as shown by the measured data, is a difficult parameter to define and measure.

The probability of occurrence of a given attenuation level or more precisely, the probability that the attenuation has equaled or exceeded a given level, is extremely useful in the design of systems where rain attenuation plays a significant part. A knowledge of this factor provides the basis for the power margin requirements for the link or conversely will indicate the expected outage time for a given link margin.

Attenuation distributions at 20 and 30 GHz for Rosman, N.C. during July and August 1974, the two heaviest rainfall months, are shown in Figure 4-11. For 20 GHz, the attenuation exceeded 12 dB for 0.68% of the 547 minute test time; for 30 GHz the attenuation exceeded 28 dB for 0.1% of the 492 minute test time.

The ATS-6 MWE was operated on a call-up basis during rain periods. Other experiments, primarily HET and often PLACE, had priority for operations over the MWE, hence all rain periods could not be monitored.

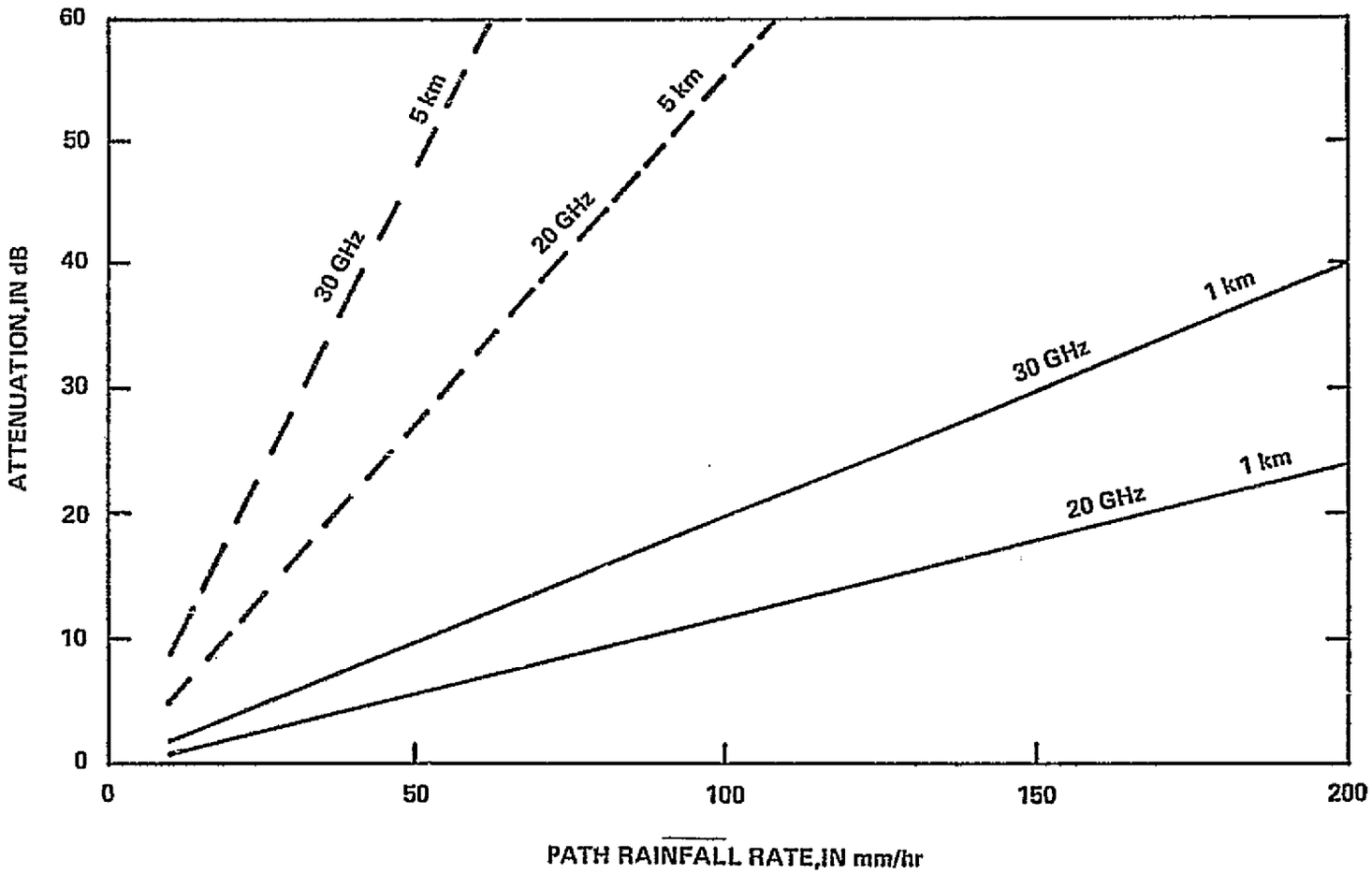

Figure 4-10. 20 & 30 GHz Attenuation, with Laws and Parsons drop-size distribution

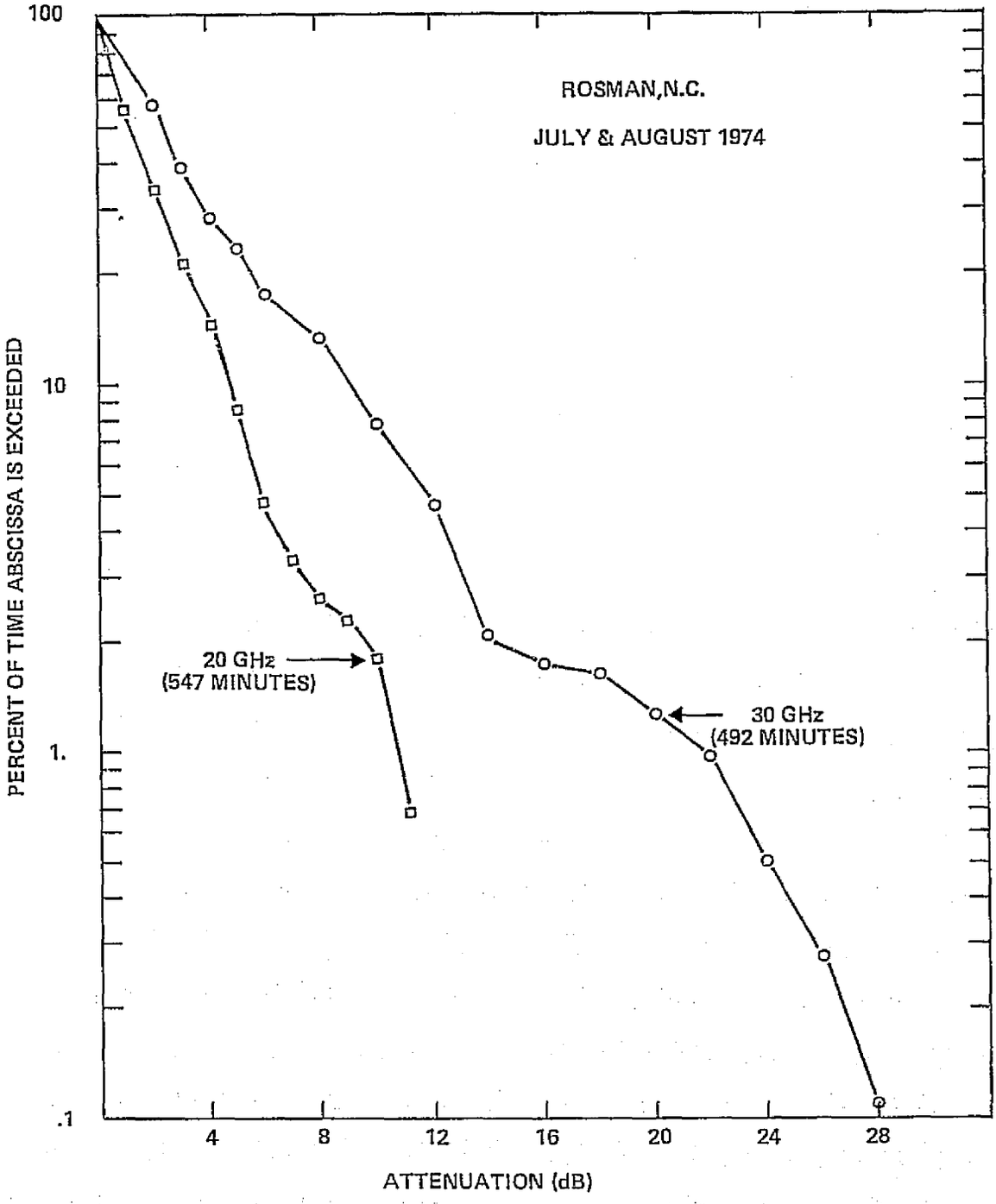

Figure 4-11. 20 & 30 GHz Attenuation Distributions for Rosman, N.C., July-August 1974

C-2

The rainrate distribution for Rosman was continuously monitored with ten raingauges located along the azimuth track of the satellite. Figure 4-12 shows the rainrate distribution for the entire two month July-August period, and for the period during which 20 and/or 30 GHz measurements were made. The distributions were measured at a raingauge co-located with the ground station antenna. The period of attenuation measurements, 600 minutes, represents 32% of the total time during July and August when rainfall greater than 1mm/hr was measured. If the attenuation measurement period is a reasonable sample of the rainrate statistics for the total two month period, an estimate of the attenuation statistics for the total two month period can then be developed. The reasonableness of this assumption is verified by superimposing the upper curve of Figure 9 on the lower curve. The similarity of the slopes of the displaced curve indicates that, up to 37 mm/hr, the attenuation measurement period was a representative sample of the rainfall statistics for the entire month.

The July-August estimate of 20 and 30 GHz attenuation can then be developed from ordered pairs of measured attenuation and rainfall rate for a given percent of time on the distribution curves given in Figures 4-11 and 4-12. This technique, similar to that described for ATS-5 measurements, [19] is developed on Figure 4-13 for the 20 GHz attenuation data. For example, the rainrate during the attenuation measurement period exceeded 30 mm/hr for 2.5% of the time, (point A). The measured attenuation for the same percentage time was about 8 dB, (point B). The rainrate exceeded 30 mm/hr for .11% of the total July-August period, (point C), therefore, the attenuation for the entire two-month period would be expected to exceed 8 dB for that same percent of time, or .11%, (point D). Using this approach a prediction curve for 20 GHz was developed where rainrate and attenuation data were available, in this case up to the 10 dB level. The 30 GHz attenuation distribution can be derived in a similar manner and is shown on Figure 4-14. The results depicted on these curves give an indication of the kinds of margins required at Rosman for the two heaviest rainfall months. For allowable outage time of ninety minutes for July-August, (.1%), then link margins of 8 dB at 20 GHz and 14 dB at 30 GHz are required. Conversely, a system with a link margin of 10 dB, could have expected outages totaling 82 minutes at 20 GHz and 196 minutes at 30 GHz. Data for the remaining months of ATS-6 operations at Rosman are presently under reduction, and similar statistics for the full eleven month period will be developed.

The duration, or length of the fade, is also an important parameter in the evaluation of rain attenuation. Figure 4-15 shows a fade duration histogram for Rosman for 931 minutes of 30 GHz measurements during July, August, September 1974 and January, February 1975.

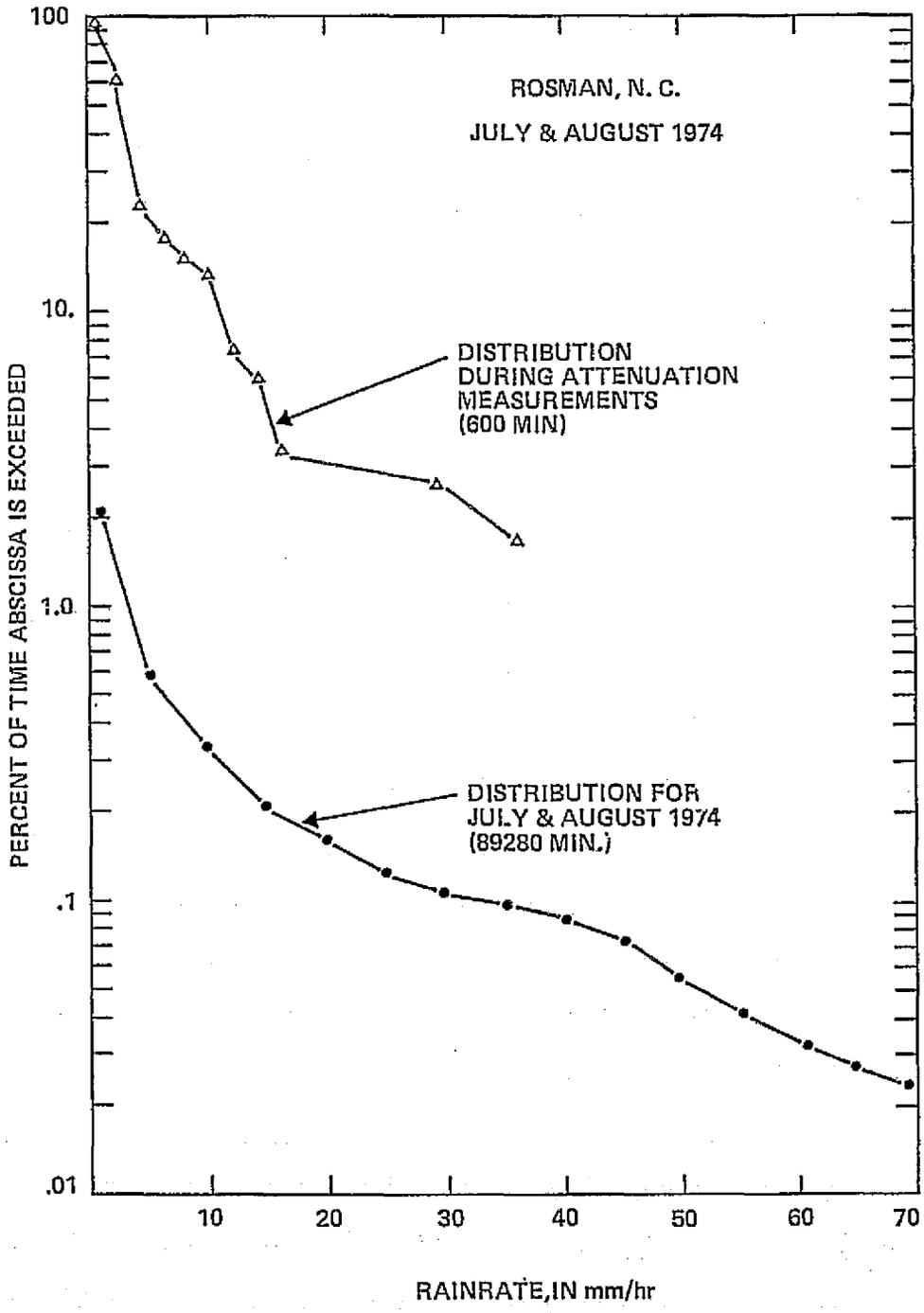

Figure 4-12. Rainrate Distributions for July and August, Rosman, N.C.

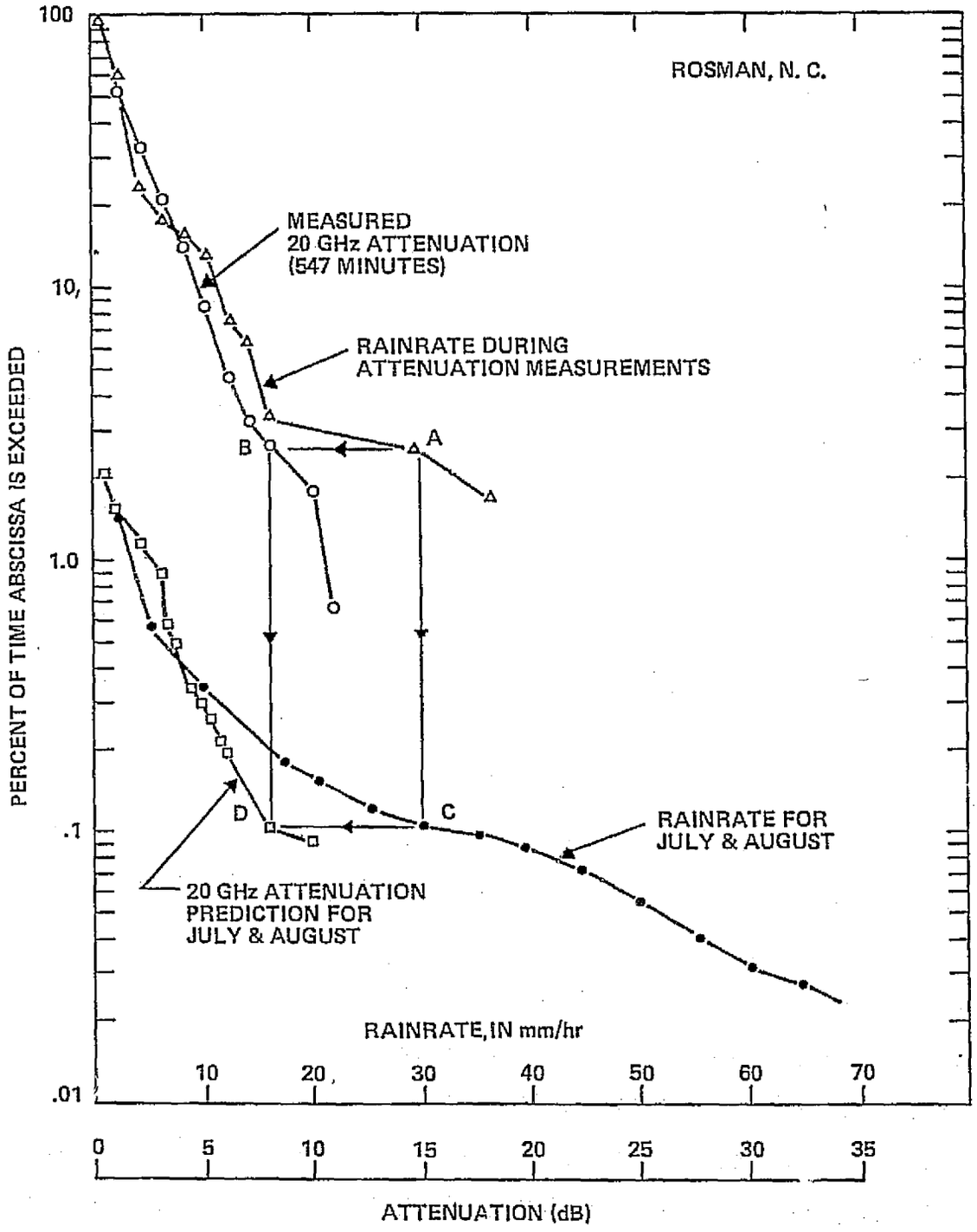

Figure 4-13. 20 GHz Attenuation Distributions for July-August

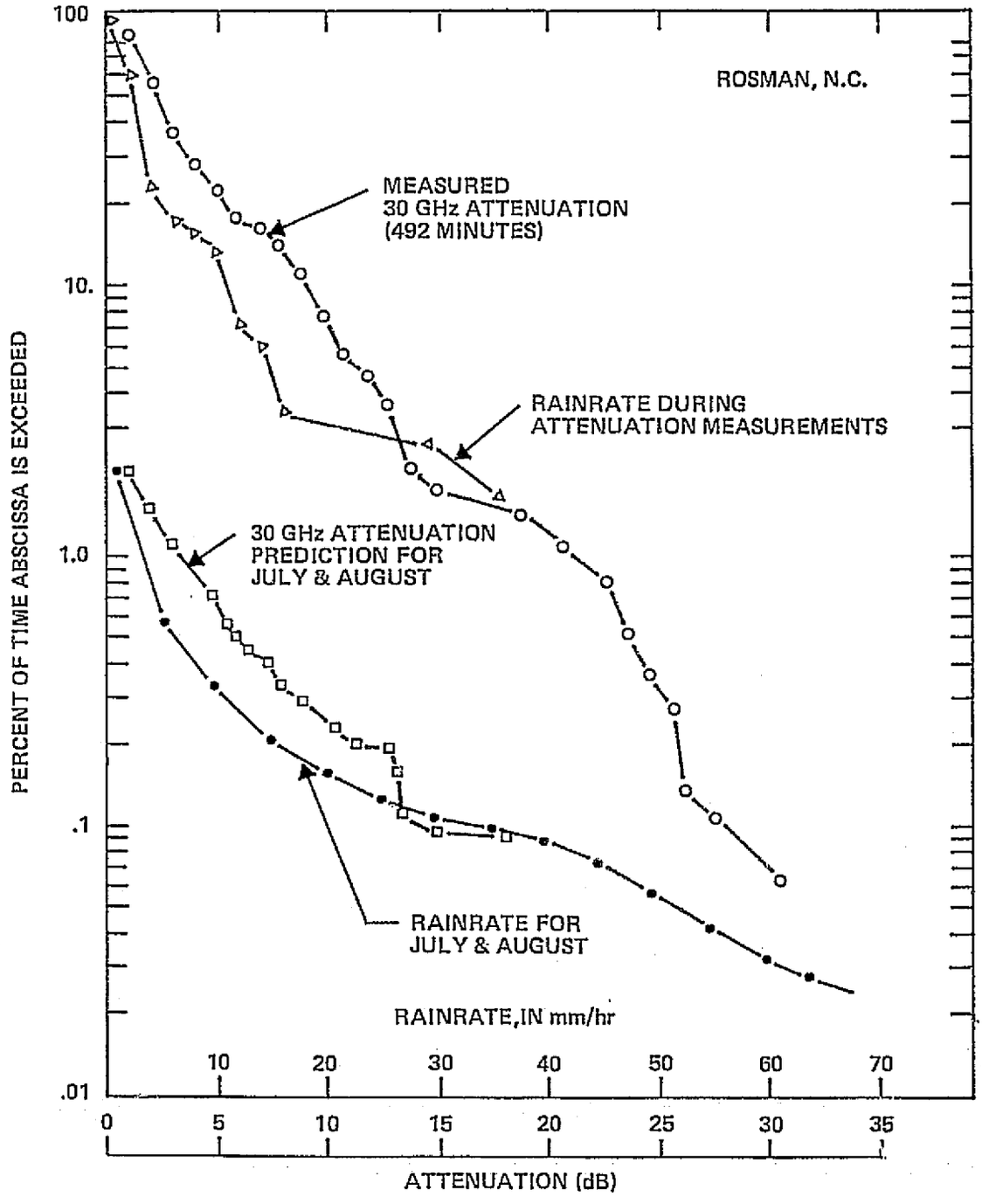

Figure 4-14. 30 GHz Attenuation Distributions for July-August

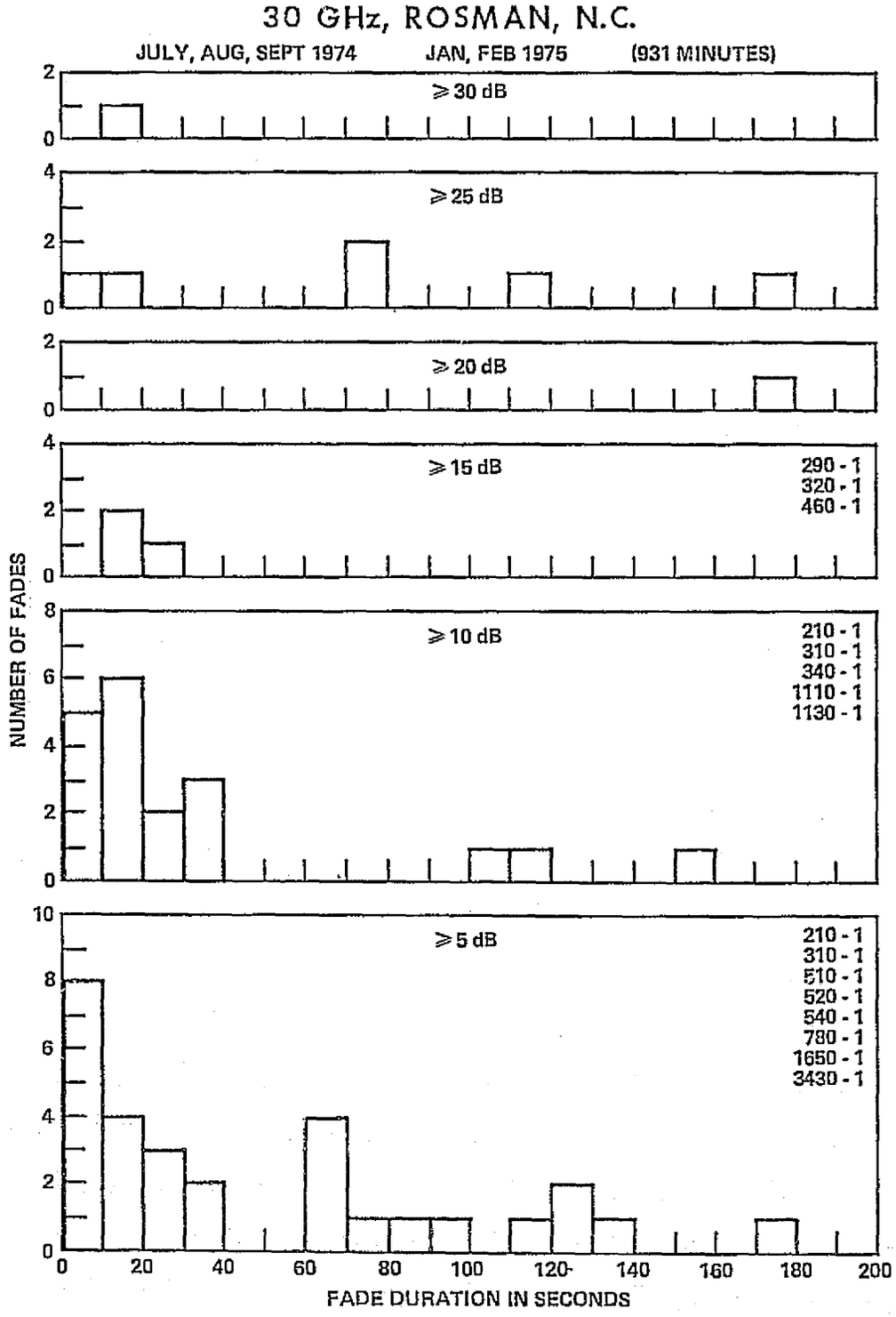

Figure 4-15. Fade Duration Histogram, Rosman, N.C., Rosman, N.C.

Fade duration data for the 30 GHz attenuation is presented in 5 dB increment steps. A ten second time bin size has been employed in these histograms. For convenience only time bins up to 200 seconds have been plotted, the higher bin values and the number of fades associated with each bin (usually one fade) are listed on each figure. As shown in Figure 4-15 a wide fade duration distribution exists for fades ≥ 5 dB. Fade durations up to 3430 seconds have been obtained. The longer duration fades are characteristic of continuous rain that exists over a long period of time. It is noticed that as the fade threshold increases the fade duration for the number of fades decreases. These shorter duration fades are characteristic (level ≥ 15 dB) of thunderstorms or periods of high intensity rainfall. A drastic decrease in the fade duration characteristics occurred between the 10 dB and 15 dB threshold level. Because of the limited amount of high attenuation data (> 20 dB) little information concerning fade duration trends can be obtained from the histograms to date.

The attenuation ratio, expressed as the ratio of attenuation at 30 GHz in dB, to the attenuation at 20 GHz in dB, is a useful parameter for a number of reasons. A knowledge of attenuation ratio characteristics could provide a means for predicting the attenuation at one frequency, given the attenuation at another. Also, attenuation ratio measurements are very sensitive to drop size distribution variations, hence an estimate of the drop size distribution could be developed. However, both of the above applications require a consistent or at least a predictable relationship between the attenuation ratio and other measured parameters.

Assuming that the attenuation varies as a power of the rainfall rate, Eqs. (5) and (6), then the attenuation ratio is

$$\frac{A_{30}(\text{dB})}{A_{20}(\text{dB})} = 2.40029\, R^{-0.06510} \tag{7}$$

A more useful expression is available by solving for R in Eq. (5) and substitute in Eq. (7). The result gives the attenuation ratio as a function of the 20 GHz attenuation:

$$\frac{A_{30}(\text{dB})}{A_{20}(\text{dB})} = 2.04860 \left(\frac{L}{A_{20}}\right)^{0.05916} \tag{8}$$

Where L is the path length, in km, and A_{20} is in dB. Note that the attenuation ratio is dependent on path length, and for a given attenuation at 20 GHz, it is not in general possible to predict the attenuation at 30 GHz, unless L is known.

Measurements of attenuation ratio with the MWE have shown that the ratio varies widely with each event, and during the event itself. Examples of attenuation ratio measurements for four rain periods at Rosman are shown in Figures 4-16, 17, 18 & 19. The dashed lines on the plots are the expected values of attenuation ratio for the given path length L. Figure 4-20 shows an example of the variation of the ratio during a fourty minute segment of the rain event on July 4. As expected, the ratio varies significantly, from 1 to 4, indicating the changing drop size and path length conditions of each event.

A more useful evaluation of attenuation ratio is accomplished by comparing the long term statistics of 20 and 30 GHz attenuation and developing a ratio for a given percent of time.

The attenuation ratio for Rosman for the July-August period, (see Figure 4-11), is shown on Figure 4-21 as the crossed-circle points. The attenuation ratio developed from the predicted curves of Figures 4-13 and 4-14 is also shown on Figure 4-21 as the solid dots. The dispersion of the ratio is reduced significantly, with ratios ranging from 1.5 to 2.1. A best fit power curve for the measurement ratios (crossed-circle points) is shown by the solid curve on Figure 4-21. The resulting curve was

$$\frac{A_{30}(dB)}{A_{20}(dB)} = 1.8755\, A_{20}^{-0.0306}, \qquad (9)$$

which is very close to the prediction curve for a constant 1 Km path length, and approaches a 1.7 ratio for large values of 20 GHz attenuation.

Measurements from other locations and seasons of the year will be compared to the above results as they become available, to determine if consistent trends in the attenuation ratio variations are observed.

SCINTILLATIONS

Rapid amplitude fluctuations, or scintillations, have been observed at Rosman, GSFC, and at other participating sites [20]. The amplitude scintillations have been observed at both 20 and 30 GHz, and in clear and rainy weather conditions. Figure 4-22 shows an example of 20 GHz atmospheric scintillations during an overcast day at GSFC. The scintillation amplitude increased from about .5 dB to 3 dB, peak to peak, during the passage of a cloud through the earth-satellite path. The fluctuation rate was fairly constant, at about 16 cycles per minute, or 0.27 Hz. The scintillations lasted for about 200 seconds, then settled back to the initial levels.

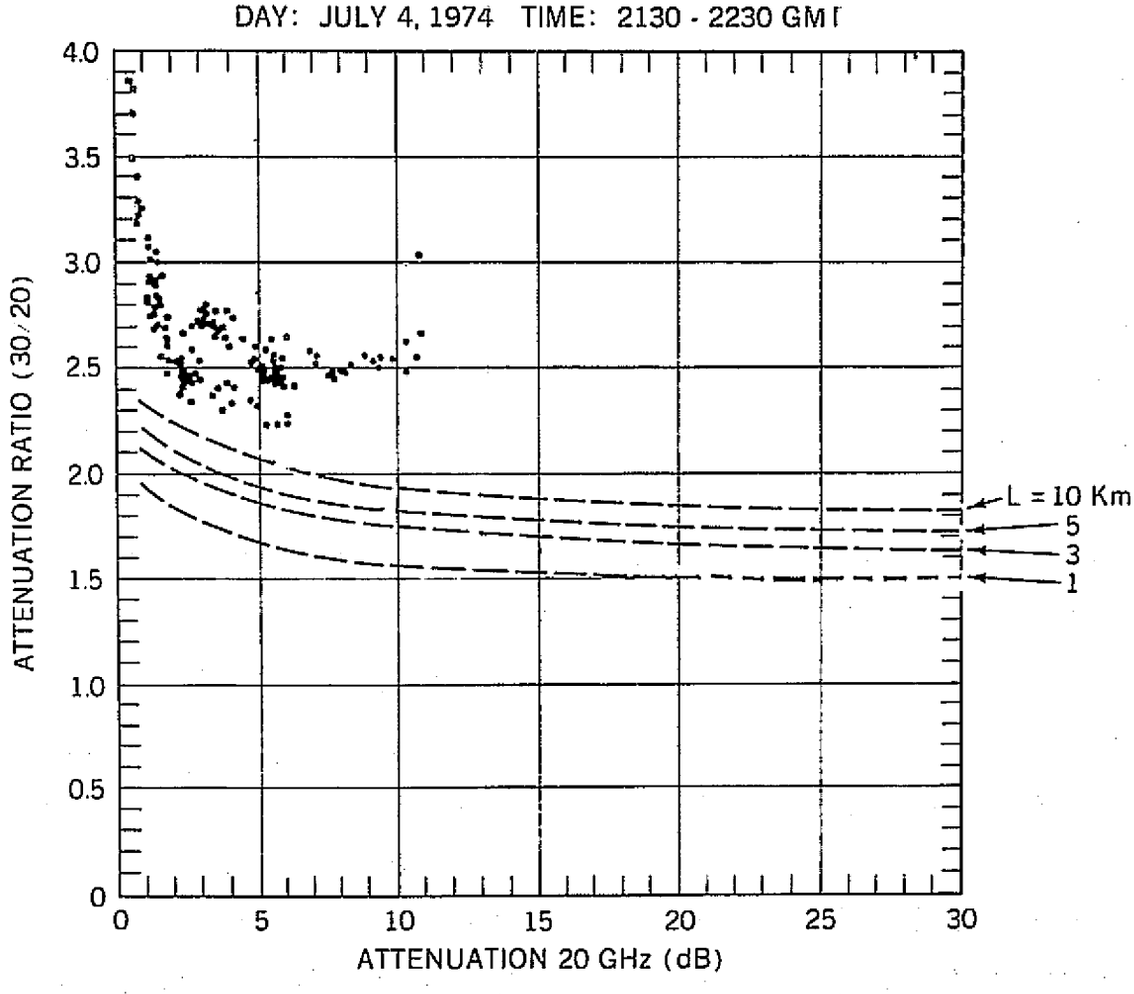

Figure 4-16. Attenuation Ratio Measurements, Rosman, N.C.

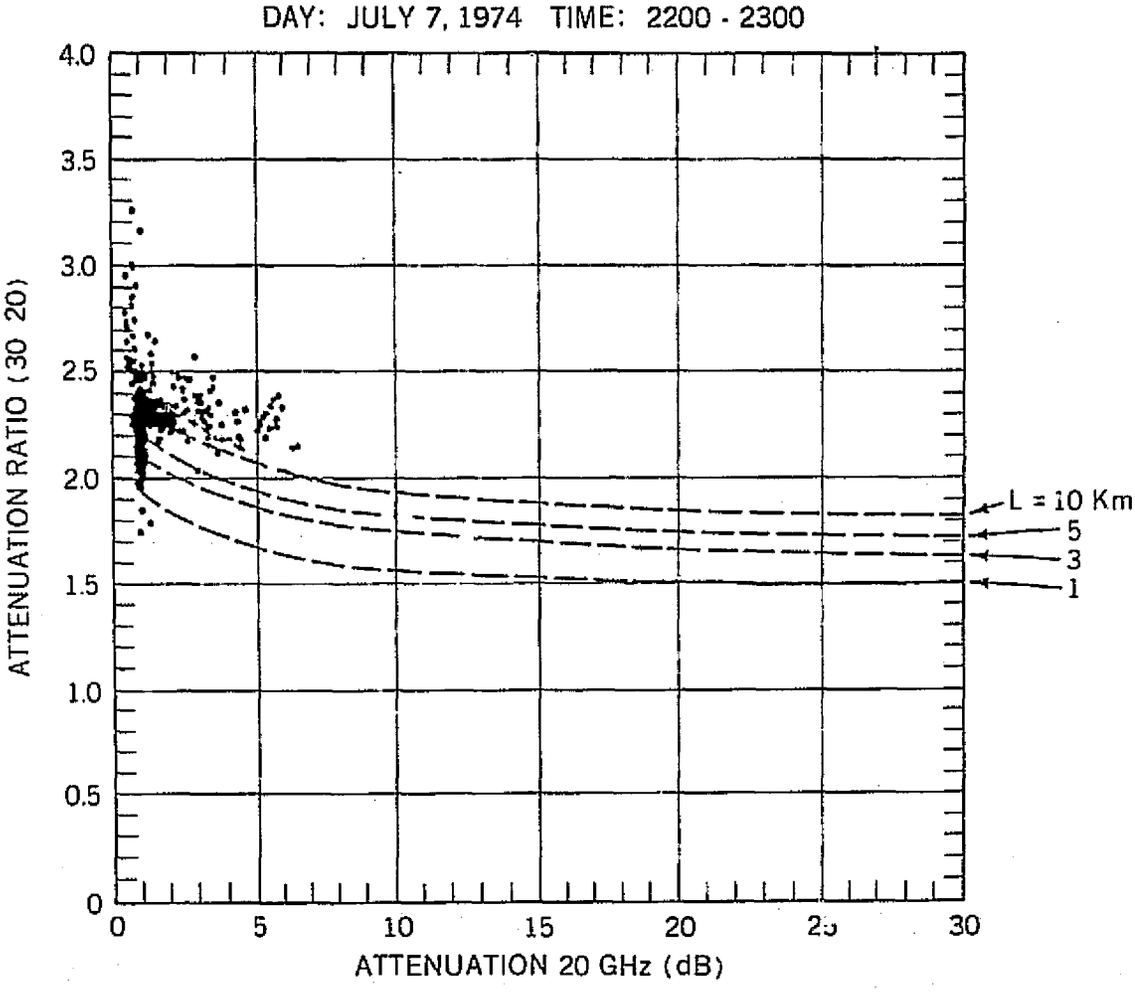

Figure 4-17. Attenuation Ratio Measurements, Rosman, N.C.

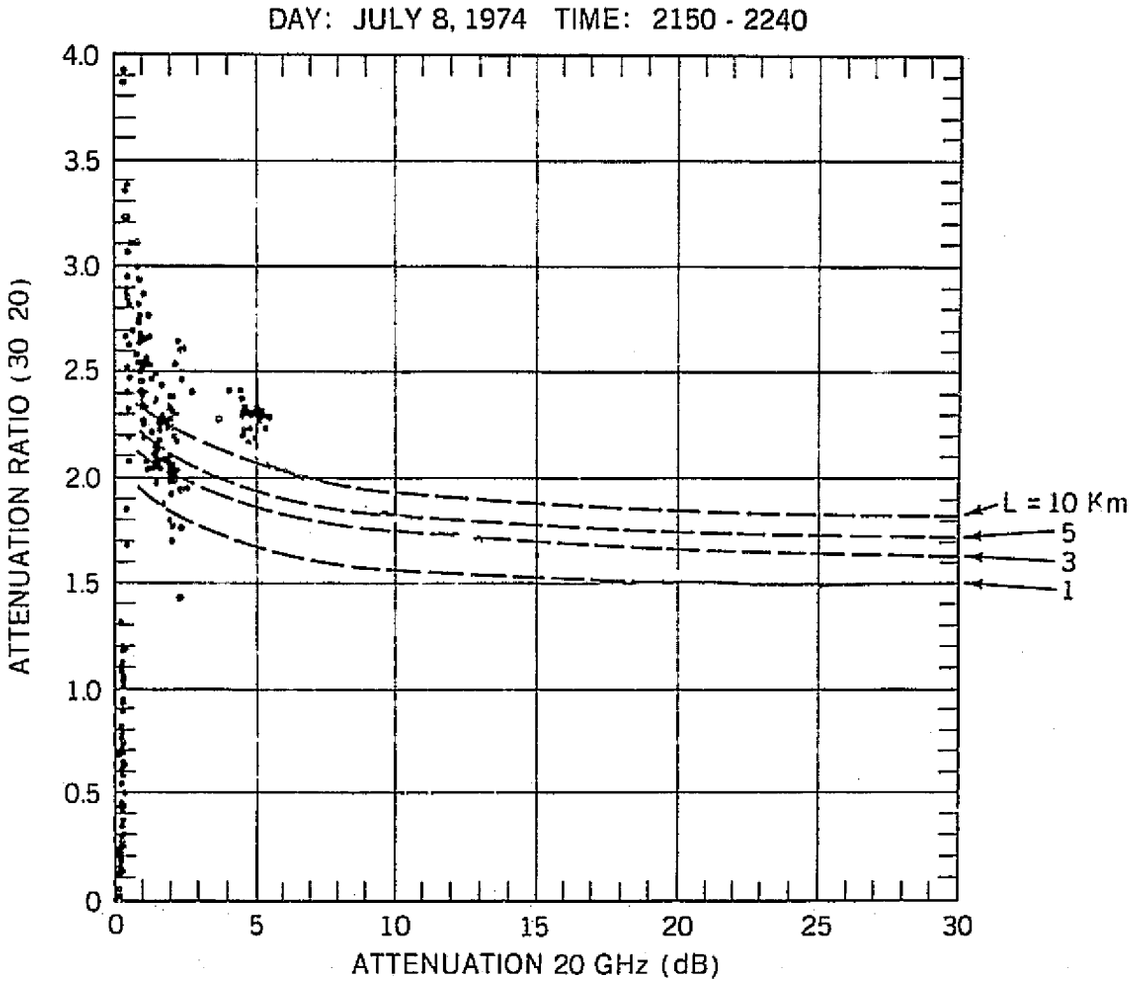

Figure 4-18. Attenuation Ratio Measurements, Rosman, N.C.

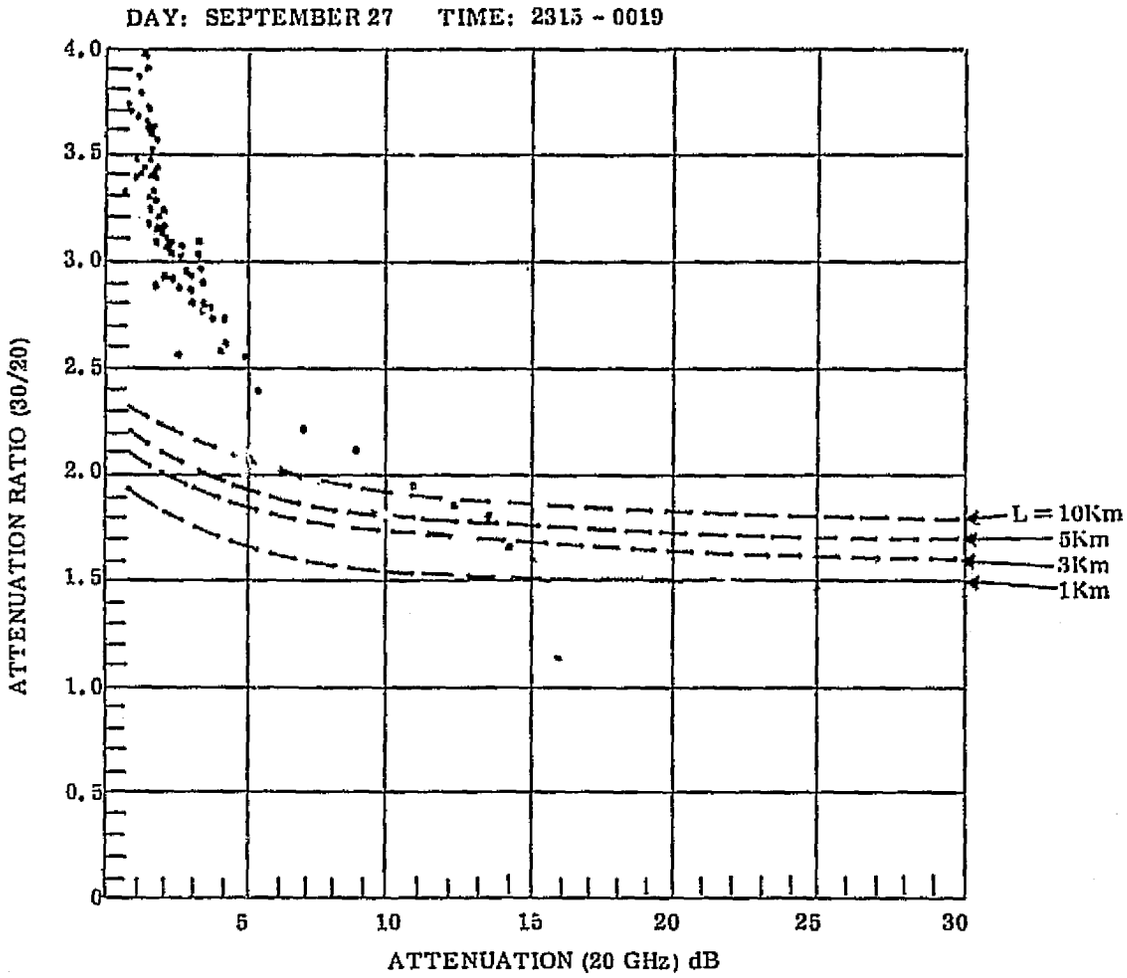

Figure 4-19. Attenuation Ratio Measurements, Rosman, N.C.

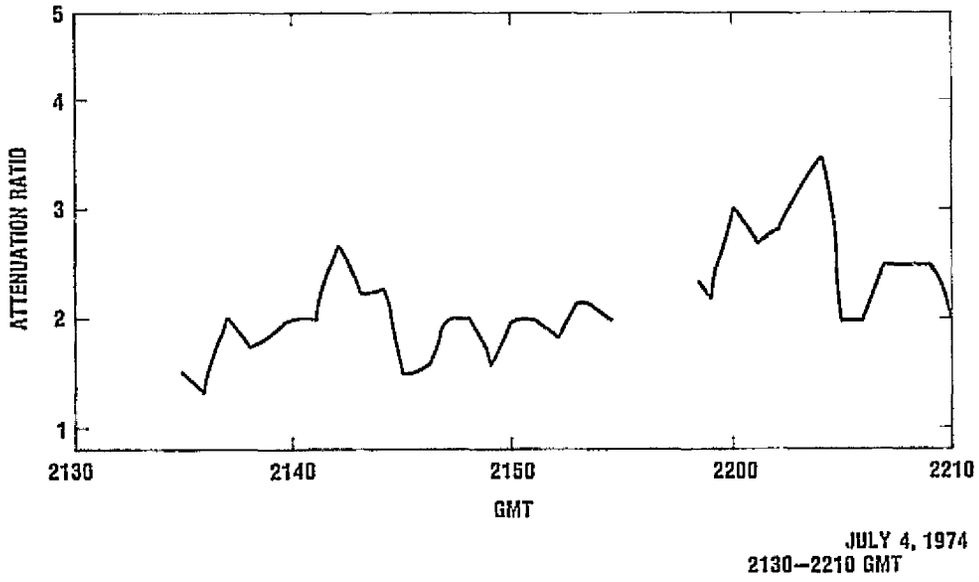

Figure 4-20. Attenuation Ratio Time Plot

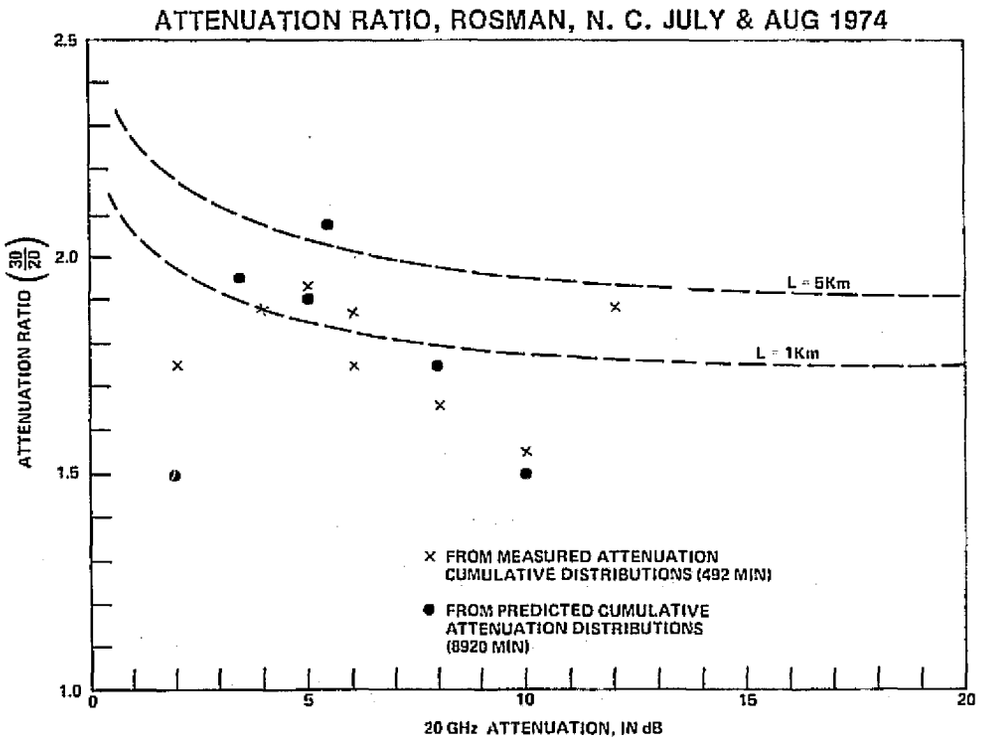

Figure 4-21. Attenuation Ratio from Attenuation Statistics

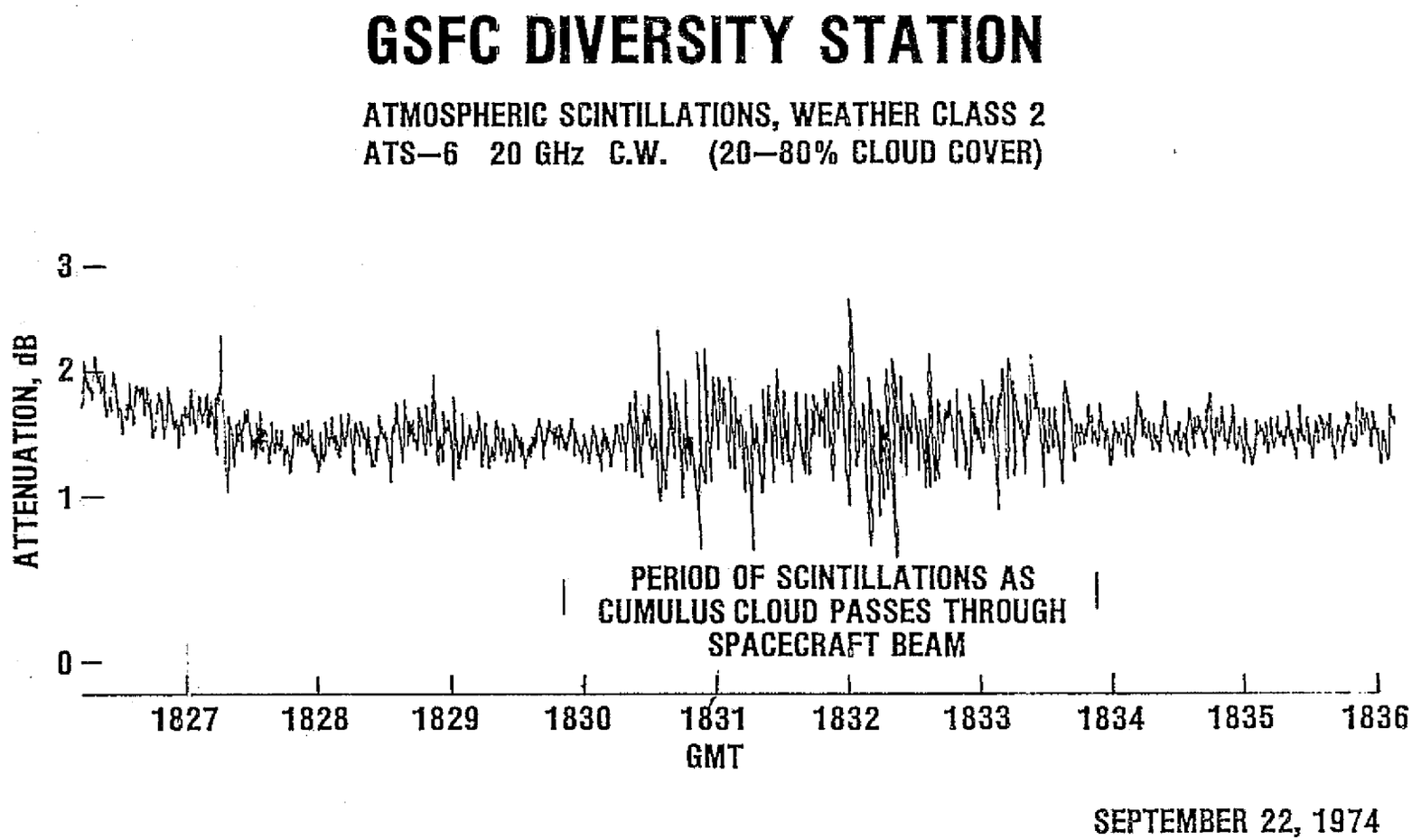

Figure 4-22. Amplitude Scintillations During Cloud Movement, GSFC

Examples of scintillations observed on a clear, cloudless day are shown in Figure 4-23. The three events occurred within a fifteen minute period, and each consisted of a short burst of rapid amplitude scintillations which reached peak to peak amplitudes of 3 dB. The fluctuation rate appeared to be about 200 Hz., and each lasted from 0 to 20 seconds. The scintillations were not caused by man-made sources, such as passing aircraft or nearby radar transmissions. The spectra of the scintillations, observed with a high resolution spectrum analyser, are shown in Figure 4-24. The spectra of the three bursts do not appear similar, however, most of the energy appears to be below 50 Hz.

The cause or causes of scintillations of the types observed are not immediately evident. Clear air turbulence has been suggested as a possible source. Additional data from other locations are available and are under study.

BANDWIDTH COHERENCE

The wideband frequency characteristics of the 20 and 30 GHz space channel were evaluated in the multitone mode of the MWE. In this mode, a carrier and 8 equally spaced side-tones are transmitted in the 20 and 30 GHz bands. A comb of nine tones is generated, four on either side of the carrier, spaced 180 MHz apart, resulting in a total spectrum of 1440 MHz in each band. The measurements consist of the amplitude of each tone (eighteen total) and the relative differential phase between sideband pairs (eight total pairs).

The amplitudes of the side-tones are adjusted by the modulation index to be approximately equal, and all eighteen tones are calibrated by the automated receiver calibration system, described above. The relative differential phase output voltage, V_ϕ, is proportional to:

$$(\phi_u - \phi_c) + (\phi_L - \phi_c) \qquad (10)$$

where ϕ_u, ϕ_L, ϕ_c, are the phases of the upper tone, lower-tone, and carrier, with respect to an arbitrary reference. This function provides a measure of the linearity of the channel frequency-phase characteristics. In an ideal linear system, V_ϕ would be zero, however, system noise and bandwidth limitations in a practical system cause a residual value for V_ϕ. Because of the sensitive nature of this measurement, all phase outputs were calibrated for each data run, at three input levels, and both with and without the parametric amplifier in the system. Nevertheless, the relative phase measurements were found to be extremely difficult to maintain, and only sparse data is available.

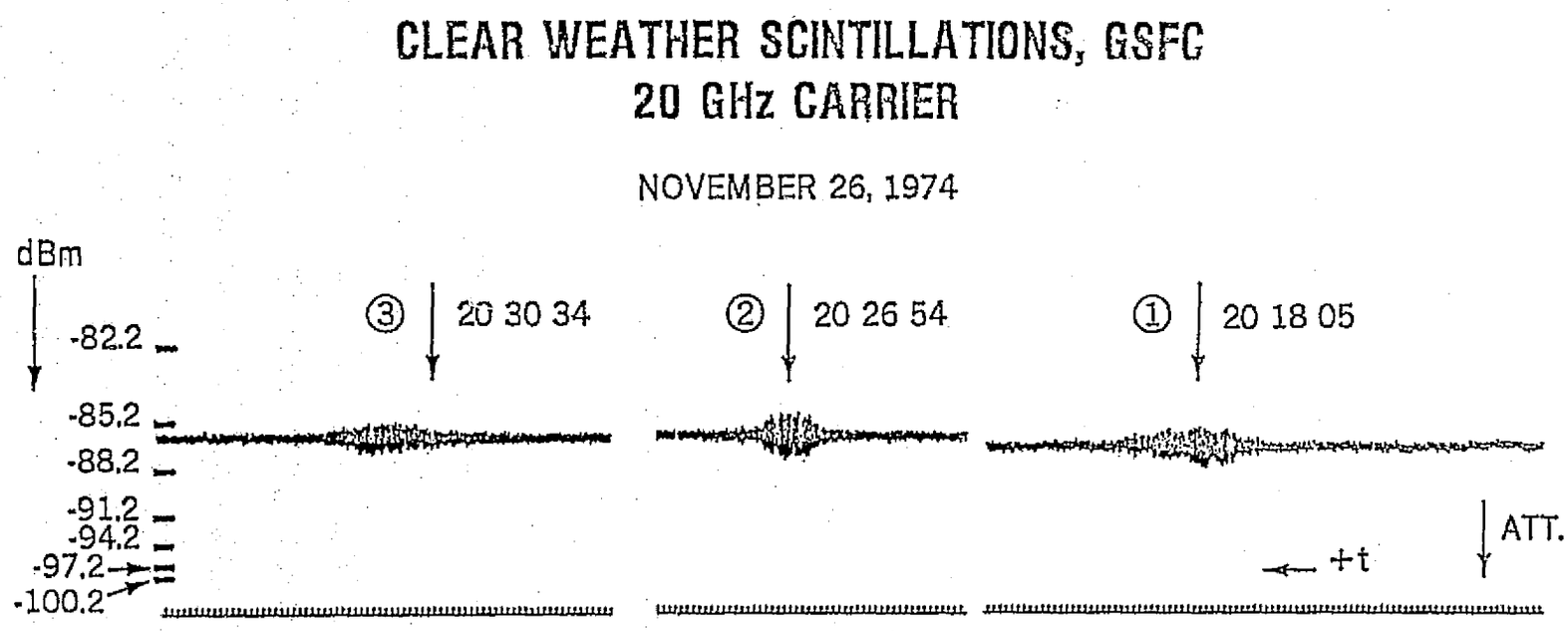

Figure 4-23. Clear Weather Scintillations, GSFC

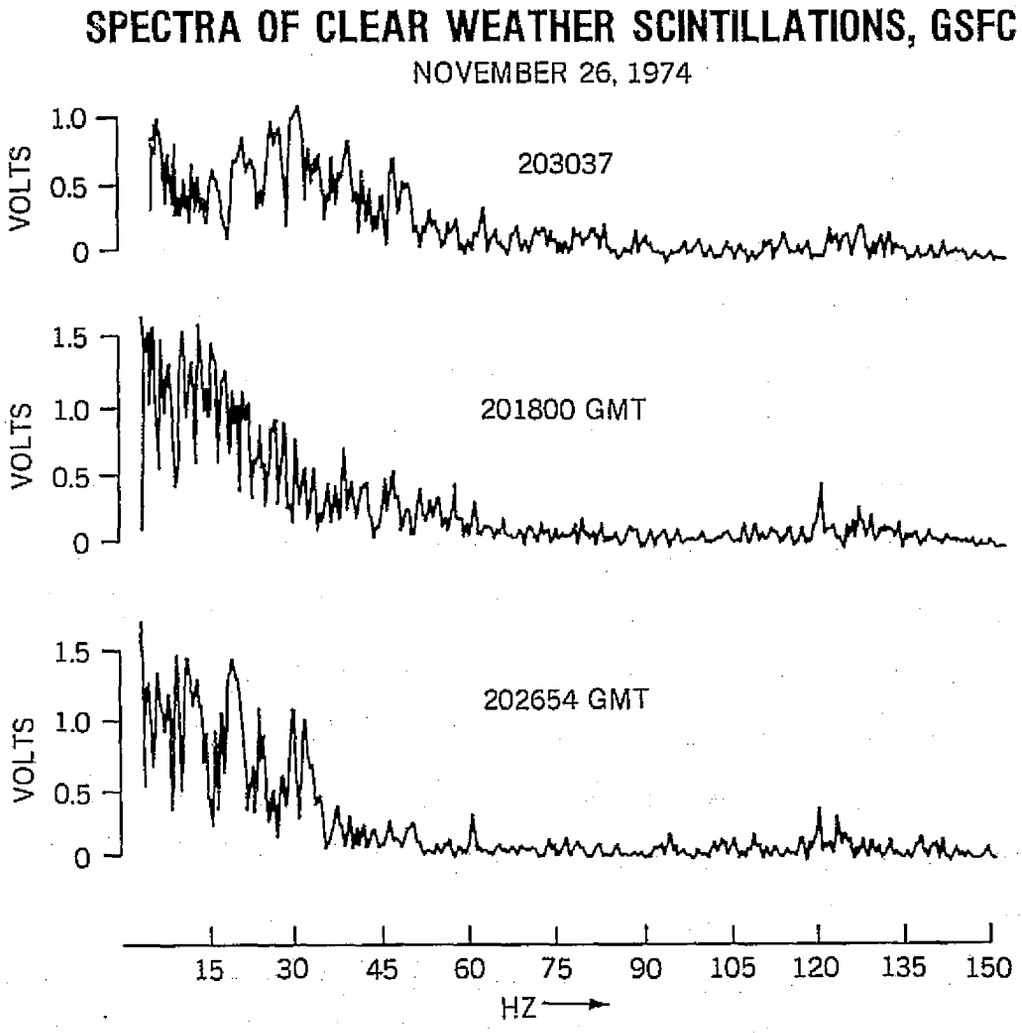

Figure 4-24. Spectra of Clear Weather Scintillations, GSFC

In the vast majority of measurement periods, the amplitude variations of the sidetones, when compared to the carrier variations, were within the system measurement accuracy of ±1 dB. The measurements were made by comparing one second averages of each amplitude, with a sampling rate of forty per second. An example of a period where some selective amplitude fading was observed is shown in Table 4-2. Each line on the table represents a four second average value of the 20 and 30 GHz carrier attenuations, in dB, and the side-tone differential attenuation, also expressed in dB. The time scale, starting at 20 minutes 0 seconds, and progressing to 24 minutes 28 seconds, is shown on the left column of the table. Three different segments, each thirty-six seconds long, are shown. During the first two segments, the side tone differential attenuation values remained within the measurement accuracy. During the last segment, however, the 30 GHz carrier attenuation began to exceed 20 dB, and the outer side-tones, ±720, exhibited variations of up to 6.9 dB.

At these high attenuation values, however, the measurement accuracy could be degraded above the ±1 dB value by receiver noise and the reduction in dynamic range of the receiver output voltage. These factors are considered to be the main causes in the amplitude variations observed, rather than a selective fading effect caused by rain scattering and absorption in the channel.

An example of the 20 GHz differential phase fluctuations during a rain event is shown in Figure 4-25. The solid lines are minutely averages and the dots are the minutely variance values for each plot. The +720 (20.72 GHz) and -720 (19.28 GHz) sidetone amplitudes are shown, along with the relative differential phase between the two sidetones, referenced to an arbitrary value. The phase fluctuations show some correlation with the amplitude fluctuations for the second attenuation peak. Also, the variance of the phase measurement remained at about 4°, which is the sensitivity of the measurement. A total phase variation of about 30° occurred during the measurement period.

The examples of amplitude and phase variations given above were developed from one-second average digital records of the data. Thus they would detect "long-term" or slow fluctuations in the measured data, but would be insensitive to rapid fluctuations and scintillation which may be present. The short term channel characteristics of the MWE data observed at Rosman and GSFC are under analysis with analog multichannel recordings and a special purpose correlator/spectrum analyzer developed for the ATS-5 Millimeter Wave Experiment. Estimates of the channel time-frequency transfer function, and important parameters such as coherence bandwidth, coherence time, fading bandwidth are developed. The initial analysis of this data is proceeding and will be reported as results are available.

Table 4-2
Multitone Amplitude Variations, Rosman, N.C., September 27, 1975

		20 GHz									30 GHz								
MM	SS	-720	-540	-360	-180	CARR	+180	+360	+540	+720	-720	-540	-360	-180	CARR	+180	+360	+540	+720
20	0	0.5	0.5	0.5	0.5	0.0	0.5	0.5	0.5	0.6	1.1	1.1	1.0	1.2	0.3	1.2	1.2	1.2	1.3
20	4	0.5	0.5	0.5	0.5	0.0	0.5	0.5	0.5	0.5	1.1	1.1	1.1	1.2	0.3	1.2	1.2	1.1	1.2
20	8	0.7	0.7	0.7	0.7	0.0	0.7	0.7	0.6	0.7	1.1	1.1	1.1	1.3	0.4	1.2	1.2	1.1	1.3
20	12	0.7	0.7	0.7	0.6	0.0	0.7	0.7	0.7	0.7	1.1	1.1	1.0	1.2	0.4	1.2	1.3	1.2	1.4
20	16	0.7	0.7	0.7	0.6	0.0	0.7	0.7	0.6	0.7	1.2	1.1	1.1	1.2	0.4	1.2	1.2	1.2	1.4
20	20	0.8	0.8	0.7	0.7	0.0	0.8	0.8	0.7	0.7	1.1	1.1	1.0	1.2	0.7	1.2	1.3	1.2	1.4
20	24	0.9	0.8	0.8	0.8	0.0	0.9	0.9	0.8	1.0	1.1	1.1	1.1	1.3	0.8	1.2	1.3	1.3	1.5
20	28	0.8	0.7	0.7	0.7	0.0	0.8	0.8	0.7	0.7	1.1	1.1	1.1	1.3	0.7	1.2	1.3	1.3	1.5
20	32	0.9	0.9	0.9	0.9	0.0	0.9	0.9	0.8	1.0	1.1	1.0	1.0	1.2	1.1	1.2	1.2	1.3	1.4
20	36	0.8	0.9	0.8	0.7	0.0	0.8	0.8	0.8	0.9	1.0	0.9	1.0	1.2	1.1	1.2	1.2	1.3	1.3
22	40	0.9	1.2	1.0	0.9	2.4	1.2	1.1	1.2	1.3	0.7	0.9	0.9	1.1	6.8	1.2	1.1	1.0	0.8
22	44	1.0	1.2	1.0	0.9	2.5	1.2	1.1	1.2	1.5	0.6	0.8	0.7	1.1	7.3	1.1	1.1	0.8	0.7
22	48	1.0	1.2	1.0	0.9	2.8	1.2	1.1	1.2	1.5	0.5	0.6	0.5	1.2	8.0	0.9	1.0	0.6	0.4
22	52	1.0	1.3	1.0	0.9	3.2	1.2	1.1	1.3	1.4	0.1	0.2	0.1	0.9	8.8	0.6	0.8	0.2	-0.0
22	56	1.1	1.4	1.0	0.9	3.2	1.2	1.2	1.3	1.5	0.1	0.2	0.1	0.9	9.0	0.5	0.8	0.2	-0.2
23	0	1.0	1.3	1.0	0.8	3.5	1.1	1.1	1.2	1.5	-0.3	-0.2	-0.4	0.6	9.7	0.1	0.3	-0.3	-0.5
23	4	1.0	1.3	1.0	0.7	3.4	1.1	1.1	1.3	1.5	-0.1	-0.1	-0.2	0.7	9.4	0.3	0.6	-0.1	-0.5
23	8	1.1	1.3	0.9	0.7	3.6	1.1	1.1	1.3	1.5	-0.3	-0.2	-0.3	0.6	9.7	0.1	0.4	-0.2	-0.6
23	12	0.9	1.3	1.0	0.7	3.7	1.1	1.1	1.2	1.3	-0.5	-0.4	-0.4	0.4	10.0	-0.1	0.2	-0.4	-0.9
23	16	1.0	1.4	1.0	0.8	3.4	1.2	1.1	1.4	1.5	-0.0	0.1	0.0	0.8	9.1	0.5	0.7	0.1	-0.4
23	52	0.9	1.3	1.1	0.6	6.7	1.2	1.2	1.3	1.5	-0.8	0.0	0.0	0.7	14.5	0.9	0.3	0.5	-0.6
23	56	0.7	1.3	1.0	0.4	7.2	1.0	1.0	1.3	1.6	-0.5	0.5	0.5	1.3	15.3	1.1	1.0	1.0	-0.8
24	0	0.6	1.3	1.0	-0.0	8.2	0.6	0.6	1.2	1.3	-1.2	0.1	-0.1	0.6	17.3	0.9	0.6	0.4	-2.2
24	4	0.9	1.3	1.0	-0.4	9.3	0.1	0.1	1.1	0.8	-1.5	-0.1	-0.4	0.7	19.4	0.5	0.5	-0.0	-3.3
24	8	0.8	1.2	1.0	-0.7	10.0	-0.2	-0.3	0.9	0.5	-2.0	-0.5	-1.0	-0.1	20.8	0.0	0.0	-0.4	-4.7
24	12	0.4	0.8	0.6	-1.2	10.7	-0.7	-0.7	0.6	0.0	-2.4	-0.0	-0.6	-0.1	21.6	0.1	-0.2	-1.2	-5.1
24	16	0.2	0.7	0.4	-1.5	11.3	-1.0	-1.0	0.3	-0.2	-2.1	0.2	-0.9	0.1	21.9	0.6	-0.3	-0.7	-5.1
24	20	0.0	0.5	0.2	-1.7	11.6	-1.2	-1.3	0.1	-0.4	-2.5	-0.1	-0.9	0.1	22.6	-0.7	-0.5	-1.5	-5.8
24	24	-0.0	0.5	0.1	-1.9	12.0	-1.4	-1.5	0.0	-0.7	-2.5	-0.0	-0.8	-0.3	23.1	-0.1	0.0	-1.7	-6.3
24	28	-0.2	0.2	-0.0	-2.1	12.4	-1.2	-1.8	-0.3	-0.9	-2.4	-0.5	-1.0	-0.0	23.5	-0.6	-0.4	-1.9	-6.9

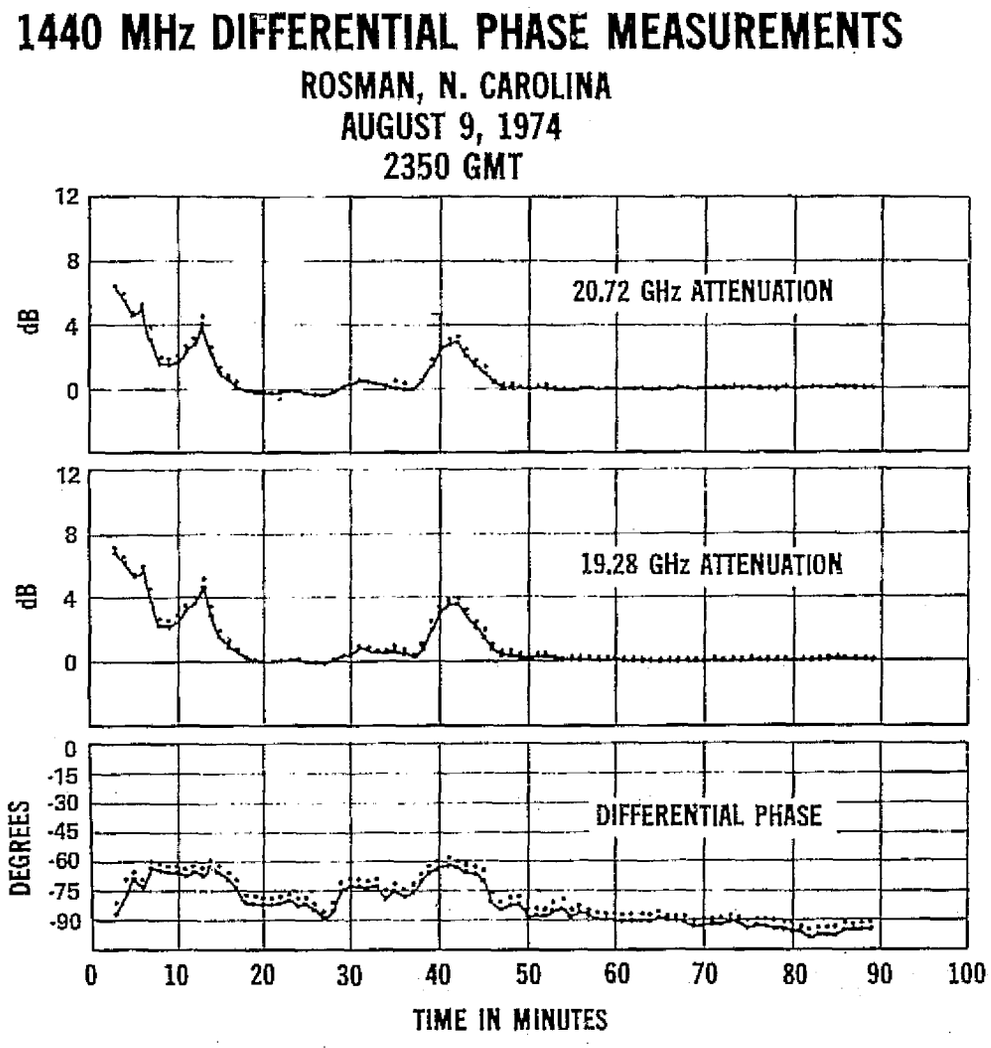

Figure 4-25. 1440 MHz Differential Phase Measurements, Rosman, N.C., August 9, 1974

COMMUNICATIONS TESTS

The ATS-6 MWE provided the first operational millimeter wavelength communications link from an orbiting satellite. A 40 MHz noise bandwidth channel, 6 GHz up, 20, 30, and 4 GHz down, was used extensively for both analog and digital test transmissions.

The first successful color video transmitted through a millimeter wave space link was demonstrated at Rosman on July 12, 1974, with signal to noise ratios of 31.5 dB at 20 GHz, and 36.5 dB at 30 GHz. Video quality was good and compared favorably with the 4 GHz downlink. Numerous attempts were made to observe video signal degradation during heavy rain at Rosman, but all were unsuccessful. The complexity of the uplink-downlink operations required all video tests to be pre-scheduled, and only light rains occurred during the test periods.

Digital video tests using a variable bit rate quadraphase modem were implemented in March 1975 at Rosman. Examples of 20, 30, and 4 GHz digital measurements are shown on Figure 4-26. During this clear weather four hour test a known code was transmitted to ATS-6 and the bit error rate (BER) for the three downlinks plotted. The BER for the closed loop (no satellite) is shown by the dashed line and solid points. When the satellite link was introduced in the system, the BER for the 20 and 30 GHz links had a negligible degradation from the closed loop calibration. No digital rain measurements were available, however, rain attenuation was simulated by rotating the ground antenna polarization during a digital transmission. The results showed that the modem performed as expected with reduced input signal to noise ratios up to 3 dB [21].

ATTENUATION PREDICTION FROM RAIN GAUGES AND RADARS

In addition to direct attenuation measurements, extensive correlative measurements using rain gauges and meteorological radars were implemented at Rosman for the investigation and validation of attenuation prediction techniques [1].

A dual frequency on-beam radar, co-located with the Rosman receiver terminal, was directed along the earth-satellite path to ATS-6. A set of ten tipping bucket rain gauges was deployed along the aximuth track of the earth-satellite path, out to a distance of 2.5 Km. The major characteristics of the radar and rain gauge systems are summarized on Figure 4-27. Figure 4-28 shows the radar antennas, and Figure 4-29 shows a rain gauge in the field. The on-beam radars, at 8.75 GHz and 3.0 GHz, have a range-gated resolution increment of 100 meters along the path, with a range of 25.6 Km. The radar return power is a function of the drop size distribution and can be related directly to the attenuation at 20 or 30 GHz through

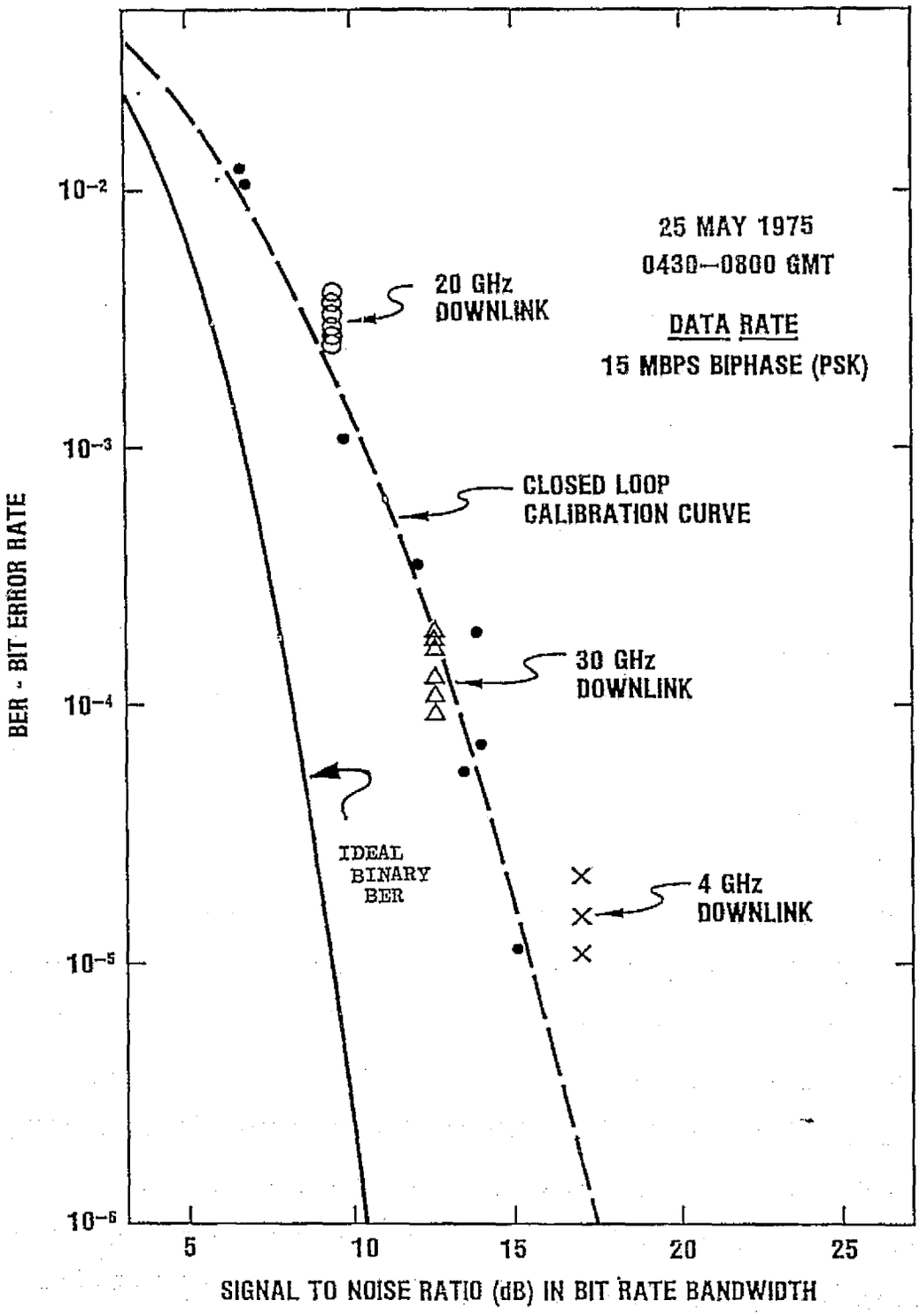

Figure 4-26. ATS-6 Digital Communications Link Measurements

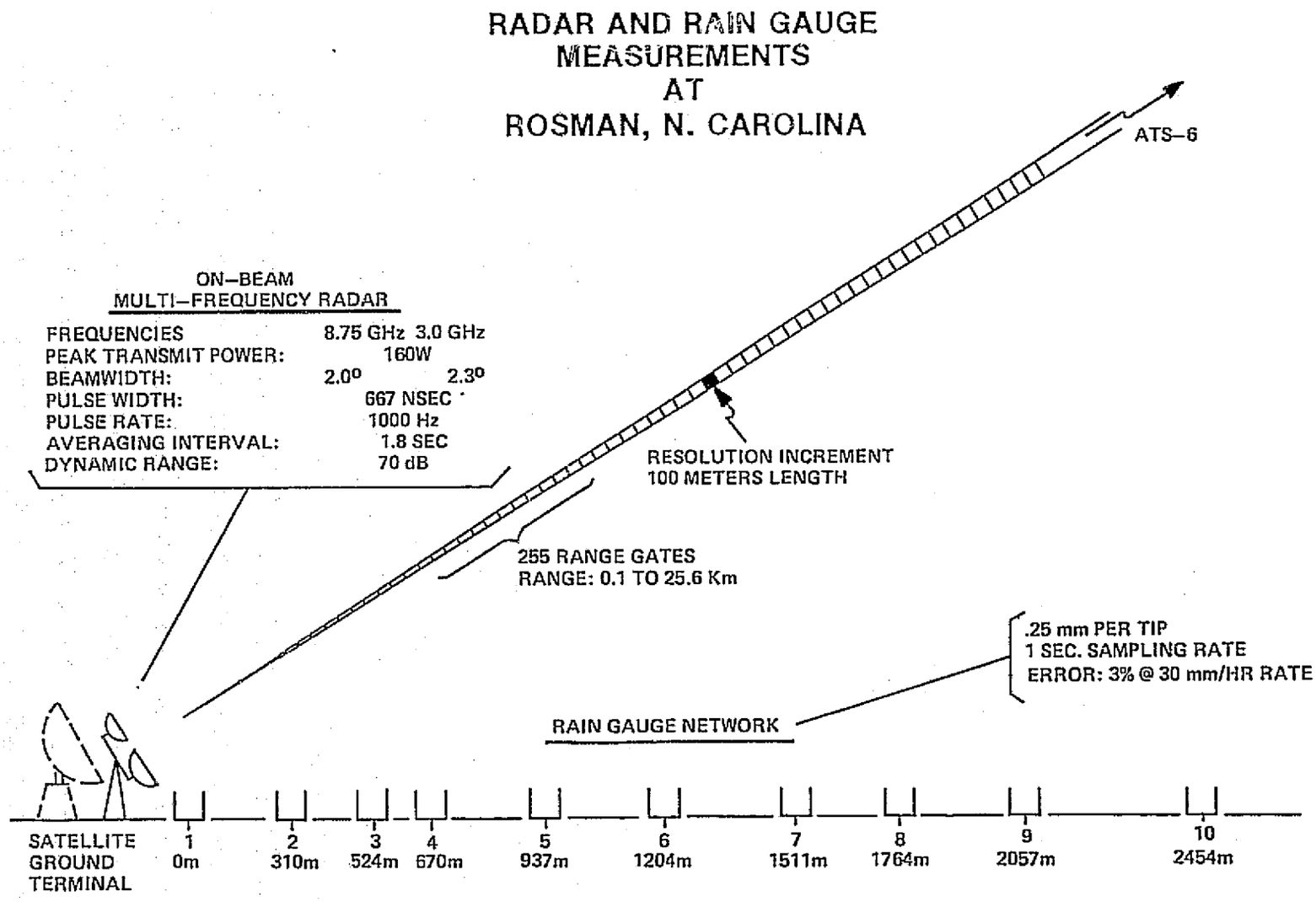

Figure 4-27. Radar and Rain Gauge Measurements at Rosman, N.C.

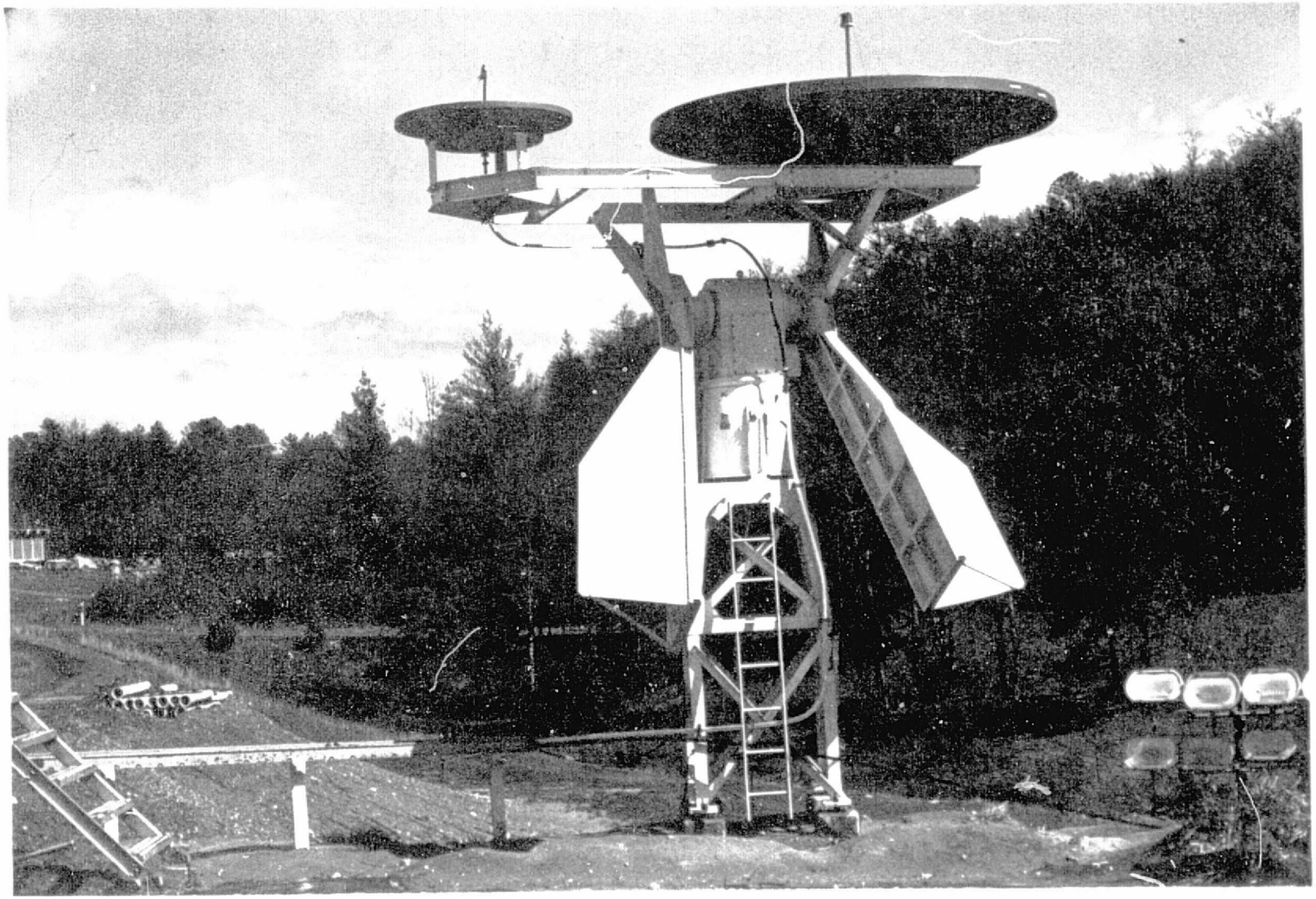

Figure 4-28. 8.75 GHz and 3 GHz On Beam Radar Antennas, Rosman, N.C.

Figure 4-29. Rain Gauge, Rosman, N.C.

an assumed drop-size distribution. Utilizing the folowing empirical relationship for continuous rain between rainfall rate and reflectivity factor, Z,

$$Z = 200\, R^{1.6} \tag{11}$$

and the attenuation relationship for 20 and 30 GHz, (Equations 5 and 6), the attenuation at 20 and 30 GHz can be developed [22]. The resulting expressions for the 20 and 30 GHz attenuation are:

$$A_{20}(\text{dB}) = \sum_{i=2}^{256} .2 \times 10^{-3}\, Z_i^{0.6313} \tag{12}$$

$$A_{30}(\text{dB}) = \sum_{i=2}^{256} .64 \times 10^{-3}\, Z_i^{0.6313} \tag{13}$$

where Z_i is the measured reflectivity factor of the ith range increment, in mm^6/m^3. Figures 4-30 and 4-31 are examples of results of direct attenuation measurements compared with predictions from the 8.75 and 3 GHz radars. In the 20 GHz case, the 8 GHz radar gave a slightly better prediction, however, both radars had a resulting RMS difference of less than 2 dB. The predictions at 30 GHz had larger RMS differences, (see values on Figure 4-31), but tended to give better correlation at the higher attenuation values.

Since the reflectivity factor Z is empirically related to the rain rate, R, it is possible to also use the radar to predict the rainfall rate along the path directly. This computed value can then be compared to the rainfall rate measured by the rain gauge directly under that point in the path. As expected, the results show that the correlation for the nearer rain gauges is good, but degrades as the distance along the path increases. Figure 4-32 shows the predicted (dashed) and measured (solid) rain rates for the rain gauges at 310, 937, and 2454 meters. Figure 4-33 shows an example of how well the 8 GHz radar can predict the measured rainfall at the near rain gauge for a highly variable rain event.

The radar measurements studies at Rosman are continuing, and the preliminary results summarized here provide only a sample of the versatility and utility of the meteorological radar as a powerful tool for rain attenuation evaluation.

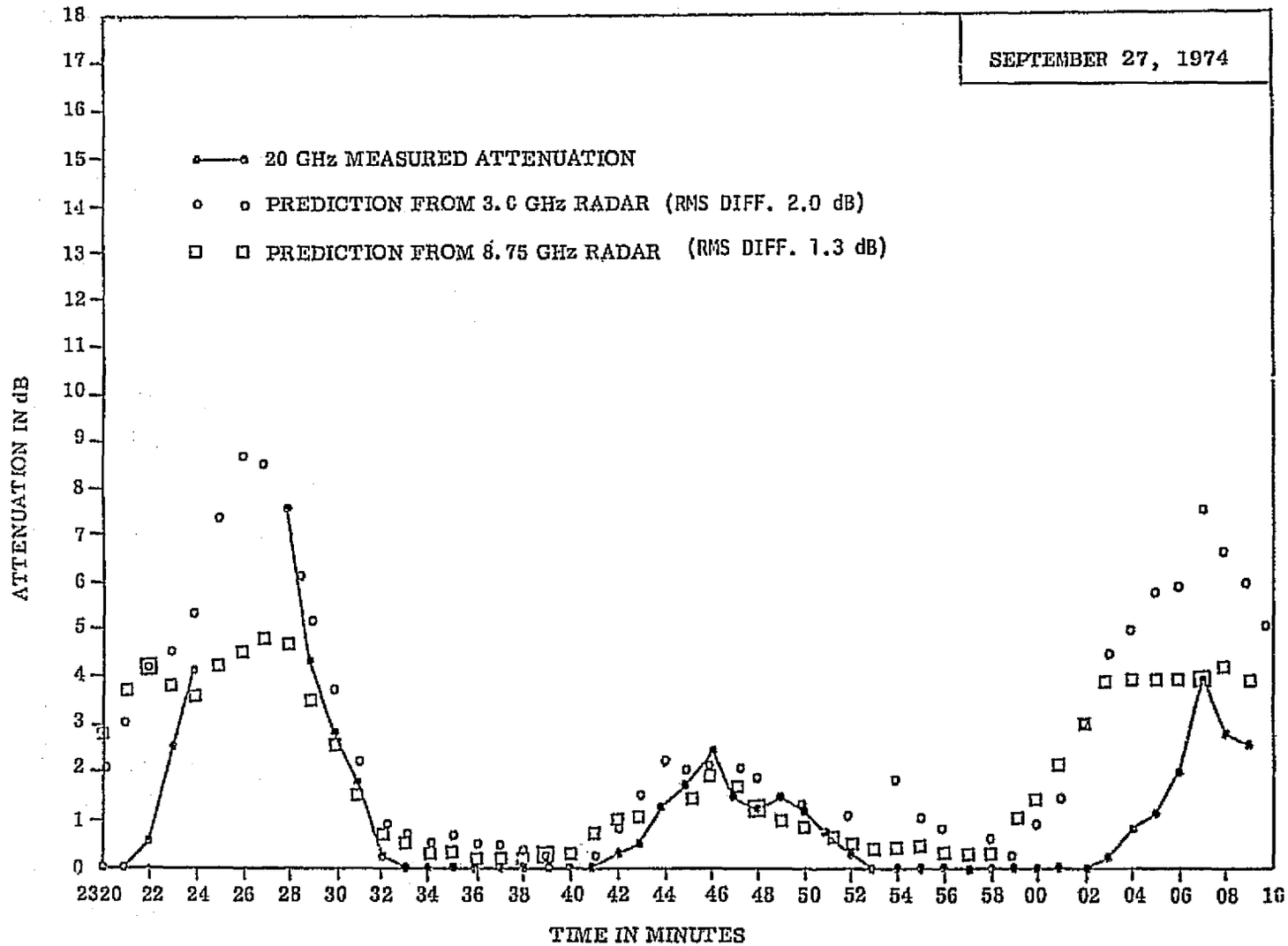

Figure 4-30. 20 GHz Attenuation Prediction From On-Beam Radar Measurements

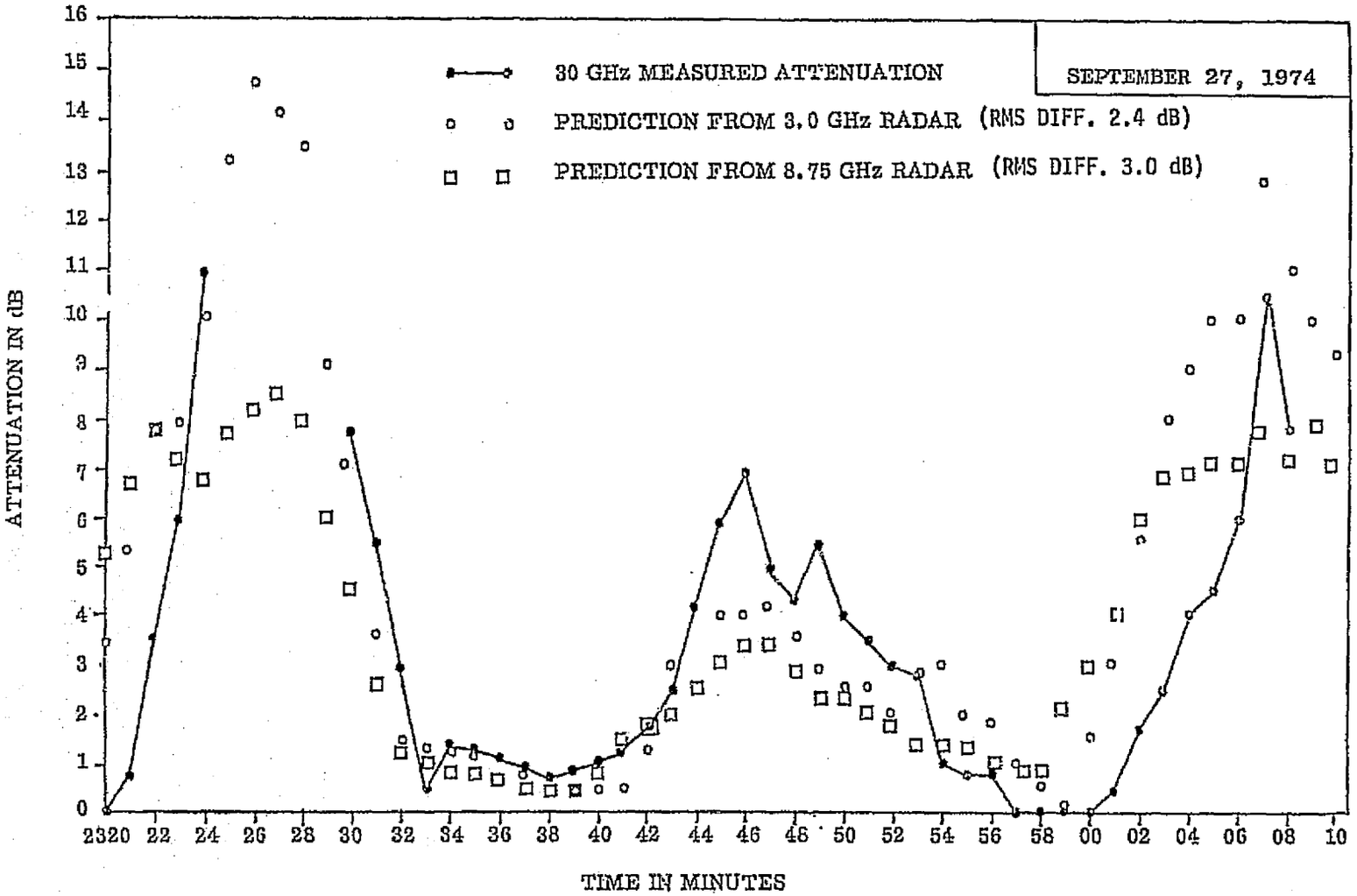

Figure 4-31. 30 GHz Attenuation Prediction From On-Beam Radar Measurements

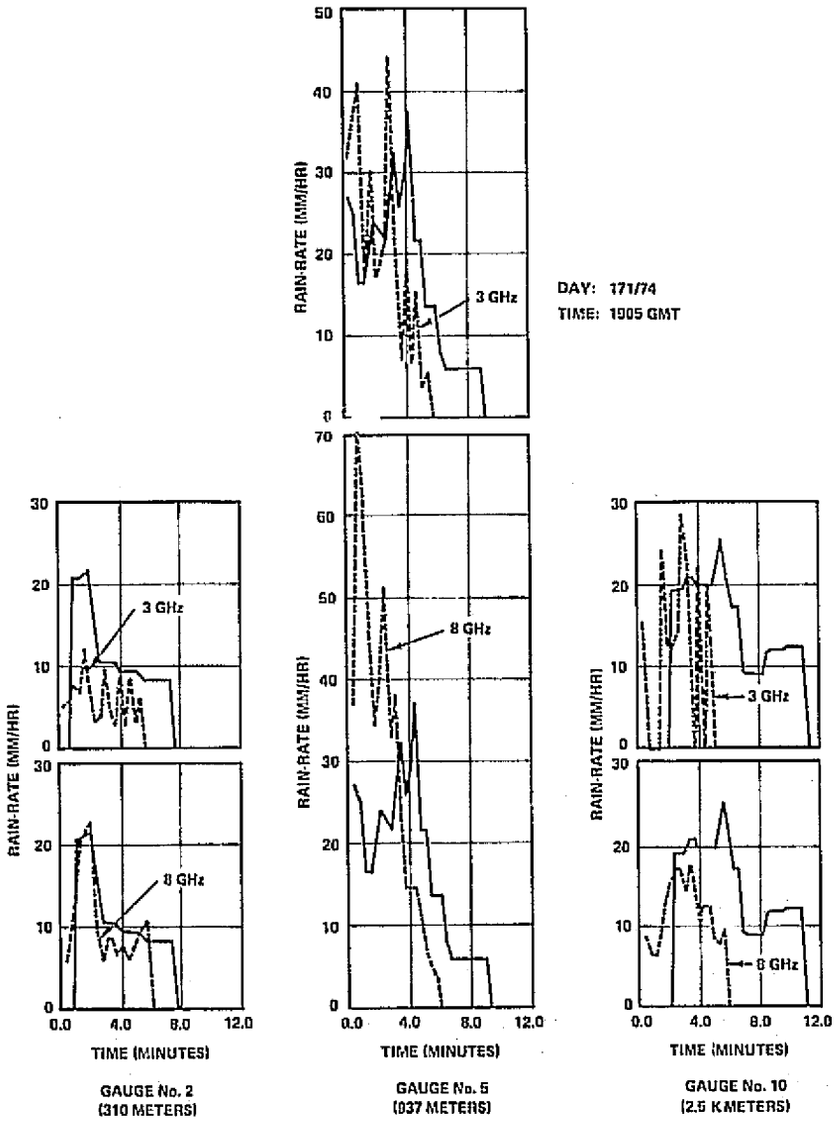

Figure 4-32. Rain Rate Prediction from Radar Measurements

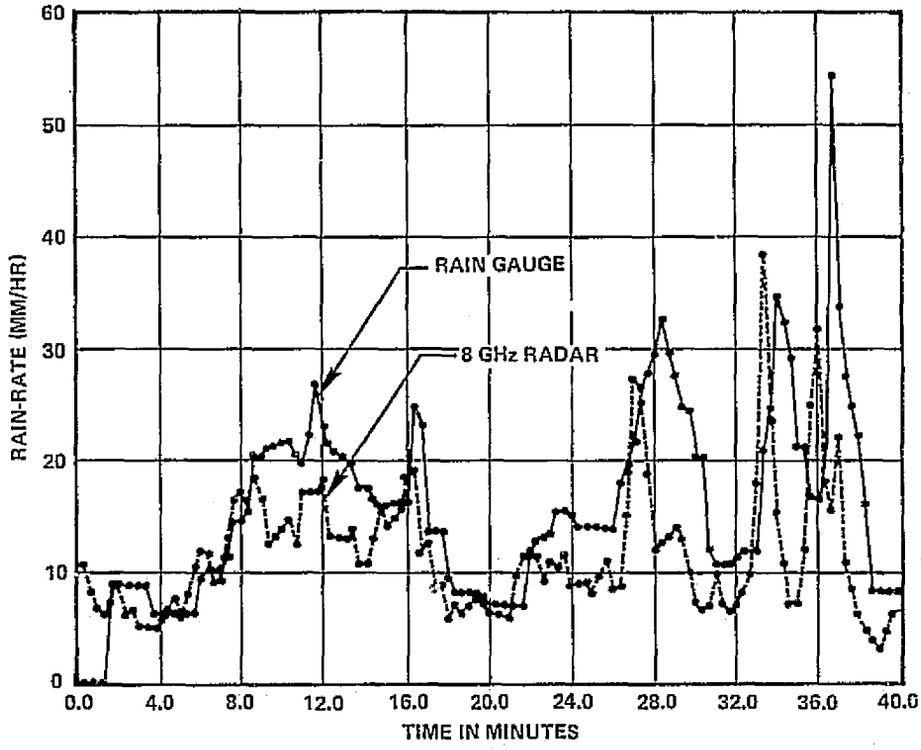

RAIN GAUGE #2 (310 METERS)
DAY 323/74
TIME 2150 GMT

Figure 4-33. Rain Rate Computed from 8 GHz Radar Compared with Measured Rain Rate

SUMMARY

The ATS-6 Millimeter Wave Experiment logged over 1140 hours of operating time from July 1974 through June 12, 1975, when the satellite moved out of range for the SITE experiments. Nearly 500 test periods were utilized by the participants, of which over 300 were unscheduled "call-up" requests. As could be expected in a multi-experiment operation of this type MWE participants missed many useful rain periods when the satellite was not available because of priority conflicts with other experiments.

The results of the data reduced to date, however, have shown that rain attenuation in the 20 and 30 GHz is a significant factor in space communications systems design. Link margin requirements will require site diversity techniques for adequate reliability at 30 GHz, and possibly for 20 GHz systems as well.

The character and magnitude of amplitude scintillations observed at both 20 and 30 GHz was an unexpected result of the MWE, particularly for the clear weather periods.

Results to date indicate that rain-induced attenuation predominates over bandwidth decoherence effects on 20 and 30 GHz links. This would imply that, for practical operational systems with 10 to 15 dB of margin and less than 1000 MHz bandwidth, decoherence is not a system design constraint.

The communications tests demonstrated the technology and feasibility of millimeter wave communications in space, which will be a major component of the next generation of space applications programs.

The verification of the validity of meteorological radar techniques to measure space propagation characteristics was a basic objective of the MWE, and the initial results indicate that techniques can be developed which provide reliable prediction for an earth space rain attenuation model.

The MWE is expected to continue operations while the ATS-6 is at the 35° East position with participating terminals in the United Kingdom and the European continent.

REFERENCES

[1] L. J. Ippolito, "The ATS-F Millimeter Wave Propagation Experiment," NASA/GSFC Document X-751-71-460, October 1971.

[2] L. J. Ippolito, "Effects of Precipitation on 15.3 and 31.65 GHz Earth Space Transmissions with the ATS-5 Satellite," Proc. IEEE, Vol. 59, No. 2, pp 189-205, February 1971.

[3] J. W. Ryde and D. Ryde, "Attenuation of Centimetre Waves by Rain, Hail, and Clouds," Rept. 8516, General Electric Co. Research Labs., Wembly, England, August 1944.

[4] K. L. S. Gunn and T. W. R. East, "The Microwave Properties of Precipitation Particles, Quart. J. Royal, Met. Society, Vol. 13, pp 550-563, July 1965.

[5] R. G. Medhurst, "Rainfall Attenuation of Centimeter Waves: Comparison of Theory and Experiment," IEEE/AP, Vol. 13, pp 550-563, July 1965.

[6] K. L. Wulfsberg and E. E. Altshuler, "Rain Attenuation at 15 and 35 GHz, IEEE/AP, Vol. 20, No. 2, pp. 121-187, March 1972.

[7] G. G. Haroules and W. E. Brown, "Radiometric Measurement of Attenuation and Emission by the Earth's Atmosphere at Wavelengths from 4 cm to 8 mm," IEEE/MTT, Vol. 16, No. 9, pp. 611-620, September 1968.

[8] R. W. Wilson, "Sun Tracker Measurements of Attenuation by Rain at 16 and 30 GHz," Bell System Technical Journal, pp. 1383-1404, May-June 1969.

[9] L. J. Ippolito, "Millimeter Wave Propagation Measurements from the Applications Technology Satellite (ATS-V)," IEEE/AP, Vol. 18, No. 4, pp. 535-552, July 1970.

[10] D. B. Hodge, "A 15.3 GHz Satellite to Ground Path-Diversity Experiment Utilizing the ATS-5 Satellite," Radio Science, Vol. 9, No. 1, pp. 1-6, January 1974.

[11] R. K. Crane, "Propagation Phenomena Affecting Satellite Communication Systems Operating in the Centimeter and Millimeter Wavelength Bands," Proc. IEEE, Vol. 59, No. 2, pp. 173-188, February 1971.

[12] D. C. Hogg, "Millimeter-Wave Communication through the Atmosphere," Science, Vol. 159, pp. 39-46.

[13] R. D. Craft, Jr., "Attenuation Statistics at 15.3 GHz for Clarksburg, MD," COMSAT Technical Review, Vol. 2, No. 1, pp. 221-225, Spring 1972.

[14] Straiton, Pate and Fannin, "Statistics on Earth-Satellite Attenuation at Two Texas Locations," Telecomm. Aspects of Freq. between 10 & 100 GHz, AGARD-CP-107, Gausdal, Norway, pp. 20-1,9, September 18-21, 1972.

[15] H. W. Evans, "Attenuation on Earth-Space Paths at Frequencies up to 30 GHz," The 1971 International Conference on Communications Record, Montreal, Canada, pp. 27-1,5, June 14-16, 1971.

[16] "Earth-Satellite Propagation Above 10 GHz – Papers from the 1972 Spring URSI Session on Experiments with the ATS-5 Satellite," NASA-GSFC Document X-751-72-208.

[17] J. O. Laws and D. A. Parsons, "The Relation of Raindrop-size to Intensity," Trans. Am. Geophysical Union, Vol. 24, pp. 432-460, 1943.

[18] J. S. Marshall and W. Mc K. Palmer, "The Distribution of Raindrops with Size," Journ. of Meteorology, Vol. 5, pp. 165-166, August 1948.

[19] L. J. Ippolito, "Summary and Evaluation of Results from the ATS Millimeter Wave Experiment," see ref. 16, pp. 8-1 to 8-27.

[20] "Minutes of Second ATS-6 Millimeter Wave Experimenter's Conference," Goddard Space Flight Center, December 19-20, 1974, dated February 28, 1975.

[21] Tu, Kahle, and Batson, "ATS-6 Quadraphase Transmission Tests," Instrument Society of America Conference, Milwaukee, Wisconsin, Oct. 6, 7, 8, 1975.

[22] "ATS-6 Millimeter Wave Propagation Experiment Data Analysis Report," Report No. F1S-75-005, prepared by Westinghouse Electric Corporation for NASA Goddard Space Flight Center, February 1975.

Preliminary Report On

ATMOSPHERIC ATTENUATION STUDIES ON ATS-6 SATELLITE 20/30 GHZ BEACON SIGNALS

D. J. Fang and J. M. Harris
COMSAT Laboratories
Clarksburg, Maryland 20734

ABSTRACT

The study is a part of a program of COMSAT praticipation in the NASA ATS-6 millimeter wave experiment. In the initial data collection phase, the measurement equipment included: (1) A 3 meter diameter antenna-receiver system for accepting 20 GHz satellite CW signals and a radiometer system at 11.7 GHz for monitoring sky noise temperature. (2) A 4.6 meter diameter antenna-receiver system capable of receiving 20 and 30 GHz main CW signals plus radiometers at 20 and 30 GHz. (3) Six rain gauges along the bore sight path toward the satellite for recording instantaneous rainfall rates. (4) A weather radar at 5.4 GHz for detecting the motion pattern of the rain cloud in large scale.

Data analysis is done on an event-by event basis by using received satellite signals as basic reference for correlation with other information derived from the radiometers, the rain gauges and the radar. Important physical characteristics for prominent individual events of heavy rain storms are identified.

I. INTRODUCTION

There are "windows" in the frequency spectrum above 10 GHz where water vapor and oxygen absorption are relatively low. Two such windows are the frequencies below 20 GHz and a band from about 27 to 38 GHz. It follows that potential for future earth-satellite communications is greater in these bands. However, the essential propagation data base needed by system designers for predicting microwave communication system margin is not yet available.

COMSAT Labs' participation in the NASA ATS-6 Millimeter Wave Experiment (MWE) was aimed at collecting propagation data at Clarksburg, Maryland using the ATS-6 20/30 GHz beacons as the transmitting source and obtaining data for the long base-line diversity experiment jointly with NASA/GSFC, NRL and Westinghouse (Friendship). The data should be applicable to the general Washington, D.C. area and to other locations of similar climatological patterns.

The measurement equipment included three beacon signal receivers (two for 20 GHz and one for 30 GHz), three radiometers (11.6, 20 and 30 GHz), six rain gauges beneath the boresight path toward the satellite, and one weather radar (5.4 GHz). The hardware aspects of these systems are discussed in Section II. Analysis of beacon signal data is oriented toward event-by-event analysis of each measured occurrence of precipitation-induced attenuation, as long term statistics of signal attenuation were not available because of the rarity of the satellite beacon transmission during precipitation events (due to the low priority accorded the MWE during most of the stay of ATS-6 at its western station). Details of the data analysis are given in Section III.

An important facet of the work which was not anticipated in the initial study program was the low-elevation-angle measurement of the satellite transmission. This measurement was made during the period when ATS-6 moved gradually from its original location at 94°W Long. to its present location at 35°E Long. It was found that strong scientillations occurred at low elevation angles, and that there was a large increase of signal level as the satellite descended towards the horizon into the diffraction region. Preliminary analysis of the data is shown in Section IV. Conclusions are presented in the last section of the paper.

II. SYSTEM CONFIGURATION

Measurements were performed at COMSAT Labs, Clarksburg, Maryland, some 40 miles northwest of Washington, D.C. Figure 5-1 shows the location of the Clarksburg site relative to the other diversity sites at NRL, GSFC, and Westinghouse. The measurement system can be summarized as follows:

(1) A 3 meter diameter transportable antenna-receiver system that included a 20 GHz receiver for receiving satellite beacon signals and a radiometeric receiving system at 11.6 GHz for observing sky temperature using thd same antenna.

(2) A 4.6 meter diameter antenna-receiver system that included 20 and 30 GHz receivers for the satellite beacon signals and two radiometric receivers at 20 and 30 GHz for observing sky temperature using the same 4.6 meter antenna.

(3) A network of 6 rain gauges extending for 7 kilometers underneath the boresight path toward the satellite for examining the precipitation under the propagation path.

(4) A weather radar at 5.4 GHz for detecting the motion pattern of the rain cloud in large scale.

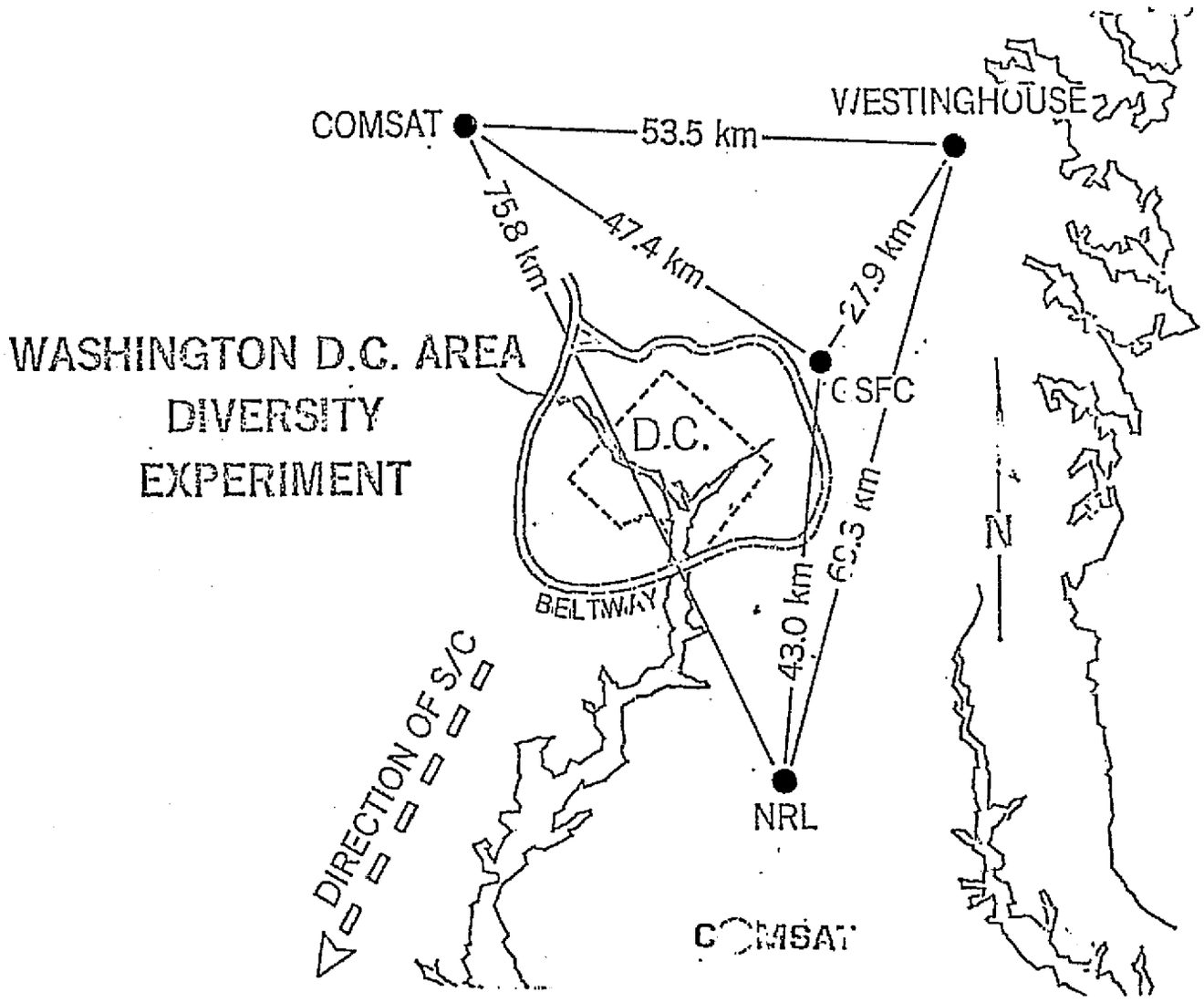

Figure 5-1. Location of COMSAT, Clarksburg Measurement

Figure 5-2 and 5-3 are the block diagrams of the 3 meter and 4.6 meter systems. The antennas are solid-surface aluminum paraboloids equipped with focal-point feeds and polarization rotators. Both antennas have servo-controlled elevation and azimuth positioners and decimal position readouts with a resolution of 0.1° and .01° for the 3 meter and 4.6 meter antennas, respectively. The nominal pointing direction to ATS-6 was 204° south from true north at an elevation angle of 42°.

As indicated in Figures 5-2 and 5-3 tunnel diode and uncooled parametric amplifiers are used in the 20 GHz front-ends of the 3 meter and 4.6 meter systems, respectively. The 30 GHz system has a low noise mixer front end. IF-signal processors which detect the down-converted signals by individual narrow-band phase-locked receivers give output amplitudes that are proportional to the satellite beacon signal attenuation levels. These outputs are then fed to strip-chart recorders or to data acquisition computers. Important performance parameters are shown in Table 5-1 (3m system) and Table 5-2 (4.6m system).

Both antenna systems are equipped with on-line radiometric subsystems. Operating in a Dicke-switched mode, these radiometers also include a noise source at known temperature for calibration purposes. The A.I.L. (Airborne Instrument Laboratories) radiometric receivers, (Model 2392C) produces an output voltage proportional to the sky noise temperature. In the switched mode, the output is the net change of sky noise temperature from that of a clear sky day. Performance parameters of the AIL radiometric receivers are summarized in Table 5-3.

The rain gauges are the tipping bucket type, where each tip represents 0.01 inch (0.25 mm) of rainfall accumulation. The gauges are aligned beneath the satellite bore-sight path at distances of 0, 0.92, 1.08, 3.23, 5.53 and 7.4 kilometers from the beacon receiver. Each gauge is equipped with a mechanically driven strip-chart recorder with a time accuracy of better than 3 minutes per week.

The radar system is an RCA AVQ-10 weather radar operating at 5.4 GHz. Three different ranges of 20, 50 and 150 nautical miles can be selected. Maximum elevation angle is 35°. A super-8mm camera can be attached to the PPI scope for for filming the radar echoes. Since the radar slant path is lower than the ATS-6 slant path, no attempt has been made to incorporate the radar data for detailed analysis. However, the radar has proved useful as a device to predict the approach of a precipitating cloud.

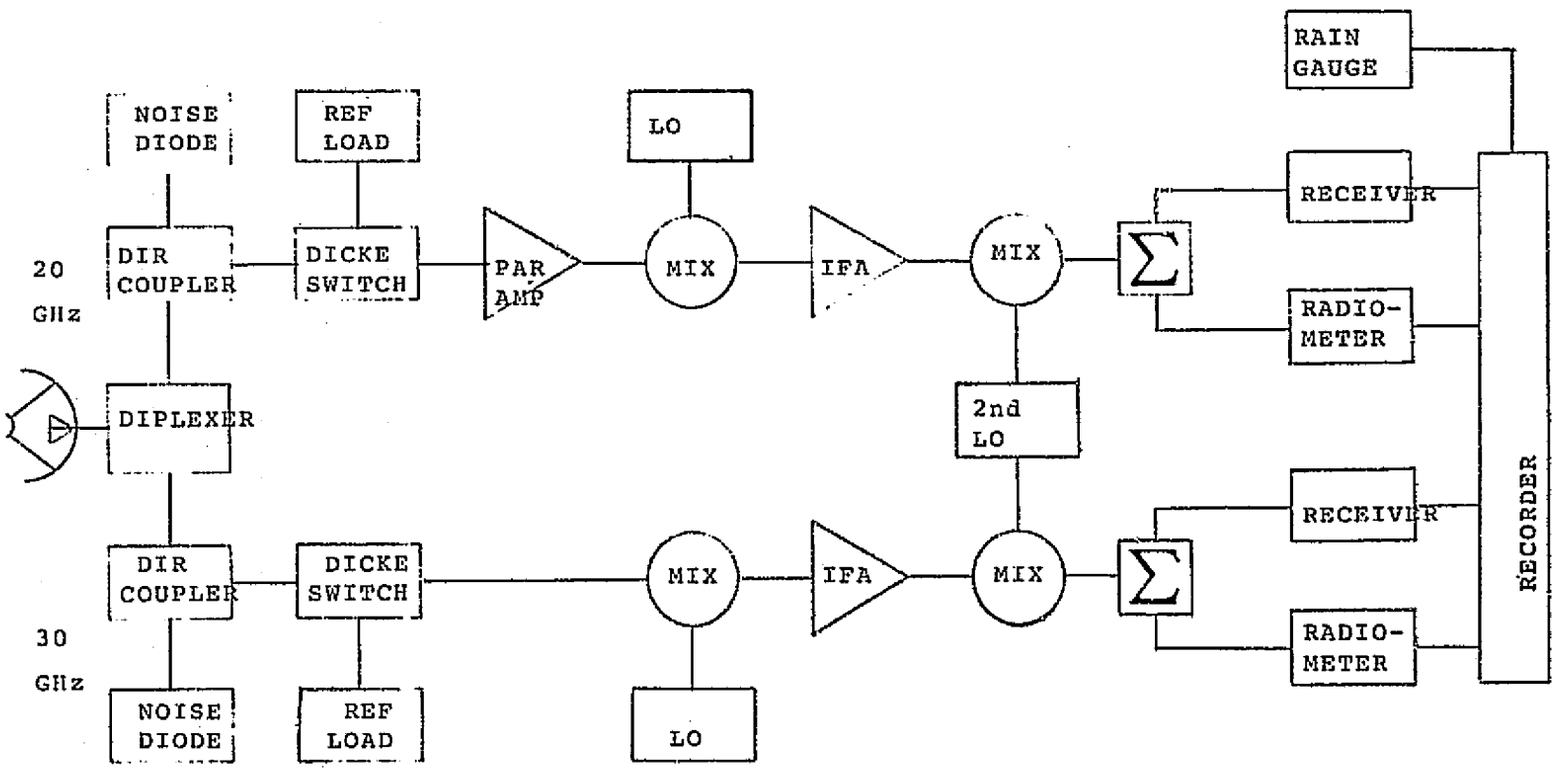

Figure 5-2. Block Diagram: 20/30 GHz Receive/Radiometer System

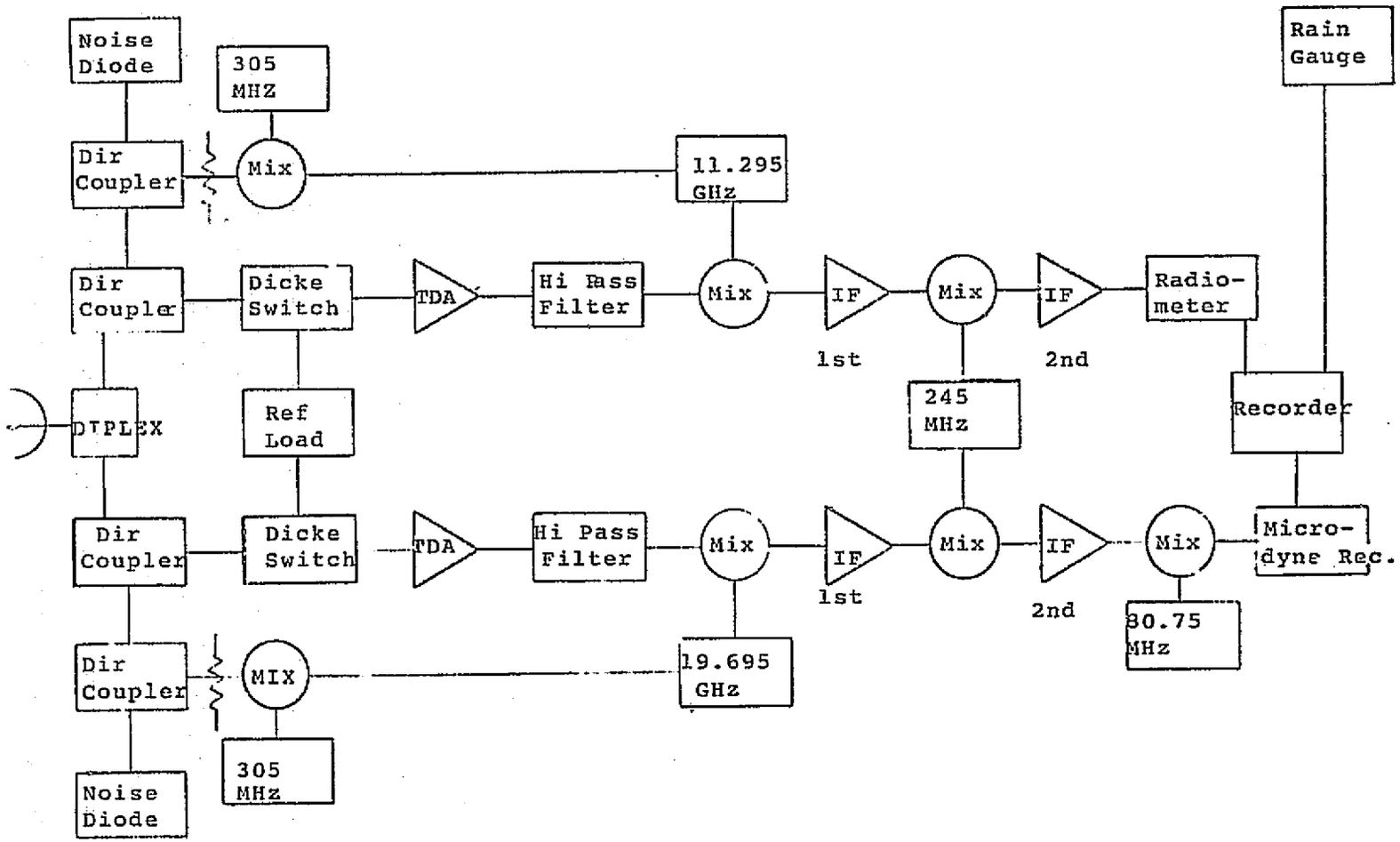

Figure 5-3. Block Diagram: 11.6 and 20 GHz Receiver/Radiometer Transportable System

Table 5-1
Important Performance Parameters of 3m Antenna System

	11.6 GHz	20 GHz
Antenna Gain	48.7 dB	53.5 dB
Pointing Accuracy	±.1°	±.1°
Noise Figure	5 dB	8 dB
Radiometer Sensitivity	1°K	–
Radiometer Bandwidth	100 MHz	–
Receiver Bandwidth	–	10 KHz

Table 5-2
Important Performance Parameters of 4.6m Antenna System

	20 GHz	30 GHz
Antenna Gain	57 dB	60.5 dB
Pointing Accuracy	±.01°	±.01°
Noise Figure	4 dB	8 dB
Radiometer Sensitivity	1°K	1°K
Radiometer Bandwidth	100 MHz	100 MHz
Receiver Bandwidth	10 KHz	10 KHz

Not all of the above systems were ready for measurement at the same time, as shown in Table 5-4. Delays in preparation of the 4.6m system were caused by the continuous slippage of the shipping schedule of the parametric amplifier. On the other hand, the systems haev performed well once operational.

III. DATA ANALYSIS

An important contraint on the entire experiment was the lack of availability of millimeter wave 20/30 GHz beacon transmissions from the satellite during precipitation events. The priority of the millimeter wave experiment was not high. There were regular weekly transmission times assigned at an average of about one hour per day. These transmission times, although used by COMSAT for data collection and equipment calibration, were not really useful due to the fact that precipitation rarely occurred on site at these times. Requests were

Table 5-3
Performance Parameters of AIL Radiometric Receivers

IF bandwidth	100 MHz (5 to 105 MHz)
Noise figure	7 dB
Input impedance	50 ohms
Input SWR	<2 to 1 over entire passband
Gain modulation	-3 to +3 dB, in 0.06-dB steps and continuous control of 0.1 dB
IF gain	85 dB (maximum)
IF gain control	0 to -41 dB, in 1-dB steps
Switch rate	5 to 500 Hz, stability ±0.05 percent
Switching waveform	Square wave
RF switch drive	0 to -14 volt square wave into 10,000 ohms
Switched system output	±5 volts maximum at 2 ma
Total power output	-5 volts maximum at 2 ma
Integration time constants:	
Switched system	0.1, 1, 3, 5, 10 and 30 seconds
Total power system	1, 5, and 10 seconds
Monitor points	Second detector current; synchronous detector balance
DC reference	Up to 3.0 volts (for use with total power output)
Input power	47 watt nominal (capable of operation at 105 to 125 and 220 volt AC, 50 to 440 Hz).

Table 5-4
System Availability Chart

System	Equipment	Available Since	Comment
Transportable System	20 GHz CW-Receiver	July 1974	Varian 620 computer was equipped for automatic tracking and data collection. But it over flowed frequently. Most time only manual operation was used.
	11.7 GHz Radiometer	July 1974	
	Rain Gauge	July 1975	
15-Foot System	20 GHz CW-Receiver	March 1975	Due to interference problem the 20 GHz radiometer was turned off when CW-Receiver was taking data.
	20 GHz Radiometer	March 1975	
	30 GHz CW-Receiver	April 1974	Paramp not available dynamic range 15-18 dB.
Others	5.4 GHz Radar	September 1974	For visual observation only
	Rain Gauges	February 1975	Total of 6, counting the one on site

made consistently to NASA ATS Operations Control Center for 20/30 GHz beacon transmission whenever precipitation was occurring or anticipated. Positive responses to the requests were infrequent. There were several occassions when beacon transmissions were abruptly terminated while valuable experimental data in a thunderstorm condition was being collected.

With the above constraint in mind, data analysis was performed largely on an event-by-event basis. This includes:

(i) Correlation of the satellite 20 GHz beacon data and the radiometric sky temperature data.

(ii) Correlation of the 20 GHz and 30 GHz signal attenuation level.

(iii) Correlation of the satellite 20 GHz beacon signals and data from the rain-gauge network.

Another phase of data collection, not included with the original plan, involved observation of the satellite descending toward the horizon in late May and early June of 1975. The low-elevation angle data will be presented in a separate section.

(i) Correlation of the satellite 20 GHz beacon data and the radiometric sky temperature data.

A typical data sample is shown in Figure 5-4, (the event of March 19, 1975, lasting 150 minutes). The scattergram of the data is shown in Figure 5-5. Empirical fit curves are shown as dashed lines. Theoretically derived attenuation curves using linear scaling for ambient sky temperature of 278°K and 300°K are also shown.

(ii) Correlation of the 20 GHz and 30 GHz signal attenuation level.

A typical data sample is shown in Figure 5-6, the event of June 6, 1975. A scattergram of the data is shown in Figure 5-7.

(iii) Correlation of the satellite 20 GHz beacon signals and data from the rain-gauge network.

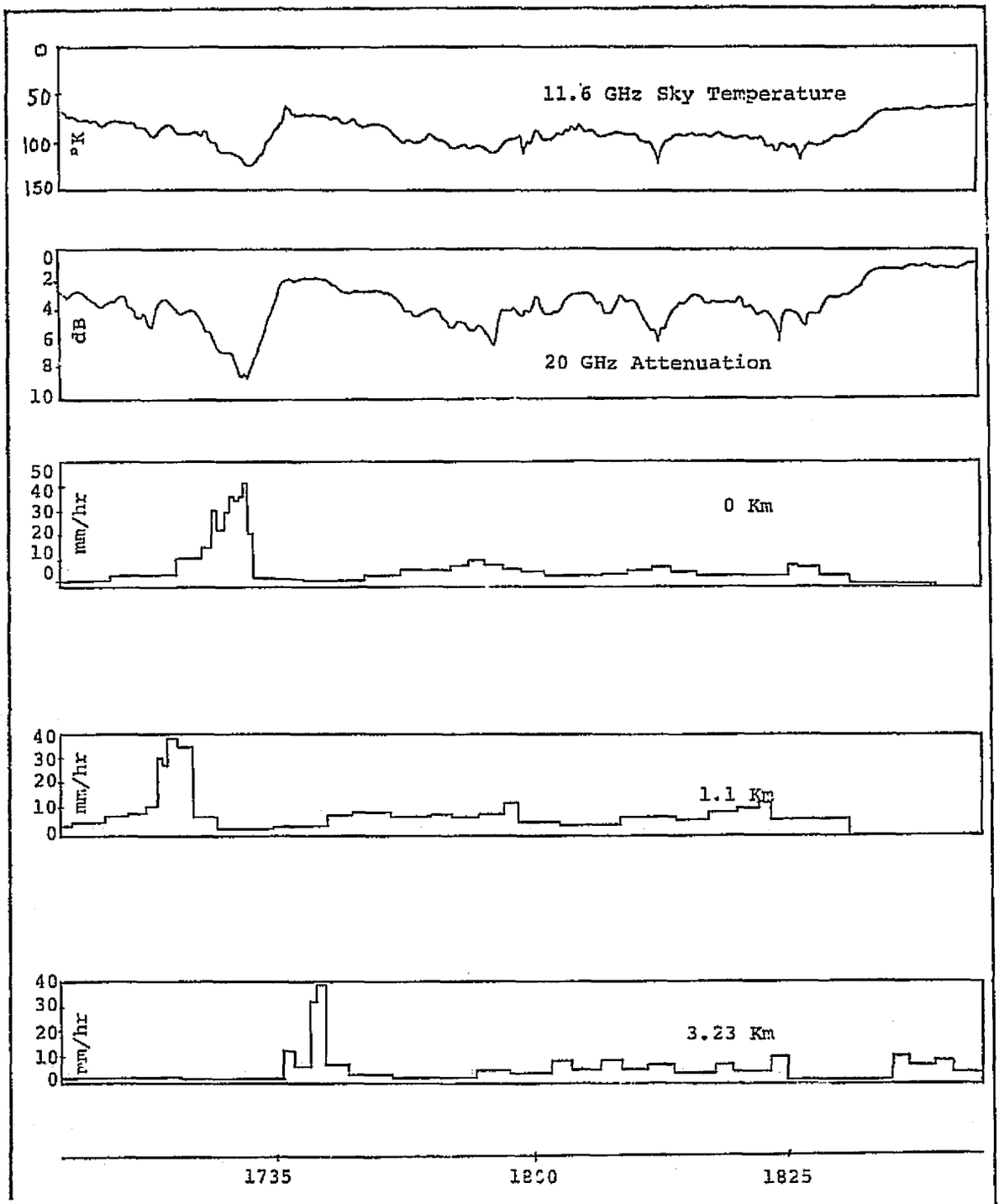

Figure 5-4. Typical Precipitation – attenuation record measured at Clarksburg, Maryland. Ground rain gauges were 0 km, 1.1 km and 3.23 km from 20 GHz receiver and 11.6 GHz radiometer.

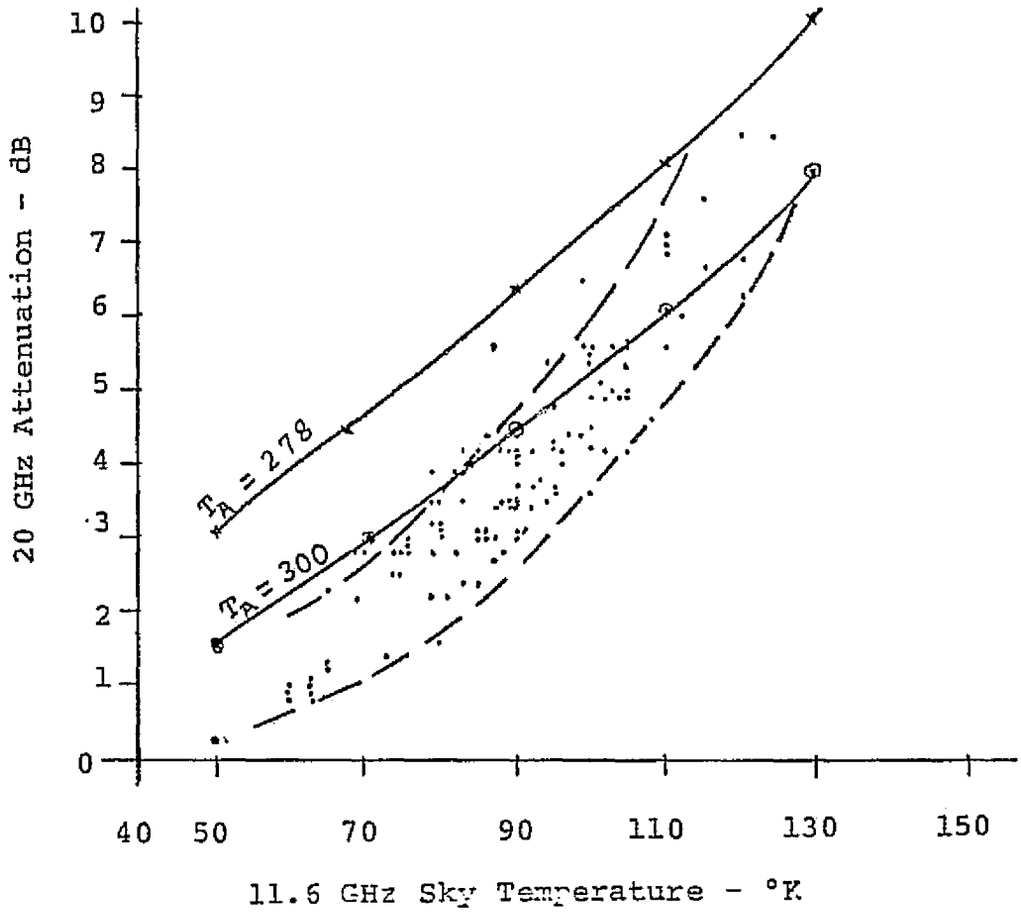

Figure 5-5. Scattergram of 20 GHz attenuation vs. 11.6 GHz sky temperature from data given in Figure 4. Solid lines theoretically derived for ambient temperature T .

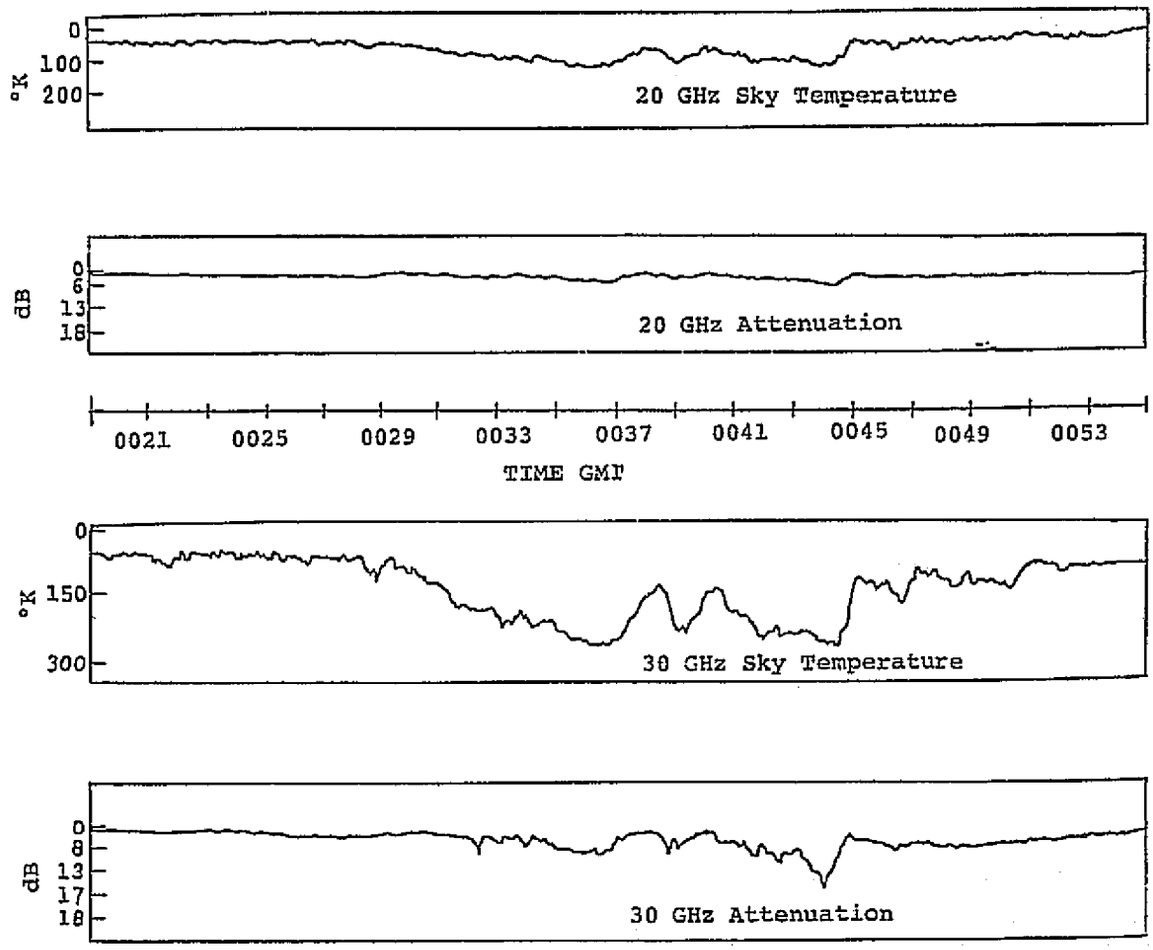

Figure 5-6. Typical records of simultaneously measured 20/30 GHz radiometric sky temperatures and 20/30 GHz ATS-6 signals.

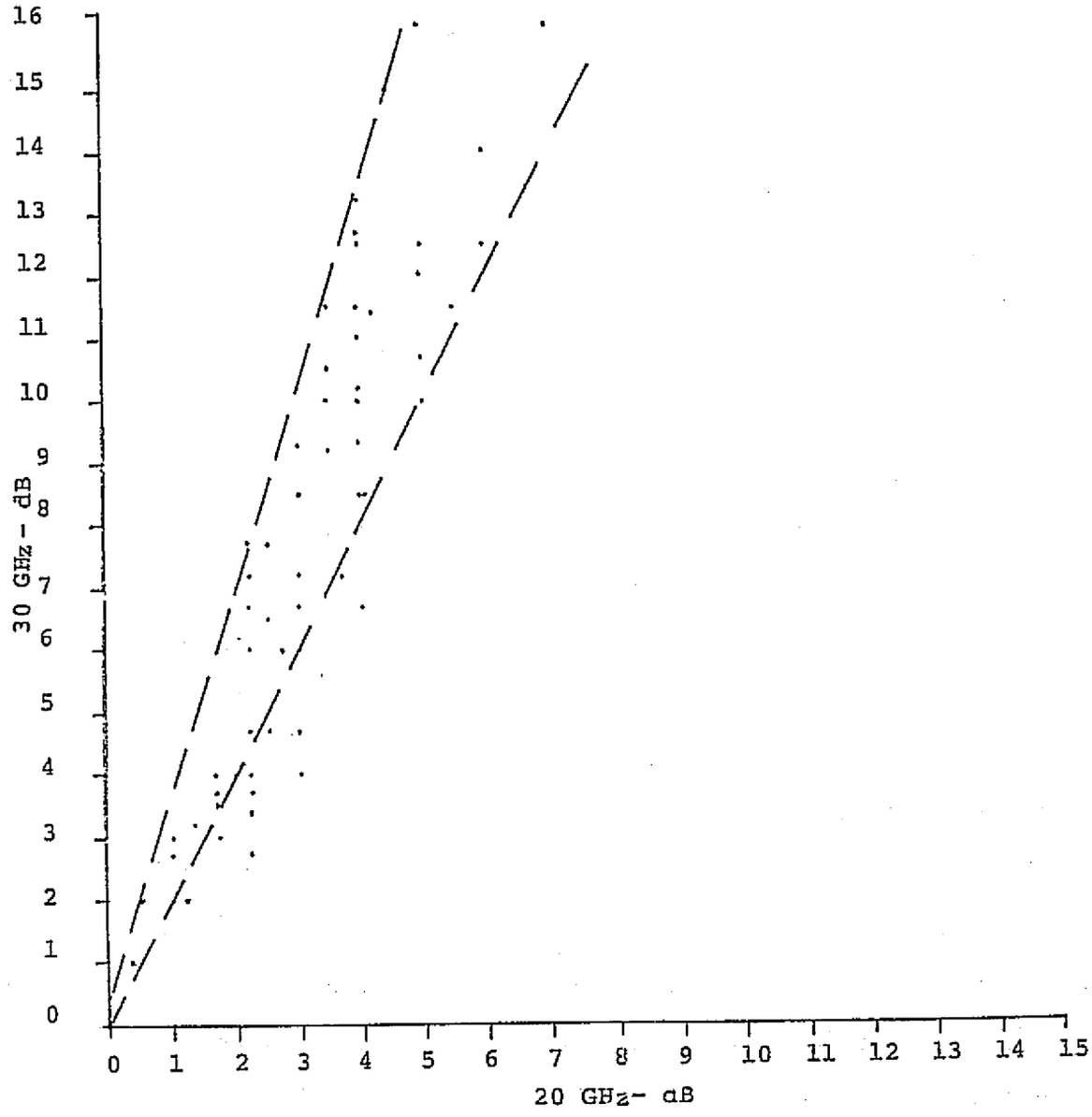

Figure 5-7. Scattergram plot of 30 GHz Attenuation vs. 20 GHz attenuation measured June 6, 1975.

A basic problem in estimating the microwave attenuations over a satellite – earth propagation path based on rain-gauge data is that for a given storm event, the attenuation and the rain-fall records very often do not have a consistent detailed correlation. As shown in Figure 5-4, it is seen that while the radiometer curve correlates well with the satellite signal level, the data from rain gauges do not have a consistent correlation with the 20 GHz curve. A particularly puzzling point is the peak registered on the rain gauge 3.23 km away from the receiver.

We have collected and analyzed the data containing the apparent discrepancies in time and magnitude as those shown in Figure 5-4. A model for adjusting the rain gauge data is provided as follows:

Let the rain-rate measured at an instant t by a ground rain gauge by $R_G(t)$ which consists of raindrops of sizes from 0.05 to 0.7 centimeter with falling velocity V ranging from 2 to 9 meters/sec. It follows that

$$R_G(t) = \sum_V R_V(t) \tag{1}$$

where $R_V(t)$ is the portion of rain-rate falling at terminal velocity v. If the rain gauge is located h meters vertically below the slant propagation path, then $R_V(t)$ penetrates across the path at an advanced time h/v, when there is no wind. Therefore, the actual rain fall $R_h(t)$ at height h and instant t' is

$$R_h(t') = \sum_{t,v} R_V(t)\ t - \frac{h}{v} = t' \tag{2}$$

The summation is over all the components of $R_V(t)$ in $R_G(t)$ for an all t and v such that $t - h/v = t'$. The decomposition of R_G into R_V for a different advanced time with h = 1000 meters is shown in Table 4-5.

Table 4-5

Actual Rain Rate at 1000-Meter Height Estimated from a Ground Rain Gauge Rainfall Reading (The estimate is based on Laws and Parsons drop size distribution and Davies' terminal velocity profile [Medhurst, 1965 IEEE paper]

Actual Rain Rate at 1000-m Height Advanced Time (minutes)										Ground Measured Rain Rate (mm/hr)
8.09	4.14	3.09	2.57	2.25	2.07	1.95	1.89	1.85	1.83	
0.07	0.13	0.05	0	0	0	0	0	0	0	0.25
0.14	0.46	0.39	0.17	0.16	0.02	0.01	0	0	0	1.25
0.18	0.07	0.82	0.48	0.20	0.08	0.04	0	0	0	2.5
0.24	1.02	1.55	1.11	0.59	0.29	0.13	0.05	0.02	0	5
0.33	1.44	3.06	3.18	2.16	1.26	0.54	0.29	0.15	0.09	12.5
0.43	1.9	4.6	5.98	4.98	3.20	2.05	0.88	0.53	0.48	25
0.6	2.7	6.25	9.95	10.45	7.8	5.45	3.35	1.65	1.8	50
1.0	4.6	8.8	13.9	17.1	18.4	15.0	9.0	5.8	6.4	100
1.5	6.15	11.4	17.55	20.85	26.55	24.15	17.85	11.55	12.45	150

The model has been applied to the rain-rate records collected from the 6 rain gauge networks in correlating rain data with the ATS-6 20 GHz beacon signals. In most cases, the method has the merit of relocating and dispersing the peaks of precipitation curves of field rain gauges in the direction of better alignment with the pattern of attenuation curves. Figure 5-8 is the outcome of the adjusted rain-rate distribution of the same event shown in Figure 6-4. Assuming that the same rain rate of a rain gauge applies over the distance between the middle points of the two adjacent rain gauges, attenuation can then be estimated from theoretical considerations. The estimated value and the actual 20 GHz attenuation value are compared in Figure 5-9. The scattergram, Figure 5-9(b) derived from the adjusted rain data of Figure 5-8 exhibits a significant improvement in comparison with the scattergram, Figure 5-9(a), derived directly from Figure 5-4.

IV. LOW ELEVATION ANGLE MEASUREMENT

In late May, 1975 ATS-6 began to move slowly from its original location toward its new position over the Indian Ocean. The path vector elevation angle at the COMSAT Labs' receivers station decreased steadily to zero over a three week period of time. While the 20 GHz and 30 GHz beacon signals were not continuously available, several hours of data were collected at varying elevation angles. As ATS-6 approached the horizon, (local horizon was at an elevation angle of 1.2°), strong scintillations occurred as well as an increase in the average level of the received signals.

The scintillations appear to be caused by irregular refraction and scattering in the earth's lower atmosphere. Although antenna tracking difficulties and calibration errors, among other things, may also have contributed to the signal variations, a continuous effort was made to minimize this effect. The magnitude of the scintillations showed a strong dependence on path elevation angle and local climatological conditions. Peak-to-peak magnitude of the variations grew to greater than 10 dB during the final hours of data acquisition near 3° elevation angle. In addition, sharp nulls in the signal level were frequently observed and believed to be caused by angle of arrival or low elevation angle multipath. These scintillations have a periodicity in the range of 15 seconds to greater than 1 minute that showed a large dependence on the local weather. A typical record of simultaneous 20 GHz and 30 GHz scintillations is given in Figure 5-10(a) and 5-10(b).

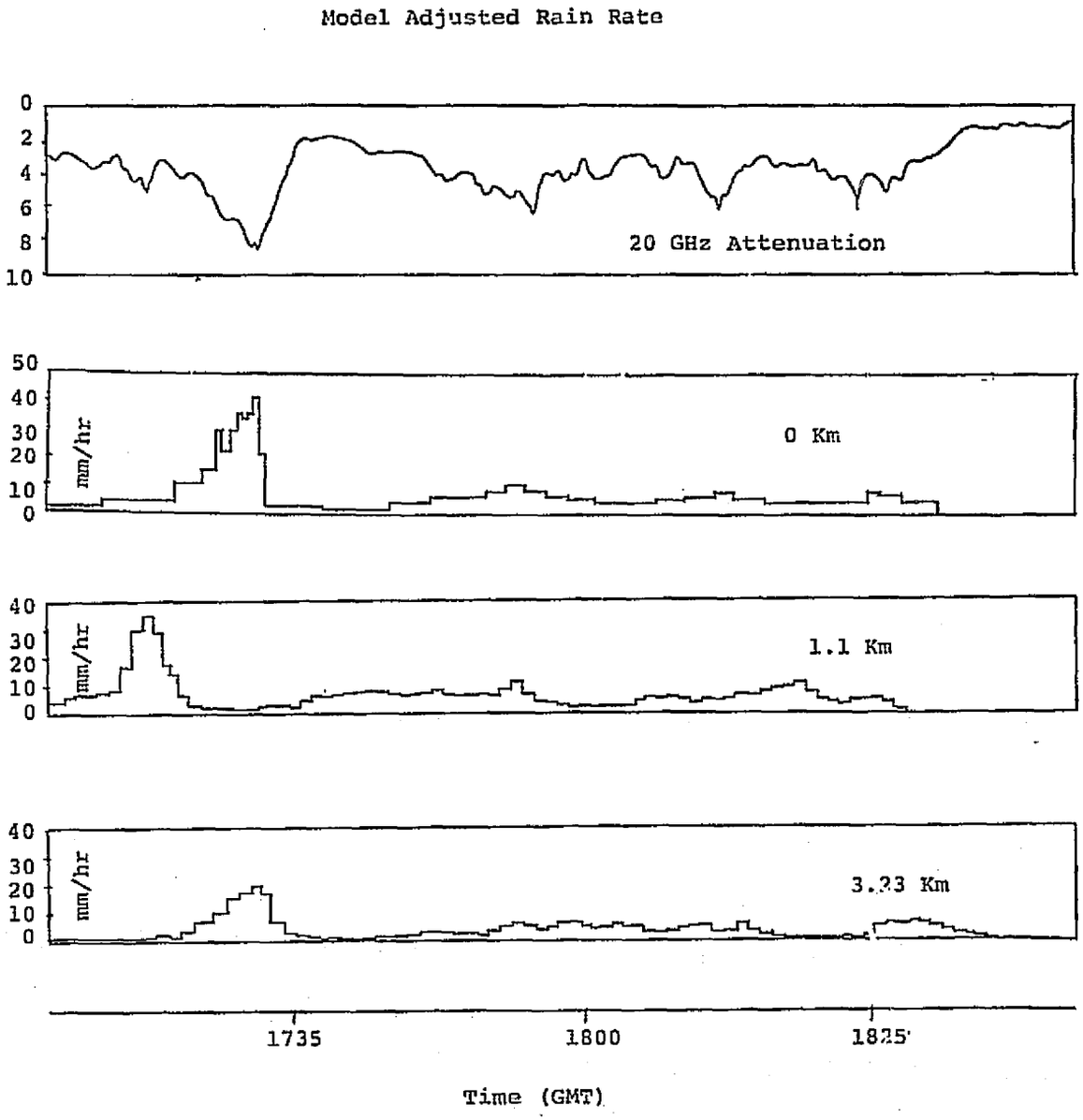

Figure 5-8. Model adjusted rainrate from original data given in Figure 4.

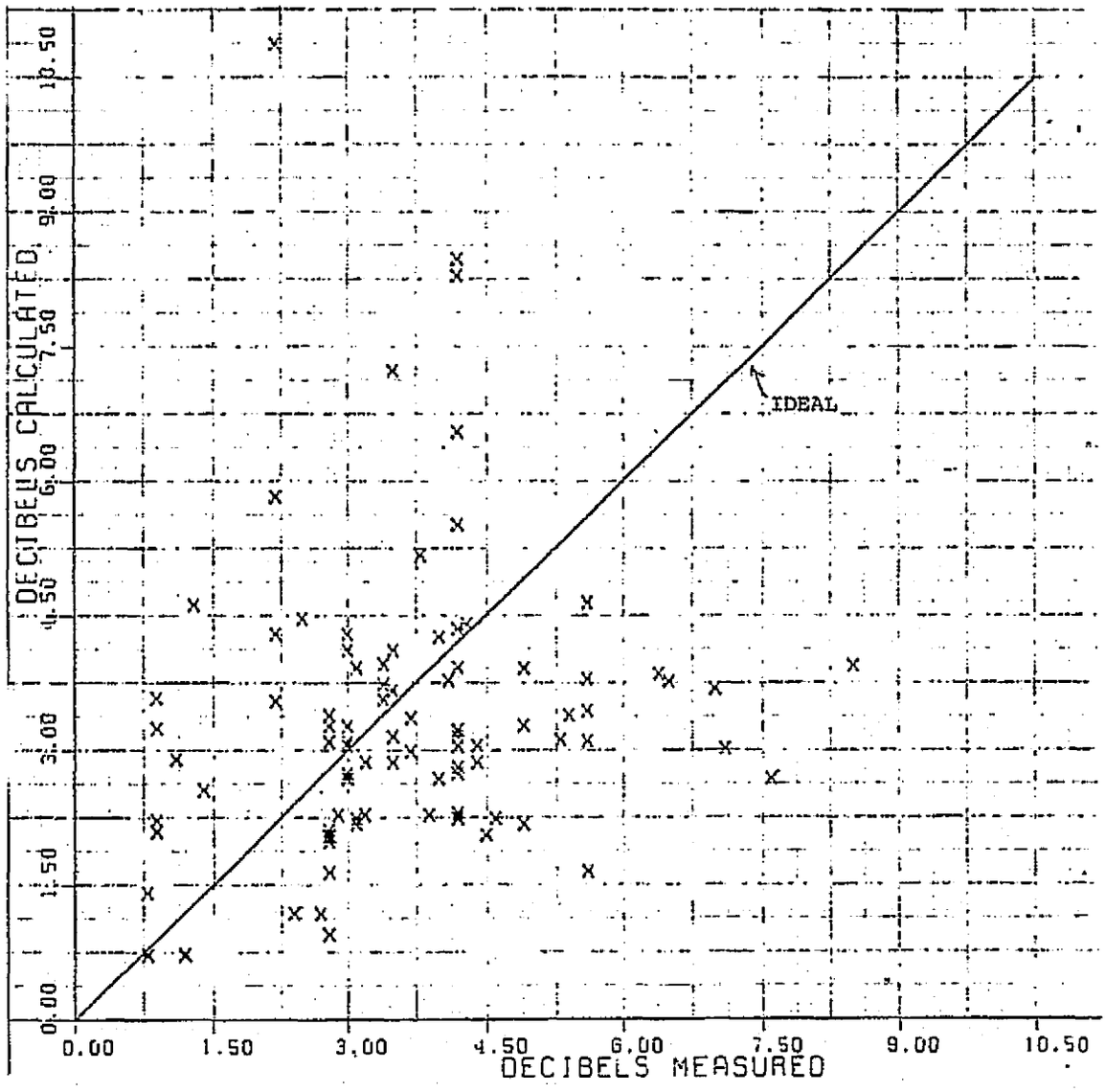

Figure 5-9(a). Scattergram of 20 GHz attenuation calculated vs. measured for 2 hour period on March 19, 1975 using original rain data from Figure 4.

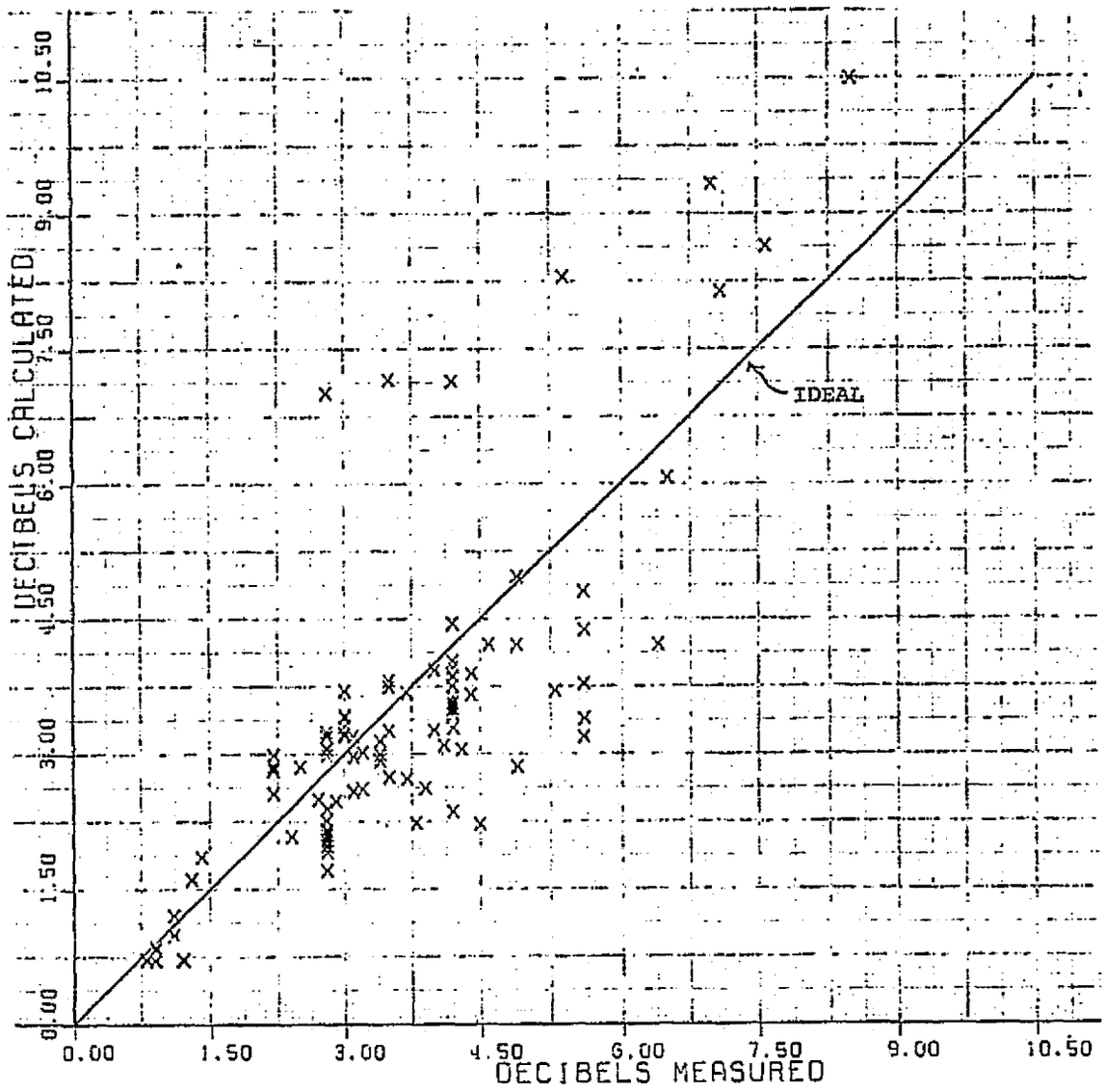

Figure 5-9(b). Scattergram of 20 GHz attenuation calculated vs. measured for 2 hour period on March 19, 1975 using model adjusted rain data from Figure 8.

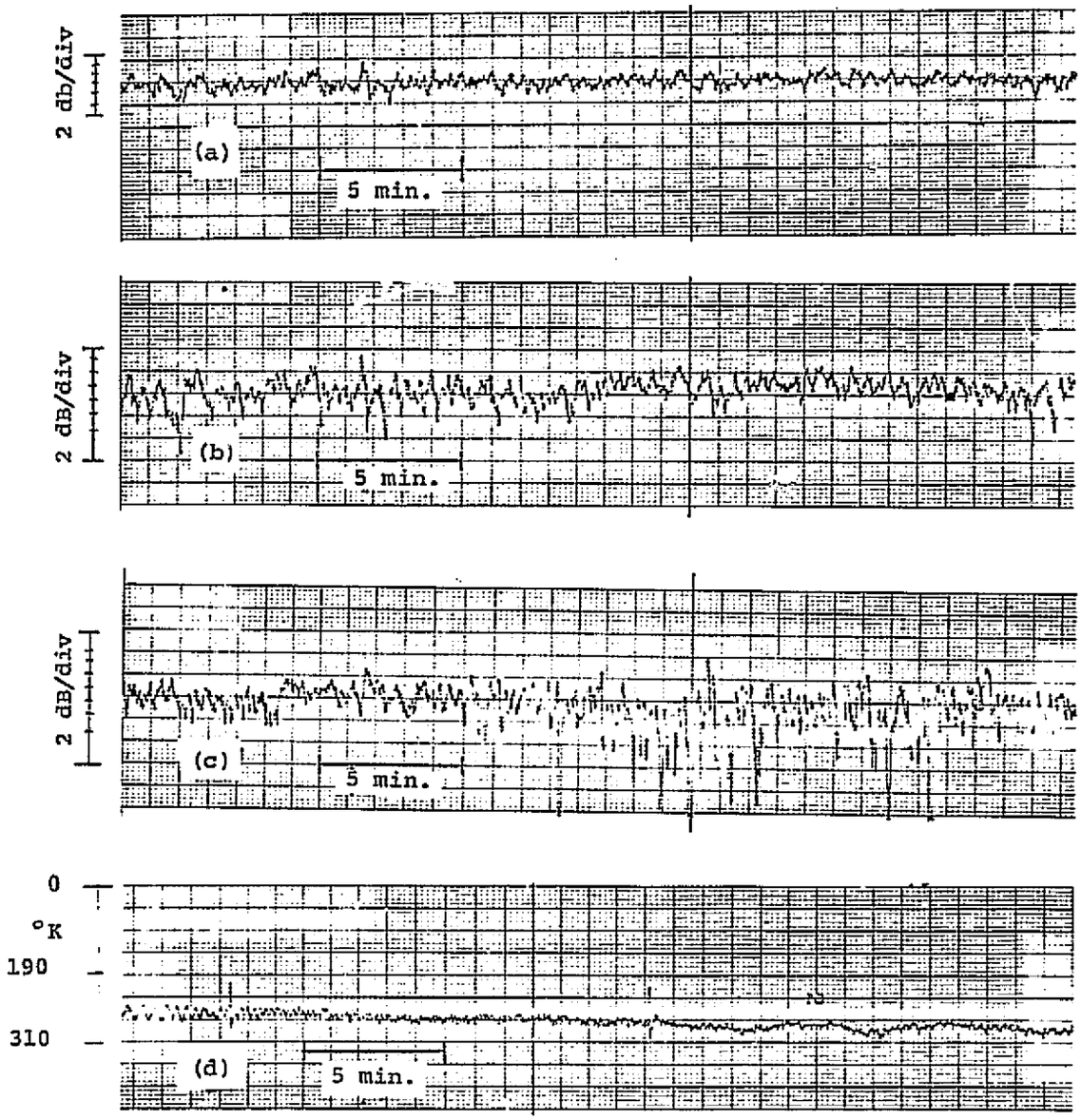

Figure 5-10. Recordings of 20/30 GHz low elevation angle signals. (a) and (b) show steady variations at 20 GHz and 30 GHz respectively. (c) and (d) show simultaneous recordings of 30 GHz ATS-6 signal and 30 GHz radiometer as light rain began. Antenna elevation angle 6.5°.

While several different physical mechanisms are probably responsible for the scintillations recorded, the occurrence of low elevation angle scintillation was expected. As noted earlier, the observed effect was no doubt a result of the combined influence of scattering by tropospheric irregularities, angle of arrival variations, rain, etc. However, most notable and identifiable was the effect of water-laden rain clouds and rain. The weather radar operated at the receiving site proved particularly useful in identifying the presence and movement of cloud systems. An interesting example is the 30 GHz recordings shown in Figures 5-10(c) and 5-10(d). Steady variations in the signal level of 5 dB peak-to-peak had been continuously recorded for well over an hour when the scintillation magnitude increased, significant absorption was also occurring as indicated by the average decrease in the signal strength and the radiometers. Figure 5-11 shows the extreme contrast in nature of scintillation recorded during rain and during early morning clear skies.

Since the scintillation magnitude is expected to be proportional to the path length through the lower atmosphere, the magnitude would be expected proportional to the cosecant of the antenna elevation angle. Because of the extreme variability of the local weather throughout the time when scintillations were recorded, the relationship between elevation angle and scintillation magnitude cannot be easily obtained. In spite of the strong effect of the weather however, some elevation angle dependence is evident from the data. The peak-to-peak magnitude of the 30 GHz scintillations were generally greater than that simultaneously recorded at 20 GHz. This fact was particularly evident during cloud and rain scintillations.

V. CONCLUSION

As we have mentioned, due to the rigid assignment of priorities, there was a considerable amount of difficulty in securing the 20/30 GHz beacon transmission from the satellite when heavy precipitation was in progress at the Clarksburg experiment site. This severely curtailed the data base on the whole experiment.

On the other hand, the program did yield many important results. For example, a new and more efficient method of estimating the slant-path microwave attenuation using a network of rain gauges was established. From event-by-event analysis, one can determine the accuracy of using a radiometric measurement of sky temperature as a substitute of direct satellite-signal attenuation measurement. The validity of using a radiometer to derive the yearly attenuation statistics, will be shown in the final report of this program when a one-year radiometric

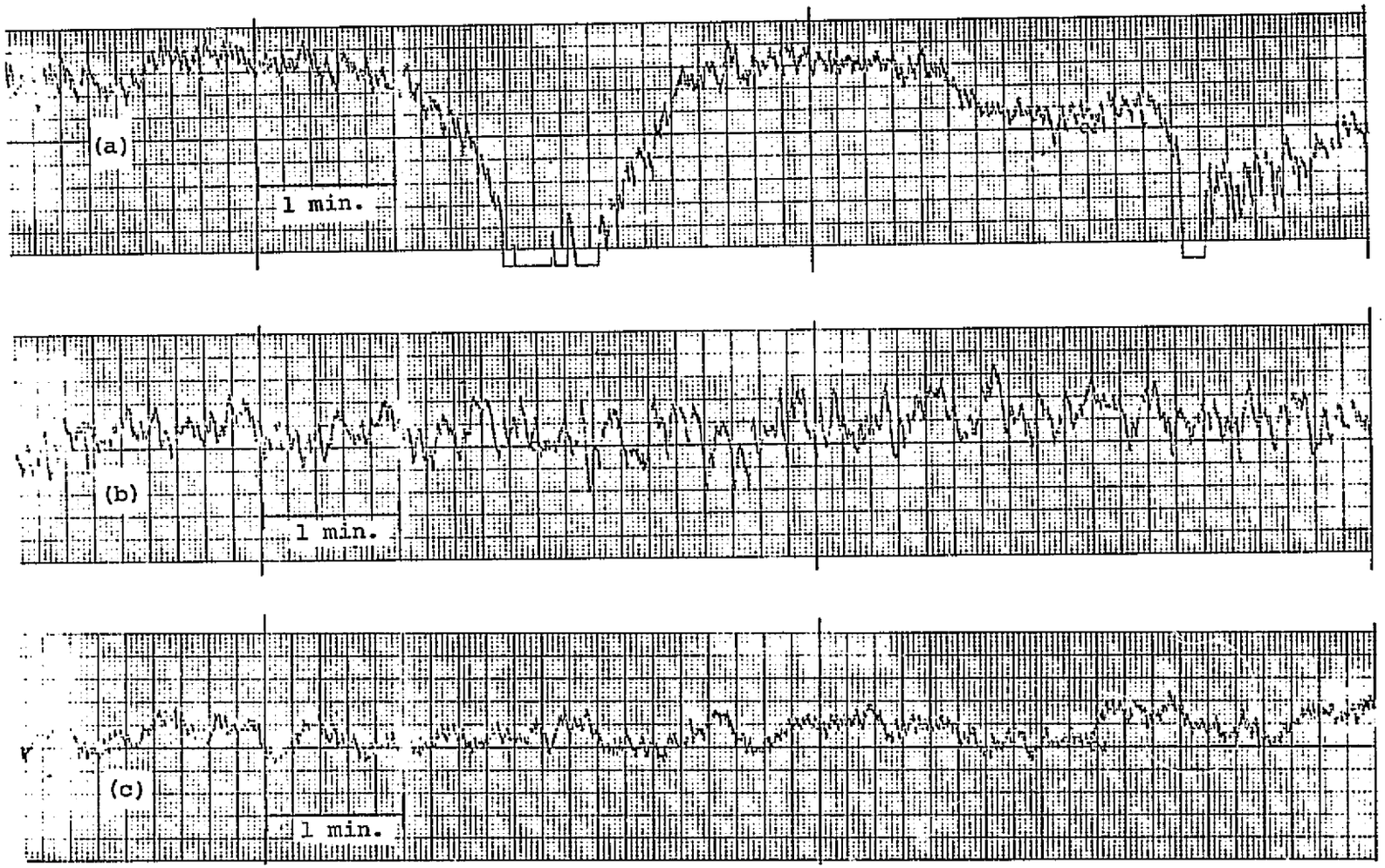

Figure 5-11. 20 GHz Recordings:

(a) Rapid scintillations during moderate rainfall at ~6° elevation angle.

(b) Strong scintillations during heavy local cloud cover at ~6° elevation angle.

(c) Slow scintillations during overcast skies at ~3.5° elevation angle.

observation has been completed. Other meaningful analyses which will be generated later from the existing data base include an estimate of the scattering effect in radiometric measurement obtained by comparing the data at 11.6, 20 and 30 GHz frequencies, and the low-elevation propagation characteristics obtained by studying the records of the descending satellite. All these will be useful in identifying the precipitation phenomena that degrade microwaves communications at 20 and 30 GHz.

RESULTS FROM THE ATS-6 20 GHz DEPOLARIZATION EXPERIMENT AT VIRGINIA POLYTECHNIC INSTITUTE AND STATE UNIVERSITY

by

C. W. Bostian, W. L. Stutzman, E. A. Manus, P. H. Wiley, and R. E. Marshall
Electrical Engineering Department
Virginia Polytechnic Institute and State University
Blackburg, Virginia 24061

1. INTRODUCTION

The The VPI&SU ATS-6 experiment was primarily concerned with the depolarizing effects of precipitation at millimeter wavelengths. Since raindrops, snowflakes, and ice crystals are not spheres, they scatter electromagnetic waves anisotropically and change their polarization. This depolarization will produce crosstalk in communication systems which employ orthogonal polarizations for frequency re-use, and an understanding of atmospheric depolarization phenomena is necessary for the design of future earth-satellite systems.

Depolarization is described quantitatively by two related variables; these are illustrated in Figure 6-1. The cross polarization ratio (CPR) is the decibel ratio of the cross polarized component of the received electric field to the co-polarized component.

$$CPR = 20 \log_{10} \left| \frac{E_{cross}}{E_{co}} \right| \qquad (1)$$

Since it is directly related to the electric field, the CPR is more frequently used by investigators studying the scatteri ng process itself. Communicators are more concerned with cross talk and the relevant parameter here is the cross polarization isolation (CPI). In a two-channel communications system the CPI is the decibel ratio of the power received from the co-polarized transmitter to the power received from the cross-polarized transmitter. Thus

$$CPI = 10 \log_{10} \frac{\text{power received from co-polarized transmitter}}{\text{power received from cross-polarized transmitter}} \qquad (2)$$

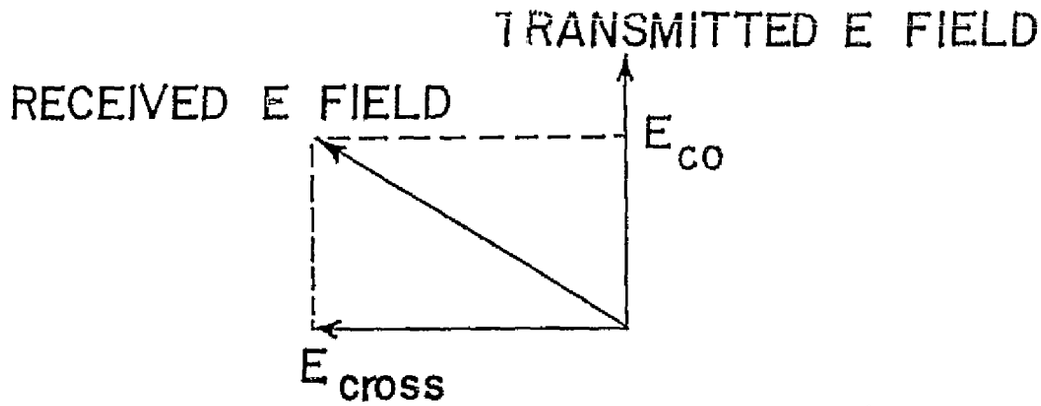

$$CPR = 20 \log_{10} \left| \frac{E_{cross}}{E_{co}} \right|$$

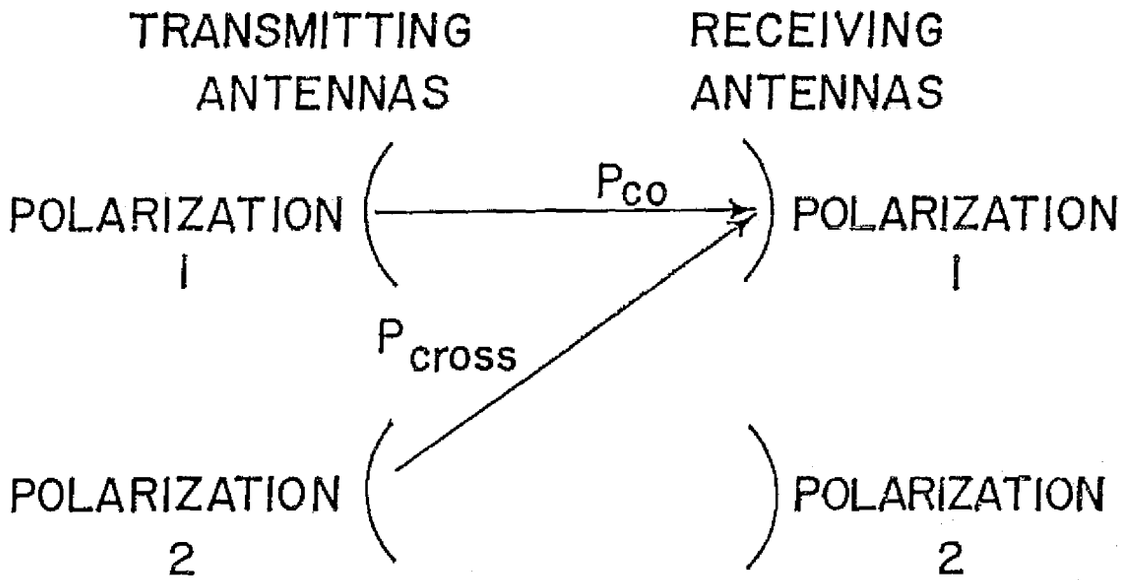

$$CPI = 10 \log_{10} \frac{P_{co}}{P_{cross}}$$

Figure 6-1. Definition of depolarization parameters.

The relationship between CPR and CPI is discussed in the literature [1,2]; in practice the CPI value is essentially the negative of the CPR value and the terms and numerical magnitudes are often interchanged.

Several groups are studying or have studied depolarization in terrestrial millimeter wave radio systems and at least two mutually consistent theoretical models have been developed [3,4]. The theoretical problem is complicated, but if one assumes that all of the drops are aligned and that their size and shape distributions are known, it is possible to calculate CPR and CPI as a function of path averaged rainfall rate, path length, and canting angle (the angle between the minor axes of the drops and vertical). The predictions of the theoretical models agree well with experimental data taken on linearly polarized ground paths, but the extent to which the existing models must be modified to describe satellite path depolarization is at present unknown. Additional statistical data is needed and will be collected when the Communications Technology Satellite becomes operational.

Depolarization on a ground to satellite path may be different from depolarization along a ground path for three reasons. These are (1) differences in size and shape distributions of the raindrops, (2) the presence of snow and ice in the freezing layer, and (3) the possible influence of cirrus cloud ice crystals. To investigate these factors and to study depolarization effects in satellite communications systems, several experiments are planned or in progress. The first measurements were made at 4 GHz by Roger Taur [5] of Comsat; our group and our colleagues at Bell Laboratories [6] worked at 20 GHz with ATS-6, and later efforts are planned by A. T. and T. [7], Comsat and NASA.

2. EXPERIMENT DESCRIPTION

The ATS-6 satellite transmits a linearly polarized signal at 20 GHz; in our experiment we measured the incoming power in the co-polarized and cross-polarized components of the incident signal. From these we can compute the CPR. Under clear weather conditions, the CPR is small (-28 to -50 dB, depending upon antenna alignment); precipitation depolarization causes it to rise.

Figure 6-2 shows the 4 ft. (1.22 m) antenna and terminal building for the experiment. A Ku-band radar, shown on the roof of the building, is used to probe weather conditions along the satellite path.

A block diagram of our experimental system appears in Figure 6-3. In addition to the CPR of the incoming signal, it records attenuation and ground-level rain and wind data. All of the equipment is under the real-time control of a dedicated Raytheon PB-440 digital computer (See Fig. 6-4) which updates the antenna

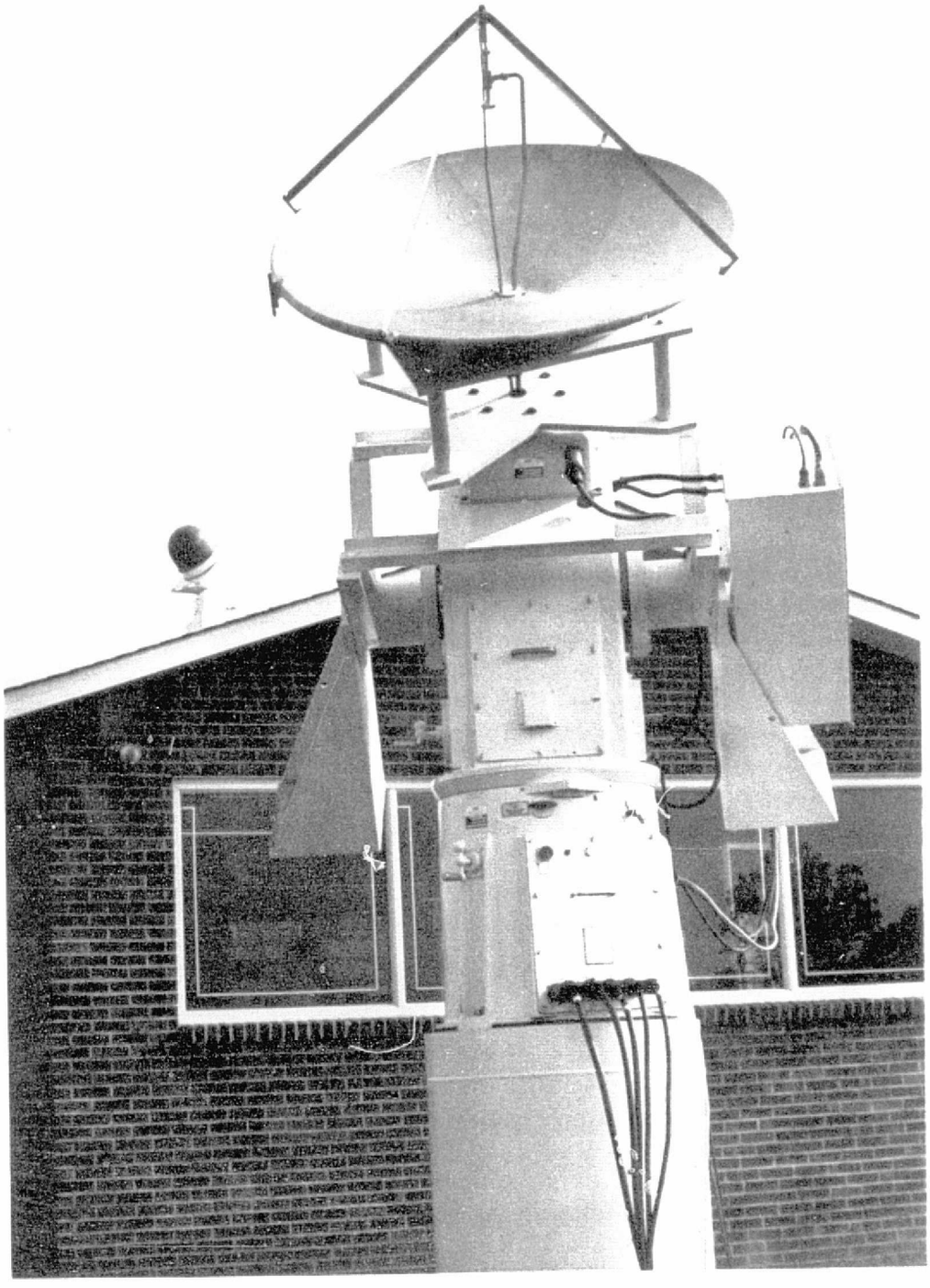

Figure 6-2. VPI&SU Antenna System

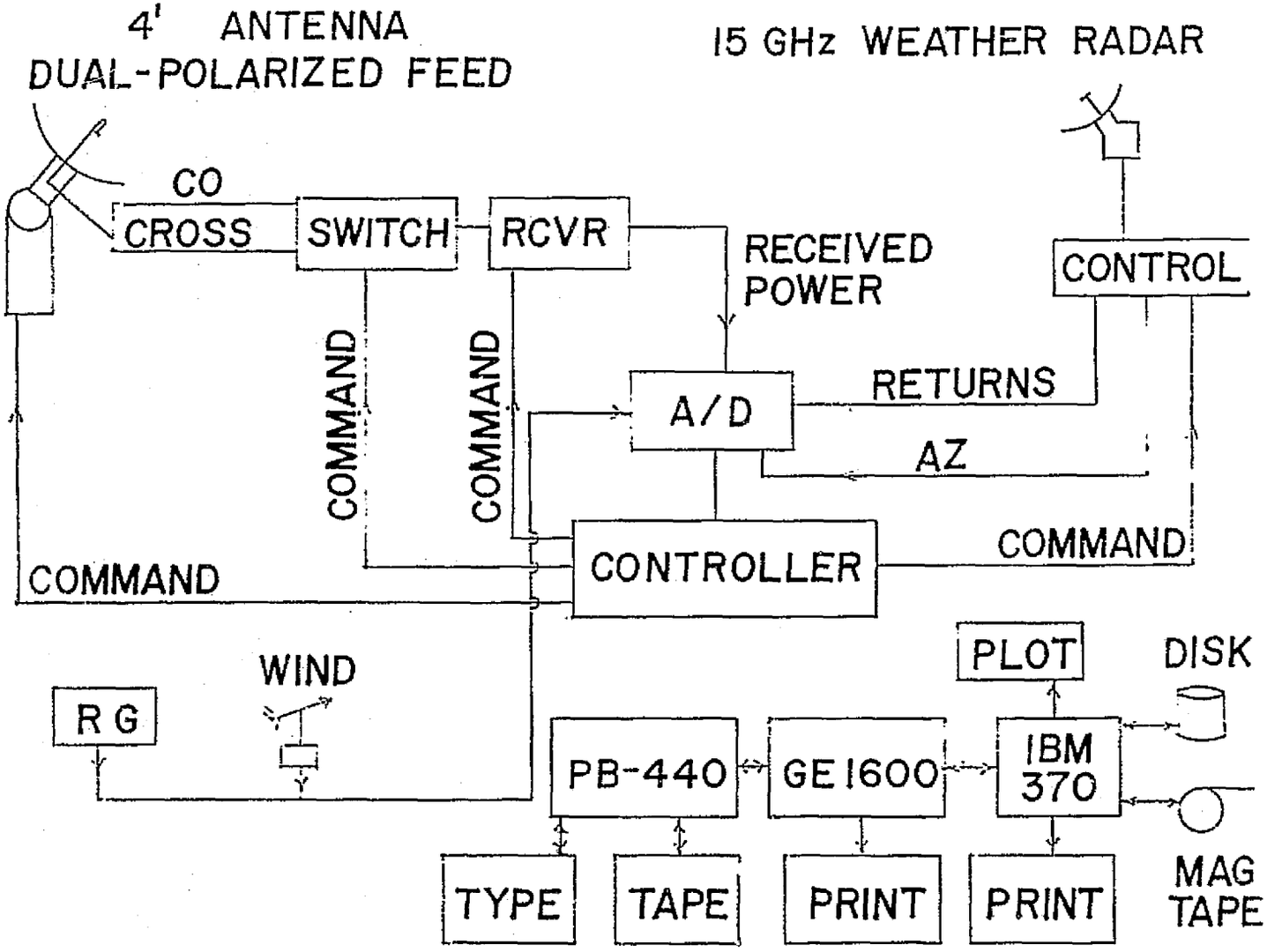

Figure 6-3. Experimental system block diagram.

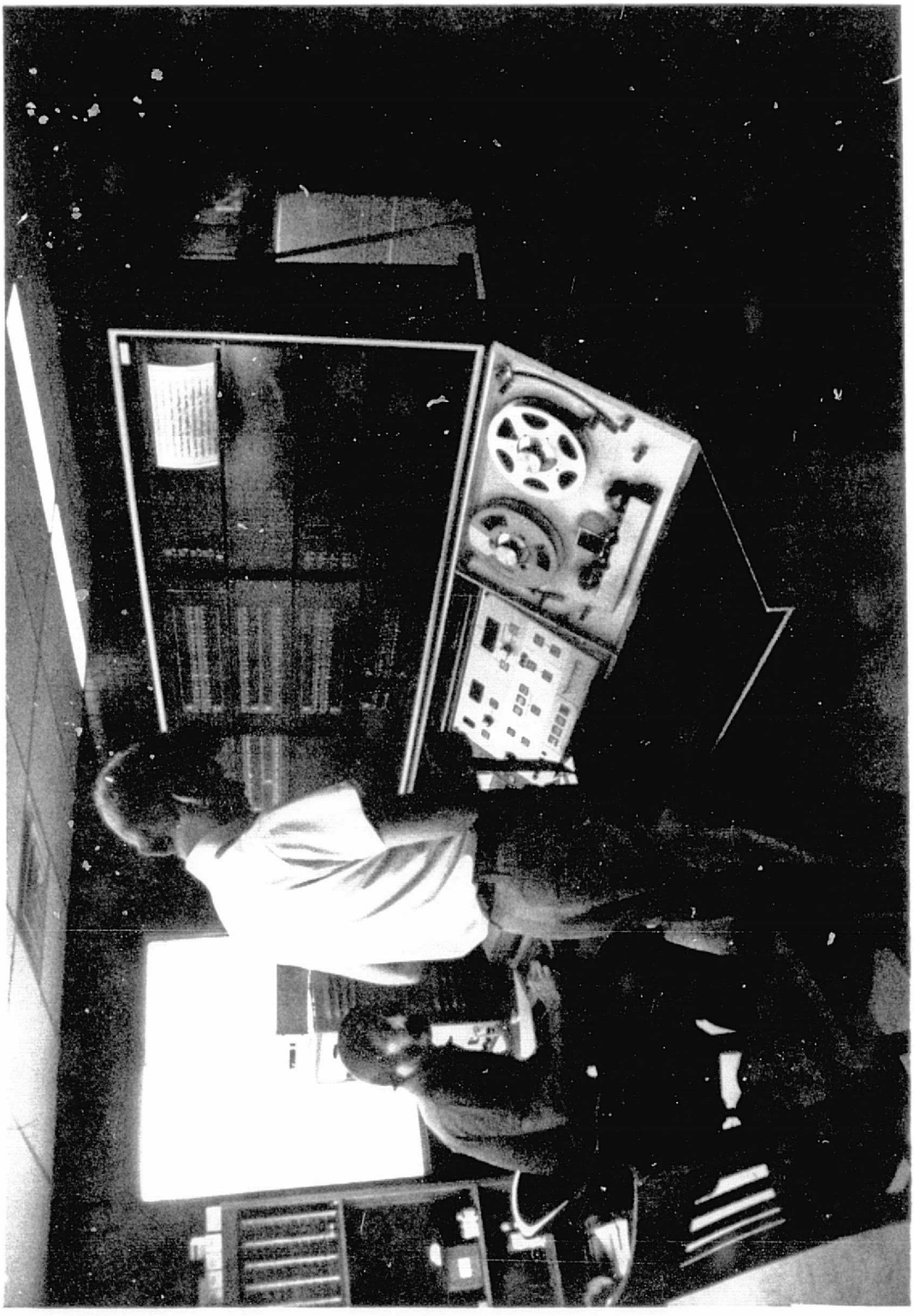

Figure 6-4. Raytheon PB-440 Computer.

pointing at ten-minute intervals and performs initial data processing. The receiver switches between the cross-polarized and co-polarized antenna feeds once every two seconds. The receiver, antenna controls and radar display are shown in Figure 6-5.

The results from the experiment were in the areas of rain effects, snow effects, low elevation angle effects, and clear weather effects. These results are discussed in the remainder of this paper. More details on the experiment and results are available in the literature [8].

3. RAIN DEPOLARIZATION

In order to successfully collect data, it is necessary that (1) the satellite be available with correct pointing and be operating nominally, (2) the ground station equipment be operating properly, and (3) a relatively intense rain event occur. During the ATS-6 project, these three requirements were seldom satisfied simultaneously. Thus, a large data base for satellite to ground propagation at 20 GHz does not yet exist. There are essentially only three storms which have data worthy of reporting; those of March 30, May 27 and June 12, 1975. In this section we shall discuss the data obtained from the first two of these storms, and the June 12 storm will be discussed in Section 5 because it occurred during low elevation angle pointing.

Almost all of the rain data was collected during the last few months of the project. Typically, data reduction procedures are developed by processing a few storms by hand and then writing computer programs to replace the hand computations. With the short time frame for data reduction, the computer programs were not developed until very late in the project. Thus, for the sake of expediency all data presented in this section was obtained from chart recordings and processed by hand.

On March 30, 1975, the first significant rain depolarization data was collected. In Figure 6-6 the rain rate, CPR, and the attenuation were plotted for the storm. The CPR and attenuation data points represent samples taken at one-minute intervals and the blank spaces are times when the receiver lost phaselock. The rain gauge data in Figure 6-6 are from three tipping bucket gauges. Gauge 1 (solid line) is directly beside the receiving antenna. Gauge 2 (dashed line) is 650 feet away and approximately 650 feet directly below the radio path. Gauge 3 (dotted line) is approximately 2500 feet away in the general direction of the satellite and about 2500 feet below the path. Since our 15 GHz radar indicated the rain was about 9 miles deep (in the direction of the satellite) and 3 miles high, we suspect that gauge 3 may have malfunctioned and reported only during the most intense rain.

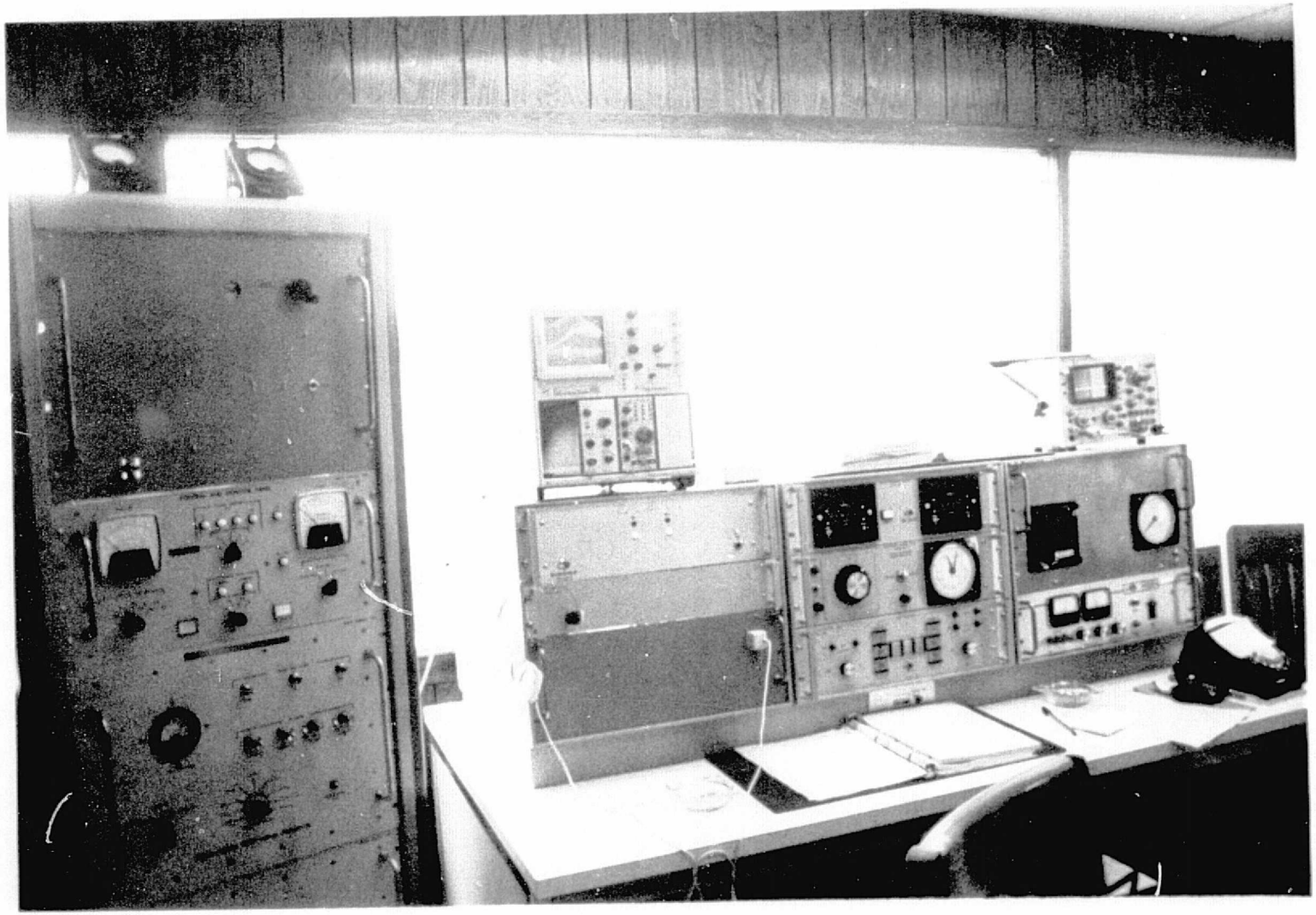

Figure 6-5. Receiver, Antenna Controls and Radar Display

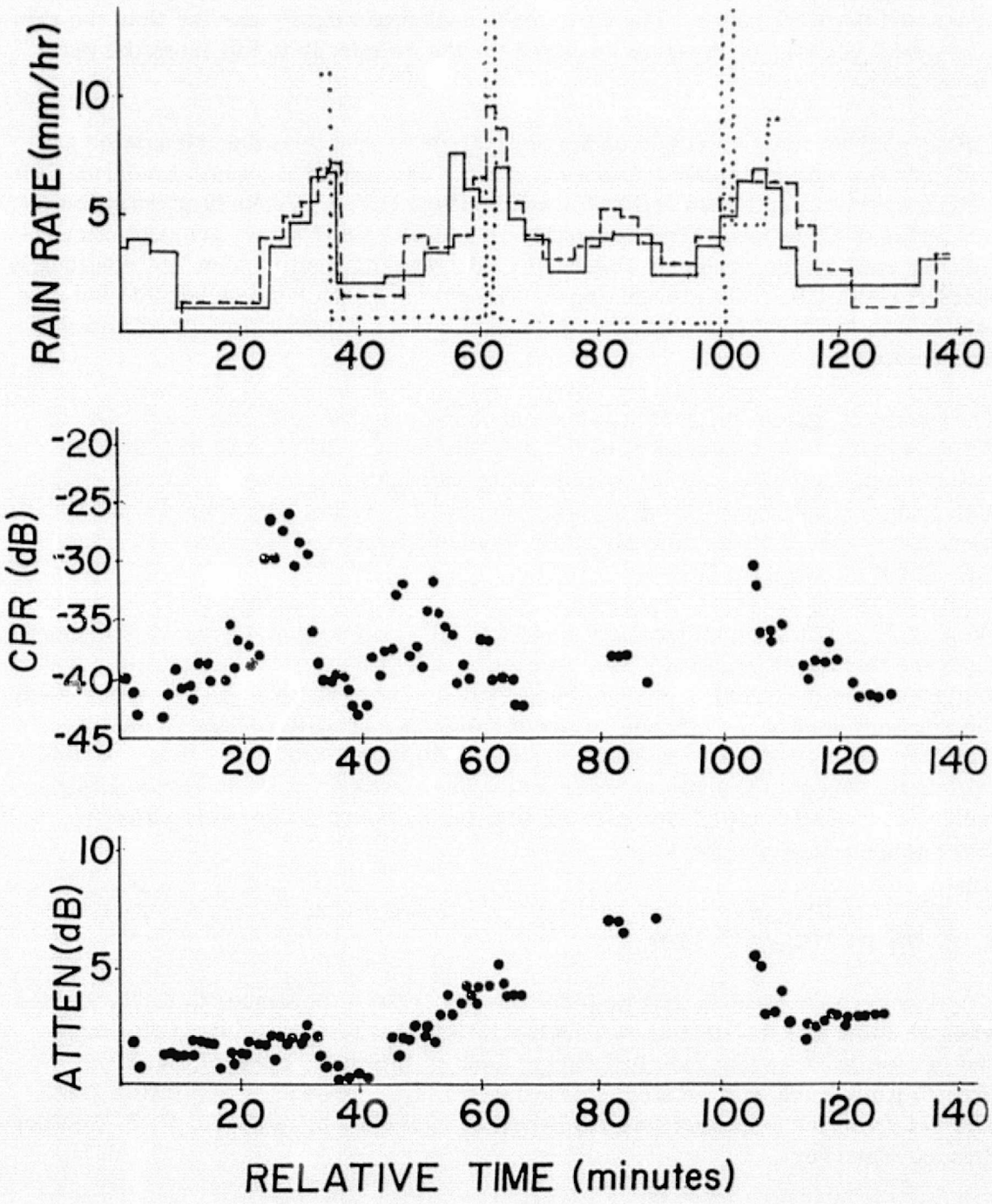

Figure 6-6. Rain depolarization data from the storm of March 30, 1975.

A striking feature of these data is the strong correlation between the rain rate peaks and the CPR peaks. The CPR peaks occurred slightly earlier than the rain rate peaks because of the time required for the raindrops to fall from the path to the gauges.

Unlike what we have observed on terrestrial radio systems, the attenuation and CPR are not well correlated with each other. The plot of attenuation versus CPR from terrestrial path data follows a well-defined curve. Peaks of attenuation and peaks of CPR occur simultaneously [9]. Figure 6 7 shows average attenuation for each integer value of observed CPR. The attenuation does not continually increase with CPR. No explanation is offered for the lack of correlation between attenuation and CPR from satellite path data. More experimental observations are needed.

The storm of March 30, 1975 was the only hard rain for which we were able to get data prior to the movement of the satellite toward 35° E. As the satellite moved east, the clear weather polarization angle that we observed at our station began to increase toward 0° from its nominal -21° value. It passed through 0° when the spacecraft was directly south of us and increased to about +50° when we lost signal on June 13, 1975.

On May 27, 1975, the polarization angle was +6°, and on that day we experienced a severe thunderstorm with fading in excess of 14 dB. The data for this storm are presented in Figure 6-8. The blank portions in the attenuation data are when the receiver lost phaselock due to power failures. The interesting feature is that there was essentially no change in the CPR during this rain. One possible explanation for this is that the polarization angle was so close to vertical that the incident electric field was aligned with the raindrop minor axes and thus there was no depolarization.

4. SNOW DEPOLARIZATION

A severe snowstorm lasting from November 30 – December 2, 1974, yielded what we think are the first snow depolarization data for a satellite path. Snow and occasional freezing rain fell during most of this time interval, but from time to time there was considerable variation in the ground precipitation rate. The net snow accumulation was measured at 10 inches by our local U. S. Weather Service observer.

Since the spacecraft operational restrictions prevented us from obtaining a continuous look at the signal from beginning to the end of the storm, we made a series of separate observations, each several hours in length. After the storm was over, we made clear sky calibration runs on December 3 and 6 to aid in data analysis.

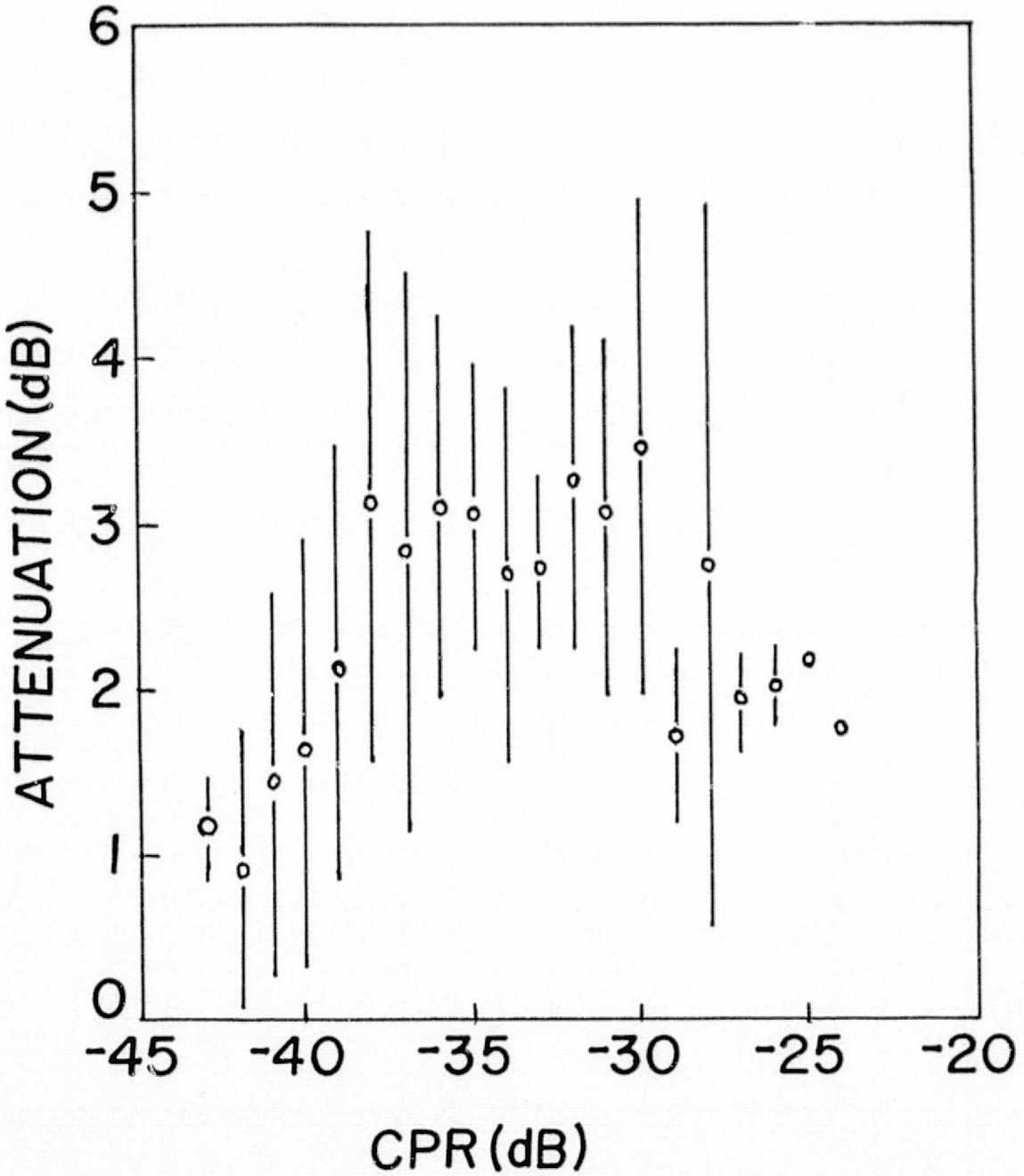

Figure 6-7. Attenuation versus CPR for the storm of March 30, 1975. Each point represents the average attenuation at each 1 dB interval of CPR. The vertical bars extend ± one standard deviation from the average.

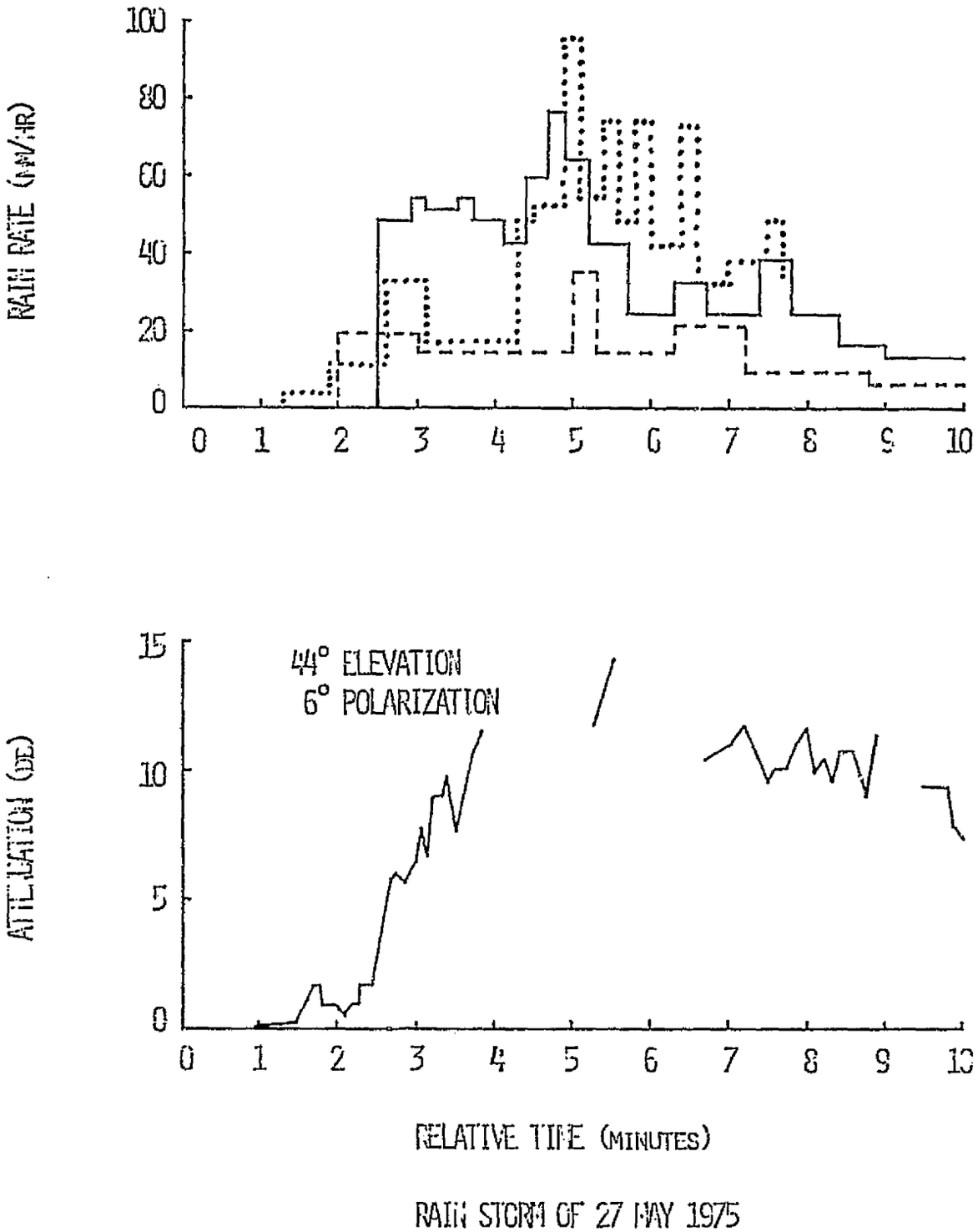

Figure 6-8. Data from storm of May 27, 1975. No CPR was observed.

Figure 6-9 displays average measured values of attenuation and cross polarization ratio versus time for the data runs between November 30 and December 6, 1974. Breaks in the time axis emphasize that this figure is a collection of data from five different runs spread over six calendar days.

The θ variable in Figure 6-9 is the antenna polarization angle. Under clear weather conditions at the time of measurement the incoming signal was polarized at or near $\theta = -19.5°$, but with this antenna polarization the cross-polarized component was below the receiver phaselock threshold. Since then, we have improved the receiver sensitivity to the point that it maintains lock on the cross-polarized components. But at that time we normally operated the antenna at $\theta = -16.5°$; this provided a clear weather isolation of -28 dB and enabled the receiver to work properly. However, on December 2, the snow depolarization was such that we were able to make measurements at $\theta = -19.5°$.

On November 30 and the early part of December 1, heavy snow was falling. During the second run on December 1, the ground snowfall rate was negligible, but heavy cloud cover remained and surprising attenuation and CPR values were measured. On December 2, the satellite was available during an intense snow shower. As the hour progressed, the snow rate decreased and we saw corresponding changes in the attenuation and CPR. Unfortunately, we had to relinquish use of the satellite before the snow ended.

Snow depolarization is somewhat more difficult to analyze than rain depolarization because at present a theoretical model is nonexistent even for a terrestrial path and in addition, we have no handy "snow rate" parameter analagous to rain rate. One approach is to plot attenuation versus CPR and examine the result. This is done in Figure 6-10 for all of the data presented in Figure 6-9.

The data in Figure 6-10 bear some resemblance to the attenuation versus cross polarization isolation plots calculated for rain depolarization in terrestrial radio systems using non-ideal antennas [10]. Figure 6-11 is a typical plot for a 19.3 GHz, 1 km, rain-filled path with 45° linear polarization and a variety of residual (clear weather) CPR values [10]. This is not a theoretical model for our 20 GHz snow data for the satellite path; it is introduced to show the trend of these surves and the effect on them of the residual isolation.

The effect of varying our antenna polarization angle is to change the residual CPR. At $\theta = -16.5°$, the clear weather CPR is -28 dB; the measured data at $\theta = -16.5°$ bear some resemblance to the -30 dB theoretical curve for rain.

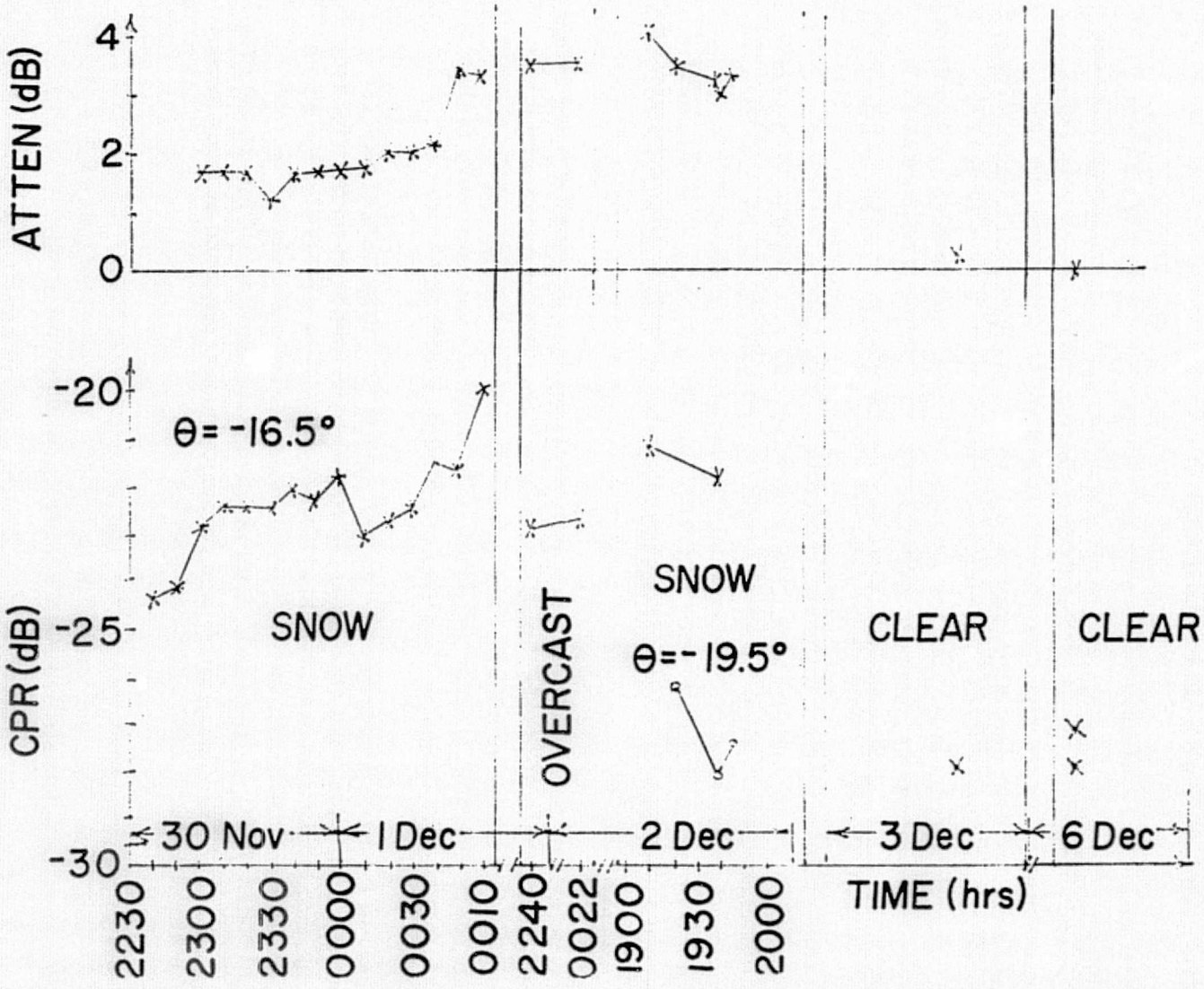

Figure 6-9. Attenuation and CPR data for the snowstorm of November 30 – December 2, 1974.

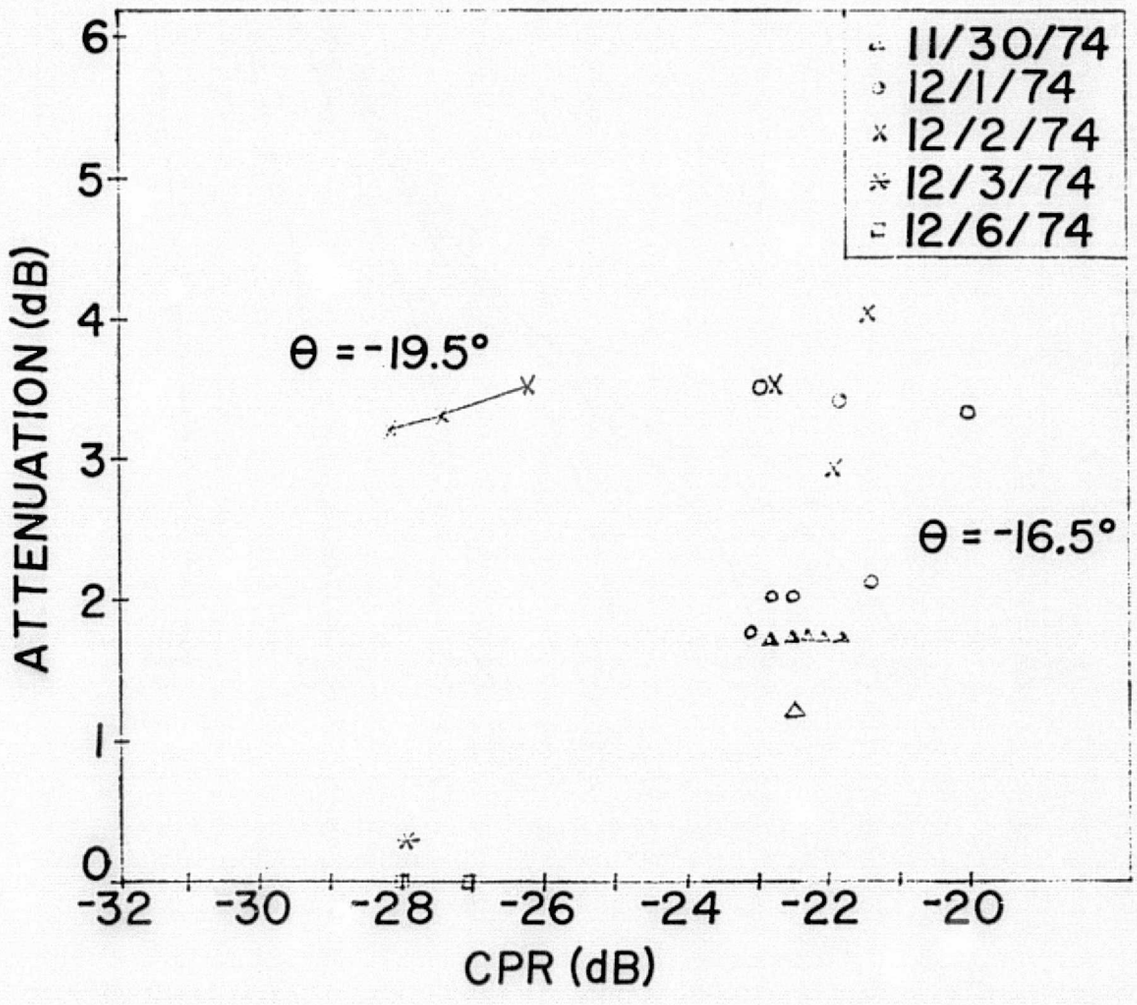

Figure 6-10. Attenuation versus CPR for the November 30 – December 2, 1974, snowstorm and subsequent clear weather calibration periods.

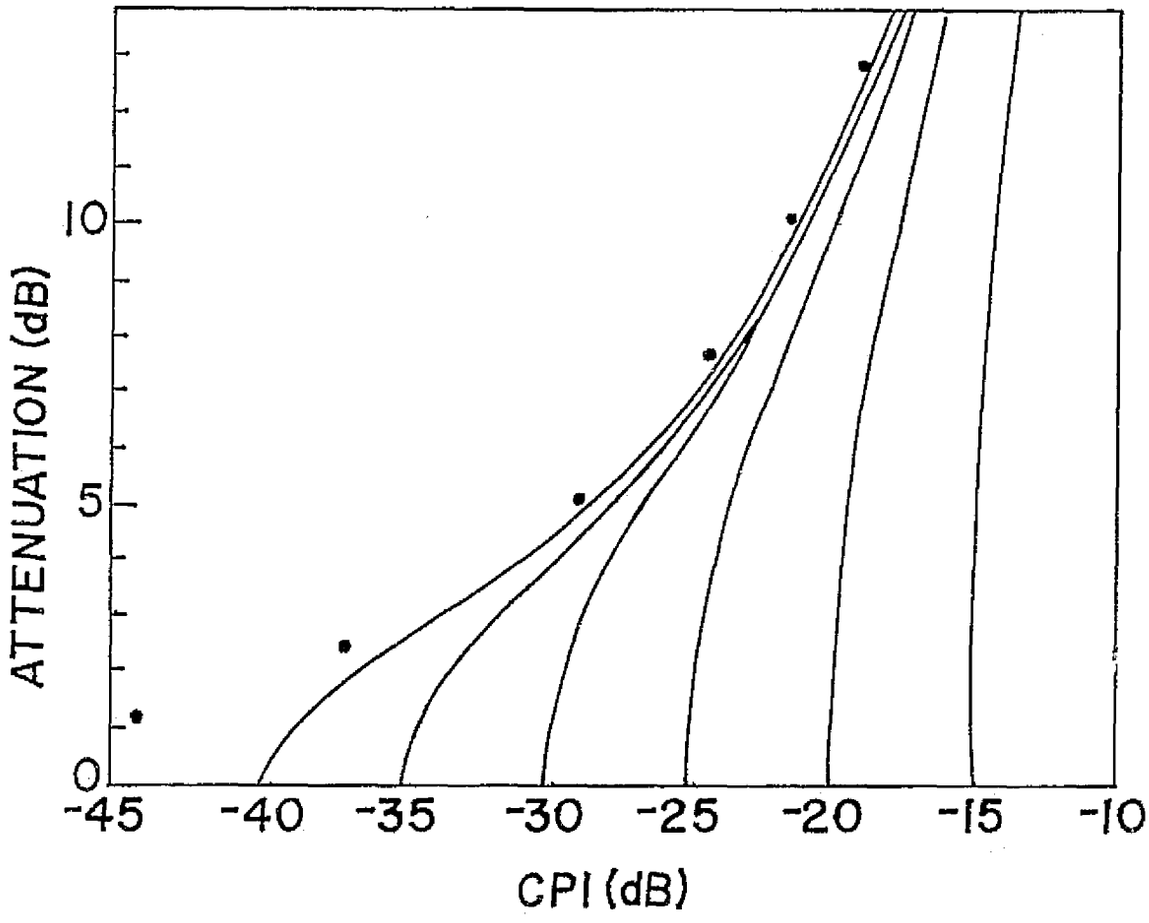

Figure 6-11. Rain induced fade versus cross polarization level (including antenna effects) at 19.3 GHz, a 1 km path, and 45° linear polarization. Points indicate scattering model theory for no antenna effects.

A question to be resolved about all of this is where do the depolarization and attenuation occur? Is it in the obvious snowflakes near the ground, or is it in the clouds overhead, or do both play a part? Certainly our data of 2240 (UT) on December 1 through December 2, 1974, implicate the clouds, because little or no ground precipitation occurred during this time. On the other hand, the attenuation and CPR levels noted 1900 – 1950 on December 2, 1974, were correlated with the snow intensity at ground level by visual observation of the snow and the radar A-scope. When both clouds and snow were gone, the clear weather signal levels returned to their normal values. The obvious conclusion is that ground precipitation and higher altitude phenomena both play a role; the only sure way to separate the two is to compare snow depolarization data measured simultaneously on terrestrial and satellite paths.

Another potential source of error related to the antennas is apparent depolarization resulting from off-axis reception.* Ghobrial and Watson [11] first reported this as being caused by refractive effects on long paths; on a satellite path it could conceivably come from refraction or from antenna pointing errors. To eliminate both possibilities we made plots of CPR versus azimuth and elevation offset during the clear weather tests of December 6. These showed the CPR levels associated with off-axis reception to be well below the values measured during the storm (at least for the high residual CPR associated with $\theta = -16.5°$) and would seem to eliminate off-axis reception as a source of error in our data.

A striking feature of the snow data displayed in Figure 6-10 compared to rain data from a terrestrial link [2] is the large depolarization observed for a given attenuation. To get a CPR of -28 dB (the leftmost $\theta = -19.5°$ point in Figure 6-10) with rain on a ground path would require at least 7 dB attenuation and possibly as much as 20 or 30 dB, depending on path length and raindrop canting angle.

Some theoretical case may be made for associating small attenuation and severe depolarization with scattering by bodies which are relatively loss-less but lack rotational symmetry. Certainly snowflakes and high altitude ice crystals fit this description, but the very fragmentary data available for snow do not necessarily support this conclusion. Watson [12] working at 11 GHz with a 13.7 km path reported a huge fade (24 dB) in wet snow accompanied by a CPR of -22 dB. On the other hand, a rain fade of only 8 dB on the same path was associated with a -20 dB CPR. Since our frequency is almost twice that of Watson's and his snow was wet while ours was dry, it is very possible that he could have been dealing with scatterers that were relatively more isotropic than ours were. Some Russian work [13] at a much higher frequency also indicates that, for the same water content, snow attenuates more highly than rain, but this tells us nothing about depolarization. Clearly more research is needed. We should operate a terrestrial path link and a satellite downlink simultaneously, and also study the high altitude conditions with a polarization diversity radar.

5. MEASUREMENTS AT LOW ELEVATION ANGLES

At the conclusion of this experiment we were able to monitor the satellite more or less continuously for elevation angles ranging from about 9° down to 1°. This gave our group and many of the other East Coast ATS-6 Millimeter Wave Experiment participants a unique opportunity to study 20 GHz propagation at extremely low angles.

*So far as could be determined, snow and ice accumulation on our antenna reflector and feed were negligible throughout the storm.

During the observing periods the weather changed rapidly, alternating between sunshine, rain, and fog; at times all three seemed to be occurring simultaneously on different segments of the path. For this reason it was frequently difficult to associate changes in the received signal with any particular weather condition.

Narrative Discussion of the Data

When the satellite was at 22° elevation, our antenna pedestal went out of control and broke a number of cables. We were able to repair the equipment and re-acquire the signal at 9.12° elevation, but our data have an unfortunate gap between these two angles.

At the time we re-acquired the satellite the clear weather signal was 12 dB below what it had been at 45° elevation. This measurement provided the first set of points in Figure 6-12 which shows the overall behavior of the co-polarized signal. The maximum and minimum signals occurred no more than four (4) minutes apart. These represent two sets of observations taken before and after a light rain.

The data measured at 7.61° elevation was taken after a storm that reached 30 mm/hr and before a 6 mm/hr sprinkle. Although the weather radar indicated no rain along the downlink, the sky was partly cloudly and there was light rain in the area. The time between the maximum and minimum signal strengths was no more than two (2) minutes. The clearest sky observed during tests below 10° elevation (excluding 1.1°) occurred at the elevation angle of 5.6°. The sky was hazy; however, the weather radar gave no indication of rain within 15 miles of the station. The scintillation frequency was approximately 1/6 Hz. As the elevation angle moved to 5.46°, rain began moving into the area. The 1 dB scintillation was observed before the rain entered the path. At one time rain extended nine (9) miles up the path. As the rain began to dissipate, the signal, as expected, began to increase. Before the signal returned to the clear weather reference, it started down again even though the radar indicated that the rain had completely dissipated along the path. The receiver then lost and regained phase lock three (3) times in ten minutes although there was no radar indication of rain along the path. When the receiver did regain phase lock on a strong signal, the co-polarized signal would fall about 0.5 dB/sec until the receiver again lost phase lock. After the receiver re-acquired the 20 GHz CW signal for the third time, the signal strength returned to the clear weather level with the same scintillations observed initially at 5.46° elevation. The data measured at 5.11° elevation were taken after a storm that reached 25 mm/hr. The data taken from 4.95° to 4.80° elevation were not interrupted by rain; however, the sky was hazy along the path. The scintillations tended to become larger and

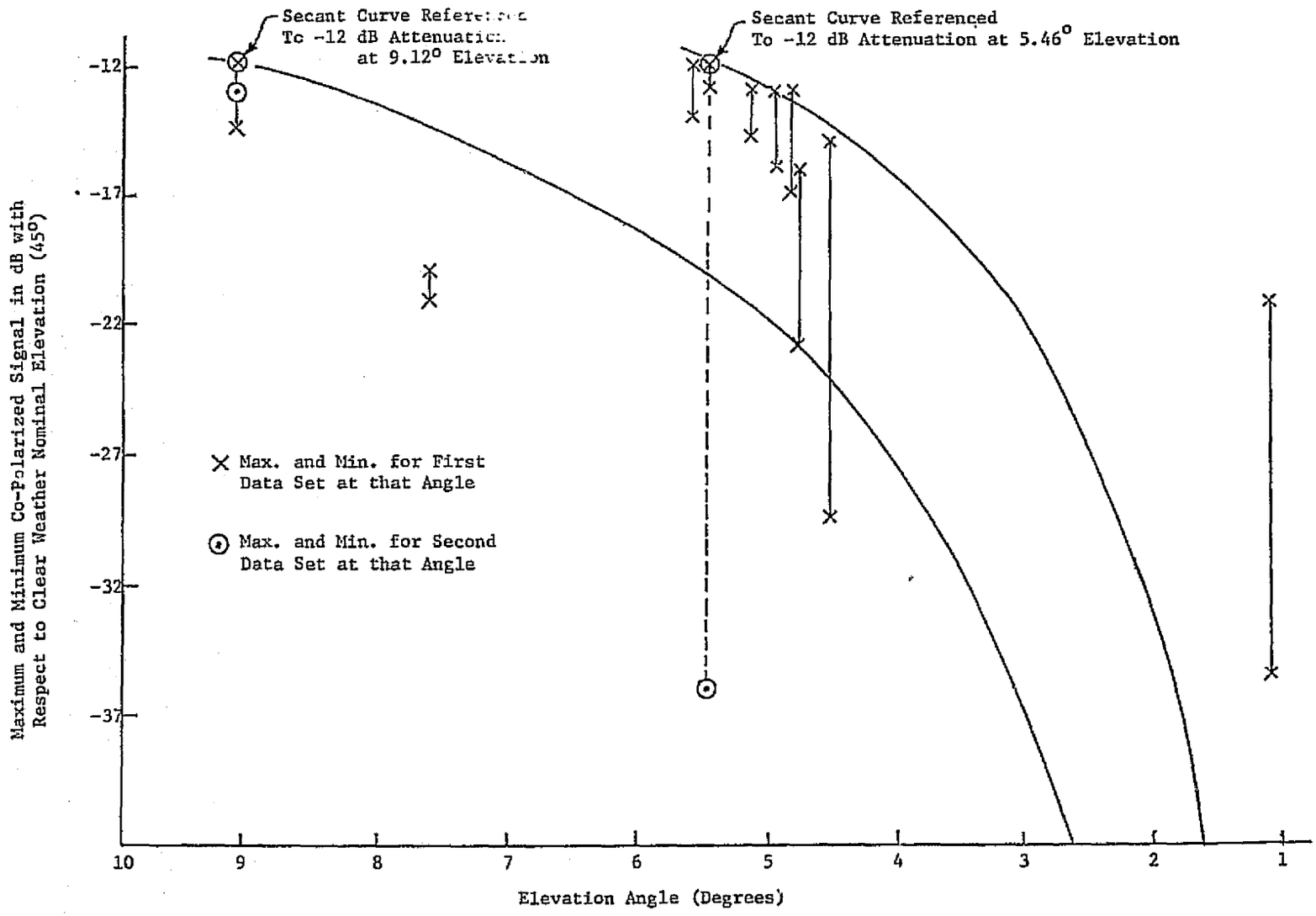

Figure 6-12. Attenuation data at low angles.

more frequent as the angle decreased. A 15 mm/hour drizzle preceded the measurements at 4.8° elevation; and although there was no radar indication of rain along the path, the signal level never came up to the clear weather reference. The scintillation patterns were composed of the higher frequency variations noted at 5.46° elevation but superimposed on sixty (60) second scintillations of the magnitude indicated in Figure 6-12. The large variation indicated at 4.54° elevation only occurred once. The remaining twelve (12) minutes of data taken at 4.54° elevation produced scintillations up to 8 dB of the type described at 5.46° elevation. The sky was partly cloudy at this time.

Antenna Pattern Broadening

After the satellite was re-acquired at 9.12° we noticed a pronounced broadening of the antenna radiation pattern in the elevation plane. The signal remained quite sharp in azimuth but in elevation the 3 dB points were frequently separated by several degrees. The same effect was noted by our colleagues at Comsat Laboratories.

On the last day that we were able to receive the signal, the broadening disappeared and the elevation pattern returned to its former sharpness. At this time the peak co-polarized signal occurred at an elevation angle of 1.1°, and the boresight telescope indicated that at this elevation the antenna was pointed <u>below</u> the crest of a nearby mountain! Presumably the propagation mechanism was knife-edge diffraction, but in that case the signal should have originated from the crest of the mountain.

We think that multipath propagation was responsible for the pattern broadening. Given the low elevation angle, and assuming horizontal stratification in the atmosphere, it is easy to hypothesize rays entering the receiving antenna from a statistical distribution of elevation angles. Certainly the scintillations, and the focusing and cross polarization effects (both described below) that we saw indicate the presence of multipath.

Clear Weather Attenuation at Low Angles

As the satellite elevation angle decreased, the tropospheric part of the propagation path lengthened. In a horizontally stratified atmosphere this would cause a decrease in signal strength proportional (in dB) to the secant of the elevation angle. Our intent was to measure the co-polarized signal clear-weather level at 45° elevation and look for this secant behavior. This effort was complicated by the lack of any data between 22° and 9.12°. Taking the signal levels at 9.12°

and 5.46° elevation as references, we have plotted two secant curves in Figure 6-12. These show fair agreement with the data in the 9° to 4° range. Of course at extremely low angles the norizontal stratification model breaks down.

Rain Attenuation at Low Angles

We were able to observe significant rain attenuation at 7.59°, 5.35°, and 4.70°. The results are displayed in Figures 6-13, 14, 15. In each case these display attenuation (calculated from the clear-weather signal level immediately before or after the storm) and the rain rate at the rain gauge located beside the receiving antenna. The correlation between the rain rate and attenuation in Figures 6-13 and 6-15 is outstanding. The high attenuation for a given rain rate is a result of the extremely long rain path.

Polarization Effects at Low Angles

The polarization response of our antenna was a sharp "V" at 45° elevation; below 9.12°, however, the polarization null became very wide and measuring the polarization angle with precision was more difficult. Nevertheless finding the null location and finding the average of the two polarization angles for which the co-polarized and cross-polarized signal levels were equal both gave similar results. Presumably the broadening was due to multipath.

At first the measured polarization angles tracked the theoretical predictions. Thus, for measurements made at 9.12° elevation and 7.61° elevation the polarization angle was +49.0°. Data taken at 5.60° to 5.11° were recorded at a polarization angle of +52.0°. As expected the polarization angle moved to 52.5° for the data sets at 4.95° and 4.85° elevation; however, at 4.80° the polarization angle was measured to be +47.0° and it moved to +46.0° at 4.54° elevation.

We have no explanation for this reversal at 4.8°. Perhaps it is related to the clear weather polarization angle effects noted at higher elevation.

The 12 dB loss in signal level between 45° and 9.12° that was discussed earlier forced us to remove the last 12 dB of front-end attenuation from the copolarized channel. Given the limited dynamic range of the ATS receiver, this meant that we would only measure CPR values greater than -20 dB. Rain depolarization of this magnitude requires considerably harder rain than we experienced; hence we observed no rain depolarization at extremely low angles. However, we did record one case of severe CPR increase due to multipath; this appears in Figure 6-14.

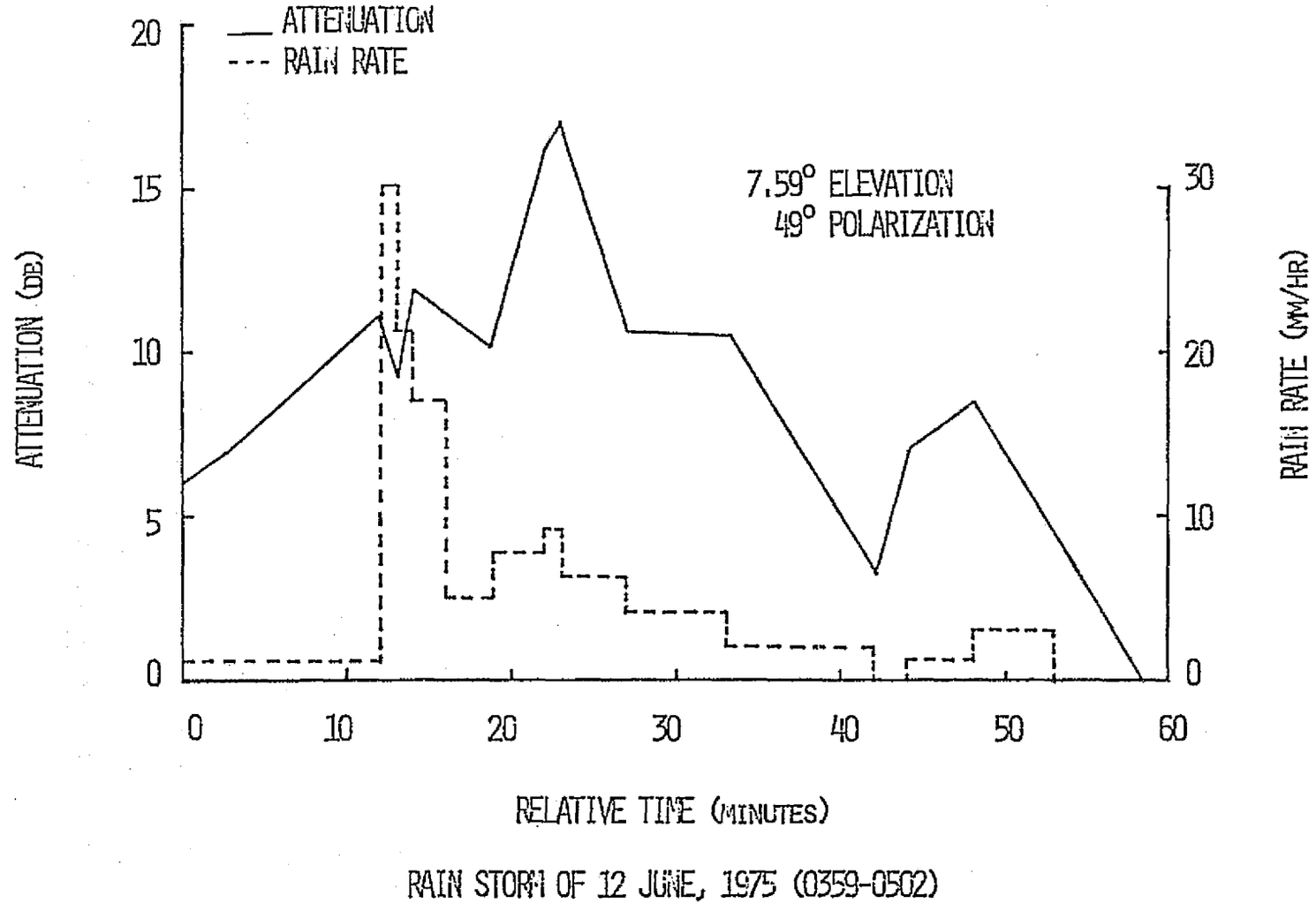

Figure 6-13. Data from rain storm of June 12, 1975 (0359-0502)

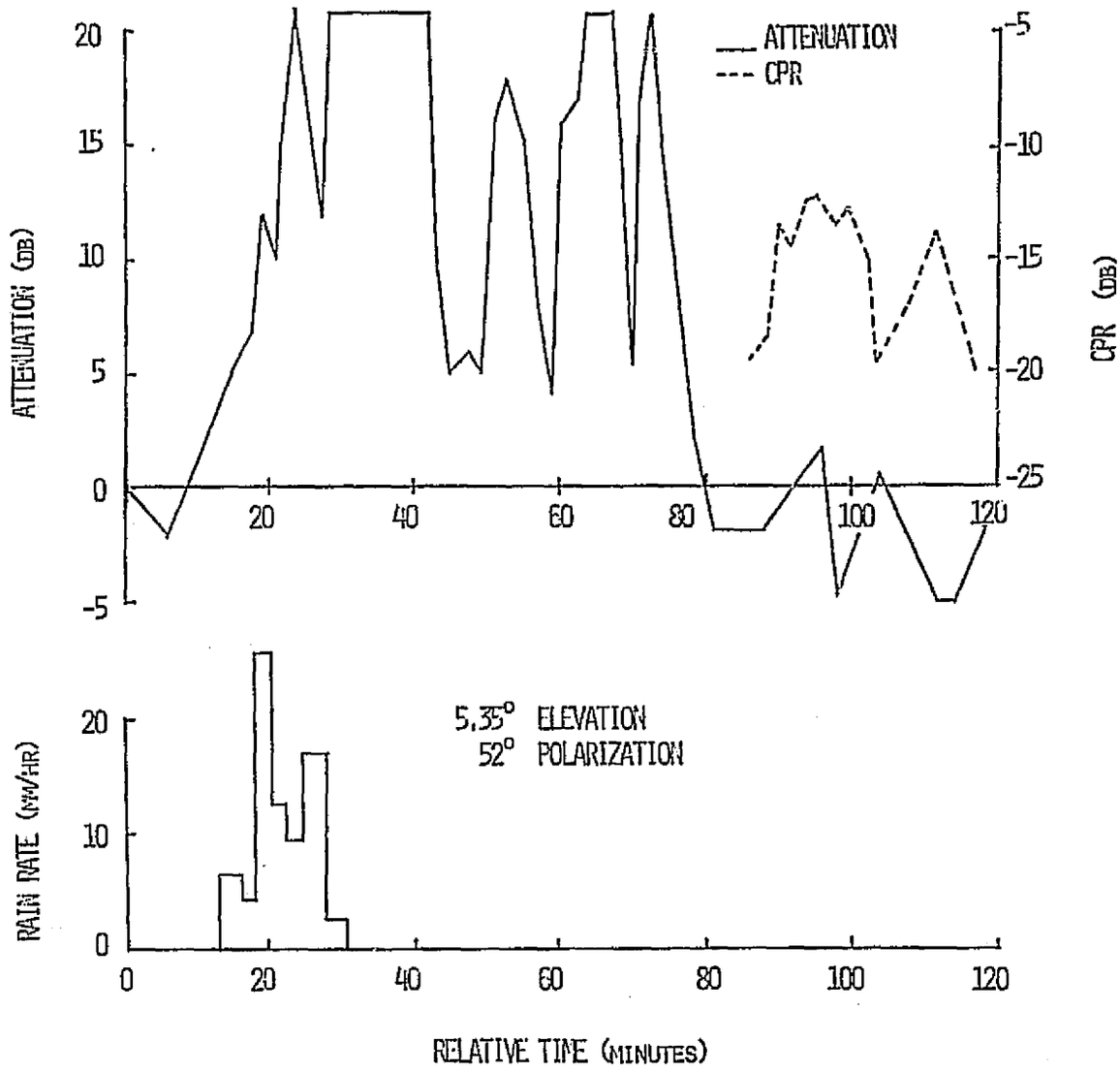

Figure 6-14. Data from rain storm of June 12, 1975 (1615-1810)

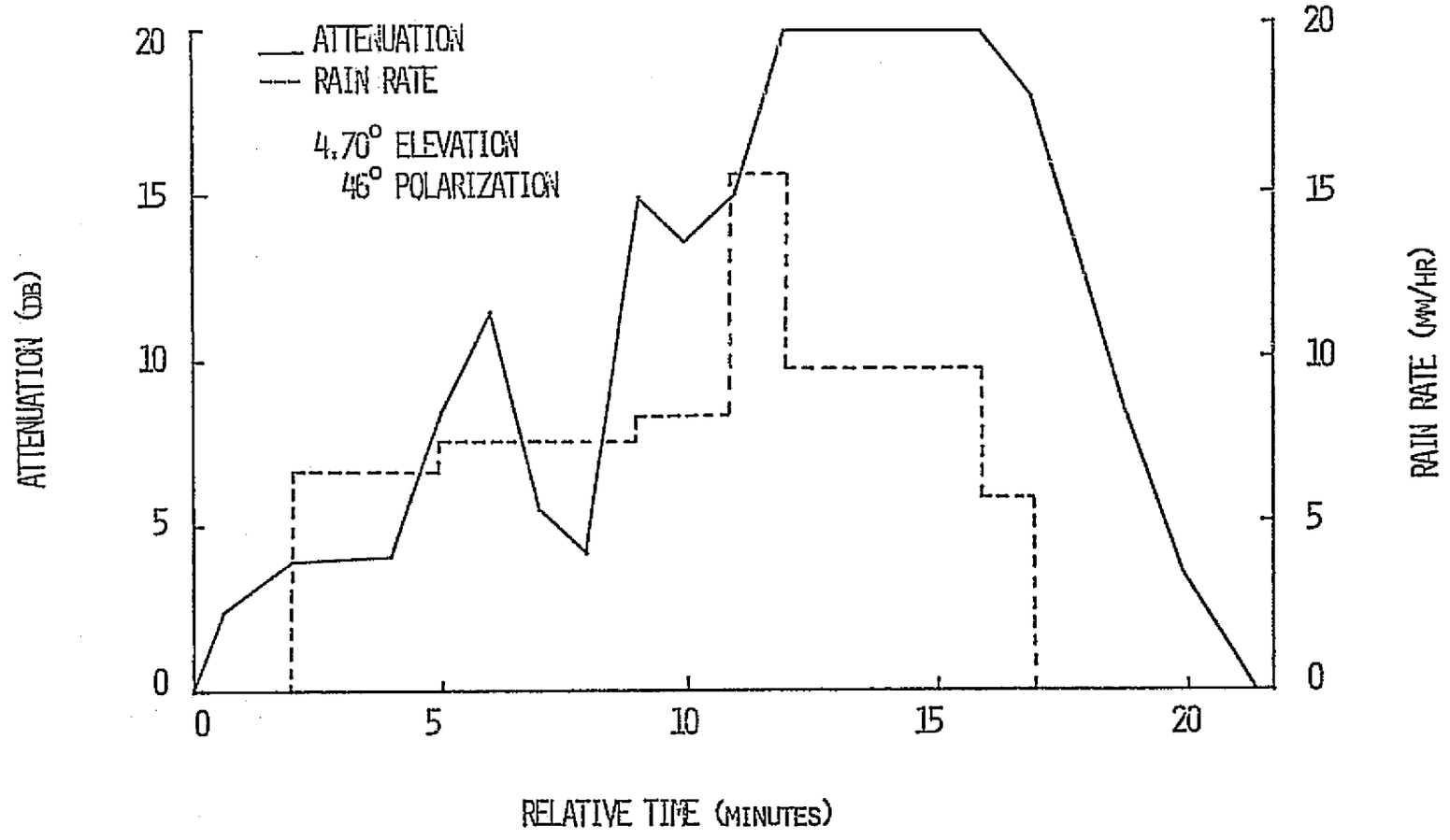

RAIN STORM OF 12 JUNE, 1975 (2053-2113)

Figure 6-15. Data from rain storm of June 12, 1975 (2053-2113)

The event began at about 1735 on June 12 when the copolarized signal level abruptly jumped from 20 dB below clear reference to as much as 5 dB above (an attenuation of -5 dB). Simultaneously, the CPR rose sharply and peaked at about -12 dB. Negative attenuation and high CPR continued for about 40 minutes. When we saw this happening, the operator carefully rechecked the antenna polarization angle and found it to be correct.

What was observed here appears to be a case of severe multipath. The 6 dB increase in co-polarized signal level over clear weather corresponds exactly to the arrival of equal-amplitude in-phase signals at the co-polarized channel. The situation for the cross-polarized signal is more complicated, but we feel that it can be explained as follows. The cross-polarized pattern of the antenna has a sharp null on axis. For the same incident polarization, a signal arriving off axis will be out of the null and the antenna will receive a larger cross-polarized component than it would if the signal came in on-axis. This is the central point of Watson's work on clear weather depolarization on ground paths. Since the phase response of the antenna also varies with angle of arrival, the CPR measured by an antenna for two signals with the same polarization but different arrival angles will be very similar to the CPR measured for two signals with slightly different polarizations and (perhaps greatly) different phases.

An analytical treatment of the second situation is relatively straight forward. Consider the electric field vectors drawn in Figure 6-16, where $\overline{E}_{NI}$ represents the normal incident signal and $\overline{E}_{MP}$ is a multipath signal which differs in orientation from $\overline{E}_{NI}$ by θ "spatial" degrees and is out of phase with $\overline{E}_{NI}$ by ϕ "phase" degrees. The total received electric field $\overline{E}_T$ is given by

$$\overline{E}_T = \overline{E}_{NI} + \overline{E}_{MP}. \tag{3}$$

Its complex polarization factor [14], ρ, is

$$\rho = \mathrm{CSC}(\theta)\, e^{-j\phi} + \mathrm{COS}(\theta). \tag{4}$$

From ρ we may calculate the Stokes parameters of $\overline{E}_T$ and from there we may calculate the average power received by the co-polarized and cross-polarized antenna fields. The ratio of these quantities is the CPR. This was done and the results are presented in Figures 6-17, 18 and 19.

At first glance, these results are somewhat surprising since, for example, two signals differing in polarization by only 1° can produce a CPR of +40 dB if their relative phase difference is near 180°. This happens because for this particular combination of parameters the cross-polarized components add and the co-polarized components subtract. Hence, multipath depolarization is potentially a more serious problem at low elevation angles than is rain depolarization.

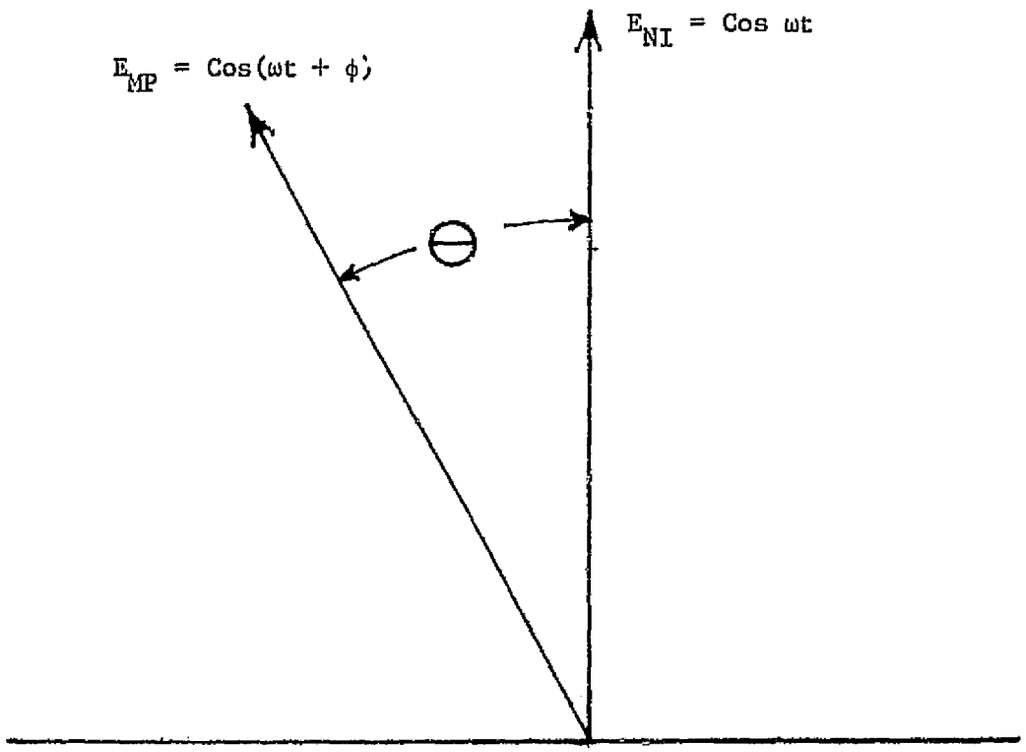

Figure 6-16. Relative spatial and temporal orientation of direct E_{NI} and multipath E_{MP} electric fields arriving at the receiver.

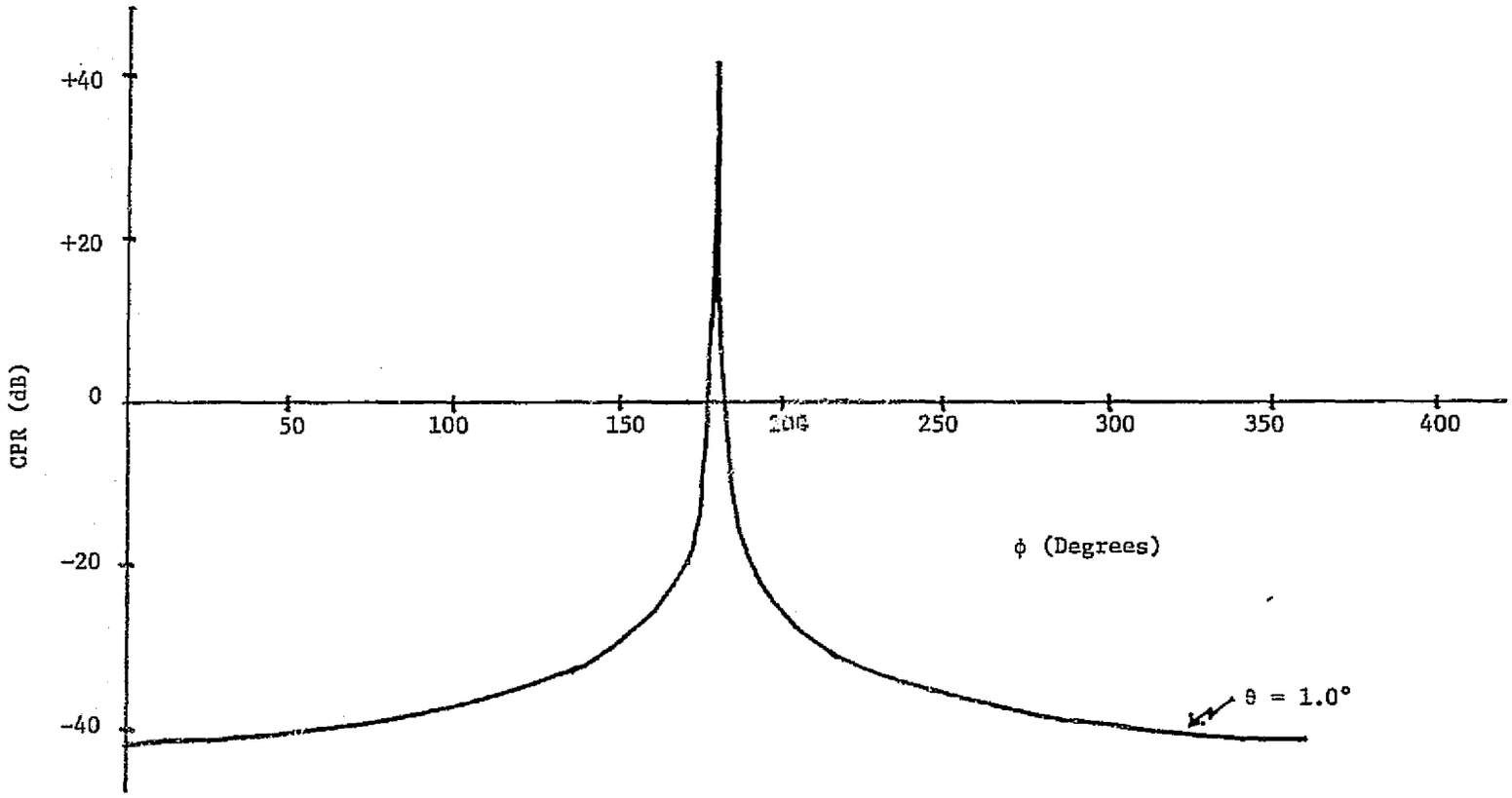

Figure 6-17. Cross polarization ratio due to a boresight signal and an equal amplitude mulitude signal displaced 1 degree from the boresight linear polarization and separated ϕ degrees in phase

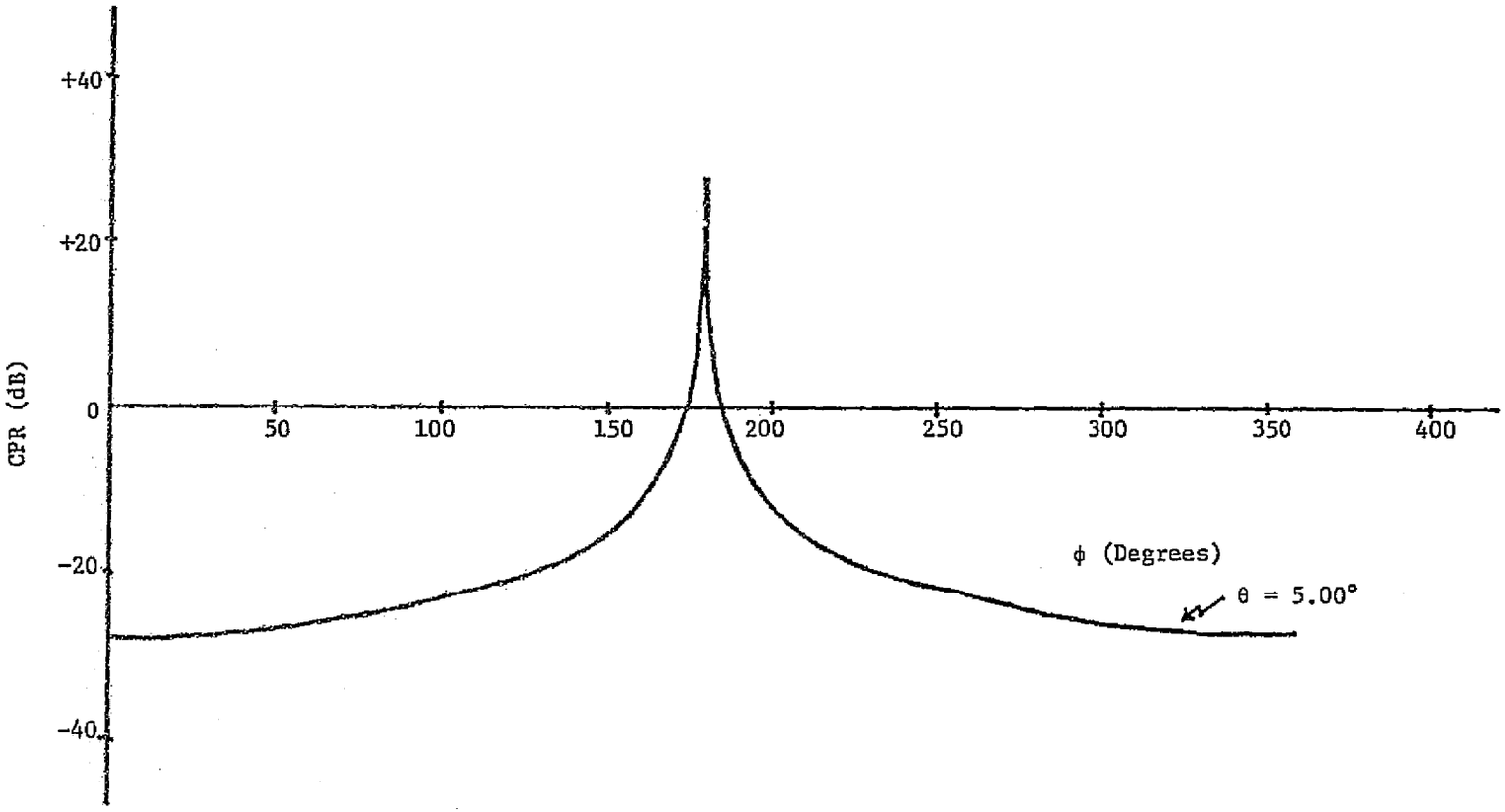

Figure 6-18. Cross polarization ratio due to a boresight signal and an equal amplitude multipath signal displaced 5 degrees from the boresight linear polarization and separated ϕ degrees in phase

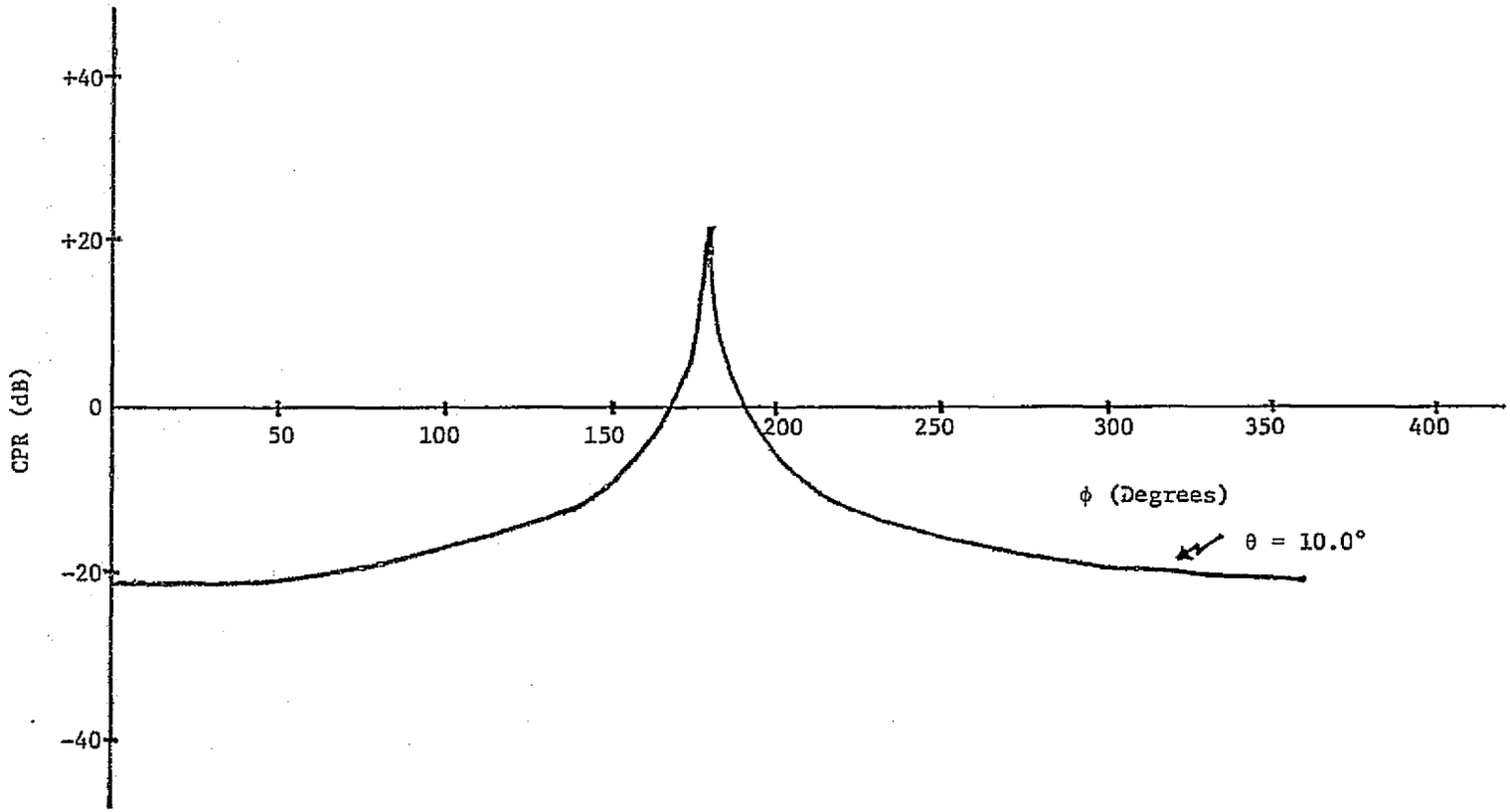

Figure 6-19. Cross polarization ratio due to a boresight signal and an equal amplitude multipath signal displaced 10 degrees from the boresight linear polarization and separated ϕ degrees in phase

6. CLEAR WEATHER EFFECTS

In the simplest kind of a dual-polarized satellite communication system, the ground antenna polarization would be aligned with the nominal clear weather polarization of the satellite signal and left for long periods without adjustment. With linear polarization, the proper antenna alignment may be found by rotating the receiving antenna until the cross polarized signal components pass through a null. But even with perfect polarization alignment and clear weather, cross polarization coupling in the transmitting and receiving antenna will cause the system to retain a finite level of cross polarization isolation; this is called the residual isolation of the system (better than -50 dB for our station). The clear weather isolation observed in a dual polarized satellite communications system depends upon the residual isolation and the accuracy of the antenna polarization alignment. Slightly misaligned "good" (high isolation) antennas may be used to simulate aligned "poor" (lower isolation) antennas. If the satellite or ground antenna alignments change, the clear weather cross polarization isolation will change with them. This will raise the crosstalk level, and the designer must allow a crosstalk margin large enough to absorb the clear weather variations and rain effects or else develop some means for periodic polarization matching.

When the ATS-6 experiment began, the consensus of NASA engineers was that the spacecraft attitude control system was so precise that no ground antenna polarization adjustments would be necessary to maintain a residual isolation close to optimum. The theoretical clear weather polarization of the ATS-6 signal at VPI (when the spacecraft antenna is pointed at VPI) is -17°, where the minus sign indicates a westward or right-hand tilt as seen by an observer standing at our station and facing the spacecraft. Our initial measurements indicated an actual value of -19.5°; given the uncertainties involved in making an absolute measurement of the polarization angle, this was acceptably close to the theoretical prediction and for about seven months we kept our antenna polarized at -19.5°.

In December 1974 and January 1975 our station was off the air for receiver repairs and modifications and after resuming operations, we rechecked the clear weather polarization angle. To our surprise, it had changed to -21.4°. We could find no reason for the change and began a program of measuring the clear weather polarization whenever the spacecraft was available. Table 6-1 presents the results of measurements made in February and March 1975. The values indicated have a mean of -20.97° and a standard deviation of 1°. A much larger sample is needed to more accurately establish the 3σ value.

The spacecraft yaw is supposed to be held to within 0.05°. A careful review of the spacecraft telemetry data by the satellite controllers and repeated checks of our antenna positioning system have shown no mechanical misorientations that

could cause the observed polarization angle changes. Before each measurement our antenna pointing is carefully adjusted to maximize the received signal (to an accuracy of ±0.1°); hence, off-axis reception [11] would not seem to be at fault.

Table 6-1
Measured Clear Weather Polarization Angles
with Spacecraft Antenna Directed at VPI&SU

Date (UT)	Time (UT)	Polarization Angle
6 Feb. 1975	2100	-21.4°
7 Feb. 1975	1900	-21.1°
20 Feb. 1975	2200	-20.5°
28 Feb. 1975	2230	-21.6°
4 March 1975	1917	-21.6°
10 March 1975	1800	-21.7°
20 March 1975	2005	-18.9°

At present the cause of these clear weather variations is unknown. In all possibility they lie in some undetected error in the spacecraft control system or in the ephemeris data that go into it rather than any propagation phenomenon, but whatever the cause, variations like this would degrade any dual polarized satellite communications system. With our equipment a 1° rotation in either direction reduces the clear weather CPR from about -40 dB to about -35 dB. This in itself would not be unacceptable for a commercial system, but the effect should be watched by other investigators.

7. CONCLUSIONS

The ATS-6 satellite signal on 20 GHz was used to measure depolarization along a satellite-to-ground path. Possible sources of depolarization are rain along the path, snow along the path, multipath effects at low elevation angles, and clear air effects. The data base was not sufficiently large in any of these areas to form statistically meaningful conclusions from the experiment. Also not enough is known to develop an accurate theoretical model. However, the experiment revealed several trends which in many cases are supported by simple theoretical explanations.

It was found that there is more depolarization on a satellite path (at -21.5° polarization angle) due to rain for a given rain rate than has been observed for a terrestrial link. From our measurements of one rain storm at a polarization angle near vertical, we tentatively conclude that depolarization may be significantly less for a dual polarized system whose polarizations are vertical and horizontal.

From several measurements made during snow we conclude that snow can introduce significant depolarization (and without high attenuation). Higher altitude phenomena may contribute to this depolarization.

Observations at very low elevation angles showed that attenuation can be introduced during clear weather by multipath effects. When rain is present further significant attenuation is also present. Furthermore, depolarization occurs.

REFERENCES

[1] P. A. Watson, "Crosspolarization isolation and discrimination," Electronics Letters, Vol. 9, pp. 516-517, November, 1973.

[2] C. W. Bostian, W. L. Stutzman, P. H. Wiley, and R. E. Marshall, "The influence of polarization on millimeter wave propagation through rain," Final Report, NASA Grant NGR-47-004-091 VPI&SU, Blacksburg, January 1974. (Available from NTIS as NASA CR-143686).

[3] P. A. Watson and M. Arbabi, "Rainfall cross polarization at microwave frequencies," Proc. IEE (London), Vol. 120, pp. 413-418, April, 1973.

[4] P. H. Wiley, W. L. Stutzman, and C. W. Bostian, "A new model for rain depolarization," Journal de Recherches Atmospheriques (France), Vol. 8, pp. 147-153, January-June, 1974.

[5] R. R. Taur, "Rain depolarization: theory and experiment," Comsat Technical Review, Vol. 4, pp. 187-190, Spring 1974.

[6] D. A. Gray, "Depolarization of ATS-6 satellite 20 GHz beacon transmitted through rain," USNC/URSI June 1975 Meeting Abstracts." Urbana, Illinois, p. 30.

[7] D. C. Cox, "Design of the Bell Laboratories 19 and 28 GHz satellite beacon propagation experiment," IEEE 1974 ICC Digest, June, 1974.

[8] C. W. Bostian, W. L. Stutzman, E. A. Manus, P. H. Wiley, and R. E. Marshall, "A 20 GHz Depolarization Experiment Using the ATS-F Satellite," Final Report, NASA Contract NAS5-21984, to be published.

[9] C. W. Bostian, W. L. Stutzman, P. H. Wiley, R. E. Marshall, "Initial Results of an Experimental Study of 17.65 GHz Rain Attenuation and Depolarization," 1972 International IEEE G-AP Symposium Digest, pp. 250-253, December, 1972.

[10] C. W. Bostian, "Antenna and path interaction in rain depolarization," 1974 International IEEE AP-S Symposium Digest, pp. 392-394, June, 1974.

[11] S. I. Ghobrial and P. A. Watson, "Cross polarization during clear weather conditions," IEEE Conf. on Propagation of Radio Waves at Frequencies Above 10 GHz, (IEE Conference Publication 98).

[12] P. A. Watson, et. al., "Cross Polarization studies at 11 GHz," Final Report European Space Research Organization Contract 1247/SL, University of Bradford, England, June, 1973.

[13] Yu, S. Babdin, et. al., "Attenuation of radiation at wavelength of 0.96 mm in snow," Radio Engineering and Electronic Physics, Vol. 15, No. 12, pp. 2171-2174, 1970.

[14] P. Beckmann, The Depolarization of Electromagnetic Waves, Boulder, Colorado: The Golem Press, 1968.

SUMMARY OF BATTELLE-NORTHWEST PARTICIPATION IN THE ATS-6 MILLIMETER-WAVE PROPAGATION EXPERIMENT

Karl C. Davis
Battelle-Northwest Laboratories
Richland, Washington 99352

Abstract

Attenuation on a space-to-Earth path was measured at 20 GHz for a ground terminal at approximately 1 km elevation in an arid (16 cm annual precipitation) region of eastern Washington State. Precipitation intensity and radiometric sky temperature at 20 GHz were also measured. Attenuation greater than 1 dB was observed only in the presence of wet snow on antenna surfaces. The most intense rain observed, 22 mm/hr, was accompanied by a measured sky temperature of 180 Kelvin implying a ground-to-space attenuation of 4.6 dB.

INTRODUCTION

Battelle-Northwest participateion in the ATS-6 Millimeter-Wave Propagation Experiment was designed to determine the effect of Pacific Northwest weather on satellite-to-Earth propagation at 20 GHz. Battelle Observatory has a 30-foot (9.1 meter) diameter Cassegrain antenna system (Figure 7-1) located in the southeastern part of Washington State on the Hanford ERDA Reservation. The site was chosen for minimum meteorological interference with millimeter-wavelength radio astronomical observation, in particular for low precipitable water. The region is arid, receiving an average of about 160 mm total precipitation per year. The antenna is located near the top of a 1,060-meter-high ridge close to the Observatory's optical astronomy and geophysical observing equipment.

INSTRUMENTATION

The major instrument used was a 20 GHz receiver-radiometer system installed on the 30-foot antenna to measure received 20-GHz carrier level and simultaneously radiometric sky temperature in the same antenna pattern at similar frequencies. A single balanced diode mixer was used for both purposes. The mixer input port was switched between the antenna and an ambient temperature waveguide termination at a 1 kHz rate. Figure 7-2 is a block diagram of the parts of

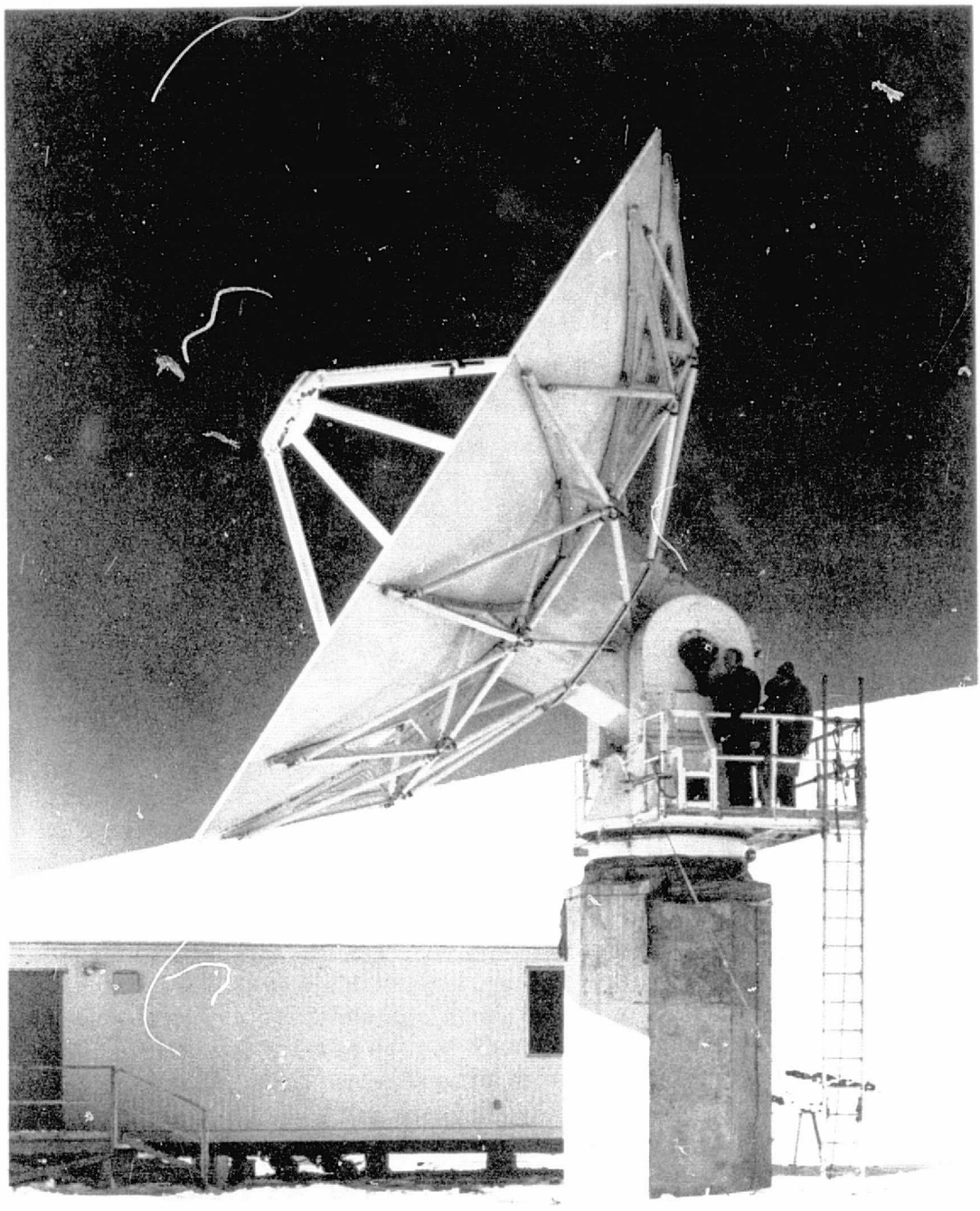

Figure 7-1. Battelle-Northwest 30-foot radio telescope

RECEIVER PACKAGE

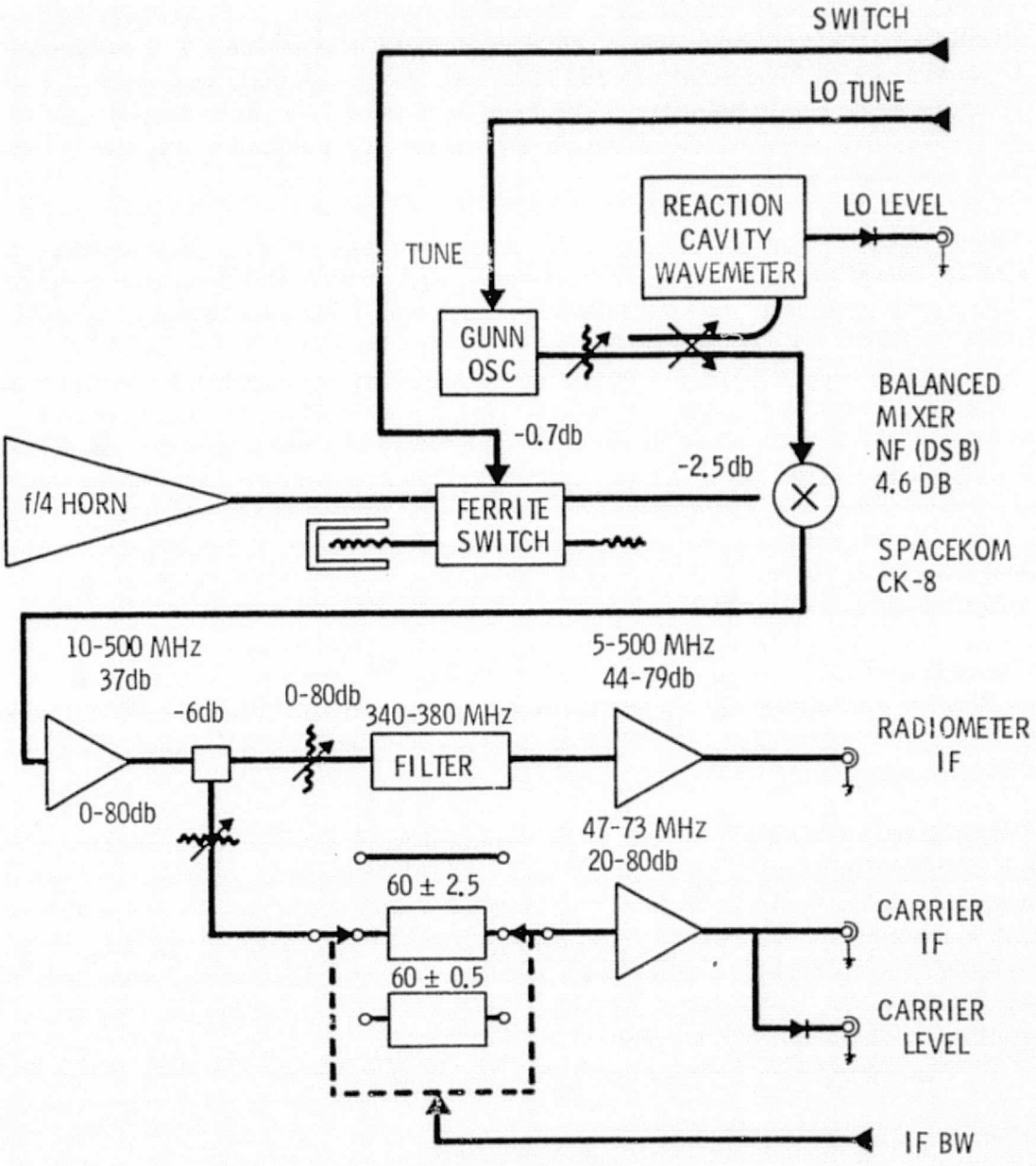

Figure 7-2

the receiver radiometer mounted in the antenna. A photograph of the antenna-mounted unit showing most of the RF components appears as Figure 7-3. A single IF preamplifier fed a power splitter and filters to define separate carrier and radiometer IF channels. The carrier IF system had remotely switchable filters defining passbands of 60 MHz ± 13, ±2.5, and ±0.5. The radiometric IF passband was fixed at 340 to 380 MHz. No RF preselector was used so both channels were double sideband. The local oscillator was set to 19.940 GHz to put the 20-GHz signal in the center of the carrier IF passband. Figure 7-4 shows the frequencies used.

Carrier level was measured by a wide dynamic range (30 dB) video detector and a 1-kHz-tuned amplifier-rectifier feeding a logarithmic amplifier and recorder. The carrier amplifier channel bandwidth used was 1 MHz and the post detection-tuned amplifier bandwidth was 20 Hz. Computed fade margin for the ATS-6 20-GHz transmitter using the parabolic antenna was approximately 50 db for this configuration for unity signal-to-noise. The RF switching, AC measurement technique actually determined the difference between total power from the ambient temperature waveguide load in a 2-MHz passband and the 20-GHz signal. The computed signal-to-comparison-noise ratio was 30 dB. We would like to point out that this level of performance was achieved without a high-stability local oscillator or a phase-locked receiver by making use of signal modulation produced by the ferrite switch.

The radiometer IF channel output was detected and synchronously rectified to measure the difference between radiometric sky temperature and ambient waveguide load temperature. The difference was recorded on a second channel of the data recorder.

A tipping bucket rain gauge with heated collecting funnel was used to determine precipitation intensity. Each bucket tip, representing 0.01" (0.24 mm) of water, was recorded with the 20-GHz signal level and sky temperature. The rain gauge was located about 100 meters from the antenna in an open area. Additional instruments were provided to measure wind speed and direction, relative humidity, temperature, and barometric pressure. A block diagram of the control room equipment appears in Figure 7-5.

OPERATING PROCEDURE

The receiver-radiometer system was operated almost continuously with the antenna pointed at the zenith. For 20-GHz path attenuation measurements, the look angles for the appropriate time interval supplied by the National Aeronautics and Space Administration were entered in the tracking computer and the antenna

Figure 7-3. Antenna-mounted RF package

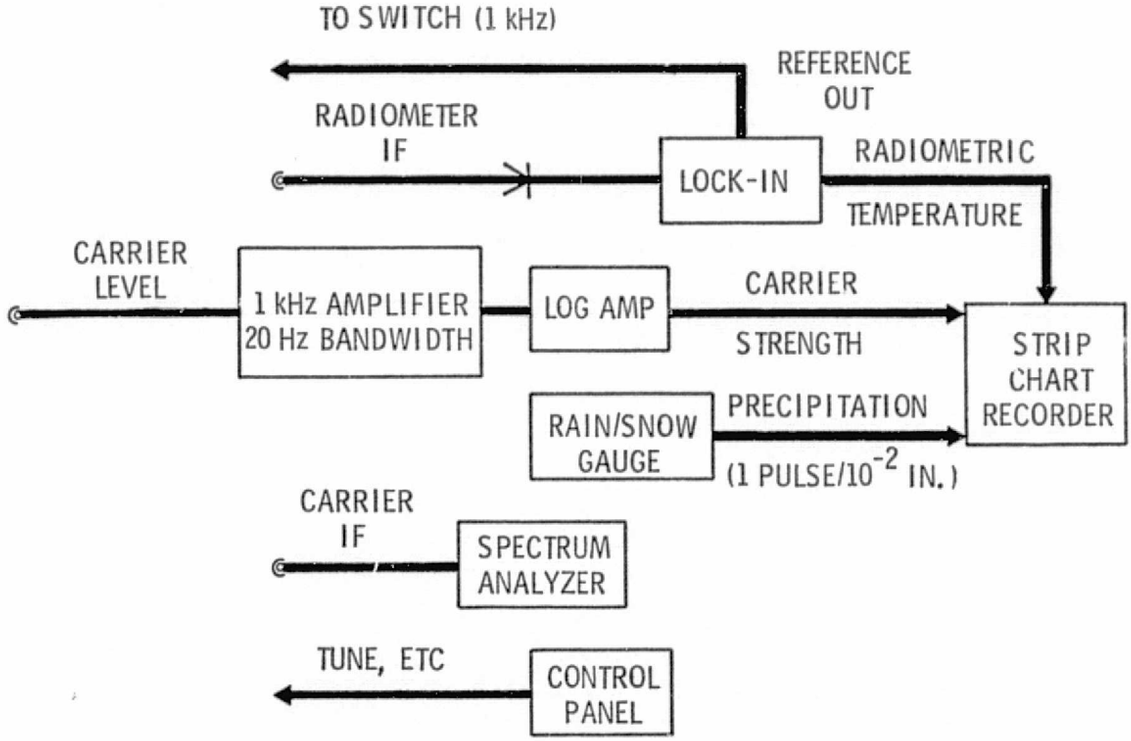

Figure 7-5

slewed to the designated initial position. The computer interpolated linearly between provided values to update the antenna position every 60 seconds. Manual fine adjustment of position was performed to "peak" received signal strength at the start of measurements. The local oscillator was tuned manually, if necessary, to center the received signal in the 60-MHz carrier signal IF channel. This manual tuning procedure, using a spectrum analyzer to locate the received signal, was the weakest link in the acquisition procedure. It was found that the signal margin for acquisition was approximately 30 dB at most favorable satellite pointing.

RESULTS

All components were installed by March 19 and the first attempt at satellite acquisition was successful on March 20. Routine operation began with a clear weather calibration March 21 and continued until loss of satellite June 3. Weather

at our site was slightly drier and cooler than normal for this time period. Average total precipitation for the period is 28 mm, and 25 mm was measured this year, (see Figures 7-6 and 7-7).

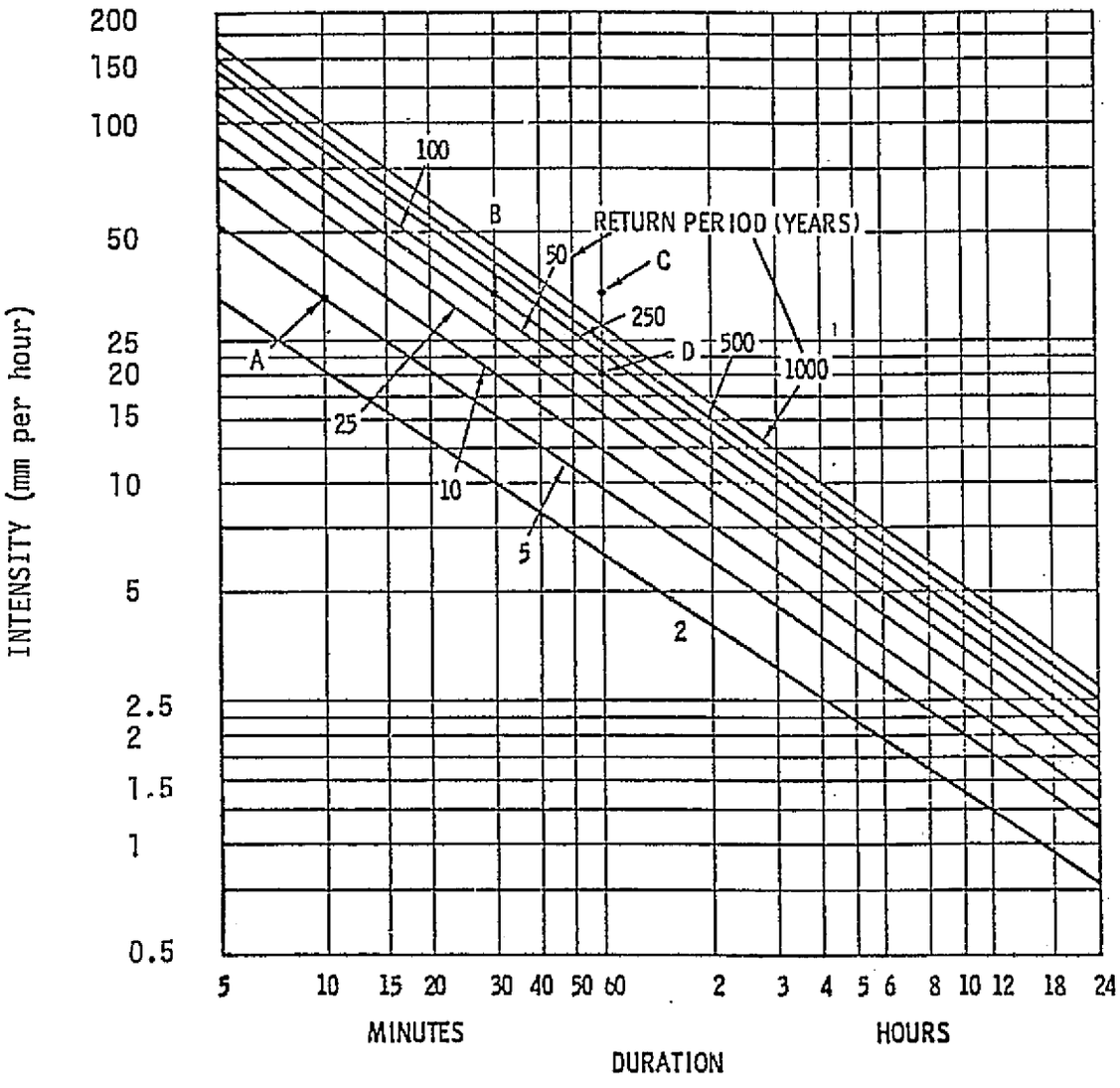

Figure 7-6

C-3

AVERAGE MONTHLY PRECIPITATION INTENSITY FACTORS (I)
BASED ON THE PERIOD 1946-1970

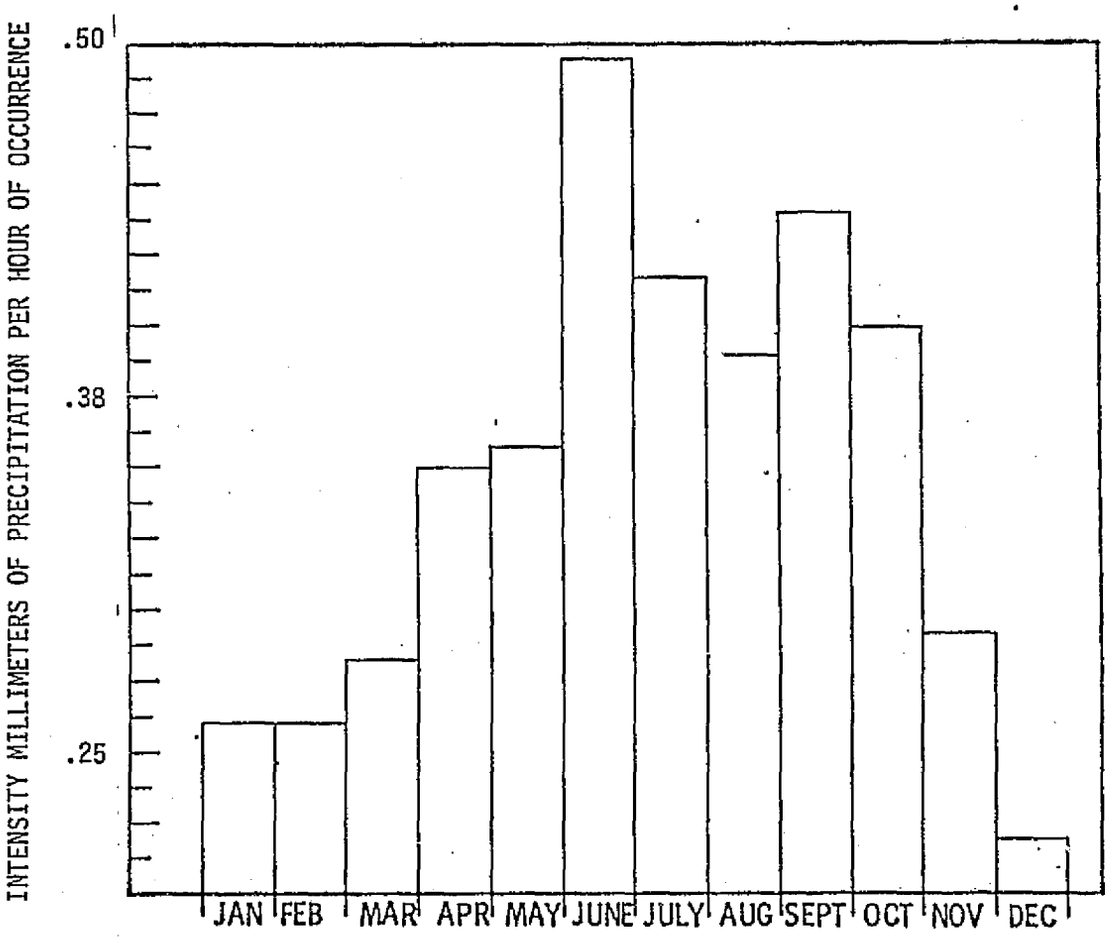

Figure 7-7

20-GHz ATTENUATIONS

The 20-GHz transmitter was observed for a total of 14 hours. There was measurable precipitation, i.e., intensity greater than 0.3 mm per hour during approximately 4 of these hours. The highest intensity precipitation through which 20-GHz signal attenuation was measured was wet snow equivalent to 1.5 mm of water per hour. No significant attenuation, i.e., greater than 1 dB, was observed which could be attributed to atmospheric absorption or scattering. Attenuation exceeding 10 dB and radiometric sky temperatures approaching ambient, above 250 Kelvin, were observed on this occasion but occurred half an hour to an hour after passage of the precipitation and coinciding with the melting of snow on most of the

reflector surface. Similar attenuation and sky temperature were observed on another occasion following snow and coinciding with the melting of snow on the antenna. There was substantially identical behavior of measured zenith sky temperature on a third occasion about an hour after a light fall of wet snow. Our conclusion is that the observed high attenuations were due to wet or melting snow on the antenna primary reflector and/or feed cover rather than atmospheric path attenuation.

SKY TEMPERATURE

Observations of zenith sky temperature have been made almost continuously since operation began. In addition to the incidents described above, we observed significantly elevated sky temperatures in the following cases:

Precipitation Rate mm/hr	Radiometric Sky Temperature	Implied Attenuation
1.2	160 Kelvin	3.5 dB
2.3	127 Kelvin	2.5 dB
22*	180* Kelvin	4.6 dB*

The first two cases occurred in May and may have been snow, sleet, hail, or rain. Our heated rain gauge does not distinguish between the various forms. Relative timing of the precipitation and the rise in sky temperature imply that these were not due to melting snow and are probably genuine path attenuations. Since both events occurred at night during unattended operation, we do not know the weather class at our mountain site (which often differs markedly from that observed in the valley). The case marked "*" occurred while the site was manned and more detailed information is available. On July 30 there was a short period of intense rain, at least intense for this area. The antenna was pointed to 30° elevation and 120° azimuth, representative of ATS-6 look angles and, in this case, the direction in which the storm appeared most intense by visual observation. Peak rain intensity, recorded at the antenna site, was 0.06" in four minutes (approximately 22 mm/hr) and coincided with an observed radiometric sky temperature of 180 Kelvin, suggesting an atmospheric attenuation of 4.6 dB.

SUMMARY

The ATS-6 millimeter-wave propagation experiment has as its goal the characterization of the Satellite-Earth propagation path at 20 and 30 GHz and the correlation of its properties with observable radiometric and meteorological phenomena.

Our part of this experiment was to assemble and operate a 20-GHz ground station using our 9.1-meter radio telescope antenna. In operation, we observed and recorded, particularly during storms, the carrier strength of the 20-GHz beacon aboard the satellite, radiometric sky temperature, precipitation rate, and other meteorological parameters. Data analysis was performed to identify interrelationships among recorded data to aid in the prediction of path attenuation for communication links.

CONCLUSIONS

Weather conditions producing attenuation greater than 5 dB on a Space-to-Earth path at 20 GHz will probably occur less than one hour per year at our arid, eastern Washington State site.

RECOMMENDATIONS

Further atmospheric path attenuation studies for regions of low precipitation intensity are probably needed only for (1) much higher operating frequencies, or (2) where extremely low probability of outage is required.